博士論文

Development of a Magnetocaloric Heat Circulator based on Self-heat Recuperation Technology

(自己熱再生技術に基づいた磁気熱循環システムの開発)

小谷　唯

Contents

List of Tables

List of Figures

Nomenclature

ΔS_{m} magnetic entropy change [J kg^{-1} K^{-1}]

ΔT_{ad} temperature difference that can be obtained by adiabatically magnetizing a magnetocaloric material [K]

ΔT_{HEX} temperature difference during heat exchange [K]

ΔT_{min} minimum temperature difference needed for heat exchange [K]

$\dot{m}_{\mathrm{f}}$ fluid flow rate [kg s^{-1}]

ϵ porosity [-]

γ electron heat capacity coefficient [J kg^{-1} K^{-2}]

μ magnetic permeability [H m^{-1}]

μ_0 magnetic permeability of vacuum (= $4\pi\times10^{-7}$ [H m^{-1}])

μ_{B} Bohr magneton (= 9.274 009 15(23)$\times10^{-24}$ [J T^{-1}]

μ_{eff} effective magnetic moment [J T^{-1}]

ρ density [kg m^{-1}]

θ_{C} Curie temperature [K]

θ_{D} Debye temperature [K]

A amount of exergy [J kg^{-}1]

A_{discard} amount of exergy discarded with the process stream [J kg^{-1}]

A_{loss} amount of exergy destruction [J kg^{-}1 K^{-}1]

A_{min} theoretical minimum exergy destruction in heat transfer when the minimum temperature difference needed for heat exchange is set [J kg^{-}1]

a_{s} heat transfer surface [m^2]

c_{f} heat capacity of process stream [J kg^{-1}]

$C_{H,p}$ specific heat capacity at constant pressure and magnetic field [J kg^{-1} K^{-1}]

C_p specific heat capacity at constant pressure [J kg^{-}1 K^{-}1]

d_{p} diameter of particle [m]

E_{net} Net work input to the system in order to obtain the desired change in state condition of the process stream [J kg^{-1}]

f strength of tension [N]

g_{J} spectroscopic splitting factor [-]

H strength of magnetic field [A m^{-1}]

H_{eff} effective magnetic field [A m^{-1}]

I amount of enthalpy [J kg^{-}1]

I_0 amount of enthalpy at standard condition [J kg^{-}1]

J total angular momentum [-]

k heat conductivity [W m^{-1} K^{-1}]

k_B Boltzmann constant (= 1.380 6488(13)$\times 10^{-23}$ [J K^{-1}])

M strength of magnetization in a magnetic material [A m^{-1}]

N_A Avogadro constant (= 6.022 141 29(27) $\times$ 10^{23} mol^{-1})

N_s number of atoms per unit volume [m^{-3}]

p pressure [Pa]

Pr Prandtl number [-]

Q amount of heat [J kg^{-}1]

$Q_{discard}$ amount of heat discarded at the cooler [J kg $^{-1}$]

$Q_{process}$ total amount of heat needed to change the temperature of a process stream to its set temperature

$Q_{transfer}$ amount of heat transferred [J]

R gas constant (= 8.314 4621(75) [J K^{-1} mol^{-1}])

Re_p Raynolds number [-]

S amount of entropy [J kg^{-}1 K^{-}1]

S_0 amount of entropy at standard condition [J kg^{-}1]

S_E electron entropy of a magnetic material [J kg^{-1} K^{-1}]

S_{gen} overall entropy generation[J kg^{-}1 K^{-}1]

S_L lattice entropy of a magnetic material [J kg^{-1} K^{-1}]

S_M magnetic entropy of a magnetic material [J kg^{-1} K^{-1}]

S_{total} total entropy of a magnetic material [J kg^{-1} K^{-1}]

T temperature [K]

t time [s]

T_0 environmental temperature: 298.15 [K]

T_{set} temperature needed for subsequent process [K]

w_{demag} amount of work needed for demagnetization [J]

w_{mag} amount of work needed for magnetization [J]

Chapter 1

Introduction

1.1 Increasing energy demands in the world

Global warming and resource depletion has grown to become one of humanity's greatest challenges. Fig. 1.1 shows the transition of contributors of carbon-dioxide (CO_2) emission in the world from 1800-2000 [1]. Needless to say, the emission of carbon-dioxide is rising at rapid rate and can be assumed to continue growing. Although development to use renewable energy sources such as solar power, wind power, geothermal... etc. are being pursued, The World Energy Outlook (WEO) 2007 has stated that the energy generated from fossil fuel is expected to meet about 84% of the world's energy demand by 2030 [2]. Shifting the view point to Japan, Fig. 1.2 presents the transition of total CO_2 emission and CO_2 emission per person in Japan during 1990-2012 [3]. Both total CO_2 emission and CO_2 emission per person is gradually increasing. Although both values drop at 2008 due to the financial crisis and economical recession, it is rapidly growing back to the original value before 2008. Besides developing renewable energy sources and raising the efficiency of energy conversion, it is needed to radically change the ways in which we use our energy.

Fig. 1.3 shows the breakdown of carbon-dioxide emission contributors in Japan 2012 [3]. Industrial sector is responsible of 1/3 of the total carbon-dioxide emission. It is

reported by Maruoka *et al.*, that in high temperature industrial processes such as steel-making and cement making processes, almost half of the input energy is discarded as waste heat [4].

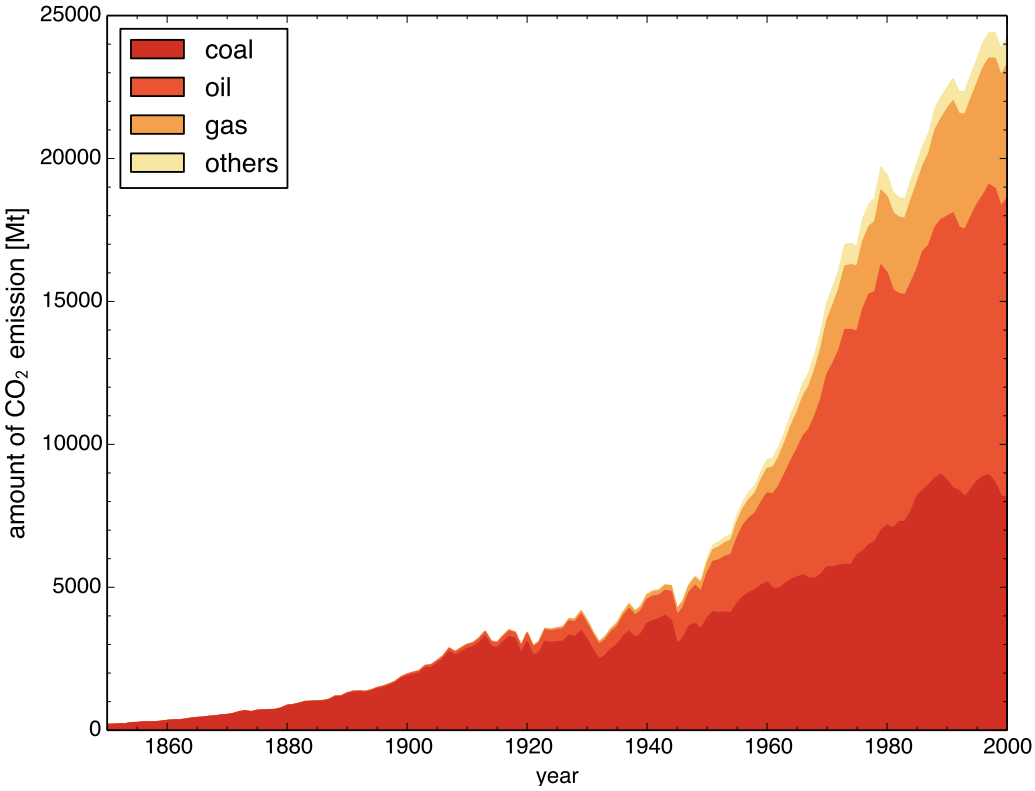

Figure 1.1: Transition of contributors of carbon-dioxide emission in the world 1800-2000 [1]

In 1997 December, the member nations of the United Nations Framework Convention on Climate Change (UNFCCC) reached an agreement to set target values to reduce the greenhouse gas emission at the 3rd Session of the Conference of the Parties (COP3) in Kyoto, Japan. Japan's target is to reduce the greenhouse gas emission to a value 6% lower than the greenhouse gas emission in year 1990. Up to 90% of the greenhouse gas emission is composed of carbon-dioxide [3]. Hence, a method to drastically reduce emission of carbon-dioxide is required.

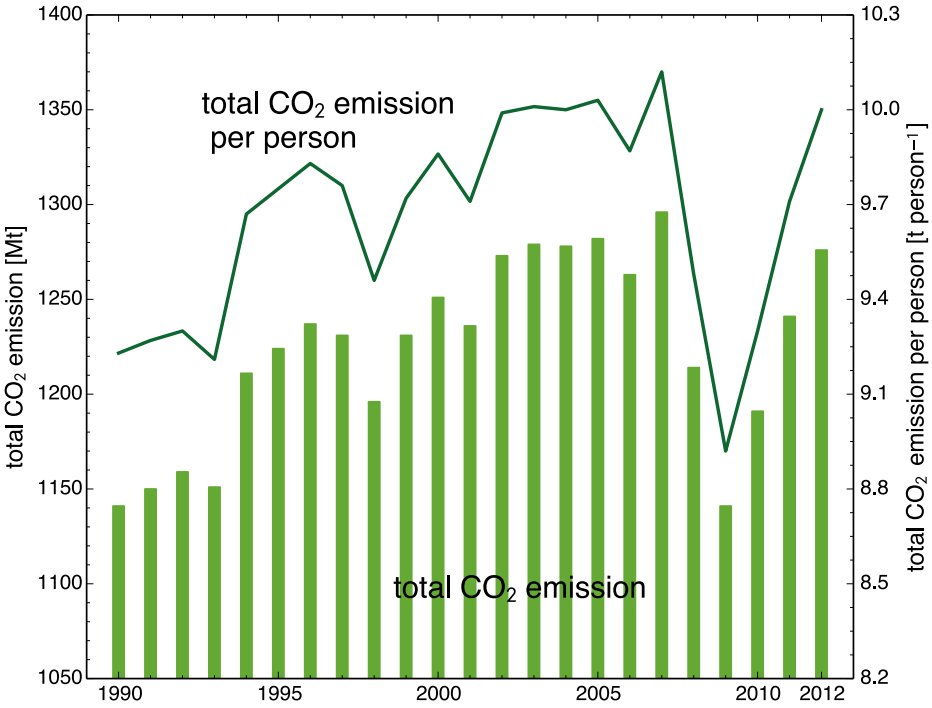

Figure 1.2: Transition of carbon-dioxide emission in Japan during 1990-2012 [3]

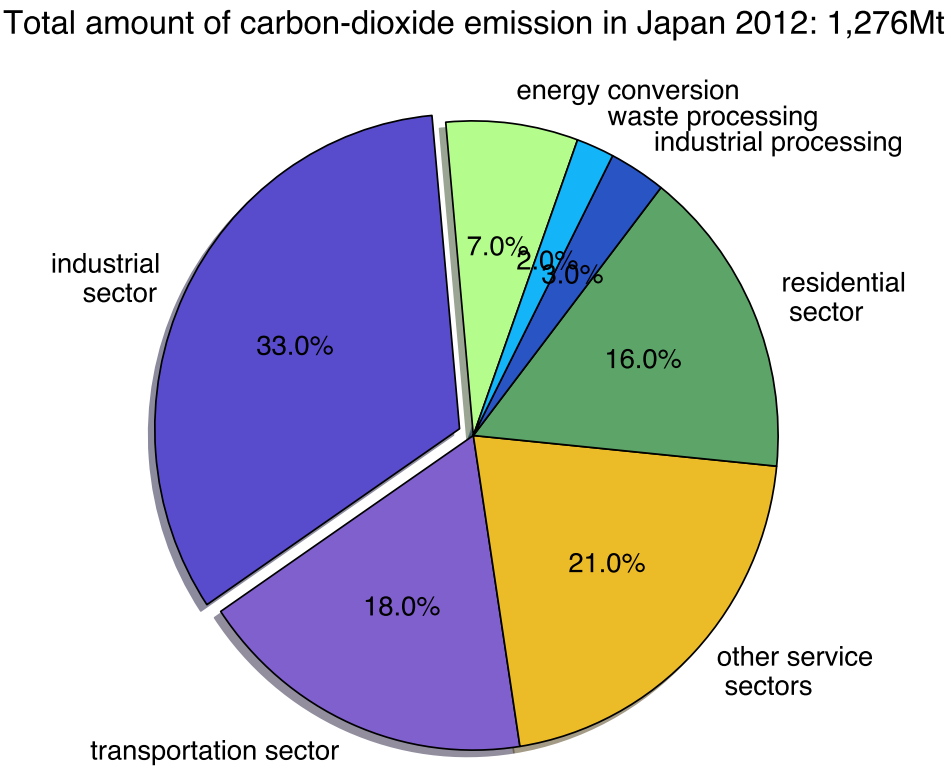

Figure 1.3: Breakdown of carbon-dioxide emission contributors in Japan (2012) [3]

1.2 Conventional heat recovery technology

Chemical processes are often comprised of various different processes. This is because the intended process (i.e. separation, reaction, drying…etc.) is usually stable near environmental conditions and energy needs to be put in to bring the condition of a feed material to a condition where the intended process will proceed spontaneously and obtain the required product. That is to say that the difference in Helmholtz and Gibbs free energy must be less than zero to drive conversion. Normally, conditions of feed material that are varied in chemical processes are temperature and pressure.

Generally, a process that involves heating or cooling starts and ends at environmental condition, which is usually defined by, environmental temperature T_0, and pressure, p_0. A schematic flow diagram of a simple heating process where the feed process stream is heated from the environmental temperature, T_0, to the set temperature, T_{set}, for the upcoming process, X, is shown in Fig. 1.4. The feed process stream is heated to the set temperature, T_{set}, at the fired heater ($1 \rightarrow 2$), via the next process, X, ($2 \rightarrow 3$), it is cooled back to the environmental temperature, T_0 ($3 \rightarrow 4$). Temperature-heat diagram of a simple process is shown in Fig. 1.5. Note that the state number correspond to the state number in the flow diagram. In the presented simple process, all of the heat needed to raise the feed process fluid temperature from environmental temperature, to the set temperature, Q_{process}, is provided at the fired heater. Due to the conservation law of energy, all of the heat provided at the fired heater, Q_{FH}, is discarded at the cooler, Q_{discard}, provided that state 2 and 3 are the same.

$$Q_{\text{process}} = Q_{\text{FH}} = Q_{\text{discard}} \tag{1.1}$$

Thus, in a simple process where no energy saving is applied, total energy consumption is equal to the heat provided to the feed process stream. Similar discussion can be made with cooling processes, all the heat taken away from the feed process stream will be given back to the effluent process stream and returns to its original temperature, T_0.

In consideration of reducing the energy consumption of these thermal processes, op-

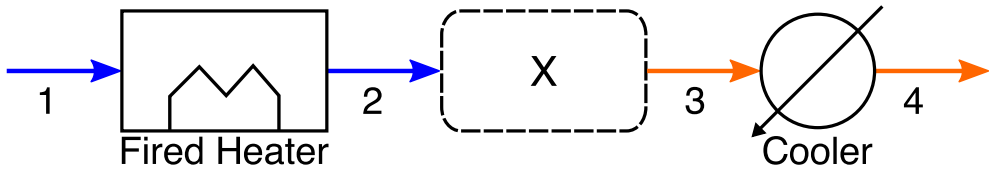

Figure 1.4: Schematic flow diagram of a simple thermal process

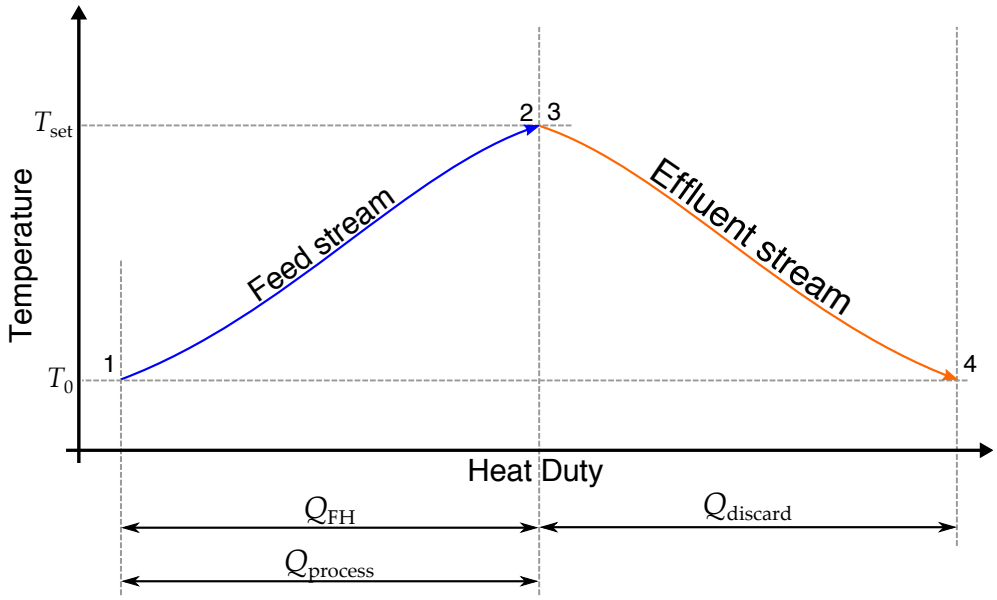

Figure 1.5: Temperature-heat diagram of a simple thermal process

timization methods represented by the pinch technology [5,6] has been applied. In pinch technology, process integration is optimized through the use of grand composite curves. By drawing the grand composite curves of the process stream in a chemical process, the heating and cooling requirements after heat recovery has taken place can graphically be seen. Pinch technology has been extended to be used area-wide in order to gain further energy savings [7]. Besides the thermal pinch analysis, due to its simplicity and effectiveness, pinch technology has been extended to be used for hydrogen distribution as hydrogen pinch analysis [8], wastewater manipulation through water-oxygen pinch analysis [9], power pinch analysis for optimizing systems comprising hybrid energy sources [10]...etc.

Fig. 1.6 shows the schematic flow diagram of a heating process with a feed-effluent heat exchanger. The feed process stream is firstly heated in the heat exchanger (HEX) (1 $\rightarrow$ 2) and then, further heated in the fired heater to the set temperature, T_{set} (2 $\rightarrow$ 3). Via the next process, X (3 $\rightarrow$ 4), the effluent process fluid is cooled at HEX as much as possible (4 $\rightarrow$ 5), and finally the rest of the heat is discarded at the cooler (5 $\rightarrow$ 6). Fig. 1.7 shows the temperature-heat diagram of the heating process with a feed-effluent heat exchanger. The composite curve is "pinched" so that the smallest temperature difference during heat exchange in the HEX is ΔT_{min}. The sum of the amount of heat provided at the HEX, Q_{transfer}, and amount of heat provided at the fired heater, Q_{FH}, is the total amount of heat provided to the feed process stream, Q_{process}.

$$Q_{\text{process}} = Q_{\text{FH}} + Q_{\text{transfer}} \tag{1.2}$$

If the enthalpy of state points 1 and 6 are the same, from the conservation law of energy, all of the heat provided at the fired heater is discarded at the cooler.

$$Q_{\text{FH}} = Q_{\text{discard}} = Q_{\text{process}} - Q_{\text{transfer}} \tag{1.3}$$

By applying a feed-effluent heat exchanger, it is possible to recover part of the process stream heat, leading to reduction of energy consumption of about 70-80% [11].

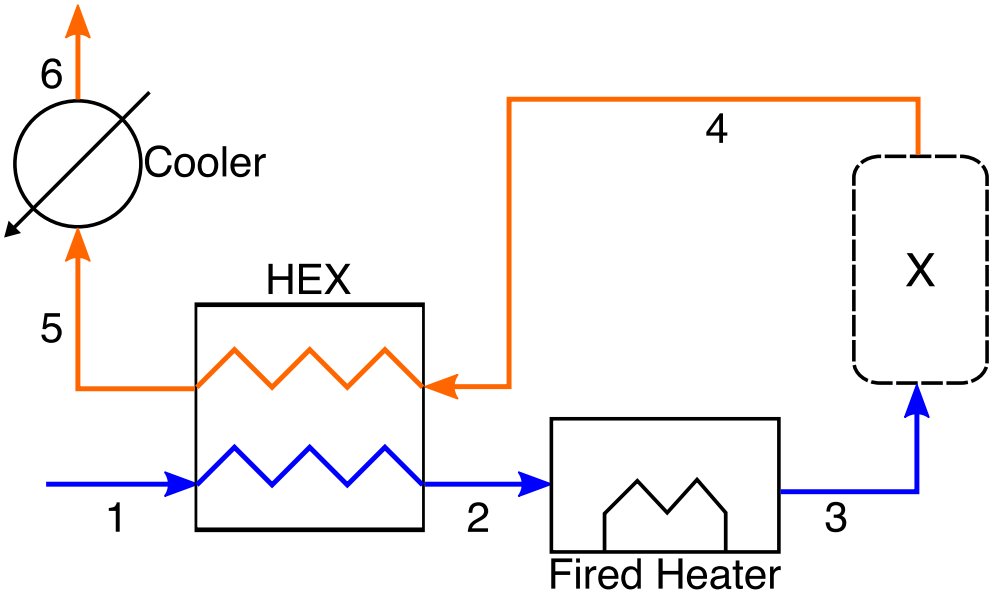

Figure 1.6: Schematic flow diagram of a thermal process with a feed-effluent heat exchanger

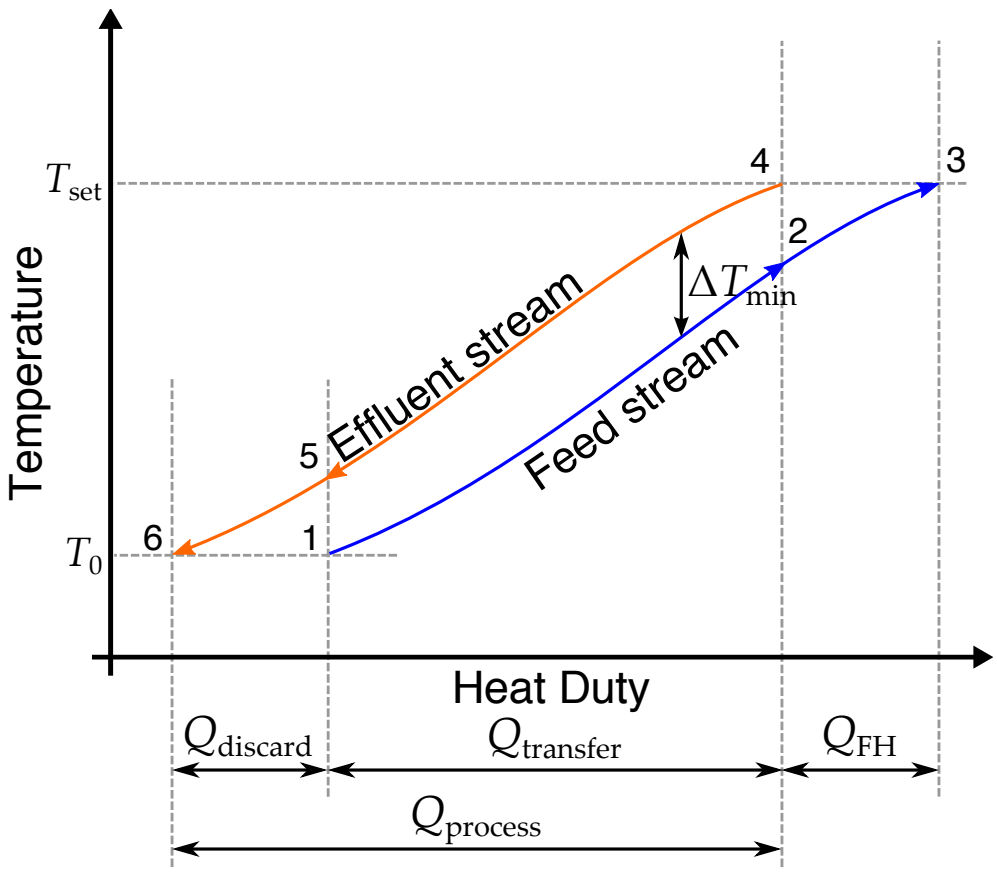

Figure 1.7: Temperature-heat diagram of thermal process with a feed-effluent heat exchanger

1.3 Self-heat recuperation technology

1.3.1 Exergy recuperation principle

In order to make use of energy, energy must be transformed from one form to another. On doing this conversion, it is also possible to split one form of energy into two different types of forms or, combine two different types of energy forms into one. All energy conversion can be categorized into four different types of energy conversion [15]. Fig. 1.8 shows the types of energy conversion in the energy conversion diagram.

type I is when energy at high exergy rate is transformed to energy with low exergy rate due to exergy destruction. A typical example is when chemical energy is transformed to heat due to combustion.

type II is when energy is transformed to an energy form which is same to the initial energy form. A typical example is conversion from electricity to work.

type III is when energy at medium exergy rate is divided into energy with high exergy rate and energy with low exergy rate. A typical example is thermal engine where chemical energy at medium exergy rate is divided in to electricity with high exergy rate and heat with low exergy rate.

type IV is when energy at high exergy rate and energy at low exergy rate is converged to create energy at medium exergy rate. A typical example is a heat pump where electricity with high exergy rate and heat at environmental temperature with low exergy rate is converged to create heat at a higher temperature with medium exergy rate.

In the conventional thermal processes, heat is firstly created by type I energy conversion, then, it is transferred to the feed process stream. Combustion (type I) energy conversion is associated with large exergy destruction. On the contrary, *Kansha et al.* proposed a thermal process based on type IV energy conversion [11], so called self-heat

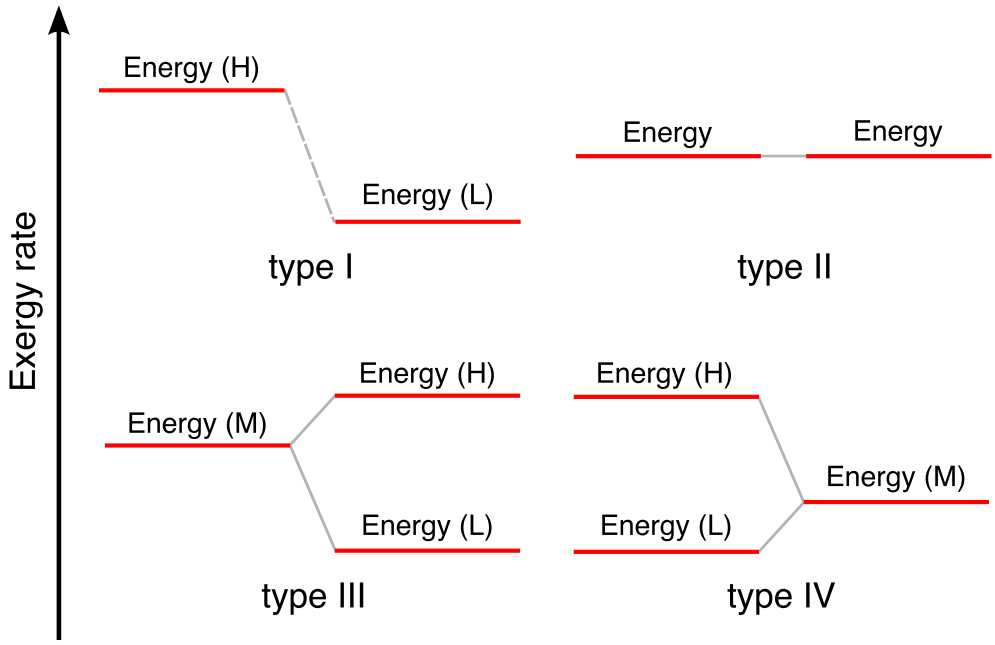

Figure 1.8: The four types of energy conversion [15]

recuperation technology. In a self-heat recuperative process, by providing work (exergy rate of 1.0), the heat at low exergy rate is recuperated. The recuperated heat is reutilizes to heat the feed process stream, thus all of the process stream heat is circulated.

1.3.2 Self-heat recuperative thermal process

Self-heat recuperation technology based on exergy recuperation principle has been proposed in year 2009 by *Kansha et al.* [11]. Fig. 1.9 shows the schematic flow diagram of a self-heat recuperative thermal process for heating. The feed process stream is heated from the environmental temperature, T_0, to the set temperature, T_{set}, in the HEX ($1 \rightarrow 2$). Via the next process ($2 \rightarrow 3$), it is adiabatically compressed to gain enough temperature difference needed for heat exchange, ΔT_{HEX} ($3 \rightarrow 4$). The effluent process stream is then put into the HEX where all of the process stream heat is given to the feed process stream ($4 \rightarrow 5$). Part of the compression work is recovered by the expander ($5 \rightarrow 6$) and the rest of the heat is discarded ($6 \rightarrow 7$). Fig.1.10 shows the temperature-heat diagram of a self-heat recuperative process.

In a self-heat recuperative process, all of the process stream heat, Q_{process}, is circulated within the system.

$$Q_{\text{process}} = Q_{\text{transfer}} \tag{1.4}$$

The total energy consumption, which is the net work input, E_{net}, is the difference between the work provided for compression, w_{comp}, and the work recovered at the expander, w_{exp}. If the state of points 1 and 7 are the same, the amount of net work input, E_{net}, is equal to the amount of heat discarded at the cooler, Q_{discard}.

$$E_{\text{net}} = w_{\text{comp}} - w_{\text{exp}} = Q_{\text{discard}} \tag{1.5}$$

In a self-heat recuperative process, all of the process stream heat is circulated within the system and no-makeup heat is added. A system like this is called "heat circulator" [23]. By applying self-heat recuperation technology in thermal processes, it is reported that drastic reduction in energy consumption compared to thermal processes with feed-effluent heat exchanger can be obtained. The work provided to raise the temperature of the process fluid is conserved in the process fluid in the form of pressure and can partially be recovered.

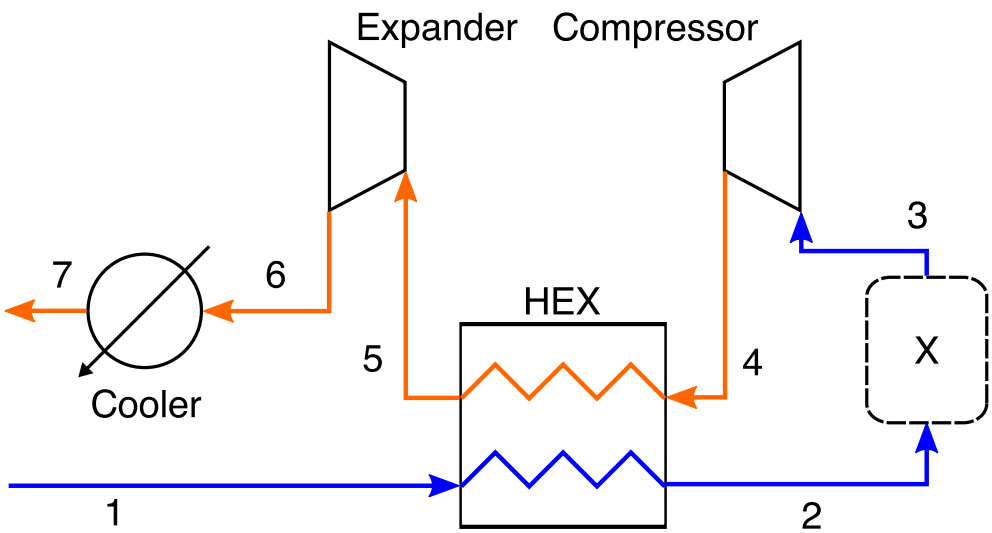

Figure 1.9: Schematic flow diagram of a self-heat recuperative thermal process

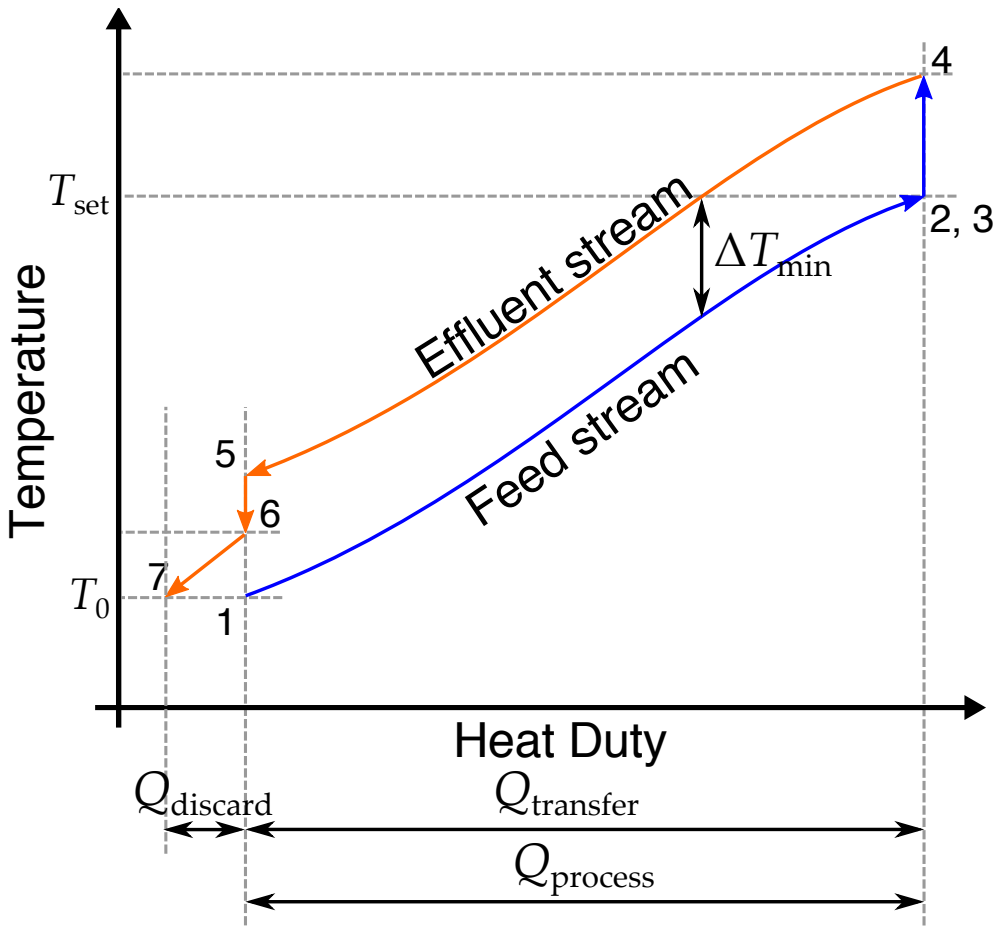

Figure 1.10: Temperature-heat diagram of a self-heat recuperative thermal process

Self-heat recuperation technology has been applied to various distillation processes [23–26], cryogenic air separation processes [27], carbon-dioxide separation process using Amine for post [28] and pre [29] combustion processes, brown coal drying processes [30,31], biomass drying processes [32–34] and seawater desalination processes [35,36]. In all of the applied processes, potential of large energy savings compared to conventional heat recovery system has been presented. In 2012, a pilot plant of bioethanol distillation was built in a joint research between the University of Tokyo and Nippon Steel & Sumikin Engineering Co. It was experimentally confirmed that it is possible to gain drastic energy savings by applying self-heat recuperation technology [37].

1.3.3 A paradigm shift of energy usage

The mindset of the conventional heat usage in a thermal process was set so that the necessary heat to change the temperature of the process stream has to continuously be provided. Various methods has been thought of to efficiently provide the necessary heat, such as heat pumping, utilizing reaction heat or integrating waste heat. Due to the conservation law of energy, all of the heat provided will be discarded, thus much waste heat exists in such processes. Various methods has been presented to utilize the waste heat as well (heat recovery, co-generation, area-wide integration with different processes . . . etc).

In an exergy recuperative process, it is still necessary to initially provide the process heat. However, the heat that has been provided is circulated within the process. Work is provided instead of heat to circulate the heat. The heat that is discarded has low exergy rate, thus has no potential usage. Since no heat is being provided, we do not need to think of a method to efficiently provide the heat, but instead, a method to efficiently circulate the heat within the system is needed.

The conventional mindset were all based on the thought that "heat must continuously be provided." Thus, the evaluation factor such as coefficient of performance (COP) cannot be applied to evaluate the energy efficiency of a self-heat recuperative process.

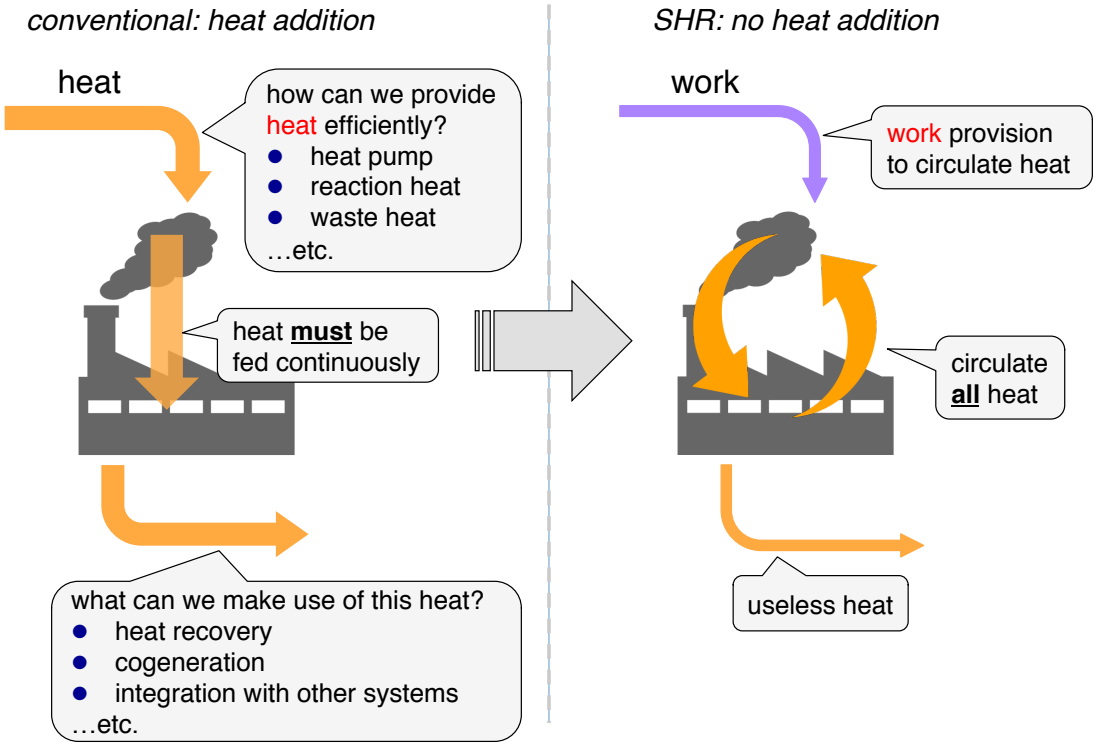

Figure 1.11: Comparison between conventional energy usage and exergy recuperative energy usage

1.4 Magnetocaloric effect

In this research, in order to expand the application of self-heat recuperation technology, a magnetocaloric heat circulator where magnetocaloric effect (MCE) is utilized to recuperate the heat exergy of the process stream is presented.

MCE is a physical chemistry phenomenon enforced when a magnetic material is subjected to varying field. It is characterized by the adiabatic temperature change, ΔT_{ad}, that can be detected when the magnetocaloric material heats up or cool down due to the varying of magnetic field [38,39]. Fig. 1.12 shows the heating and cooling of a magnetocaloric material due to MCE. When the magnetic material is subjected to increasing magnetic field, its magnetic moments will become ordered, leading to reduction of the magnetic part of the total entropy, ΔS_{m}. If the increasing of the magnetic field was performed adiabatically, the crystalline lattice of the magnetic material vibrates harder to keep constant the total entropy of the magnetic material. Thus, the temperature of the magnetic material will increase. The opposite effect occurs when the magnetic material is subjected to decreasing magnetic field, i.e. the temperature of the magnetic material will decrease.

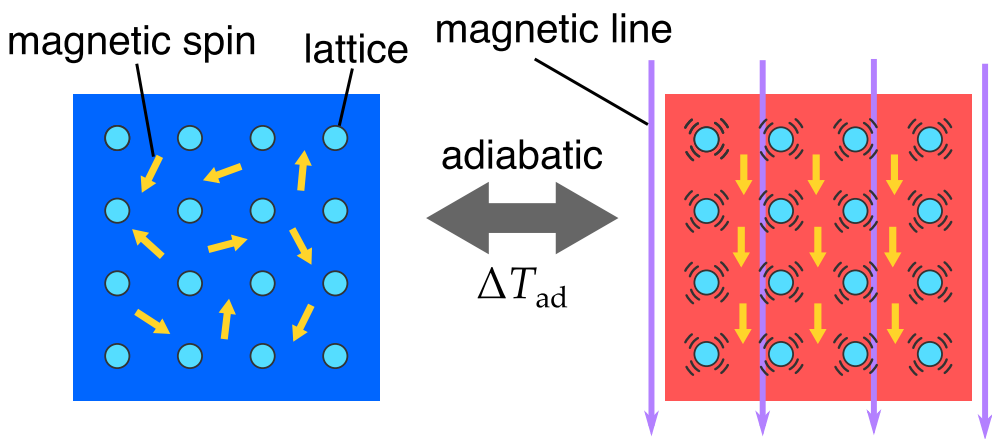

Figure 1.12: Schematic of the raise and the decrease of the temperature of the magnetocaloric material due to magnetocaloric effect

The phenomena itself was first discovered by Warburg using iron in 1881 [40]. The first practical application was presented by Debye [41] and Giauque [42] to reach extreme low temperatures by adiabatic demagnetization. Formally, the effect was seen in paramagnetic salts at cryogenic temperatures. At higher temperatures, the entropy fluctuation of the lattice becomes large compared to the effect of magnetic field variation, ΔS_{M}, thus MCE could not be observed. However, it was found that large MCE (few Kelvins per Tesla of adiabatic temperature change, ΔT_{ad}) can be seen near the ordering temperature of ferromagnetic materials known as the Curie temperature, θ_{C} [43] and extended its use to temperatures above cryogenic. Today, much research are being performed to apply MCE to refrigeration technologies, especially around room temperature [44].

1.4.1 Theory of magnetocaloric effect

At constant pressure, it is known that the total entropy, S_{total} of a magnetic material is the sum of the magnetic entropy, S_{M}, lattice entropy, S_{L}, and electron entropy, S_{E} [45]. All three entropies are dependent on the temperature, T, of the magnetic material but only the magnetic entropy, S_{M}, strongly depends on the strength of the magnetic field, H while the lattice entropy, S_{L}, and electron entropy, S_{E} are independent to the magnetic field.

$$S_{\mathrm{total}} = S_{\mathrm{M}}(T, H) + S_{\mathrm{L}}(T) + S_{\mathrm{E}}(T) \tag{1.6}$$

Fig. 1.13 shows the MCE of a magnetic material in a temperature-entropy diagram. The magnetic entropy change, ΔS_{M}, in an isothermal process is a function of temperature, T, initial strength of magnetic field, H_0, and final strength of magnetic field, H_1 and can be written as,

$$\begin{aligned} \Delta S_{\mathrm{M}}(T, H_0, H_1) &= S_{\mathrm{M}}(T, H_1) - S_{\mathrm{M}}(T, H_0) \\ &= S_{\mathrm{total}}(T, H_1) - S_{\mathrm{total}}(T, H_0) \end{aligned} \tag{1.7}$$

From the second law of thermodynamics, the derivative of entropy, S, can be written as,

$$dS(T,B) = \frac{C(T,H)_{H,p}}{T} dT \tag{1.8}$$

where $C_{H,p}$, is heat capacity of a magnetic material at constant pressure and magnetic flux density. The third law of thermodynamics, the entropy of a material at zero temperature is assumed zero, thus, Eq. 1.8 can be written as,

$$S(T,H) = \int_{T_1 \to 0}^{T} \frac{C(T,H)_{H,p}}{T} dT \tag{1.9}$$

Eq. 1.7 can be written using the above equation,

$$\Delta S_{\mathrm{M}}(T,H_0,H_1) = \int_{T_1 \to 0}^{T} \frac{C(T,H_1)_{H,p}}{T} dT - \int_{T_1 \to 0}^{T} \frac{C(T,H_0)_{H,p}}{T} dT \tag{1.10}$$

The above equation indicates, greater change in heat capacity due to the effect of magnetic field, H, will result in larger change in magnetic entropy, but the effect will gradually decrease as the temperature, T, rises.

According to the fundamental Maxwell's relation, the partial derivative of entropy, S, with respect to magnetic field density, H, at constant temperature can be written as,

$$\left(\frac{\partial S(T,H)}{\partial H}\right)_T = \left(\frac{\partial M(T,H)}{\partial T}\right)_H \tag{1.11}$$

where M is the strength of magnetization in a magnetic material. Thus, from Eq. 1.7 and Eq. 1.11, the isothermal change in magnetic entropy is

$$\Delta S_{\mathrm{M}}(T,H_0,H_1) = \int_{H_0}^{H_1} \left(\frac{\partial M(T,H)}{\partial T}\right)_H dH \tag{1.12}$$

indicating that the magnetic entropy change is proportional to the derivative of magnetization with respect to temperature.

In a reversible process, heat that is exchanged, Q, with the surroundings when a magnetic material is subjected to varying field can be written as [46],

$$\begin{aligned} Q = TdS &= T\left(\frac{\partial S}{\partial T}\right)_H dT + T\left(\frac{\partial S}{\partial H}\right)_T dH \\ &= C_{H,p} dT + T\left(\frac{\partial S}{\partial H}\right)_T dH \end{aligned} \tag{1.13}$$

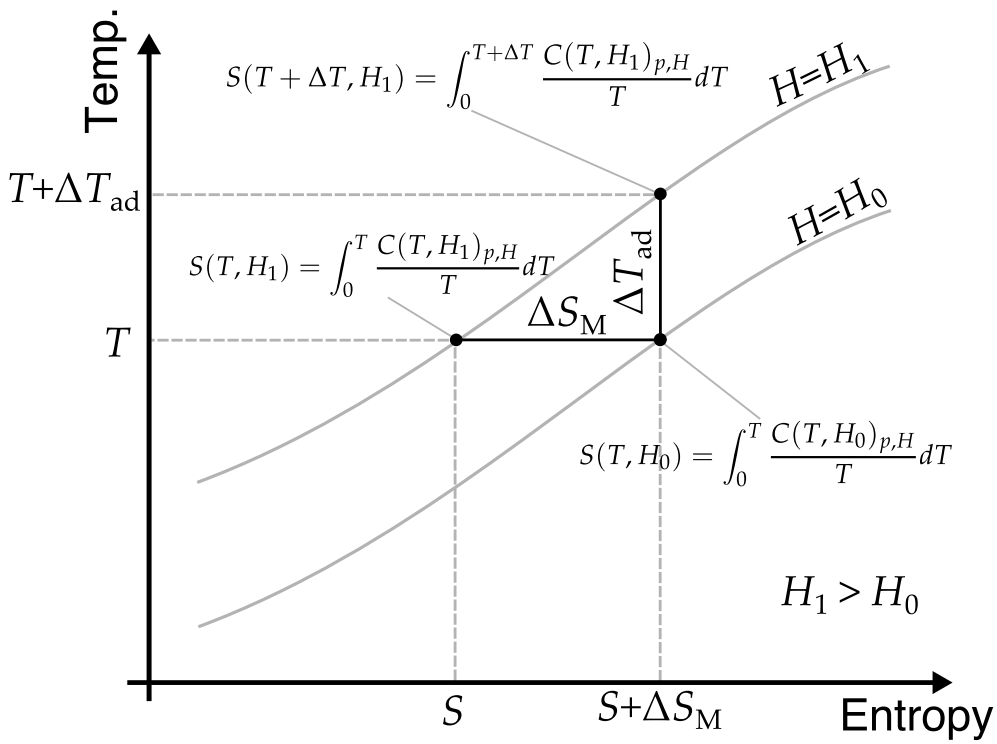

Figure 1.13: The total entropy of a magnetic material in two different magnetic field B_0 and B_1 on a temperature-entropy diagram

because entropy, S, is partially differentiable with respect to temperature, T, and strength of magnetic field, H. In an adiabatic process where $Q = 0$, from the above equation, the adiabatic temperature change due to MCE, ΔTad, when the strength of the magnetic field was varied from H_0 to H_1,

$$\Delta T_{\mathrm{ad}}(T, H_0, H_1) = -\int_{H_0}^{H_1} \frac{T}{C_{H,p}} \left(\frac{\partial S}{\partial H}\right)_T dH \tag{1.14}$$

using Eq. 1.11, the Maxwell relation, the above equation can be written as,

$$\Delta T_{\mathrm{ad}}(T, H_0, H_1) = -\int_{H_0}^{H_1} \frac{T}{C_{H,p}} \left(\frac{\partial M}{\partial T}\right)_H dH \tag{1.15}$$

Thus, it can be seen that besides the magnetization differential with respect to temperature, the ratio of heat capacity at constant magnetic field and pressure and temperature affects the size of adiabatic temperature change, T_{ad}.

In magnetic thermodynamics, the strength of magnetic field, H, is a quantity analogous to the pressure, $-p$, for gaseous thermodynamics and the strength of magnetization, M, is a quantity analogous to the volume, V. It is noted that the positive and negative of the strength of magnetic field, H, and pressure, p is different. From the first law of thermodynamics, the differential of enthalpy, dI, of a magnetic material can be written as [47],

$$dI = TdS - \mu_0 MdH \tag{1.16}$$

The enthalpy, I, of a magnetic material can be derived from the heat capacity at constant magnetic field, H, and pressure, p.

$$I(T, H) = \int_{T_0}^{T} C(T, H)_{H,p} dT \tag{1.17}$$

1.4.2 Magnetocaloric material

Theoretically, MCE occurs in every magnetic materials. At cryogenic temperatures, it is possible to see the temperature change caused by magnetic field variation with paramagnetic materials. However, at temperatures above cryogenic, the isothermal entropy

difference, ΔS_{M}, is much smaller than the fluctuation of the crystalline lattice, making the temperature change undetectable. But if magnetic field is varied at the turning temperature of a ferromagnetic material, it is possible to gain a far larger magnetic entropy change, ΔS_{m} and a detectable temperature change can be obtained. The magnetic entropy change, ΔS_{m}, is determined by the size of the effective magnetic moment, μ_{eff}

$$\mu_{\mathrm{eff}} = g\mu_{\mathrm{B}}\sqrt{J(J+1)} \tag{1.18}$$

The most popular material studied magnetocaloric material is a lanthanide, gadolinium (Gd) due to its large effective magnetic moment. Furthermore it has Curie temperature of 293 K [48–50], around room temperature making it an ideal benchmark material for room temperature magnetocaloric effect. Gd is known to have one of the largest adiabatic temperature difference, ΔT_{ad}, near room temperature. The adiabatic temperature difference, ΔT_{ad}, for Gd is around 2-3 [K T^{-1}]. MCE has been measured for other lanthanide materials such as Nd, Tb, Dy, Ho, Er and Tm [43], however Gd proved to have the largest MCE.

Table 1.1 shows the different ferro and ferrimagnetic materials and their Curie temperatures, θ_{C}. It can be seen that there are many materials and compounds with variety of Curie temperatures exists. Although the recent trends of magnetocaloric materials are focused on developing materials that show large magnetocaloric effect at room temperatures and below, for refrigeration use, it can be seen from the table that there are potentials for high temperature magnetocaloric materials as well.

1.4.3 Magnetic heat pumping

Since the temperature change obtained in magnetocaloric effect is analogous to the temperature change gained by compression and expansion for gaseous materials, it is possible to draw thermodynamic cycles such for power generation and heat pumping [51]. Some research has been performed in cryogenic temperature regions, for creating lique-

Table 1.1: Example of ferro and ferrimagnetic materials and their Curie temperature

materials	Curie temperature [K]
Co	1388
Fe	1043
$FeOFe_2O_3$	858
$CuOFe_2O_3$	728
MnBi	630
Ni	627
MnSb	587
$Y_3Fe_5O_{12}$	560
CrO_2	386
MnAs	318
Gd	292
Dy	88
EuO	69

fied hydrogen [52,53] and liquefied helium [54], but the major trend has been replacement of vapor compression heat pumps for room temperature application [39, 55].

One of the first magnetic heat pumps reported was the work by Collins and Zimmerman [56] and Heer *et al.* [57]. They were used to maintain cryogenic temperature through cyclic demagnetization of iron ammonium alum. The work by Brown [58], pushed the possibility of applying magnetic heat pumping to room temperature applications. It was reported that by using gadolinium as working material and magnetic field up to 7 [T], a no load temperature span of 47 [K] (cold end temperature is 292 [K], hot end temperature of 339 [K]) was achieved, which is far larger than the adiabatic temperature difference, ΔT_{ad}, of gadolinium. In the research performed by Brown, the magnetocaloric material work as a kind of regenerator and a heat exergy recuperator. The concept of Brown was followed by Steyert [59] and Barclay [60]. The mechanism later became known as active magnetic regeneration (AMR) and has considerably been developed over the past few years [44].

Fig. 1.14 shows the schematic of the basic concept of active magnetic regeneration. A magnetocaloric material is put inside an insulating container. The container is filled with a working fluid. The magnetocaloric material moves up and down inside the insulating container. While the magnetocaloric material is at the hot end of the insulating container, it is magnetized (adiabatic magnetization), then the heat of the magnetized magnetocaloric material is transferred to the working fluid, thus, the temperature of the working fluid at the hot end increases (isomagnetic cooling). The magnetocaloric material is then moved to cold end of the insulating container, where it is demagnetized (adiabatic demagnetization). The temperature of the magnetocaloric material will decrease, thus, the magnetocaloric material absorbs heat from the working material at the cold end of the insulating container (isomagnetic heating). The four steps will cyclically be repeated until the temperature difference between the hot and the cold end in the insulating container has saturated. The magnetocaloric material works as a regenerator and a heat exergy recuperator allowing to heat pump in between much larger temperature

difference than the adiabatic temperature change, ΔT_{ad} of the magnetocaloric material. Most of the magnetic heat pumps being developed these days follow the same mechanism, but in most structure, the magnetocaloric material is fixed and the working fluid flows back and forth to carry the heat.

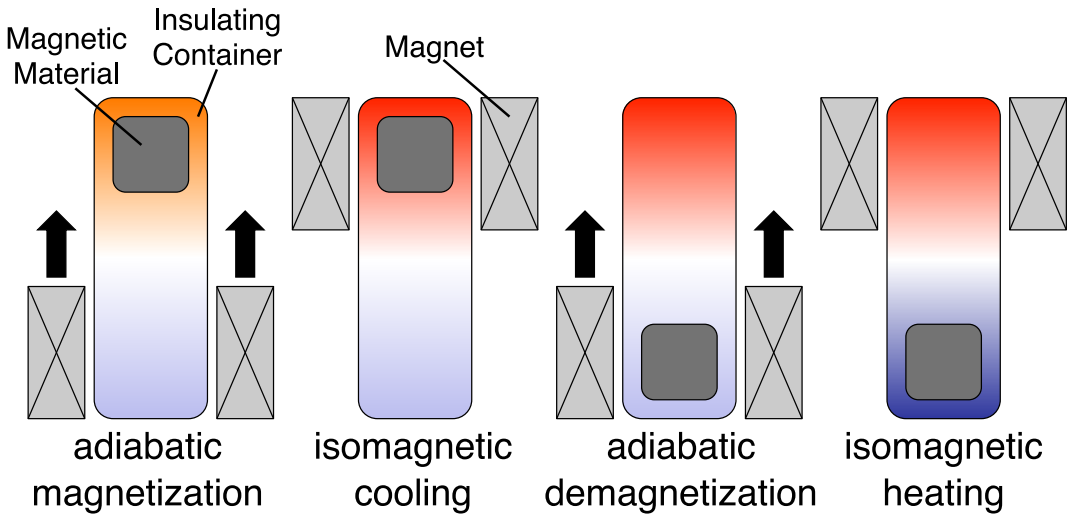

Figure 1.14: Schematic of basic concept of active magnetic regeneration

Substantial research has been performed for magnetic heat pumping at room temperature (mainly for refrigeration purpose) has been conducted, using superconducting magnets [61–63] and permanent magnets [64–67] to create the magnetic field. These studies showed that magnetic heat pumps are energy efficient and fully compatible with conventional compressive heat pumps. Also, much effort has been put in to modeling the active magnetic regenerator heat pumps to optimize their parameters and the geometry of the regenerators to gain further efficiency [68, 69].

In this research, we applied the magnetocaloric effect to heat circulators. Heat pump is a method to provide or take away heat from a system, while heat circulator is a method to circulate the heat within a system. In a process where a process stream is heated or cooled to a certain temperature and finally comes back to its original state, heat circulators can minimize the exergy destruction, A_{loss}, and the energy consumption.

1.5 Scope of this research

It was expressed in Section 1.1 the importance of shifting the ways we use energy into more energy efficient methods from the perspective of carbon-dioxide emission. The carbon-dioxide emission in Japan is in standstill, thus a drastic method to suppress the energy consumption is needed. Amongst the different sectors in which carbon-dioxide is emit, the industrial sector is the largest contributor.

In Section 1.2, the conventional methods of energy saving in thermal processes in chemical industry was introduced. The conventional energy saving is based on heat recovery principle. Optimization methods represented by the pinch-technology are being used to maximize the heat that can be recovered in a chemical process and amongst different chemical processes integrated.

Self-heat recuperation technology (Section 1.3) is an energy saving method based on the exergy recuperation principle, where all of the process stream heat in a thermal process is circulated within the system, without any addition of makeup heat. Only small amount of work is needed to circulate the heat within the system, leading to drastic energy saving in processes that involves heating or cooling of process streams. The energy saving potentials that the self-heat recuperation technology holds has been evaluated in various processes through process simulation, and also verified in a joint project between the University of Tokyo and Nipponsteel engineering Co. Ltd.

Although self-heat recuperation has proven to be effective to reduce the energy consumption in some thermal processes, there are still limitations. The limitation of the conventional self-heat recuperative process is that,

1. state of the process material is limited to gaseous materials

2. temperature range in which self-heat recuperation can be applied is limited due to operable temperature range of the compressor

3. efficiency at small scale applications may become small due to low adiabatic effi-

ciency of compressors

4. it is difficult to compare energy saving potential of self-heat recuperation because, conventional thermal processes provides heat to the system, where as self-heat recuperation provides work

Thus, the scope of this research is to expand the application of self-heat recuperation technology. In order to do so, a reference index to evaluate self-heat recuperative process alongside different energy saving technologies in thermal process is required. A heat circulator based on a method besides compression is presented and evaluated using the reference index.

Fig 1.15 shows the structure of this thesis dissertation. In order to evaluate different thermal processes with energy saving technologies applied, and to understand the limits of these technologies, in Chapter 2, an evaluation factor is set. The minimum energy consumption in thermal process is evaluated in terms of irreversibility and exergy. Thermal processes with (1) no energy saving technology applied, (2) conventional heat recovery technology, and (3) self-heat recuperation technology are graphically expressed in temperature-entropy diagram and their energy saving potentials has been compared with the minimum energy consumption in thermal processes. Furthermore, since the energy saving potential of a self-heat recuperative process cannot be measured by conventional evaluation factors, such as COP, an evaluation factor to measure the energy saving potential of self-heat recuperation has been presented.

The recuperation of heat exergy is the very essence of heat circulation by self-heat recuperation technology. In all of the conventional self-heat recuperative processes compressors were used to enforce a reversible temperature change. In Section 1.4, a method to recuperate the heat exergy of a process stream by means other than pressure variation is presented; magnetocaloric effect.

In Chapter 3, a magnetocaloric heat circulator based on self-heat recuperation technology is presented. The basic concept and the energy saving potential of a magnetocaloric

heat circulator when magnetocaloric material is the process material is evaluated in terms of temperature-entropy diagram. The analogy between the compressive self-heat recuperative processes are discussed. Also, a method to apply a magnetocaloric heat circulator to non-magnetocaloric process material is presented and evaluated.

Chapter 4 explains the conceptual design of an Active Regenerative Magnetic (AMR) heat circulator to actualize self-heat recuperation using magnetocaloric effect for non-magnetocaloric process material presented in Chapter 3. A basic one-dimensional mathematical model is constructed based on the energy balance of the AMR bed. Through thermal simulation using the constructed mathematical model, the heat circulating capability and energy saving potential of an AMR heat circulator is discussed.

Chapter 5 verifies the mathematical model of an AMR heat circulator presented in Chapter 4 by a newly constructed AMR heat circulator. The AMR heat circulator circulates the heat carried by the process stream; water. Heat of the process stream is recuperated by magnetic field variation.

Finally, the conclusion of the thesis and some work that need to be done in the future is presented in Chapter 6.

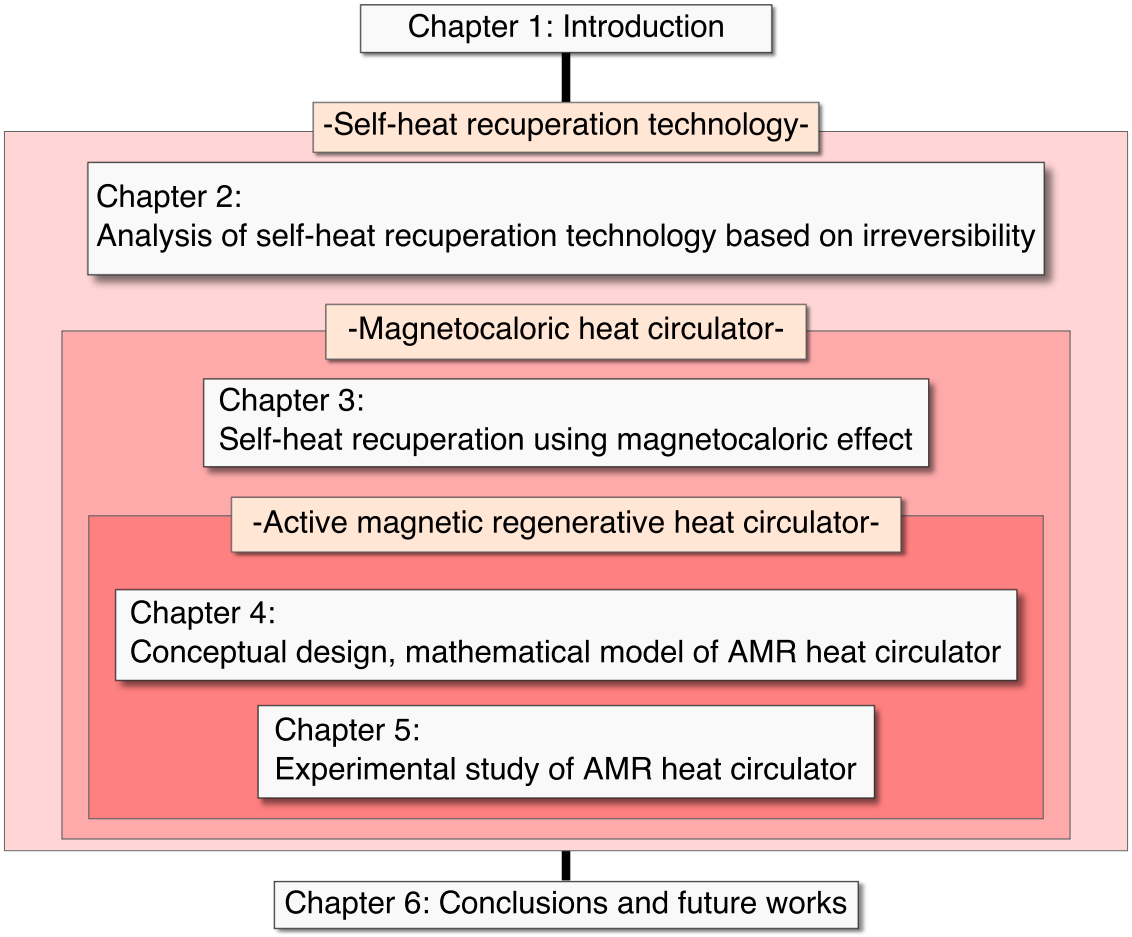

Figure 1.15: Structure of thesis dissertation

Chapter 2

Analysis of self-heat recuperation technology based on irreversibility

2.1 Introduction

Recently, Tsutsumi proposed the concept of exergy recuperation [13]. Based on the concept, Kuchonthara and Tsutsumi developed a design method for an energy-recuperative integrated gasification power generation system [14, 16]. Then, exergy recuperation has been extended to self-heat recuperation technology by Kansha *et al.* [11]. This chapter evaluates self-heat recuperative processes based on thermodynamic irreversibility and exergy. Furthermore, a method to obtain the minimum energy consumption needed in thermal processes is presented. The value obtained by such methodology can work as an evaluation index to understand the energy saving limit of thermal processes.

2.2 Exergy analysis of thermal processes

2.2.1 Evaluation factor

Fig. 2.1 shows an image of an industrial process. This industrial process continuously transforms raw material into product. In the process of converting the raw material to product, it is necessary to change the state of the raw material. If the initial state and the set state is decided, and limit the variation of state to temperature, a certain amount of heat, Q_{process}, is needed to be provided to the process stream. The amount of the required energy (or heat), Q_{process}, is fixed if the initial and the set state is decided.

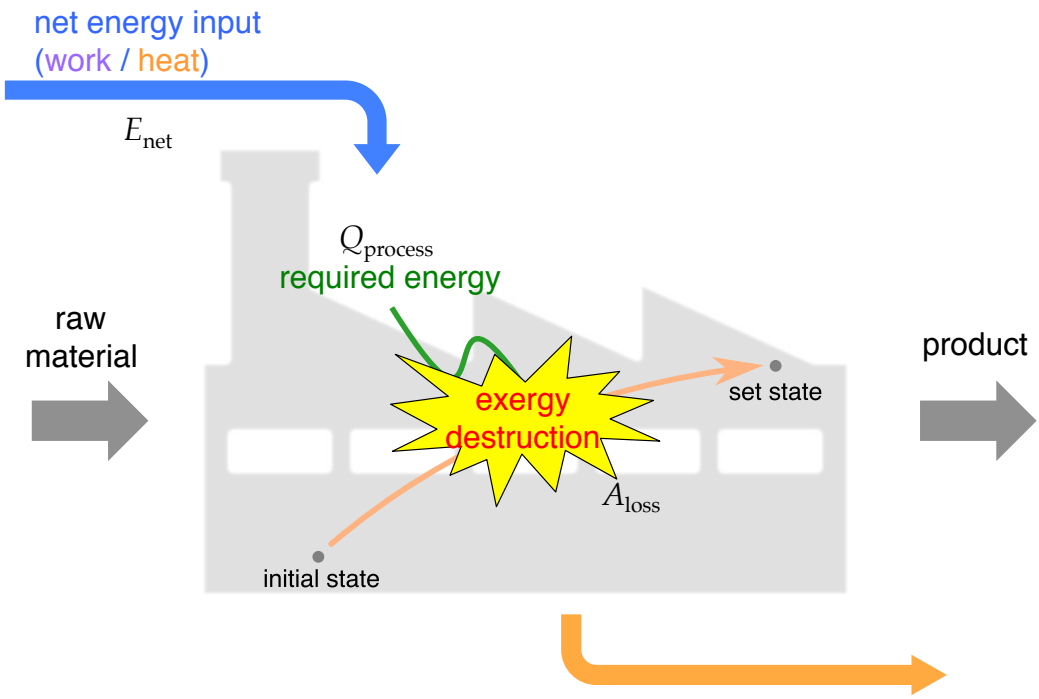

Figure 2.1: Mass and energy balance of industrial process

Focusing on the inputs and outputs of the process, in order to provide the required heat, Q_{process}, to the process stream, net energy, E_{net}, is provided. Since energy is being conserved, all of the energy provided to the process will flow out, partly with the product and the rest usually in the form of waste heat. In order to obtain the amount of energy

saved, the ratio between net energy input, E_{net}, and the required heat, Q_{process} can be used as an evaluation factor.

$$\text{evaluation factor 1} : \frac{Q_{\text{prcess}}}{E_{\text{net}}} \tag{2.1}$$

The value can show us how much energy has been saved compared to the heat provided to the process stream. The value is in similar form to the COP value often used for evaluating heat pumps. However, the two are based on a different concept.

Fig 2.2 shows a schematic of heat pump system and a self-heat recuperative system. A heat pump gains heat, Q_{cold}, from a cold reservoir and pumps that heat, Q_{hot}, to a reservoir with higher temperature by providing work, E_{net}. The objective of a heat pump is to pump the heat at T_{cold} to T_{hot}. The work, E_{net} that is required to do so is determined by,

$$E_{\text{net}} = Q_{\text{hot}} - Q_{\text{cold}} \tag{2.2}$$

and the evaluation factor COP is the heating or cooling capacity over the power input, and can be written as,

$$\text{COP}_{\text{h}} = \frac{Q_{\text{hot}}}{E_{\text{net}}} = \frac{Q_{\text{hot}}}{Q_{\text{hot}} - Q_{\text{cold}}} \tag{2.3}$$

or,

$$\text{COP}_{\text{c}} = \frac{Q_{\text{cold}}}{E_{\text{net}}} = \frac{Q_{\text{cold}}}{Q_{\text{hot}} - Q_{\text{cold}}} \tag{2.4}$$

depending on which heat is desired as the product. A self-heat recuperative process, does not have take heat from outside the system and discards an amount of heat, Q_{discard}, same as the work input. E_{net}. If were to apply the same evaluation factor, COP, to a self-heat recuperative process, since the heating capacity is the same as the power input and the cooling capacity is zero,

$$\text{COP}_{\text{h}} = \frac{Q_{\text{discard}}}{E_{\text{net}}} = 1 \tag{2.5}$$

$$\text{COP}_{\text{c}} = \frac{0}{E_{\text{net}}} = 0 \tag{2.6}$$

The value will be identical for all self-heat recuperative system, thus will not hold any actual meaning on evaluating such systems.

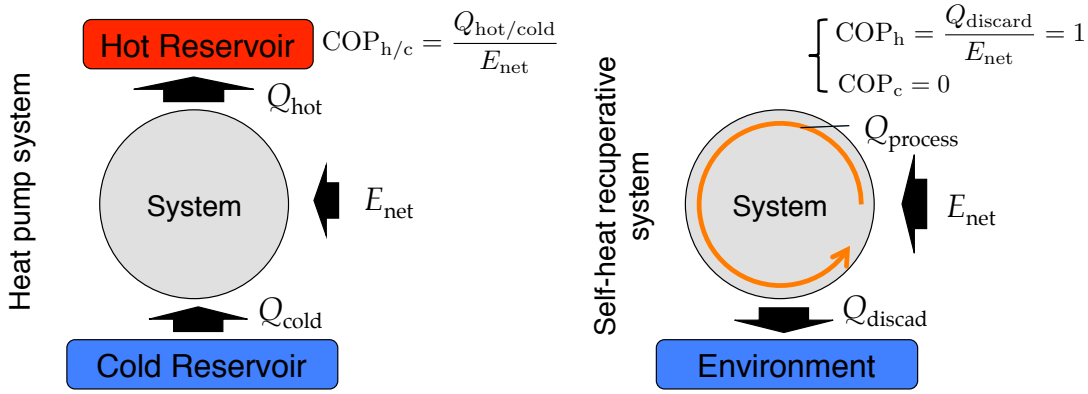

Figure 2.2: Comparison of heat pump and heat circulator

Fig 2.3 shows the temperature-entropy diagram of a reverse Brayton cycle, a reverse Brayton cycle with regeneration and a self-heat recuperative cycle. Needless to say, the first two are heat pump cycles and the third is a heat circulation cycle. A heat pump pumps heat from a cold reservoir to a hot reservoir by providing work, this is the same for regardless of applying regeneration or not. However although self-heat recuperative cycle draws a cycle similar to that of a reverse regenerative Brayton cycle, in the case of self-heat recuperation, the objective is to circulate the heat in temperature between T_0 and T_{set} and no heat is pumped. Thus, the evaluation factor for self-heat recuperative process was presented Eq. 2.1.

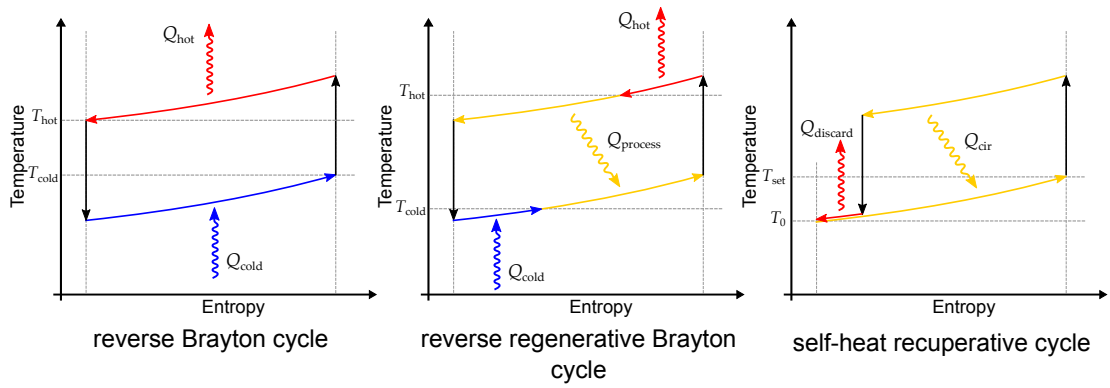

Figure 2.3: Temperature-entropy diagram of heat pump cycle, heat pump cycle with regeneration and self-heat recuperative cycle

Fig. 2.4 (left) shows the relationship between the inverse of the presented evaluation factor, $Q_{\text{process}}/E_{\text{net}}$, and the temperature range in which the heat is circulated, $T_{\text{set}} - T_0$, when the process fluid was Butane. The initial temperature, T_0 was set to 298.15 [K] and minimum temperature difference needed for heat exchange, ΔT_{min}, was set to 10 [K]. Fig.2.4 (right) shows the relation ship between COP and temperature difference in which the heat is pumped, $T_{\text{hot}} - T_{\text{cold}}$, for a reverse Carnot cycle. It can be seen that for heat pumps, the larger the temperature difference the heat is pumped, the smaller the COP value. However in the case of self-heat recuperation, when the temperature difference in which the heat is circulated, $T_{\text{set}} - T_0$, the amount of required energy, Q_{process}, grows faster than the work, E_{net}, that is needed to do so.

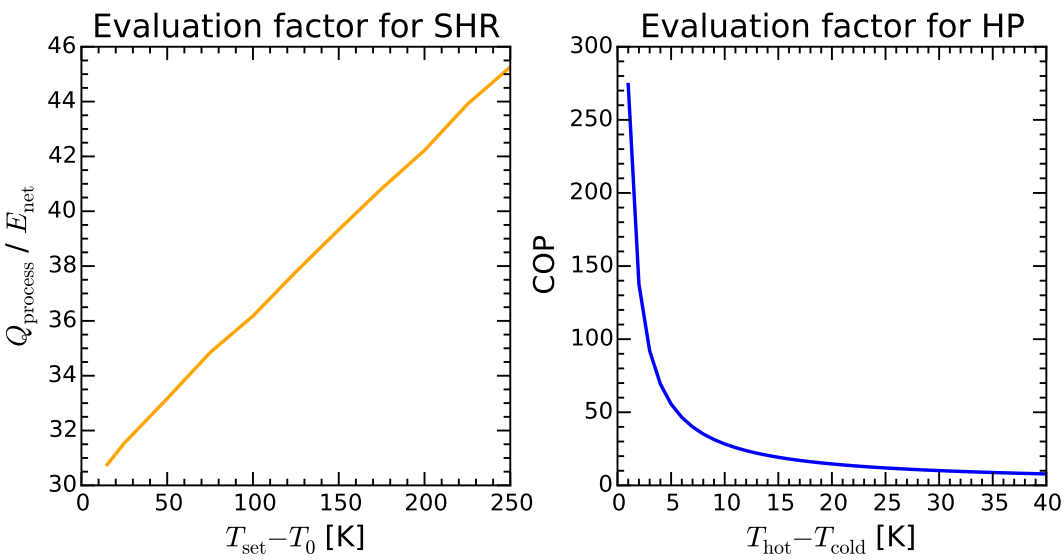

Figure 2.4: Relationship between temperature difference and evaluation factor for self-heat recuperative cycle and heat pump

Although it is possible to tell how much energy saving can be obtained by the ratio between E_{net} and Q_{process}, it cannot tell us how far it is from the ideal minimum energy saving required. In the case of heat pump, the COP of reverse Carnot cycle is the ideal minimum energy required for pumping heat at T_{cold} to T_{hot}. Thus, it is necessary to obtain

the minimum energy required for a self-heat recuperative cycle when heat is circulated in between T_0 and T_{set}.

When the required energy, $Q_{process}$ is provided to the process stream (Fig. 2.1), irreversibility takes place resulting in exergy destruction. If we were to analyze the process and obtain the minimum exergy destruction, A_{min}, the ratio between the minimum exergy destruction of a thermal process, A_{min}, and the required heat. $Q_{process}$, value can be used as a benchmark to show how far you are away from the ideal minimum energy consumption.

$$\text{evaluation factor 2} : \frac{Q_{process}}{A_{min}} \tag{2.7}$$

2.2.2 Exergy destruction due to irreversibility

The pinch analysis is based on the first law of thermodynamics and only considers the temperature as the quality parameter of the process stream and not the pressure. In order to achieve a methodology to gain further energy savings, it is needed to take into account both temperature and pressure of the process streams for optimization [12]. Many researchers have paid attention to exergy because it is based on the second law of thermodynamics and can take into account both temperature and pressure.

Exergy, A, is the maximum amount of work that can be taken out of energy. The maximum amount of work that can be taken out from heat, Q at temperature T is expressed by the Carnot efficiency as [17],

$$A = Q\left(1 - \frac{T_0}{T}\right) \tag{2.8}$$

T_0 is the temperature of the environment. Eq. 2.8 assumes heat capacity of infinite at temperature T, however in reality, heat is carried by actual materials thus the amount of heat is finite. If In order to take into account the temperature change when heat is being transferred, the following differential equation.

$$dA = dQ\left(1 - \frac{T_0}{T}\right) = dQ - T_0\frac{dQ}{T} \tag{2.9}$$

In many cases, the chemical processes are performed under constant pressure. In this case, the amount of heat, Q, is equal to the enthalpy of the process stream. Thus, Eq. 2.9 can be written using the enthalpy, I, and entropy, S, as,

$$dA = dI - T_0 dS \tag{2.10}$$

The exergy of heat at temperature T is

$$A = I - I_0 - T_0(S - S_0) \tag{2.11}$$

A is the maximum amount of work or available energy that can be taken out of heat at constant pressure.

When a system undergoes an irreversible process, entropy, S, will be generated leading to exergy destruction. The amount of available energy that can be taken out of the system will decrease by A_{loss}. If we assume the entropy generation as S_{gen}, the amount of available energy, A', can be expressed as,

$$A' = A - A_{\text{loss}} = \Delta I - T_0(\Delta S + S_{\text{gen}}) \tag{2.12}$$

From Eq. 2.11 and Eq. 2.12, the amount of exergy destruction in the system is

$$A_{\text{loss}} = T_0 S_{\text{gen}} \tag{2.13}$$

Thus due to the irreversible process, A_{loss} has been discarded to the environment at temperature T_0 as energy of no value. It can be seen that by tracking the exergy destruction, the second law of thermodynamic can easily be taken into account for analyzing processes.

2.2.3 Exergy destruction in thermal processes

Exergy destruction in a thermal process is caused by two main factors, combustion and heat exchange. Fig. 2.5 shows the energy and material flow of thermal process where no energy saving technology is applied broken down into functions. Usually, a thermal

process starts and ends at environmental temperature, T_0. Process stream A at environmental temperature, T_0, is heated to the set temperature, T_{set}, the required temperature for the subsequent process (X). The heat that is needed to raise the temperature of the process stream is provided by the reaction heat of combustion. Process stream B consist of fuel and oxygen needed for the combustion reaction. The reaction heat is first carried by Process stream B and then transferred to Process stream A. Fig. 2.6 shows the transition of exergy ratio of a thermal process where no energy saving technology is applied. The initial exergy of the fuel is reduced in two steps. The first exergy destruction is due to combustion, next is due to heat transfer.

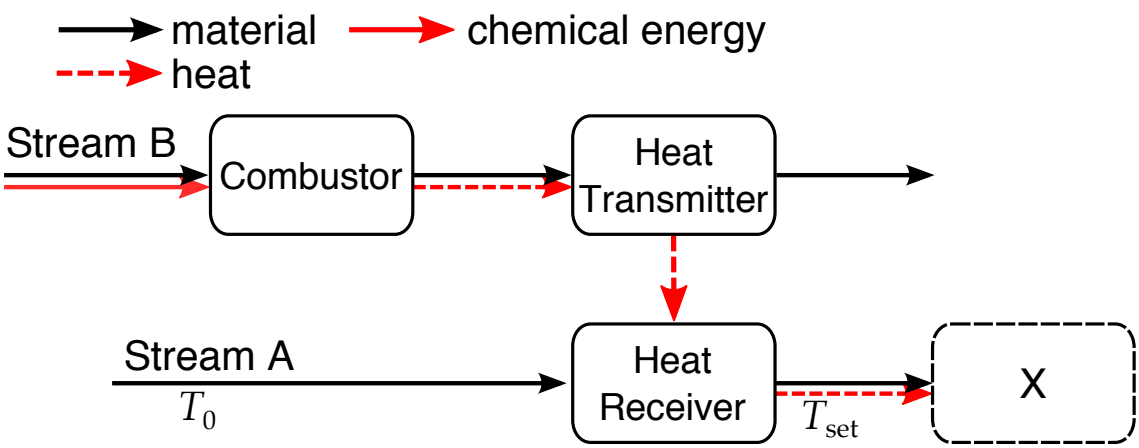

Figure 2.5: Energy and material flow of thermal process where no energy saving technology is applied

Exergy destruction due to combustion

Combustion is an unstable process which is associated with large exergy destruction [18]. According to the conservation law of energy, if no heat loss is assumed, all of the reaction heat due to combustion is transferred to the process stream. Figure 2.7 shows the exergy rate of heat carried by carbon dioxide (CO_2) at 1 [atm]. Heat does not stand on its own but is carried by some substance. Thus it is needed to calculate the exergy of the

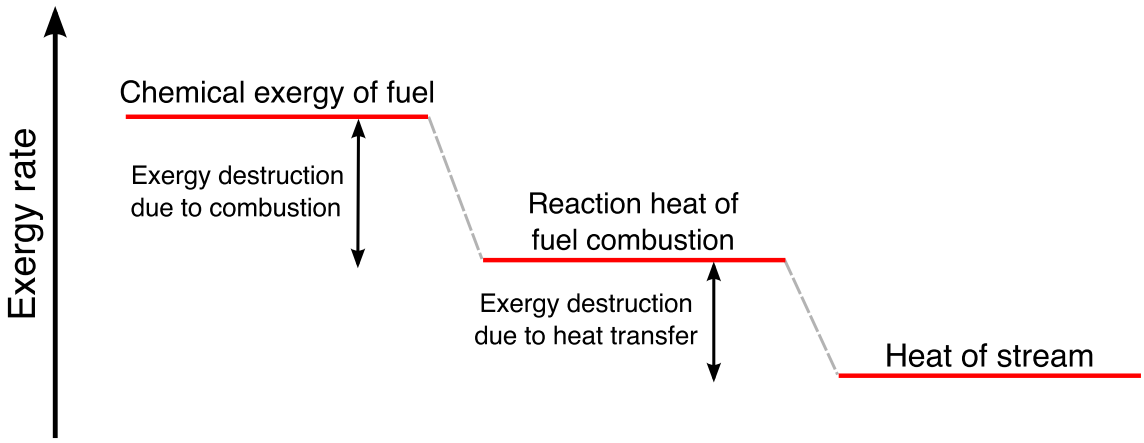

Figure 2.6: Exergy rate transition of a thermal process where no energy saving technology is applied

substance that carries the heat at a particular temperature. The exergy rate is calculated by using the Shomate equation [19, 20], its calculation method is presented in Appendix A. Considering the fact that the exergy rate of a typical fuel is around 92% [21], the fuel immediately loses about half of its exergy when it is combusted to gain heat of around 1000 [K]. Hence, although combustion may be one of the most easiest and convenient method to obtain heat for raising the temperature of a process stream, it is necessary to avoid unnecessary combustion where it is possible. It is also noted that the exergy rate of electricity is 1.0.

Exergy destruction due to heat exchange

Since temperature difference is needed for heat to transfer between one substance to another, heat transfer is always associated with irreversibility and exergy destruction. Fig. 2.8 shows the temperature-entropy diagram of heat exchange between two process streams. While the cold stream is heated from T_0 to T_{set}, the temperature of the hot stream decreases from T_{a} to T_{b}. If no heat loss is assumed, the amount of heat provided from reaction (a $\rightarrow$ b) is equal to the heat provided to the process stream (A $\rightarrow$ B). Thus,

$$Q_{\mathrm{transfer}} = \int_a^b TdS = \int_A^B TdS \tag{2.14}$$

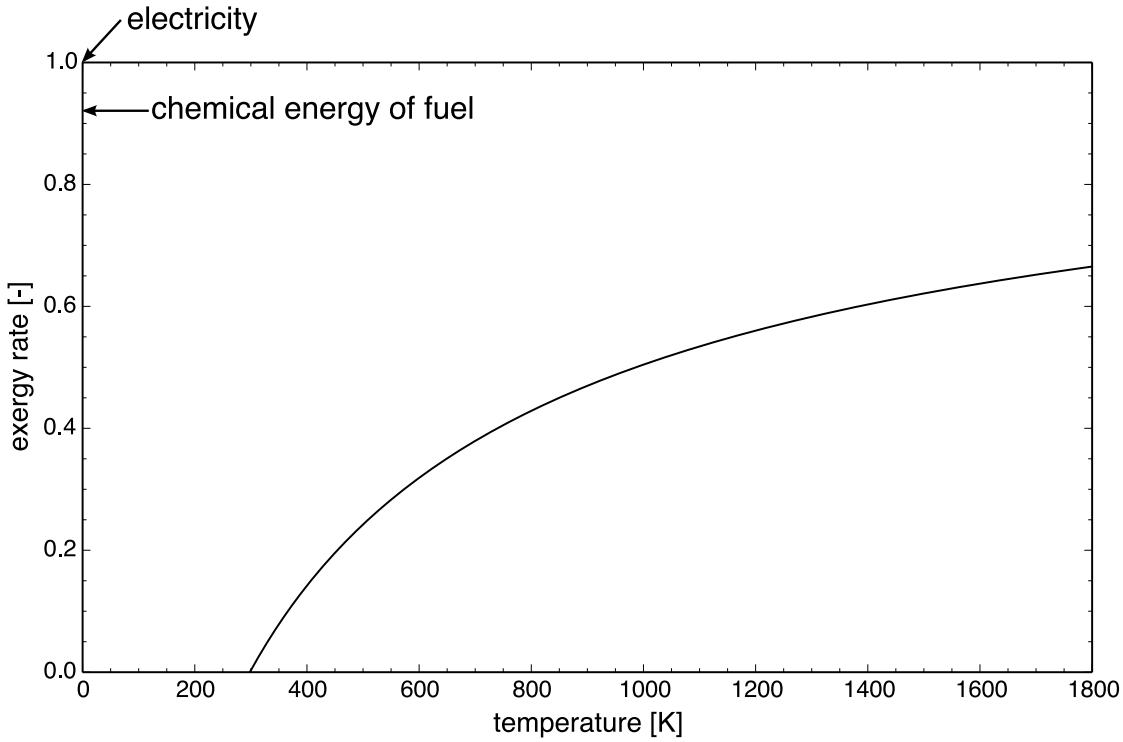

Figure 2.7: Exergy rate of heat carried by carbon dioxide at 1 [atm]

The difference between the entropy change of the hot stream, ΔS_{hot}, and the entropy change of the cold stream, ΔS_{cold} is the overall entropy generation, S_{gen} due to heat exchange between the two streams.

$$S_{\text{gen}} = \Delta S_{\text{cold}} + \Delta S_{\text{hot}} \tag{2.15}$$

Note that ΔS_{hot} is negative. From Eq. 2.13, the exergy destruction due heat exchange is

$$A_{\text{loss}} = T_0 \left(\Delta S_{\text{cold}} + \Delta S_{\text{hot}} \right) = T_0 S_{\text{gen}} \tag{2.16}$$

The exergy destruction of heat exchange between the two streams is colored yellow in Fig. 2.8. It can be seen that the larger the temperature difference during heat exchange, the larger the exergy destruction due to heat exchange.

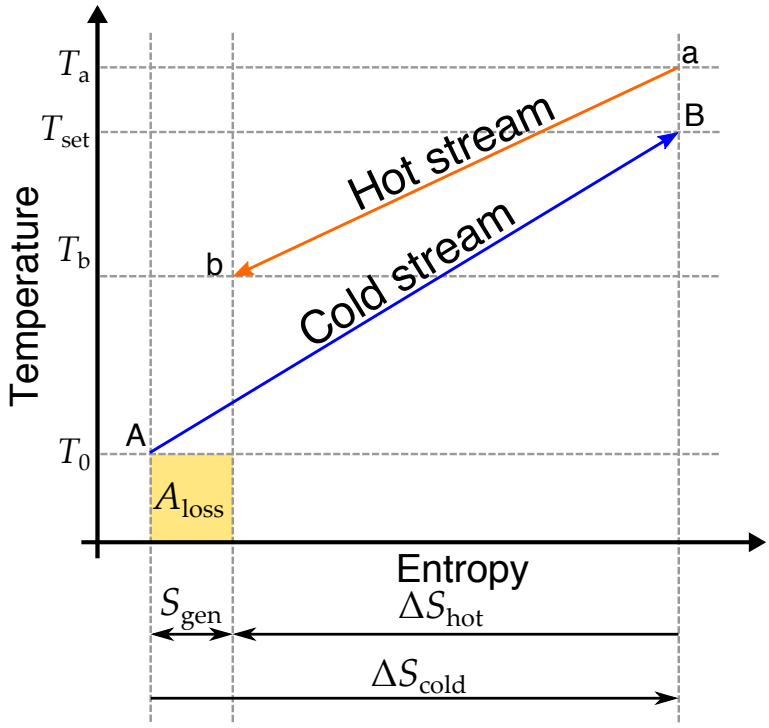

Figure 2.8: Temperature-entropy diagram of heat transfer between two process streams

2.2.4 Theoretical minimum exergy destruction in thermal processes

Industrial processes are often stable process that run for a long time once it is started. Regardless to thermal processes, in order to keep the process stable and running, it is needed to keep providing the exergy destroyed within the process. Exergy can be provided together with energy. The only two means of providing this exergy is by heat or work. It is possible to provide exergy through both, but the exergy rate of work is 1.0 while the exergy rate of heat depends on the temperature as shown in Fig. 2.7. If the required exergy is provided by heat at around 1000 [K], twice as much energy will be needed compared to a case where the exergy is provided by work because the exergy rate of heat at 1000 [K] is around 0.5. Work; usually provided in the mean of electricity, is often created via heat as a result of combustion. However, electricity created in gas turbines are usually created at a higher temperature, making it advantageous compared to heat created on site at chemical plants.

If we were to raise the temperature of a cold process stream to a certain temperature, heat will need to be transferred from a hot process fluid. When heat is transferred between process streams at different temperatures, exergy destruction will occur as described in chapter 2.2.3. If we consider a minimum temperature difference needed to heat exchange, ΔT_{min}, the entropy generation and exergy destruction will be minimum when the temperature difference during heat exchange, ΔT_{HEX}, is equal to ΔT_{min} throughout the heat exchanging process. That is to say that there is no "pinch point" from start to end of the heat exchanging process and the composite curves of the cold stream and the hot stream are completely parallel (Fig. 2.9 (left)). Fig. 2.9 (right) shows the temperature-entropy diagram during heat exchange between the hot and the cold stream when the temperature difference during heat exchange is kept constant at ΔT_{min}. Note that the two lines in the temperature-entropy diagram is not parallel. When the temperature of the cold stream is raised from T_0 to T_{set}, (A $\rightarrow$ B), the state point of the hot stream changes from point a to b. Assuming no heat loss in within the process, the heat that is transferred, Q_{transfer}, is represented by area A-B-III-I for the cold stream and area a-b-II-III in Fig. 2.9 (right) are of the same size. The minimum exergy destruction in heat transfer,A_{min}, when the temperature difference needed for heat exchange is set to ΔT_{min}, is shown as the colored area in the temperature-entropy diagram.In order for the two composite curves of the process streams to be parallel, the heat capacity of the two process fluids must be identical and can be shown by the following equation using the minimum temperature needed for heat exchange, ΔT_{min}.

$$C_p'\left(T, p\right) = C_p\left(T + \Delta T_{\mathrm{min}}, p\right) \tag{2.17}$$

where C_p and C_p' are the specific heat capacity at constant pressure for the cold process stream and the "ideal" hot stream. Thus, if the cold stream is the objective process stream, the enthalpy and the entropy of the "ideal" hot stream, I' and S', can be derived by

integrating the obtained heat capacity,

$$I'(T,p) = \int C_p(T + \Delta T_{\text{min}}, p)\, dT \tag{2.18}$$

$$S'(T,p) = \int \frac{C_p(T + \Delta T_{\text{min}}, p)}{T} dT \tag{2.19}$$

The entropy generation,S_{gen}, and the theoretical minimum exergy destruction exergy destruction when temperature difference during heat exchange is set to constant, A_{min}, can be derived from Eq. 2.15 and 2.16.

$$\begin{aligned} S_{\text{gen}} = &\left(\int^{\text{A}} \frac{C_p(T)}{T} dT - \int^{\text{B}} \frac{C_p(T)}{T} dT \right) \\ &- \left(\int^{\text{a}} \frac{C_p(T + \Delta T_{\text{min}})}{T} dT - \int^{\text{b}} \frac{C_p(T + \Delta T_{\text{min}})}{T} dT \right) \end{aligned} \tag{2.20}$$

$$\begin{aligned} A_{\text{min}} = T_0 \Bigg\{ &\left(\int^{\text{A}} \frac{C_p(T)}{T} dT - \int^{\text{B}} \frac{C_p(T)}{T} dT \right) \\ &- \left(\int^{\text{a}} \frac{C_p(T + \Delta T_{\text{min}})}{T} dT - \int^{\text{b}} \frac{C_p(T + \Delta T_{\text{min}})}{T} dT \right) \Bigg\} \end{aligned} \tag{2.21}$$

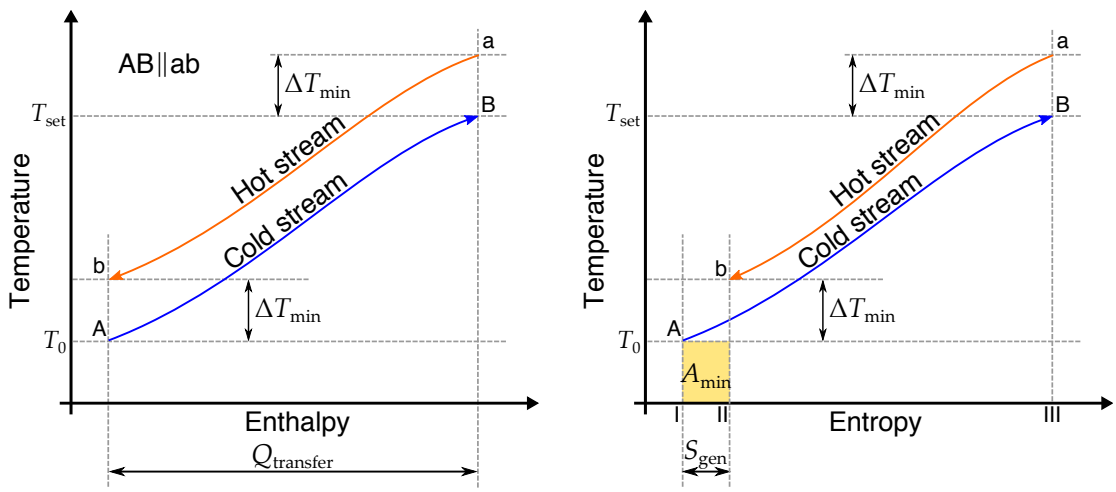

Figure 2.9: Temperature-enthalpy diagram (left) and temperature-entropy diagram (right) of process where temperature difference during heat exchange is fixed to ΔT_{min}

To understand how much exergy is being destroyed when a certain amount of heat is

transferred, the ratio of the two is defined as the evaluation factor.

$$\frac{A_{\text{loss}}}{Q_{\text{process}}} \tag{2.22}$$

When exergy loss is minimum, i.e. $A_{\text{loss}} = A_{\text{min}}$, and the amount of heat transferred, Q_{transfer}, is the amount of heat that the process stream requires, Q_{process}, the evaluation factor can be written as,

$$\frac{A_{\text{min}}}{Q_{\text{process}}}$$

Table 2.1 and Table 2.2 shows the calculation result of entropy generation,S_{gen} , and exergy destruction,A_{loss} , due to heat transfer when nitrogen (N_2) at 1 [atm] was heated by an "ideal" hot stream where temperature difference during heat exchange is kept constant to ΔT_{min}. Heat capacity of nitrogen was obtained by the Shomate equation [19, 20]. The effect of pressure loss is neglected because usually the effect of pressure loss to exergy destruction is quite small compared to the effect of temperature difference, especially for heat exchange between gaseous materials. It can be seen from Table 2.1 that the theoretical minimum exergy destruction due to heat exchange is proportional to the minimum temperature difference needed for heat exchange, ΔT_{min}. In Table 2.2, the minimum temperature needed for heat exchange, ΔT_{min}, is fixed but the set temperature, T_{set} is varied. It can be seen that the larger the set temperature, the larger the evaluation factor, ϕ, becomes. This is because the amount of heat transferred, Q_{transfer} (area A-B-III-I in Fig. 2.9 (right)) increases much more rapidly compared to the overall temperature difference during heat exchange (area A-B-a-b in Fig. 2.9 (left)) at temperatures above environmental temperature, T_0.

Fig. 2.10 shows the calculated temperature-enthalpy diagram (top) and the temperature-entropy diagram (bottom) of heat exchange between nitrogen and "ideal" hot stream when the set temperature, T_{set} is set to 350 [K] and the minimum temperature difference during heat exchange, ΔT_{min}, is set to 10.0 [K]. The enthalpy difference, ΔH, is equal for both process streams, while the entropy difference, ΔS, is different, which is the cause of entropy generation, S_{gen} leading to exergy destruction. The smaller the temperature

Table 2.1: Entropy generation, S_{gen}, and exergy destruction, A_{min}, of heat transfer between cold process stream of nitrogen at 1 [atm] and "ideal" hot stream. (ΔT_{min} varied)

T_{set} [K]	ΔT_{min} [K]	$Q_{transfer}$ [$kJ \cdot kg^{-1}$]	S_{gen} [$J \cdot kg^{-1} \cdot K^{-1}$]	A_{min} [$kJ \cdot kg^{-1}$]	$A_{min}/Q_{process}$ [%]
	2.5		1.24	0.370	0.70
	5.0		2.46	0.733	1.38
350	10.0	53.06	4.84	1.442	2.72
	15.0		7.14	2.128	4.02
	20.0		9.36	2.791	5.26

Table 2.2: Entropy generation, S_{gen}, and exergy destruction, A_{min}, of heat transfer between cold process stream of nitrogen at 1 [atm] and "ideal" hot stream. (ΔT_{set} varied)

T_{set} [K]	ΔT_{min} [K]	$Q_{transfer}$ [$kJ \cdot kg^{-1}$]	S_{gen} [$J \cdot kg^{-1} \cdot K^{-1}$]	A_{min} [$kJ \cdot kg^{-1}$]	$A_{min}/Q_{process}$ [%]
350		53.06	4.84	1.442	2.72
400	10.0	105.19	8.31	2.478	2.36
450		157.51	10.93	3.257	2.07

difference during heat exchange, the smaller the area surrounded by the two process streams will become meaning smaller exergy destruction.

The minimum exergy destruction, $A_{\min}$, obtained using the methodology presented can be fixed as a target value for designing new energy saving thermal processes. It is the minimum energy consumption that is needed for heat exchange between two process streams. There are many conventional heat recovering technologies where part of the process stream heat is recirculated aiming to reduce the energy consumption needed in thermal processes. Although it is possible to gain some reduction in energy consumption by applying these technologies, the exergy destruction caused by heat exchange cannot be reduced to value lower than $A_{\min}$. This is because temperature difference, $\Delta T_{\min}$ is needed for heat exchange and additional heat source is required to raise the temperature of the process stream heat so that it can be recovered.

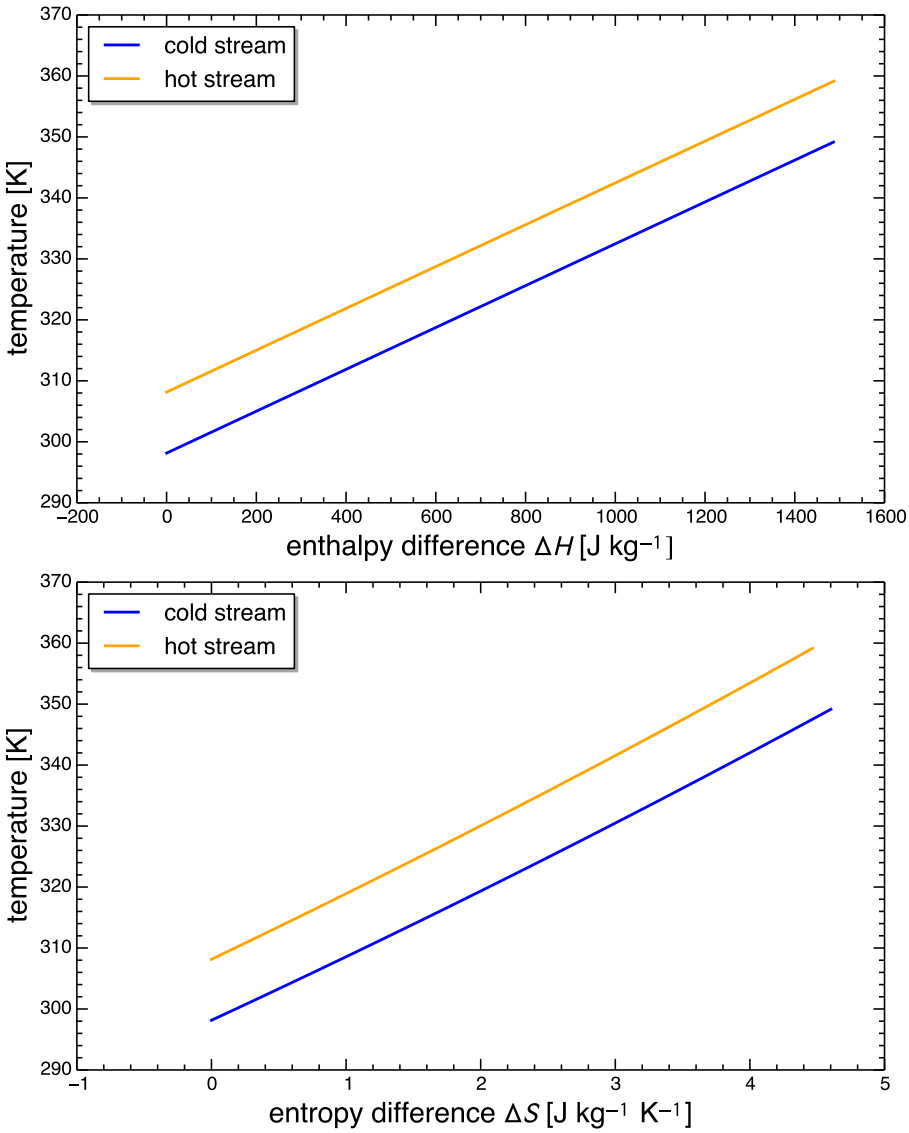

Figure 2.10: Temperature-enthalpy diagram (top) and temperature-entropy diagram (bottom) of nitrogen (N_2) at 1[atm] and "ideal" hot stream

2.3 Simplified evaluation index for thermal processes

A method to obtain the minimum exergy destruction due to heat exchange has been presented in chapter 2.2.4 which can be used as an evaluation factor for thermal processes. However, the calculation results in Fig. 2.10 (right) shows that the overall entropy generation, S_{gen} is usually quite small compared to the entropy change of the two streams, ΔS_{cold} and ΔS_{hot}, i.e. the minimum temperature difference needed for heat exchange, T_{min} is much smaller than the temperature difference that the process stream is raised ($T_{\text{set}} - T_0$). The differential of the heat heat transferred, dQ_{transfer}, is expressed as,

$$dQ_{\text{transfer}} = TdS_{\text{cold}} = -(T + \Delta T_{\text{min}})dS_{\text{hot}} \tag{2.23}$$

Using Eq. 2.23, the exergy destruction, Eq. 2.10 can be rewritten as,

$$\begin{aligned} dA &= \frac{T_0}{T}\Delta T_{\text{min}} dS_{\text{hot}} \\ &= \frac{\Delta T_{\text{min}}}{T + T_{\text{min}}} T_0 dS_{\text{cold}} \\ &= \frac{1}{(T/T_0) + (\Delta T_{\text{min}}/T_0)} \Delta T_{\text{min}} dS_{\text{cold}} \end{aligned} \tag{2.24}$$

If we assume that ΔT_{min} is much smaller than T_0 and T, and the temperature of the cold stream, T is close to the standard temperature, T_0, the minimum exergy destruction,A_{min}, due to heat transfer can simply be expressed as,

$$A_{\text{min}} \approx \Delta T_{\text{min}} \Delta S_{\text{cold}} \tag{2.25}$$

Strictly speaking, the minimum exergy destruction obtained by Eq. 2.25 will be slightly larger than the minimum exergy destruction obtained by Eq. 2.21.

Table 2.3 shows the comparison between A_{min} obtained by Eq. 2.15 and the simplified value obtained by Eq. 2.21. It can be seen that the simplified value is fairly in a good agreement with A_{min} when the set temperature, T_{set}, is close to the environmental temperature, T_0 and the temperature difference during heat exchange, T_{min} is small.

The equation to obtain the simplified A_{loss} is not only simple, but also easy to understand viscerally through the temperature-entropy diagram because it is close to the area

surrounded by the two composite curves of the process streams, which represents the temperature difference throughout the heat transfer.

Table 2.3: Comparison of minimum exergy destruction during heat exchange, A_{min} and simplified value, $\Delta T_{\mathrm{min}} \Delta S_{\mathrm{cold}}$ when nitrogen (N_2) at 1 [atm] is the cold process stream

T_{set} [K]	ΔT_{min} [K]	ΔS_{cold} $[\mathrm{J \cdot kg^{-1} \cdot K^{-1}}]$	ΔS_{hot} $[\mathrm{J \cdot kg^{-1} \cdot K^{-1}}]$	S_{gen} $[\mathrm{J \cdot kg^{-1} \cdot K^{-1}}]$	A_{min} $[\mathrm{kJ \cdot kg^{-1}}]$	$\Delta T_{\mathrm{min}} \Delta S_{\mathrm{cold}}$ $[\mathrm{kJ \cdot kg^{-1}}]$
	2.5		163.05	1.24	0.37	0.41
	5.0		161.83	2.46	0.73	0.82
350	10.0	164.29	159.45	4.84	1.44	1.64
	15.0		157.15	7.14	2.13	2.46
	20.0		154.93	9.36	2.79	3.29
400	10.0	303.82	295.51	8.31	2.48	3.04
450	10.0	427.31	416.38	10.93	3.26	4.27

2.4 Comparison of exergy destruction in thermal processes

2.4.1 Exergy destruction in conventional heat recovery systems

In a thermal process where there is no heat recovery as shown in Fig. 1.4, all of the provided heat is discarded. The temperature-entropy diagram of simple process where no heat recovering technology is applied is shown in Fig. 2.11. The process stream climbs the isobaric line when heat is given from the fired heater ($1 \rightarrow 2$). After the subsequent process (X) ($2 \rightarrow 3$), the process stream descends the same isobaric line as it discards its heat. The amount of exergy that is discarded with the effluent steam, A_{discard}, can be calculated by Eq. 2.11 and is the area colored purple. If heat at constant temperature, T_{heat}, is created by another source of energy with exergy rate 1.0, the exergy loss due to the creation of heat. $A_{\text{loss,FH,heat}}$ is the area colored green. Exergy destruction due to heat exchange between the feed stream and the created heat at constant temperature can be derived from the entropy change of the feed stream, ΔS_{feed}, and heat at constant temperature, ΔS_{heat} during heat transfer,

$$A_{\text{loss,FH,HEX}} = T_0 \left(\Delta S_{\text{feed}} - \Delta S_{\text{heat}} \right) \tag{2.26}$$

which is the area colored in yellow. The overall exergy lost, A_{loss}, from the process is the sum of the three values, A_{discard}, $A_{\text{loss,FH,heat}}$ and $A_{\text{loss,FH,HEX}}$.

Attempting to reduce the energy consumed in thermal processes, conventionally, feed-effluent heat exchanger is set to recover the heat of exhaust as shown in Fig. 1.6. The pinch analysis is one of the methods to optimize the heat exchanger network so that maximum heat is recovered. Fig. 2.12 shows the temperature-entropy diagram of thermal process with feed-effluent heat exchanger. Similar to the simple process where no energy saving technology is applied, the process stream climbs and descends the same isobaric line. However, due to heat exchange ($1 \rightarrow 2$ for feed stream and $4 \rightarrow 5$ for effluent stream), some of the heat is recovered. The heat provided at the furnace heater is

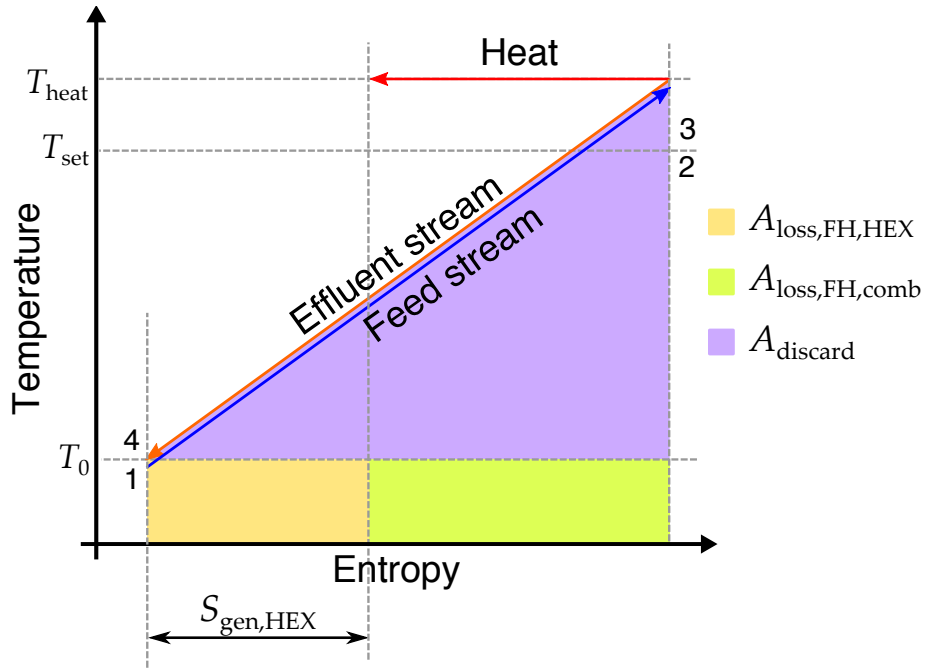

Figure 2.11: Temperature-entropy diagram of a simple thermal process

discarded at the cooler, $Q_{discard}$.

$$\int_1^2 TdS = \int_4^5 TdS \tag{2.27}$$

$$Q_{discard} = \int_2^3 TdS = \int_5^6 TdS \tag{2.28}$$

The exergy destruction due to self-heat exchange between the feed and effluent process stream, $A_{loss,HEX}$, can be expressed by the following equation,

$$\begin{aligned} A_{loss,HEX} &= T_0(S_{cold,HEX} + \Delta S_{hot,HEX}) \\ &= T_0 \Delta S_{gen,HEX} \end{aligned} \tag{2.29}$$

which is the area colored red. In a conventional process with feed-effluent heat exchanger, not all of the heat can be recovered and extra heating by the furnace is needed because temperature difference is needed for heat transfer. For excess heating, similar discussion to a simple thermal process explained above can be made. Exergy is destroyed in the process of creating heat at constant temperature, $A_{loss,FH,heat}$, and in transferring its heat to the feed process stream, $A_{loss,FH,HEX}$, colored in green and yellow respectively. It can also

be said that the sum of $A_{\text{loss,FH,heat}}$ and $A_{\text{loss,FH,HEX}}$ is the exergy destroyed in the process of changing the feed process stream state point from 2 to 3. Finally heat is discarded at the cooler (5 → 6). Exergy associated with the discarded heat, A_{discard} is represented by the area colored purple. The overall exergy lost, A_{loss}, from the process is the sum of the four values, A_{discard}, $A_{\text{loss,FH,heat}}$, $A_{\text{loss,FH,HEX}}$ and $A_{\text{loss,HEX}}$.

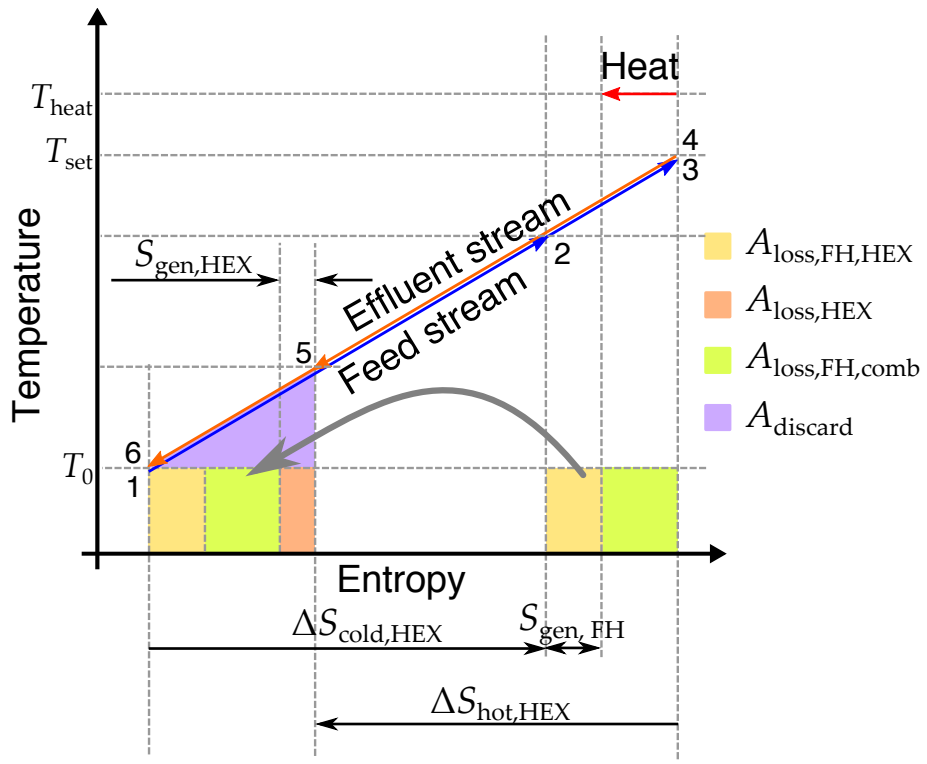

Figure 2.12: Temperature-entropy diagram of a thermal process with feed-effluent heat exchanger

Table 2.4 shows the breakdown of exergy loss in thermal processes with feed-effluent heat exchanger to recover heat when nitrogen was chosen as the process stream. In a case where no energy saving technology is applied, Q_{process} is equal to the total exergy lost in the process. Compared to Q_{process}, total exergy lost in the process with a feed-effluent heat exchanger, A_{loss}, is reduced up to 5%. However, it can be seen that by comparing the values obtained for heat exchange between with an "ideal" process stream (Table 2.1

and 2.2), that the total exergy loss, A_{loss} is still 3-7 times larger than the minimum exergy destruction needed for heat exchange, A_{min}. This is due to the exergy destruction in the fired heater, $A_{\text{loss,FH}}$. Exergy rate of heat carried by nitrogen at 350-450 K is merely around 0.3-0.4 which is much lower than the exergy rate of a typical fuel.

Table 2.4: Breakdown of exergy loss in thermal processes with feed-effluent heat exchanger when nitrogen is the process stream

T_{set} [K]	ΔT_{min} [K]	Q_{process} [kJ · kg^{-1}]	Q_{transfer} [kJ · kg^{-1}]	$A_{\text{loss,HEX}}$ [kJ · kg^{-1}]	$A_{\text{loss,FH}}$ [kJ · kg^{-1}]	A_{discard} [kJ · kg^{-1}]	A_{loss} [kJ · kg^{-1}]	$A_{\text{loss}}/Q_{\text{process}}$ [%]
	2.5		51.4	0.39	2.21	0.02	2.61	4.83
	5.0		48.8	0.72	4.47	0.02	5.21	9.64
350	10	54.01	43.59	1.25	9.00	0.16	10.42	19.3
	15		38.38	1.67	13.60	0.37	15.64	29.0
	20		33.17	1.91	18.28	0.66	20.84	38.6
400	10	106.18	95.74	2.39	7.90	0.15	9.83	
450	10	158.54	148.05	3.28	7.04	0.17	10.49	6.62

2.4.2 Exergy destruction in self-heat recuperative process

Although it was seen that it is possible to reduce the exergy destruction in thermal processes by employing a feed-effluent heat exchanger, exergy destruction in the fired heater is still quite large when the set temperature, T_{set} was at low temperatures. In chapter 2.2.4, it was described that in order to obtain the minimum exergy destruction in thermal processes, the temperature difference between the hot and the cold process stream should always be at the minimum temperature difference during heat exchange, ΔT_{min}. In a self-heat recuperative process (Fig. 1.9), the temperature of the process stream is raised through compression ($3 \rightarrow 4$) and is recirculated to heat the feed process stream. The hot and the cold process stream during heat exchange is composed of the same material so

that the heat capacity of the two process streams are very close.

Fig. 2.13 is the energy conversion diagram of a self-heat recuperative thermal process. In an energy conversion diagram, the number on the top represents the amount of energy or enthalpy and the number on the bottom represents the amount of exergy. In a self-heat recuperative thermal process, work (exergy rate of 1.0) equal to the amount of exergy destruction due to heat transfer is provided to enable heat circulation.

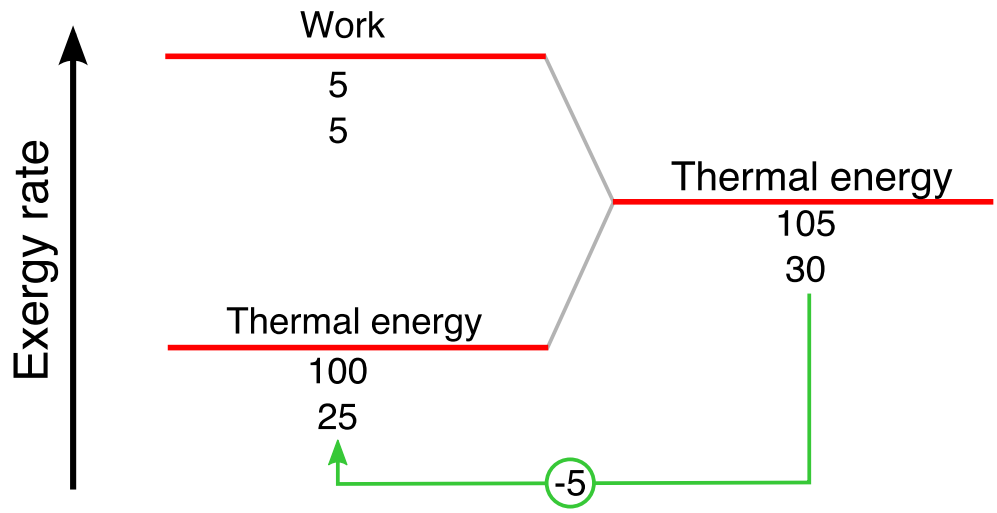

Figure 2.13: Energy conversion diagram of self-heat recuperative thermal process

Fig. 2.14 shows the temperature-entropy diagram of a self-heat recuperative process. The cycle of self-heat recuperation is composed of isobaric heating, adiabatic compression, isobaric cooling and adiabatic expansion, thus it draws a cycle similar to that of a reverse Brayton cycle. However in a reverse Brayton cycle, the amount of heat that the cycle gains from a heat source is different from the amount of heat the cycle gives to a heat sink. In a self-heat recuperative process, the heat sink and the heat source is itself and the amount of heat transferred in the isobaric heating and the cooling is the same.

$$\int_1^2 TdS = -\int_4^5 TdS \tag{2.30}$$

The exergy destruction due to heat exchange, $A_{\text{loss,HEX}}$, can be derived from the en-

tropy change during isobaric heating and isobaric cooling,

$$A_{\text{loss,HEX}} = T_0(\Delta S_{\text{cold}} + \Delta S_{\text{hot}}) \tag{2.31}$$

which is the area colored in red. The amount of exergy discarded with the effluent stream, $\Delta A_{\text{discard}}$, can be calculated from Eq. 2.11, the area colored purple. In a self-heat recuperative thermal process, the total amount of heat transferred to the feed stream, Q_{process}, is equal to the heat transferred in the heat exchanger, Q_{transfer}.

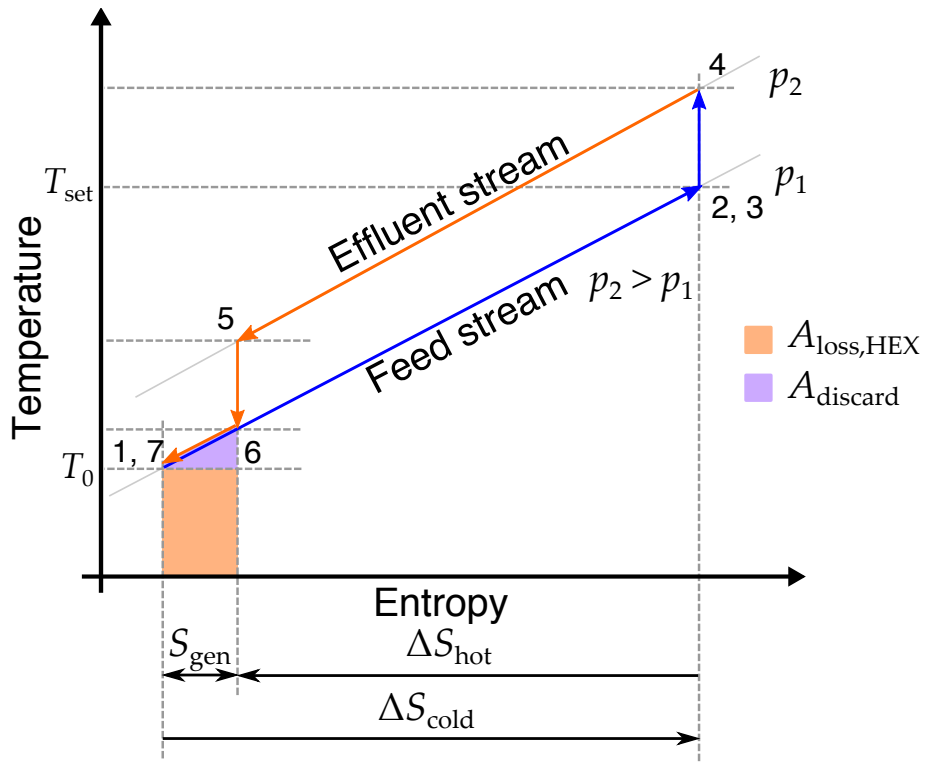

Figure 2.14: Temperature-entropy diagram of a self-heat recuperative thermal process (adiabatic pressure variation)

Table 2.5 shows the breakdown of exergy loss in a self-heat recuperative thermal process when nitrogen was chosen as the material for the process stream. Compression and expansion is assumed completely adiabatic. Exergy destruction has been reduced considerably compared to the case with feed-effluent heat exchanger (Table 2.4). Also it can be

seen that by comparing the obtained value with the minimum exergy destruction for heat transfer (A_{min} in Table 2.1 and 2.2), it can be seen that the total exergy destruction, A_{loss}, matches quite closely. If the heat capacity of feed stream and effluent stream matches completely, the exergy loss due to heat exchange, $A_{\mathrm{loss.HEX}}$, is identical to the minimum exergy destruction for heat transfer, A_{min}. However, because the heat capacity of the process stream is affected by pressure, the heat capacity of the feed and effluent stream differs slightly. As the minimum temperature difference needed for heat exchange, ΔT_{min}, increases, the pressure ratio increases, resulting in larger difference between the heat capacity.

Table 2.5: Breakdown of exergy loss in a self-heat recuperative thermal process when nitrogen is the process stream

T_{set} [K]	ΔT_{min} [K]	Q_{process} [$\mathrm{kJ \cdot kg^{-1}}$]	$A_{\mathrm{loss,HEX}}$ [$\mathrm{kJ \cdot kg^{-1}}$]	A_{discard} [$\mathrm{kJ \cdot kg^{-1}}$]	A_{loss} [$\mathrm{kJ \cdot kg^{-1}}$]	$A_{\mathrm{loss}}/Q_{\mathrm{process}}$ [%]
	2.5		0.43	0.02	0.45	0.08
	5.0		0.74	0.02	0.77	1.42
350	10.0	54.01	1.49	0.02	1.51	2.80
	15.0		2.23	0.03	2.26	4.19
	20.0		2.87	0.03	2.90	5.38
400	10.0	106.18	2.55	0.03	2.58	2.43
450	10.0	158.54	3.51	0.04	3.55	2.24

2.4.3 Discussion

In the above section, three different types of thermal processes (simple process, process with feed-effluent heat exchanger, self-heat recuperative process) were analyzed in terms

of temperature-entropy diagram and compared with the minimum exergy destruction needed for heat exchange. Table 2.6 shows the total exergy destruction, A_{loss}, of a each thermal processes when the set temperature, T_{set}, was set to 400 [K] and the minimum temperature difference needed for heat exchange, ΔT_{min}, was set to 10.0 [K] for nitrogen. The environmental temperature, T_0 was set to 298.15 [K]. Fig. 2.15 shows the comparison of $E_{\mathrm{net}}/Q_{\mathrm{process}}$ of three thermal processes and $A_{\mathrm{min}}/Q_{\mathrm{process}}$. In a simple process where no energy saving technology is applied (case 1), all of the heat that is needed to raise the temperature of the process stream is discarded along with its exergy, A_{loss}. In case when feed-effluent heat exchanger is applied (case 2), some of the exergy destruction is avoided. For a self-heat recuperative process (case 3), the exergy destruction is quite close to that for an ideal case where the temperature difference during heat exchange is always kept to ΔT_{min} (case 4).

Table 2.6: Comparison of exergy destruction in three different process, simple process (case 1), process with feed-effluent heat exchanger (case 2), self-heat recuperative process (case 3) and minimum exergy destruction needed for heat transfer (case 4) for nitrogen

case	T_{set}	ΔT_{min}	Q_{process}	A_{loss}	$A_{\mathrm{loss}}/Q_{\mathrm{process}}$
[−]	[K]	[K]	[kJ · kg^{-1}]	[kJ · kg^{-1}]	[−]
1				106.18	100
2	400	10.0	106.18	10.44	9.83
3				2.58	2.43
4	400	10.0	106.18	2.50	2.36

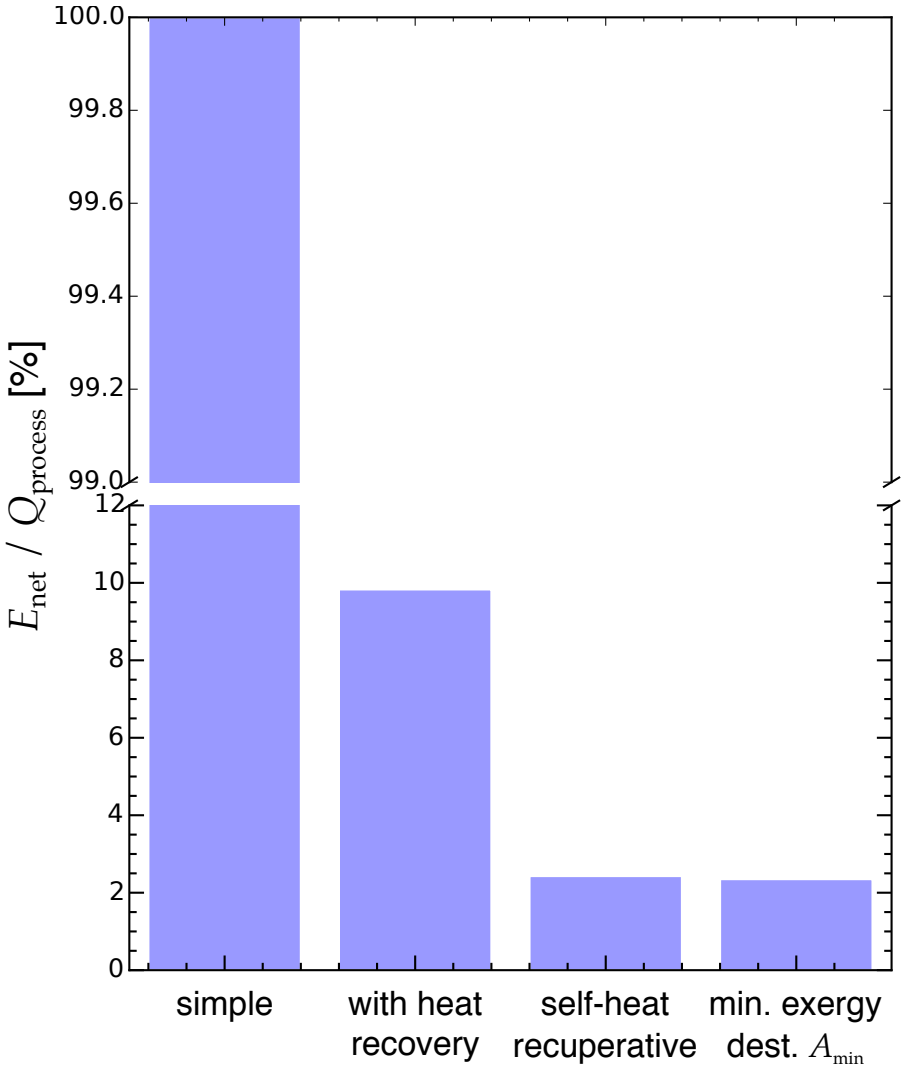

Figure 2.15: Comparison of exergy destruction in three different process, simple process (case 1), process with feed-effluent heat exchanger (case 2), self-heat recuperative process (case 3) and minimum exergy destruction needed for heat transfer (case 4) for nitrogen

2.5 Conclusion

In this chapter, thermal processes were analyzed in terms of exergy and irreversibility and two evaluation factors were set so that self-heat recuperativve process can be compared with different thermal processes regarding energy saving potentials. In order to maintain steady state in chemical process and keep the process running, all of the exergy lost during the process must constantly be provided. Thus, it is important to minimize the exergy lost in the process. It was explained that exergy destruction in thermal process is mainly caused by creation of low temperature heat and heat transfer between two process streams. The two cause of exergy destruction were graphically presented in temperature-entropy diagram so that a method to minimize the value can be derived.

A method to obtain the theoretical minimum exergy destruction in heat transfer, A_{loss}, is presented. When the minimum temperature difference needed for heat exchange, is set, exergy destruction due to heat transfer is minimum when the temperature difference during heat exchange is always at ΔT_{min}. The minimum exergy destruction in heat transfer should be the target value for thermal processes. Furthermore, a simple evaluation index that can be derived only from the minimum temperature difference during heat exchange, T_{min}, and the entropy change of the feed process stream, ΔS_{cold}. The simple evaluation value was compared with the minimum exergy destruction for heat exchange, A_{min}. It was seen that the simple evaluation value is in good agreement with the minimum exergy destruction when the minimum temperature difference needed for heat exchange, ΔT_{min}, is small and the set temperature, T_{set}, is close to environmental temperature, T_0.

Three thermal processes (simple process with no energy saving technology applied, process with feed-effluent heat exchanger and self-heat recuperative process) were compared with the minimum exergy destruction for heat transfer, A_{loss}. It was seen that a process with feed-effluent heat exchanger is capable of reducing the exergy destruction to about 10% compared to processes with no energy saving technology applied. In a self-

heat recuperative process, it is possible to further reduce the energy to about 25% of a process with a feed-effluent heat exchanger by removing the furnace heater and circulating heat through work provision. The total exergy destruction in a self-heat recuperative process is quite close to the minimum exergy destruction in heat transfer.

Chapter 3

Self-heat recuperation using magnetocaloric effect

3.1 Introduction

In a self-heat recuperative process, the recuperation and recirculation of the process stream heat is its essence. In all of the conventional self-heat recuperative process, compressors are applied to recuperate the heat exergy of the process stream [23–36]. However, method to recuperate the heat exergy of the process stream through work provision is not limited to compression. In the case of compression, the provided work enforces a change in intensive property; pressure, p. If a magnetic material is subjected to a varying field, the entropy change of the magnetic moments inside the material enforces a reversible temperature change, which is the magnetocaloric effect (MCE) [38]. With MCE, the strength of the magnetic field, H, or the magnetic flux density, B, is the intensive property which is enforced to change by providing work. It is also possible to enforce a change in tension, f, of a rubber or in strength of electric field, E, of a dielectric material to create a reversible temperature change known as the elastocaloric effect [71,72] and electrocaloric effect [73–75].

If the process stream was composed of incompressible fluids it will not be possible to

apply compression to recuperate its heat exergy. Also, the temperature range in which compressors can be used are limited due to sealing issues. In order to expand the application of self-heat recuperation, it is needed to study the other methods of recuperating heat exergy and classify them so that it is clear in which application they should be used.

MCE has been counted as a replacement of vapor compression in refrigeration technologies because no refrigerants such as CFCs (chlorofluorocarbons) with high global warming impact factor is not needed [76]. Electrocaloric effect was, until recently, too small to be used in applications [77]. In 2006, Mischenko [75] reported a large electrocaloric effect using thin film PZT ($PbZr_{0.95}Ti_{0.05}O_3$) which brought the electrocaloric effect as a serious alternative to conventional vapor compression and magnetocaloric effect [78]. However, one of the largest obstacle of achieving a sufficient temperature change by electrocaloric effect is the need to expose the material to very high electric field. The adiabatic temperature change,ΔT_{ad} , due to electrocaloric effect depends on the varying of electric field, E. In order to obtain a practical adiabatic temperature change of about 3 [K], an electric field, E, of at least about 30-60 [MV m^{-1}] is needed. Such electric field is difficult to obtain in large area, so the electrocaloric material must have very small thickness, which lead to insufficient mass of the material. Elastocaloric effect on the other hand, it is much easier for the elastocaloric material to undergo variation in stress, f. However, one of the greatest shortcoming is the fatigue life of the elastocaloric material because it undergoes constant variation in stress for a long period of time [72].

In this chapter, we focused on magnetocaloric effect as the method to recuperate the heat exergy of the process stream. This chapter describes the concept of a magnetocaloric heat circulator and how it can be applied to non-magnetocaloric process materials. The theoretical energy consumption and exergy destruction in terms of temperature entropy diagram has been obtained through simulation using the mean field theory and its energy saving potential has been discussed.

3.2 Magnetocaloric heat circulator

3.2.1 Conceptual design of magnetocaloric heat circulator

In the conventional self-heat recuperative processes, compressors has been used to recuperate the heat exergy of the process stream. However, compressors can only be applied to compressible process fluids. Also, in a small size application, the adiabatic efficiency of the compressors may become quite low, resulting in excess exergy destruction and lower efficiency. Here, we focused on MCE of a magnetocaloric material to overcome the issues the compressors hold and expand the application of self-heat recuperation technology.

Magnetocaloric heat circulator for magnetocaloric process materials

In a conventional self-heat recuperative process, a compressor was placed after the objective process, X, (Fig. 1.9: $3 \rightarrow 4$) and a expander was placed after the heat exchanger (Fig. 1.9: $5 \rightarrow 6$) to enforce a change in pressure from p_0 to p_1. In a magnetocaloric heat circulator, compression is replaces with magnetization and expansion is replaced with demagnetization thus, the strength of magnetic field, H, is varied in between H_0 and H_1. Magnetization and demagnetization of a magnetocaloric material cause a reversible temperature change, ΔT_{ad}. The process stream heat is recirculated due to cyclic magnetization and demagnetization. Fig. 3.13 shows the schematic process flow diagram of a magnetocaloric heat circulator for a magnetocaloric process material when the set temperature, T_{set}, is above environmental temperature, T_0. Instead of compressors and expanders, the heat circulator consists of a high field region, and a feed effluent heat exchanger. The temperature-heat diagram is the same as the temperature-entropy diagram for a self-heat recuperative process using compressors and expanders (Fig. 1.10).

In a counter-flow heat exchanger (HEX) the feed process stream of magnetocaloric material is raised from the environmental temperature, T_0, to the set temperature, T_{set}, for a certain process that follows, X ($1 \rightarrow 2$). Via the following process ($2 \rightarrow 3$), the effluent process stream is adiabatically magnetized to gain the temperature difference needed for

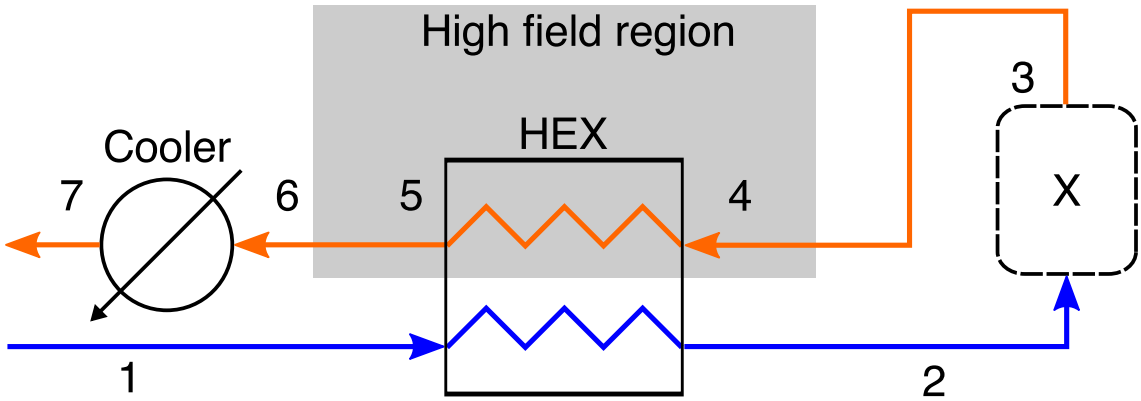

Figure 3.1: Schematic of the magnetocaloric heat circulator for a magnetocaloric process material when the set temperature, T_{set}, is above environmental temperature, T_0.

heat exchange ($3 \rightarrow 4$). The effluent process stream is then fed to the HEX so that all of the process stream heat is recirculated ($4 \rightarrow 5$). Then, the effluent process stream is demagnetized back to the initial magnetic field ($5 \rightarrow 6$), and finally, the rest of the heat is discarded at the cooler ($6 \rightarrow 7$). Thus, no heat is added but work is put in to recuperate and circulate all of the process stream heat.

$$Q_{\text{process}} = Q_{\text{transfer}} \tag{3.1}$$

If the state points of 1 and 7 are the same, from the conservation law of energy, the heat discarded at the cooler, Q_{discard}, is equal to the net work input, provided that part of the demagnetizing work, w_{demag}, can be recovered during magnetization. Thus,

$$\begin{aligned} E_{\text{net}} &= w_{\text{demag}} + w_{\text{mag}} \\ &= Q_{\text{discard}} \end{aligned} \tag{3.2}$$

note that work is needed for demagnetization rather than magnetization even though demagnetization and magnetization is analogous to expansion and compression respectively, because the positive and negative sign of strength of magnetic field, H, and pressure, p, is different (Subsection 1.4.1). The amount of net work input, E_{net}, is equal to the heat discarded at the cooler, Q_{discard}. This is because we are assuming a stable process,

thus, all that is provided must be discarded.

Similar discussion can be made for cases when the set temperature, T_{set}, is below the environmental temperature, T_0. Fig. 3.2 shows the schematic flow diagram (top) and temperature-heat diagram (bottom) of a magnetocaloric heat circulator for magnetocaloric process material when the set temperature, T_{set}, is below the environmental temperature, T_0. The feed process material at environmental temperature, T_0, is firstly magnetized to raise its temperature ($1 \rightarrow 2$). The feed process stream is cooled in the HEX ($2 \rightarrow 3$), and then demagnetized back to the original magnetic field ($3 \rightarrow 4$). Via the next process ($4 \rightarrow 5$), the effluent process stream is heated in the HEX ($5 \rightarrow 6$) to a temperature a higher than the initial environmental temperature. Finally, the effluent process stream is heated to the environmental temperature, T_0 ($6 \rightarrow 7$). The energy balance is the same as the case for magnetocaloric heat circulator for magnetocaloric process material when the set temperature, T_{set}, is below the environmental temperature, T_0 (Eq. 3.1 and 3.2).

The magnetocaloric heat circulator must be constructed so that the work needed for demagnetization, w_{demag}, can partly be compensated by the work needed for magnetization, w_{mag} [79]. One of the ways this can be accomplished is by configuring the magnetocaloric material in a circular shape as shown in Fig. 3.3. When part A of the magnetocaloric material circle is being demagnetized, it will be pulled by the magnetic field with f_1. At the same time, part B of the magnetocaloric circle is magnetized, where it is also pulled by the magnetic field with f_2. Thus, the force that is needed to keep the magnetocaloric material to circulate, f_{net}, is

$$f_{\text{net}} = |f_1| - |f_2| \tag{3.3}$$

in a magnetocaloric heat circulator, the force for demagnetization, f_1, is larger than force for magnetization f_2. If the magnetocaloric material circle was used for a heat engine, the force for demagnetization, f_1, will be smaller than the force for demagnetization, f_2, thus, work can be extracted.

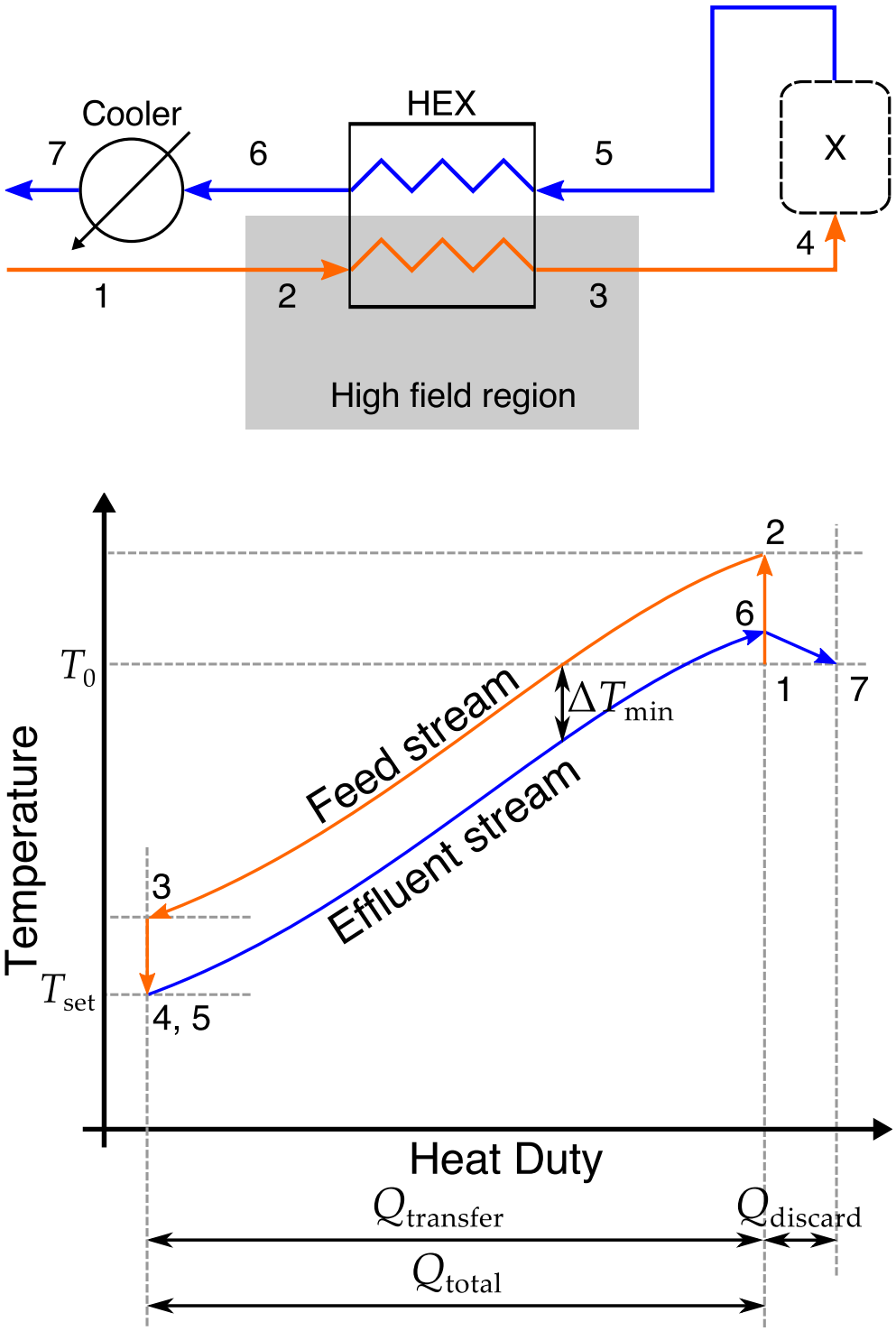

Figure 3.2: Schematic flow diagram (top) and temperature-heat diagram (bottom) of a magnetocaloric heat circulator for magnetocaloric process material when the set temperature, T_{set}, is below the environmental temperature, T_0

The net work provided from outside the system, E_{net}, can be expressed as,

$$E_{\text{net}} = \int F_2 dl + \int F_1 dl \tag{3.4}$$

where l is the length of the movement. By applying this configuration, part of the work needed for demagnetization can be compensated, which is an analogy of recovering part of the compression work by an expander.

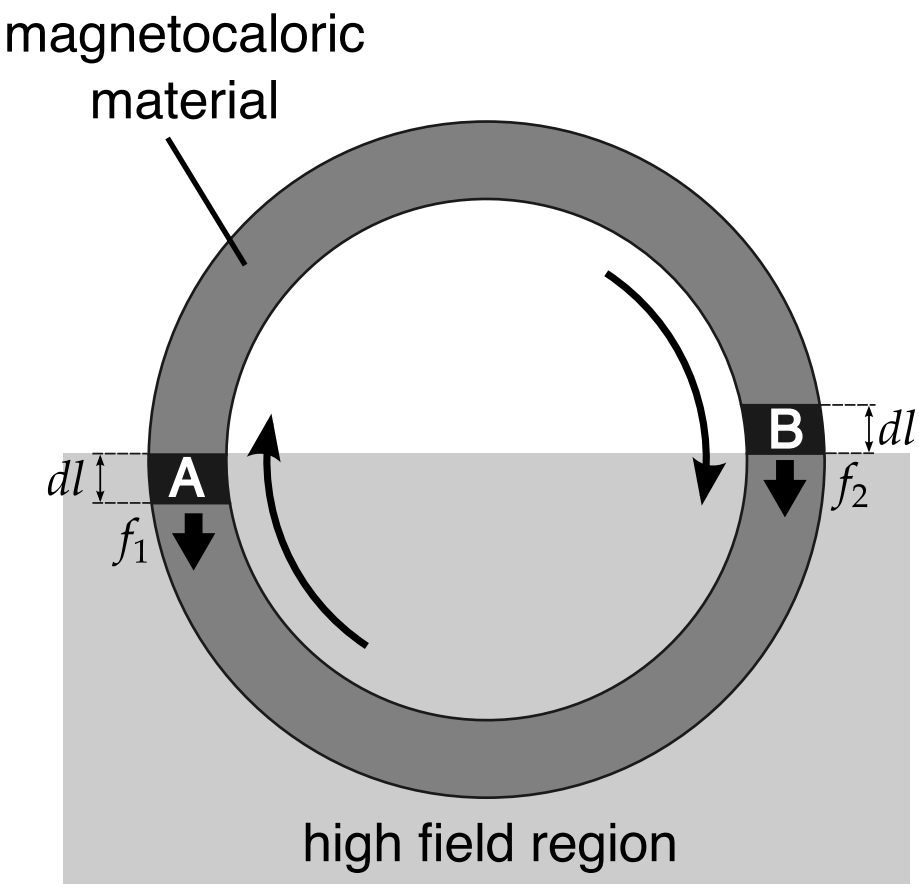

Figure 3.3: Configuration of magnetocaloric material so that magnetizing work can be recovered

Magnetocaloric heat circulator for non-magnetocaloric process materials

The above paragraphs explained the magnetocaloric heat circulator for magnetocaloric

process materials. However usually, process material is not magnetocaloric. In order to apply magnetocaloric heat circulator to non-magnetocaloric process materials, the heat of the effluent non-magnetocaloric process material can be passed to the magnetocaloric working material so that it can be recuperated, and then given to the feed non-magnetocaloric process material.

Fig. 3.4 shows the schematic flow diagram (top) and the temperature-heat diagram (bottom) of a magnetocaloric heat circulator for non-magnetocaloric process material when the set temperature, T_{set}, is above the environmental temperature, T_0; a heating process. A magnetocaloric heat circulator for non-magnetocaloric process material is made of two counter-flow heat exchangers (HEX1 and HEX2), a high field region, and working magnetocaloric material.

The feed process stream at environmental temperature, T_0, is heated to the set temperature, T_{set}, in the first heat exchanger (HEX1) by receiving heat from the magnetocaloric working material for the following process, X (a $\rightarrow$ b). Via the next process (b $\rightarrow$ c), the effluent process stream is cooled in the second heat exchanger (HEX2) by giving its heat to the magnetocaloric working material (c $\rightarrow$ d). Finally, the rest of the heat is discarded at the cooler bringing the temperature back to environmental temperature, T_0 (d $\rightarrow$ e). In HEX2, while the effluent process stream is being cooled, the working magnetocaloric material receives all of process stream heat (1 $\rightarrow$ 2), which is an isomagnetic heating process for the working magnetocaloric material. Then, the working magnetocaloric material is adiabatically magnetized so that the heat exergy can be recuperated (2 $\rightarrow$ 3). The recuperated heat is given back to the feed process stream in HEX1 (3 $\rightarrow$ 4), which is an isomagnetic cooling process for the working magnetocaloric material. Finally, the magnetocaloric working material is adiabatically demagnetized so that it will return to its original state (4 $\rightarrow$ 1).

It can be seen from the temperature-heat diagram (Fig. 3.4 bottom), the temperature difference, ΔT_{HEX} during heat exchange between the process stream and the magnetocaloric working material in the two heat exchangers, HEX1 and HEX2, is approximately

the half of adiabatic temperature change, ΔT_{ad} of the magnetocaloric working material.

The amount of magnetocaloric working material is decided so that the heat capacity of the magnetocaloric material matches the heat capacity of the process stream. Assuming no heat is lost during the heat exchange, the state of the process stream at state points a and e are the same, and the demagnetizing work, w_{demag}, is partly compensated by the magnetizing work, w_{mag}, the following equation can be realized through the energy balance,

$$Q_{\mathrm{ab}} = Q_{12} = Q_{\mathrm{cd}} + Q_{\mathrm{discard}} = Q_{34} + Q_{\mathrm{discard}} \tag{3.5}$$

$$\begin{aligned} Q_{\mathrm{discard}} &= E_{\mathrm{net}} \\ &= |w_{\mathrm{demag}} + w_{\mathrm{mag}}| \end{aligned} \tag{3.6}$$

where Q_{ab}, Q_{cd}, Q_{12} and Q_{34} denotes the amount of heat transferred when changing from state point, a $\rightarrow$ b, c $\rightarrow$ d, 1 $\rightarrow$ 2 and 3 $\rightarrow$ 4 respectively.

Fig. 3.5 shows the schematic of process flow diagram and temperature-heat diagram for cases when the set temperature, T_{set}, is below the environmental temperature, T_0, i.e. a cooling process when the process material is non-magnetocaloric. Compared to the heating process, the high field region is moved from HEX1 to HEX2 and the magnetocaloric working material is circulating in the opposite direction.

The magnetizing and demagnetizing force must compensate in order to recover part of the work as it was for the magnetocaloric heat circulator for magnetocaloric process streams. One of the configuration of a magnetocaloric heat pump for non-magnetocaloric process material is shown in Fig. 3.6. Steyert proposed a magnetic heat pump with a counter-flow heat exchanger [59]. A magnetic heat pump with a similar design has been actualized by Coelho *et al.* [80]. In a magnetic heat pump proposed by Steyert, wheel of magnetocaloric material circulates counter-flow to the working fluid. Magnetic field is applied to one half of the wheel, thus as the wheel of magnetocaloric material circulates, a part of the wheel is magnetized and while the other is demagnetized. A temperature gradient is created along the arc of the magnetocaloric material so that it is possible to heat

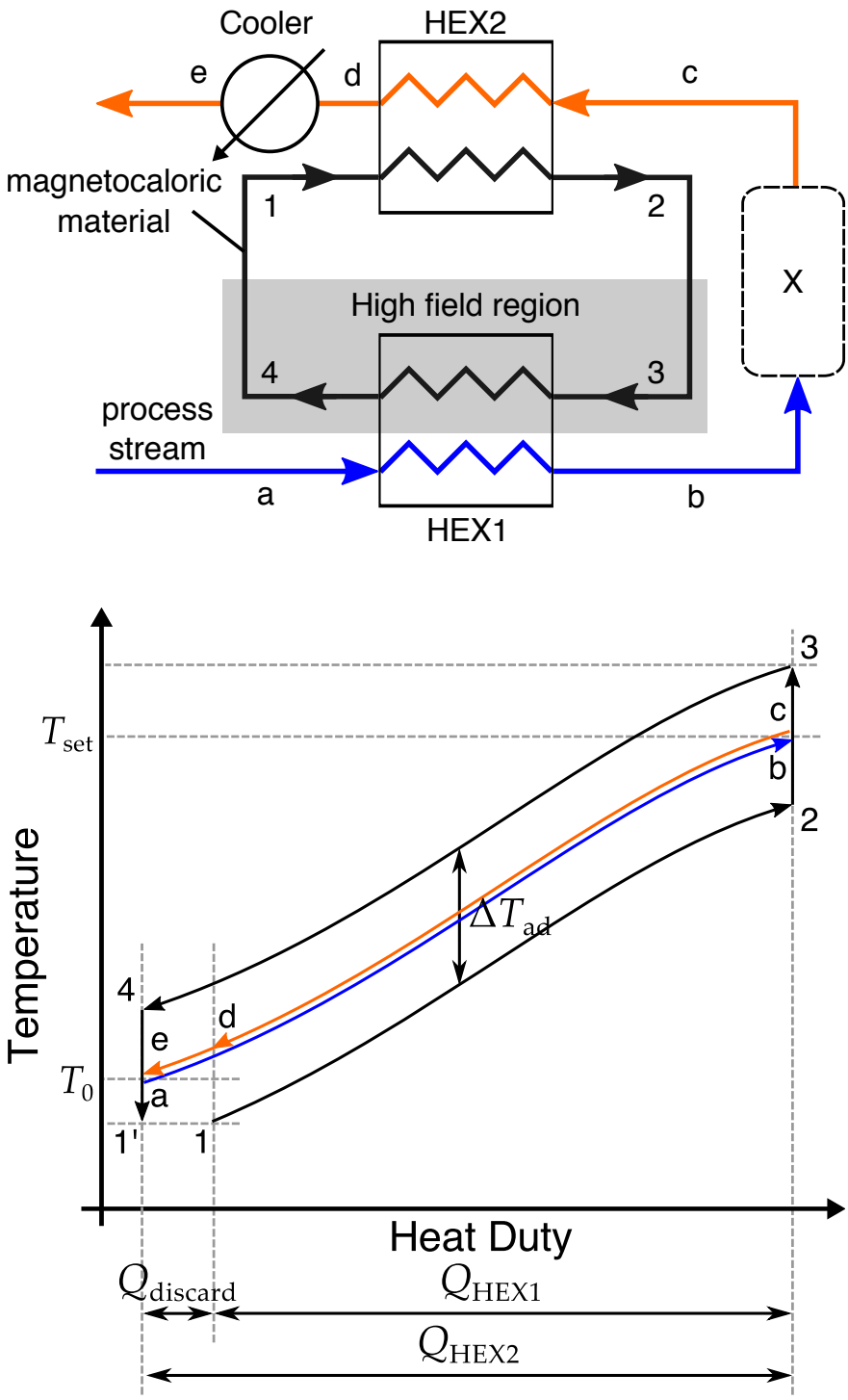

Figure 3.4: Schematic flow diagram (top) and temperature-heat diagram (bottom) of a magnetocaloric heat circulator for non-magnetocaloric process material when the set temperature, T_{set}, is above the environmental temperature, T_0

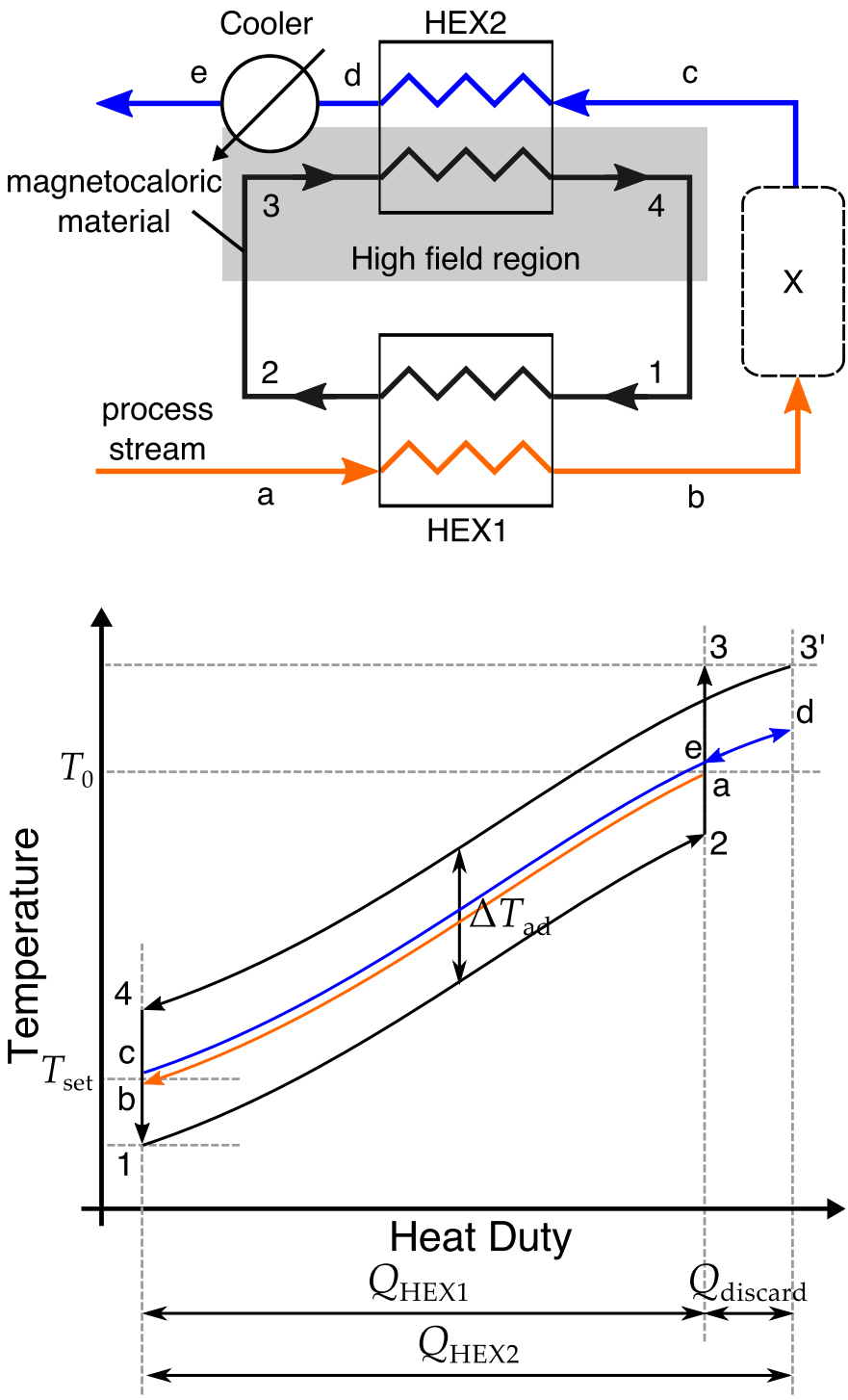

Figure 3.5: Schematic flow diagram (top) and temperature-heat diagram (bottom) of a magnetocaloric heat circulator for non-magnetocaloric process material when the set temperature, T_{set}, is below the environmental temperature, T_0

pump at a heat range larger than the adiabatic temperature change gained by magnetization, ΔT_{ad}. In the proposed magnetocaloric heat circulator, no heat sink or heat source is set but the process stream flows counter-flow to the magnetocaloric wheel. With this configuration, it is possible to circulate the heat between large temperature difference ($|T_{set} - T_0|$) than the adiabatic temperature change, ΔT_{ad}, obtained by MCE.

Scarpa classified the different magnetic heat pump configurations [81] including the configuration designed by Steyert. In all of the magnetic heat pump configurations, with small modifications, it is possible to apply to self-heat recuperation technology.

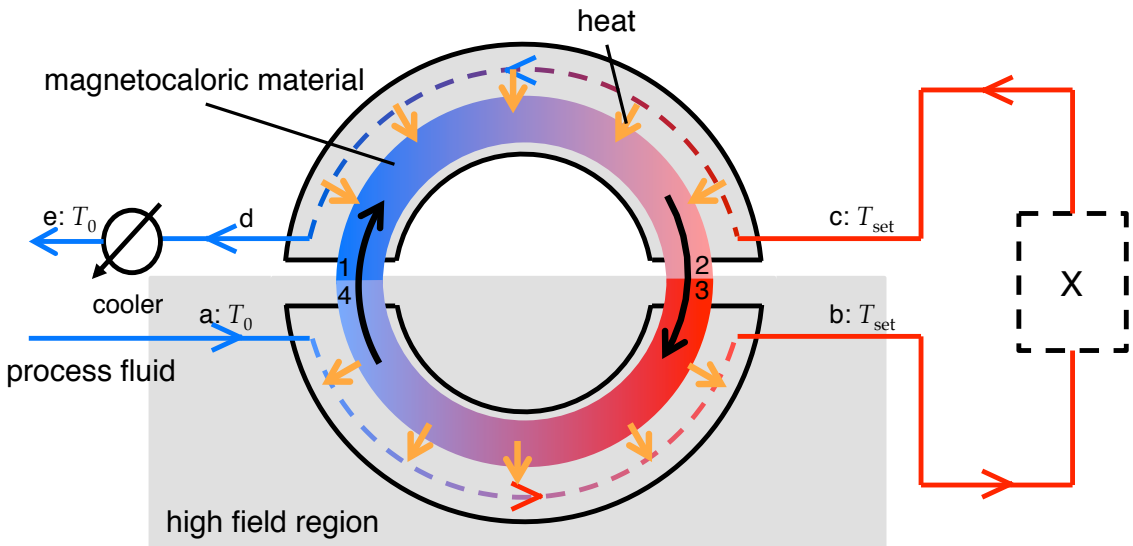

Figure 3.6: Image of Steyert like magnetocaloric heat circulator with counter-flow heat exchanger for non-magnetocaloric process material

3.3 Magnetocaloric heat circulator cycle

The magnetocaloric heat circulator can be expressed using the temperature-entropy diagram as it was for a compressive self-heat recuperative process in Chapter 2. Furthermore, the magnetocaloric heat circulator is expressed using a magnetization-magnetic field diagram so that magnetization and demagnetization work can visually be seen.

3.3.1 Temperature-entropy diagram

An self-heat recuperative process draws a cycle similar to that of a reverse Brayton cycle as presented in subsection 2.4.2. A cycle of magnetocaloric heat circulator for magnetocaloric process stream is made of isomagnetic heating, adiabatic magnetization, isomagnetic cooling process. Fig. 3.7 shows the temperature-entropy diagram of magnetocaloric heat circulator for magnetocaloric process streams for heating process (left) and cooling process (right). The two lines in gray are the isobaric line of a magnetocaloric process material at $H_1(=0)$ and $H_2(>0)$.

In a reverse Brayton cycle, entropy change of the process fluid at the heat sink and the heat source is the same because heat is transferred to outside the system. However, in a self-heat recuperative process, the same amount of heat is circulated internally, thus, in a process where the set temperature, T_{set}, is above the environmental temperature, T_0, the following equation can be realized

$$\begin{aligned} Q_{12} &= -Q_{45} \\ \int_1^2 TdS &= -\int_4^5 TdS \end{aligned} \tag{3.7}$$

Q_{12} and Q_{45} are the heat transferred during isomagnetic heating (1-2-c-a in Fig. 3.7 left) and isomagnetic cooling (4-5-b-c in Fig. 3.7 left). The smallest temperature difference during heat exchange, ΔT_{min}, is the smaller of the temperature difference between state points 4 and 3, ΔT_{43}, and state points 5 and 7, ΔT_{57}. When the temperature difference in which the heat is circulated ($|T_{\text{set}} - T_0|$) is small, the minimum temperature difference during heat exchange, ΔT_{min}, is approximately equal to the adiabatic temperature

change, ΔT_{ad}, obtained by MCE.

$$\Delta T_{ad} \approx \Delta T_{min} \tag{3.8}$$

Considering that the state points at 1 and 7 is the same, the heat discarded, $Q_{discard}$ (6-7-a-b) is equal to the net work input as written in Eq. 3.2.

Similarly, in a process where the set temperature, T_{set}, is at a temperature lower than the environmental temperature, T_0, i.e. cooling process, the following equation is realized

$$\begin{aligned} Q_{23} &= -Q_{56} \\ \int_2^3 TdS &= -\int_5^6 TdS \end{aligned} \tag{3.9}$$

Q_{23} and Q_{56} are the heat transferred during isomagnetic heating (2-3-a-b in Fig. 3.7 right) and isomagnetic cooling (5-6-c-a in Fig. 3.7 right). The smallest temperature difference during heat exchange, ΔT_{min}, is the smaller of the temperature difference between state points 3 and 5, ΔT_{35}, and state points 2 and 6, ΔT_{26}. The heat discarded, $Q_{discard}$ (6-7-b-c) is equal to the net work input as written in Eq. 3.2.

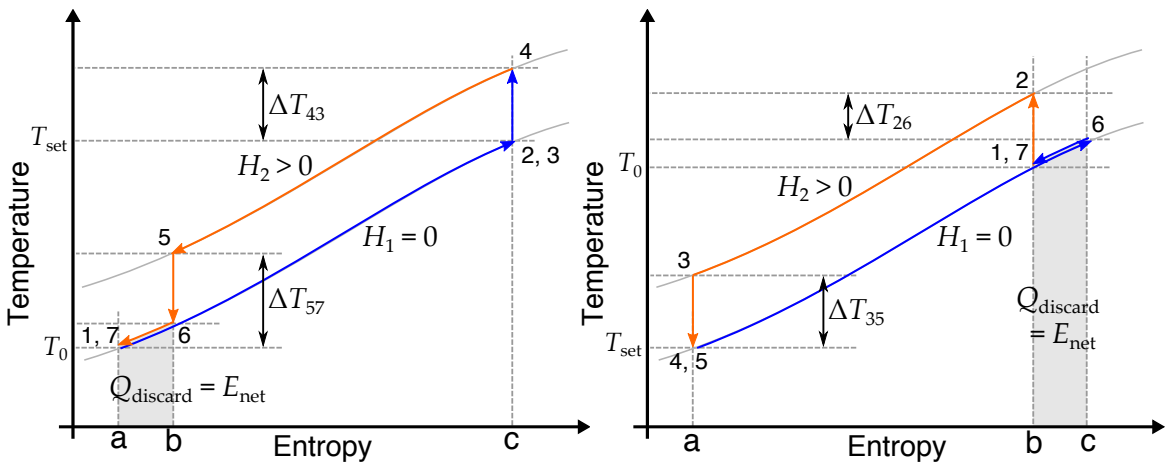

Figure 3.7: Temperature-entropy diagram of magnetocaloric heat circulator for magnetocaloric process streams for heating process (left) and cooling process (right)

Fig. 3.8 shows the temperature-entropy diagram of magnetocaloric heat circulator

for non-magnetocaloric process streams for heating process (left) and cooling process (right). In a magnetocaloric heat circulator for non-magnetocaloric process streams, the temperature-entropy diagram of the process stream goes up and down the same isobaric/isomagnetic line and the magnetocaloric material draws a reverse Brayton cycle. In a case where the set temperature, T_{set}, is above the environmental temperature, T_0, the following equation is realized,

$$\begin{gathered} Q_{\mathrm{ab}} = Q_{12} = Q_{\mathrm{cd}} + Q_{\mathrm{discard}} = Q_{34} + Q_{\mathrm{discard}} \\ \int_{\mathrm{a}}^{\mathrm{b}} TdS = \int_{1}^{2} TdS = \int_{\mathrm{c}}^{\mathrm{d}} TdS + \int_{\mathrm{d}}^{\mathrm{e}} TdS = \int_{4}^{3} TdS + \int_{\mathrm{d}}^{\mathrm{e}} TdS \end{gathered} \tag{3.10}$$

where Q_{ab} and Q_{12} are the heat transferred during the isomagnetic heating (a-b-IV-I and 1-2-IV-II in Fig. 3.8 left) and Q_{cd} and Q_{34} are the heat transferred during the isomagnetic cooling (c-d-III-IV and 3-4-II-IV in Fig. 3.8 left). The heat discarded, Q_{discard} (d-e-I-III) is equal to the net work input as written in Eq. 3.6. The smallest temperature difference during heat exchange is smallest out of the temperature difference between state points 3 and b, $\Delta T_{3\mathrm{b}}$, b and 2, $\Delta T_{\mathrm{b}2}$, 4 and d, $\Delta T_{4\mathrm{d}}$, and a and 1, $\Delta T_{\mathrm{a}1}$.

Similarly, in a process where the set temperature, T_{set}, is at a temperature lower than the environmental temperature, T_0, i.e. cooling process, the following equation is realized

$$\begin{gathered} Q_{\mathrm{cd}} = Q_{12} = Q_{\mathrm{ab}} + Q_{\mathrm{discard}} = Q_{34} + Q_{\mathrm{discard}} \\ \int_{\mathrm{c}}^{\mathrm{d}} TdS = \int_{1}^{2} TdS = \int_{\mathrm{d}}^{\mathrm{e}} TdS + \int_{\mathrm{a}}^{\mathrm{b}} TdS = \int_{4}^{3} TdS + \int_{\mathrm{d}}^{\mathrm{e}} TdS \end{gathered} \tag{3.11}$$

where Q_{cd} and Q_{12} are the heat transferred during the isomagnetic cooling (c-d-IV-I and 1-2-III-I in Fig. 3.8 right) and Q_{ab} and Q_{34} are the heat transferred during the isomagnetic heating (a-b-I-II and 3-4-I-III in Fig. 3.8 right). The heat discarded, Q_{discard} (d-e-II-IV) is equal to the net work input as written in Eq. 3.6. The smallest temperature difference during heat exchange is smallest out of the temperature difference between state points 3 and d, $\Delta T_{3\mathrm{d}}$, a and 2, $\Delta T_{\mathrm{a}2}$, 4 and c, $\Delta T_{4\mathrm{c}}$, and d and 1, $\Delta T_{\mathrm{d}1}$. When the temperature difference in which the heat is circulated ($|T_{\mathrm{set}} - T_0|$) is small, the minimum temperature difference during heat exchange, ΔT_{min}, is approximately equal to double value of

adiabatic temperature change, ΔT_{ad}, obtained by MCE.

$$\Delta T_{ad} \approx 2\Delta T_{min} \tag{3.12}$$

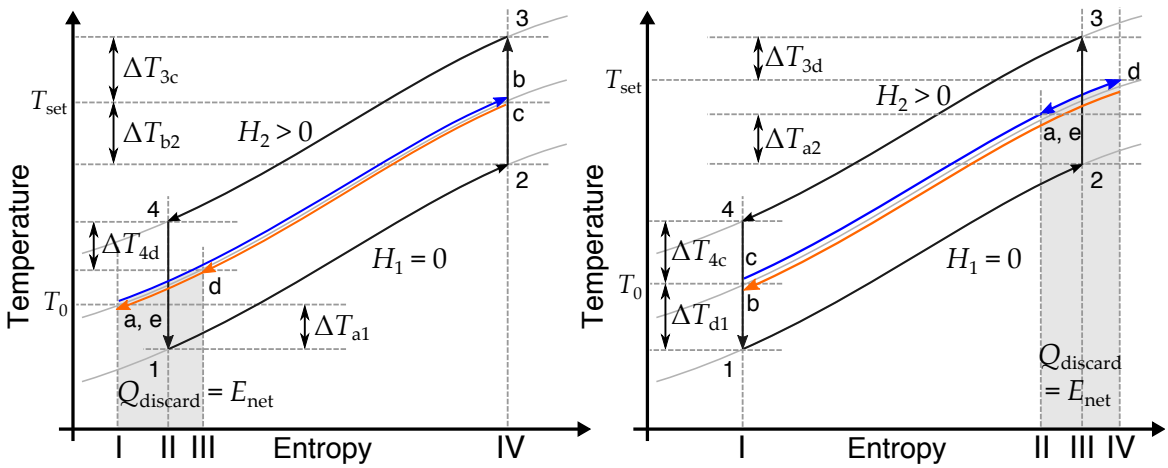

Figure 3.8: Temperature-entropy diagram of magnetocaloric heat circulator for non-magnetocaloric process streams for heating process (left) and cooling process (right)

The magnetization and demagnetization is assumed to be completely adiabatic. Irreversibility during these process is caused by hysteresis loss and electromagnetic induction heating. The effect of these causes are discussed in subsection 3.3.2.

3.3.2 Irreversibility associated with magnetocaloric effect

In subsection 3.3.1, the cycle of magnetocaloric heat circulator for magnetocaloric and non-magnetocaloric process stream has been evaluated in terms of temperature-entropy diagram. The magnetization/demagnetization was assumed as a complete adiabatic processes. However, in actuality, magnetization and demagnetization is not completely reversible and some amount of irreversibility is created. In a process that uses compressors and expanders, adiabatic efficiency, η, is often used to quantify the irreversibility during compression and expansion. For magnetization and demagnetization, the two factors

that result in irreversibility are hysteresis loss [82] and electromagnetic induction heating (eddy current) [83].

Losses due to hysteresis are inherent to the magnetic material, thus depends on the material and the temperature range in which the magnetic material subjected to magnetic field variation. The excess magnetic work needed to bring the material back to its original condition will result in production of heat. It is known that materials that undergoes a first-order transition has hysteresis. It is known that generally, the more pure and the more refined the micro structure of the solid, less hysteric the phase transition would be [84]. Material that undergoes a second-order transition generally does not show hysteresis. Dan'kov measured the hysteresis of a well known benchmark material for room temperature MCE, Gd, as close to zero [48].

Since the MCE is caused by subjecting a magnetic material through field variation, eddy current, which is also caused by field variation is inevitable. The eddy current caused by electromagnetic induction heating, causes joule heating due to the electric resistance, r, of the magnetocaloric material. The electromotive force, ϵ_{EI}, is decided by the rate of magnetic flux, Φ, that goes through the magnetic material over time, t. If we assume area that the magnetic material cuts the magnetic flux as A, the following equation is known,

$$\epsilon_{\mathrm{EI}} = A\frac{d\Phi}{dt} \tag{3.13}$$

From Equation 3.13, it can be seen that in order to reduce the electromotive force, ϵ_{EI}, two method can be thought of. 1) Reducing the time differential of magnetic flux, Φ, over time, t and 2) reducing the area, A, in which the magnetic material cuts the magnetic flux.

The eddy current, j, and the resistance, r, of the magnetic material results in joule heating, Q_{joule}

$$\begin{aligned} Q_{\mathrm{joule}} &= rj^2 \\ &= \frac{\epsilon_{\mathrm{EI}}^2}{r} \end{aligned} \tag{3.14}$$

From Equation 3.14, it can be seen that the amount of heat created by joule heating, Q_{joule},

is proportional to the electromotive force, ϵ_{EI}, squared. Thus, considering the fact that most of the magnetic materials are metals and have small electric resistance, r, if the size of the magnetic material is small and the magnetic field is varied slowly, the amount of heat created by joule heating can become negligible.

In order to handle the irreversibility during magnetization and demagnetization in a thermal process as it was handled using compressors and expanders, adiabatic efficiency, η_{total}, is set. The adiabatic efficiency is a product of efficiency due to hysteresis loss, η_{hyst}, and eddy current, η_{eddy} and can be written as,

$$\eta_{\mathrm{total}} = \eta_{\mathrm{hyst}}\eta_{\mathrm{eddy}} \tag{3.15}$$

The adiabatic efficiency for magnetization and demagnetization, η_{total}, is ratio of the amount of work needed for an adiabatic process, W_{ad}, and for an irreversible process, W_{ir}

$$\eta_{\mathrm{total}} = \frac{W_{\mathrm{ir}}}{W_{\mathrm{ad}}} \tag{3.16}$$

Kitanovski and Egolf estimated the adiabatic efficiency for magnetizing and demagnetizing Gd near room temperature as 0.97 for hysteresis loss, η_{hyst}, and 0.95 for eddy current, η_{eddy}, [85]. Thus,

$$\eta_{\mathrm{total}} = \eta_{\mathrm{hyst}}\eta_{\mathrm{eddy}} \approx 0.92 \tag{3.17}$$

The adiabatic efficiency value used by Kitanovski and Egolf is a value assumed for a single condition and can vary depending on the operating condition and material. Thus, it is needed to estimate the efficiency for each evaluating process.

3.4 Performance evaluation of magnetocaloric heat circulator

3.4.1 Simulation method

To understand the energy saving potential of a magnetocaloric heat circulator, the net energy consumption, E_{net}, and the amount of heat circulated, Q_{cir}, is calculated using the temperature-entropy diagram as explained in section 3.3. The initial environmental temperature, T_0, the set temperature, T_{set}, and the minimum temperature difference needed for heat exchange, ΔT_{min}, is set. The net work, E_{net}, needed to circulate the heat between the environmental temperature, T_0, and the set temperature, T_{set}, with the minimum temperature difference, ΔT_{min} is calculated when the process stream is magnetocaloric.

Similarly, the circulated heat, Q_{cir}, and the net work, E_{net}, needed for magnetocaloric heat circulator for non-magnetocaloric material is calculated. The temperature difference needed for heat exchange, ΔT_{HEX}, between the magnetocaloric working material and the non-magnetocaloric process stream is set to ΔT_{min}.

In order to calculate the entropy, S, of a magnetocaloric material at a given temperature, T, and magnetic field, H, mean field model was used [38]. The obtained energy consumption has been compared with a benchmark process with a feed-effluent heat exchanger (Fig. 1.6).

In a self-heat recuperative process, the amount of heat circulated, Q_{cir}, is equal to the required heat of the process stream to reach the set state, Q_{process}. The energy consumption of the thermal processes were evaluated using the evaluation factor, $Q_{\text{process}}/E_{\text{net}}$. Furthermore, the obtained value is compared with the minimum exergy destruction for thermal processes, A_{min}.

Mean-field model of a magnetocaloric material

In order to derive the isothermal entropy change, ΔS_{ad}, it is needed to know the magnetization, M. It is known from the mean-field model approximation, the magnetization,

M, of a magnetic material can be written as [70],

$$M = N_{\mathrm{s}} J g_{\mathrm{J}} \mu_{\mathrm{B}} B_J(X) \tag{3.18}$$

where N_{s} denote the number of atoms per unit volume of the magnetic material, J denote the total angular momentum, g denote the spectroscopic splitting factor and μ_{B} denote the Bohr magneton (= 9.274 009 15(23) $\times 10^{-24}$ [J T^{-1}]). The Brilliouin function, $B_J(X)$,is defined as,

$$B_J(X) = \frac{2J+1}{2J} \coth\left(\frac{2J+1}{2J} X\right) - \frac{1}{2J} \coth\left(\frac{X}{2J}\right) \tag{3.19}$$

X is expressed as follows,

$$X = \frac{g \mu_B \mu_0 H_{\mathrm{eff}} J}{k_B T} \tag{3.20}$$

where k_B denote the Boltzmann constant (= 1.380 6488(13)$\times 10^{-23}$ [J K^{-1}]), μ_0 denote the magnetic permeability of vacuum (= $4\pi \times 10^{-7}$ [H m^{-1}]) and H_{eff} denote the effective magnetic field, which is,

$$H_{\mathrm{eff}} = H + \frac{3\theta_C B_J(X) k_B}{\mu_B g_{\mathrm{J}} (J+1)} \tag{3.21}$$

from Eq. 3.20 and Eq. 3.21, we have

$$X = \frac{g \mu_B \mu_0 H J}{k_B T} + \frac{3 J \theta_{\mathrm{C}} B_J(X)}{T(J+1)} \tag{3.22}$$

It is possible to derive the magnetization, M, of a magnetic material using Eq. 3.19 and Eq. 3.22. If we rewrite

$$x = \frac{J+1}{3J} X \tag{3.23}$$

then, Eq. 3.19 and Eq. 3.22 can be rewritten as,

$$B_J(X) = \tfrac{2J+1}{2J} \coth\left(\tfrac{3}{2} \tfrac{2J+1}{2J} x\right) - \tfrac{1}{2J} \coth\left(\tfrac{3}{2} \tfrac{1}{2J} x\right) \tag{3.24}$$

$$B_J(X) = \tfrac{T}{\theta_{\mathrm{C}}} x - \tfrac{H}{N_{\mathrm{W}} M_0} \tag{3.25}$$

where N_W is the mean field constant,

$$N_{\mathrm{W}} = \frac{3\theta_C k_B}{(J+1) g \mu_B \mu_0 M_0} \tag{3.26}$$

$M_0(= gJ\mu_B N_s)$ is the magnetic moment of the magnetic material at absolute zero. Eq. 3.24 and Eq. 3.25 suggests that x can be derived as the node of Brilliouin function and line with gradient T/θ_C and intercept of $H/(N_W M_0)$. From 3.18, the Brilliouin function, $B_J(X)$ and magnetization, M, is proportional. It can be seen from Fig. 3.9 that at constant magnetic field, H, when the ratio of temperature, T, becomes larger, the gradient of the line becomes larger, resulting in magnetization, M, becoming smaller. At constant temperature, T, the larger magnetic field, H, will mean smaller intercept, resulting in larger magnetization, M.

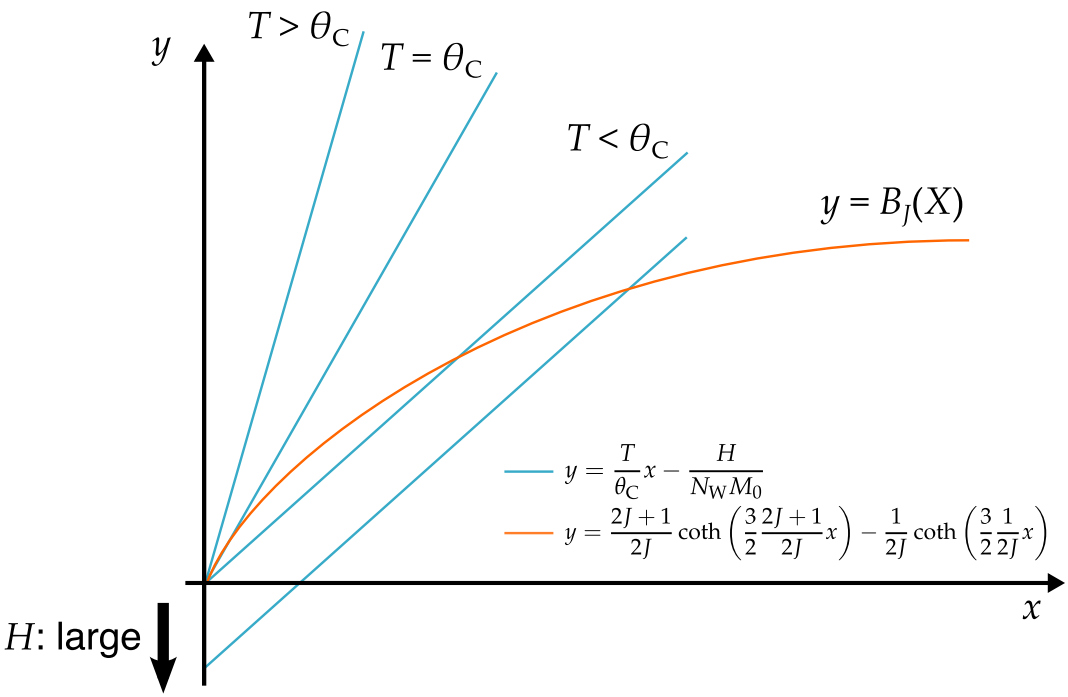

Figure 3.9: The node of Brilliouin function and line with varied gradient and intercept

From Eq. 1.12, Eq. 3.24 and Eq. 3.25, the magnetic entropy, S_M, can be derived as,

$$S_M(T,H) = R\left[\ln\sinh\left(\frac{2J+1}{2J}X\right) - \ln\sinh\left(\frac{X}{2J}\right) - XB_J(X)\right] \tag{3.27}$$

where $R(= RN_A)$ is the gas constant (= 8.314 4621(75) [J K^{-1} mol^{-1}]).

The entropy of the lattice, S_L, can be calculated using the Debye temperature, θ_D

as [38],

$$S_{\mathrm{L}}(T) = -3R\ln\left(1 - e^{-\frac{\theta_{\mathrm{D}}}{T}}\right) + 12R\left(\frac{T}{\theta_{\mathrm{D}}}\right)^3 \int_0^{\frac{\theta_{\mathrm{D}}}{T}} \frac{x^3 dx}{e^x - 1} dx \tag{3.28}$$

Finally, the entropy of the electron, S_{E} is calculated with the electron heat capacity coefficient γ,

$$S_{\mathrm{E}}(T) = \gamma T \tag{3.29}$$

the total entropy, S_{total}, is the sum of the three entropies (Eq. 1.6).

Fig. 3.10 shows the temperature-entropy diagram calculated using the mean-field approximation for gadolinium. It can be seen that around the Curie temperature, θ_{C}, of the magnetocaloric material (293 K for gadolinium), the entropy difference is larger compared to other temperature regions. Fig. 3.11 shows the isothermal entropy change, ΔS_{M}, of gadolinium when magnetic field is varied to different magnetic fields. It can be seen that the isothermal entropy change, ΔS_{M}, is proportional to the magnetic field. Fig 3.12 shows the comparison of the adiabatic temperautre difference, ΔT_{ad}, when magnetic field subjected to gadolinium was varied from 0 tesla to 1 tesla for the calculated value using the Mean Field Theory and the value measured by Benford and Brown [50]. IIt can be seen that the mean field theory has somewhat caught the behavior of the temperautre change in the vicinity of Curie temperautre of Gd.

The heat capacity of the magnetic material can be calculated by the following equation,

$$C_{H,p} = T\left(\frac{\partial S}{\partial T}\right)_{H,p} \tag{3.30}$$

Fig. 3.13 shows the heat capacity of Gd at constant magnetic field, H, and pressure, p, calculated using the mean-field model. It can be seen that the heat capacity changes rapidly near the Curie temperature, θ_{C}, of gadolinium. The gradient near the Curie temperature gradually decreases as the strength of magnetic field, H, rises. Comparing the value obtained for the heat capacity of gadolinium and the measured value by Dan'kov *et al.* [48] it can be seen that the calculated value is fairly in good agreement with the measured value,

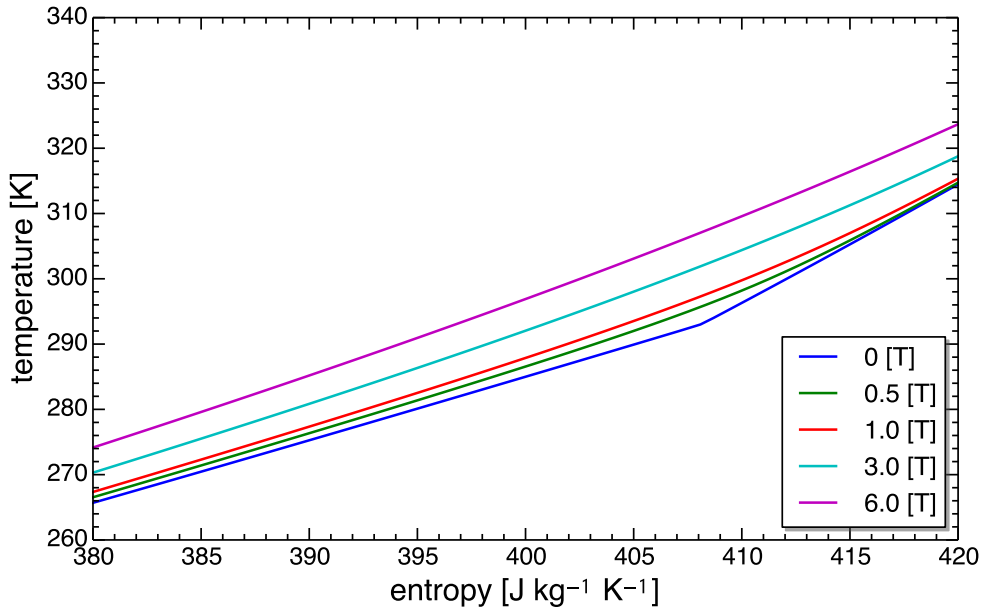

Figure 3.10: Temperature-entropy diagram calculation of Gd subjected to various magnetic fields

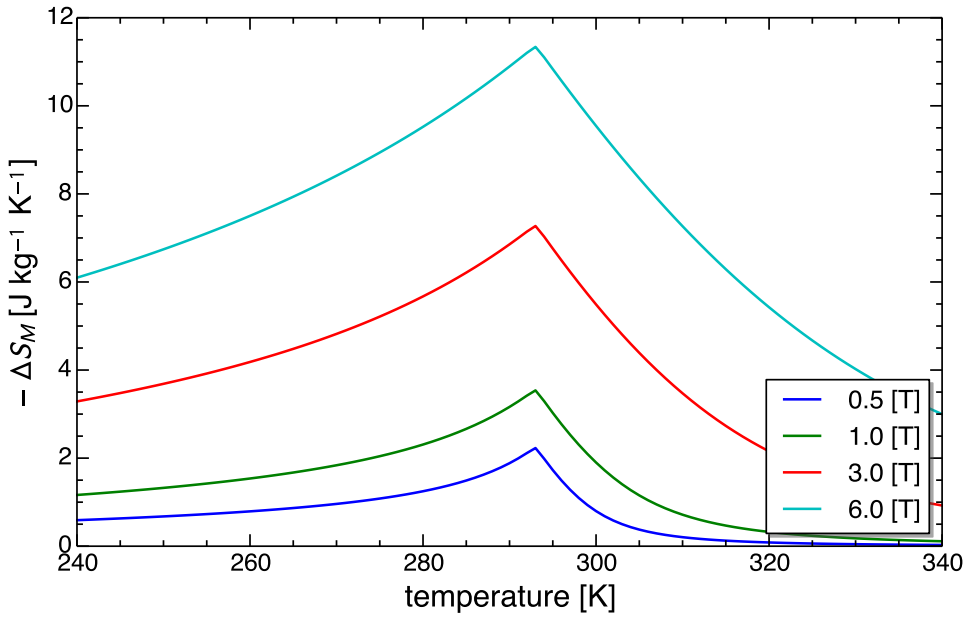

Figure 3.11: Isothermal entropy change, ΔS_{M}, of Gd subjected to various magnetic fields

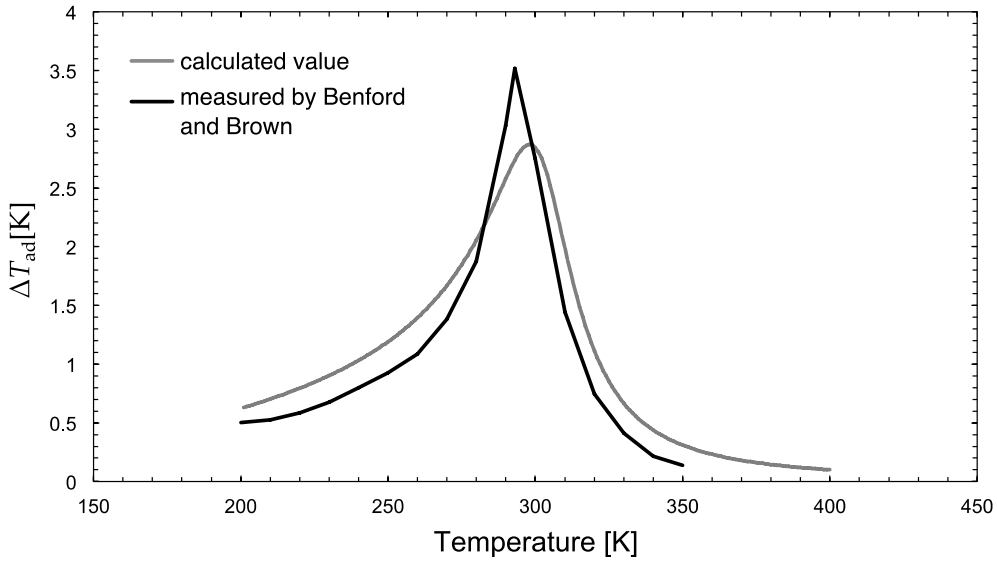

Figure 3.12: The comparison of the adiabatic temperautre difference, ΔT_{ad}, when magnetic field subjected to gadolinium was varied from 0 tesla to 1 tesla for the calculated value using the Mean Field Theory and the value measured by Benford and Brown

although it cannot reproduce the rapid rise of heat capacity at the Curie temperature.

Table 3.1 shows the parameters of major ferromagnetic materials that is needed for calculation using the mean-field model.

3.4.2 Simulation conditions

Simulation to evaluate the theoretical energy consumption has been performed under four different conditions; two for magnetocaloric process stream cases and two for non-magnetocaloric process stream case using the temperature-entropy diagram. Gd was chosen as the magnetocaloric material for all cases because its physical properties are well known [48]. Water was chosen as the non-magnetocaloric process material and its heat capacity, c_f, was assumed constant. The initial environmental temperature, T_0, was set to 298.15 K, initial magnetic field, μH_1, was set to 0 T where μ is the magnetic permeability. The pressure, p, was assumed to be 1 [atm] throughout the process. The minimum temperature difference needed for heat exchange, ΔT_{min}, was set to 2 K. It was assumed

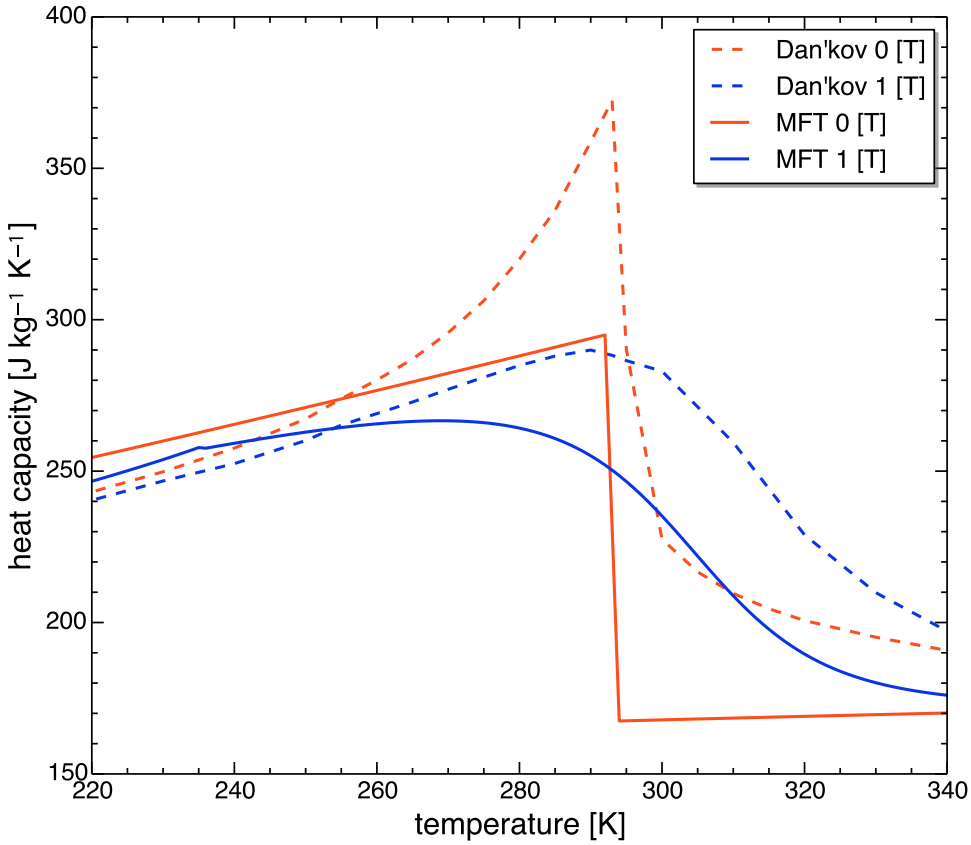

Figure 3.13: Heat capacity of Gd at constant magnetic field, H, and pressure, p, calculated using the mean-field model

Table 3.1: Parameters of major ferromagnetic materials

		Gd	Ni	Fe	Co
g	[-]	2	2	2	2
J	[-]	3.5	0.3045	1.4	0.95
θ_C	[K]	293	631	1043	1403
θ_C	[K]	184	385	420	375
γ	[mJ mol^{-1} K^{-2}]	6.38	7.04	4.90	4.40

that no heat is lost during the heat exchange and all of the heat removed from the effluent process stream is transferred to the feed process stream. Adiabatic efficiency during magnetization and demagnetization is assumed as adiabatic process (subsection 3.3.2).

When Gd is the process material, commencing from environmental temperature, T_0, the temperature of the process material is raised to 308 K (case 1), and 318 K (case 2). Similarly, when water is the process material, commencing from environmental temperature, T_0, the temperature of the process material is raised to 308 K (case 3) and 318 K (case 4) while Gd recuperates the process heat. The simulation conditions are shown in Table 3.2 and Table 3.3. Each energy consumption obtained for magnetocaloric heat cir-

Table 3.2: Simulation conditions for evaluating magnetocaloric heat circulator

environmental temperature	T_0	[K]	298.15
initial magnetic field	μH_1	[T]	0
pressure	p	[atm]	1.0
minimum temperature difference during heat exchange	ΔT_{min}	[K]	2.0

Table 3.3: Process material and set temperature, T_{set}, for different simulation cases

case	process material	T_{set} [K]	temperature change [K]
1	Gd	308.15	+10
2	Gd	318.15	+20
3	Water	308.15	+10
4	Water	318.15	+20

culator has been compared with the energy consumption using the benchmark process with feed-effluent heat exchanger under the same conditions.

3.4.3 Simulation results and discussion

Simulation results are shown in Table 3.4. Note that the minimum temperature different needed for heat exchange for calculating the minimum exergy destruction, A_{loss}, for case 3 and 4 has been doubled. It can be seen that compared to the benchmark process with feed-effluent heat exchanger, by applying a magnetocaloric heat circulator energy saving of 80-95% can be obtained. Larger energy consumption was needed for process with non-magnetocaloric process material compared to process with magnetocaloric process material because larger magnetic field is needed to ensure the minimum temperature difference needed for heat exchange, ΔT_{min}. Also, in cases where the process stream is non-magnetocaloric, exergy destruction occurs in the two heat exchange opposed to cases where the process stream is magnetocaloric, exergy destruction occurs in only one heat exchange. The temperature difference during heat exchange and the amount of heat is approximately the same in the two HEXs for non-magnetocaloric process material case and the HEX for magnetocaloric process material case, hence, the exergy destruction will double for non-magnetocaloric process material case. The result of the table is summarized in Fig. 3.14.

The energy consumption in magnetocaloric heat circulator increases as the set temperature, T_{set}, moves further from the Curie temperature, θ_{C}, of the magnetocaloric material. This is because the adiabatic temperature change, ΔT_{ad}, becomes smaller as the temperature furthers from the Curie temperature, θ_{C}, thus larger magnetic field, μH_2, is needed to ensure the minimum temperature difference needed for heat exchange in the HEXs. Nevertheless, large reduction in energy consumption can be expected.

If the magnetization and demagnetization is an adiabatic process, the area surrounded by the isomagnetic lines (Fig. 3.7; 3-4-5-6) is equal to the net work needed for heat circulation (Fig. 3.7; 6-7-a-b). This indicates that the temperature difference during heat ex-

Table 3.4: Comparison of strength of magnetic field, μH; total energy consumption, E_{net} of magnetocaloric heat circulator and benchmark process. Value is compared with minimum exergy destruction, A_{min}

		magnetocaloric heat circulator			benchmark process		
case	Q_{process}	μH_2	E_{net}	$E_{\text{net}}/Q_{\text{process}}$	E_{net}	$E_{\text{net}}/Q_{\text{process}}$	$A_{\text{min}}/Q_{\text{process}}$
	[J cycle^{-}1]	[T]	[J cycle^{-}1]	[%]	[J cycle^{-}1]	[%]	[%]
1	1680	1.35	21.8	1.3	336.5	20.0	0.75
2	3366	1.93	35.9	1.1	320.0	9.51	0.65
3	41286	2.10	861	2.1	8360	20.2	1.4
4	82073	2.98	1517	1.8	8350	10.17	1.3

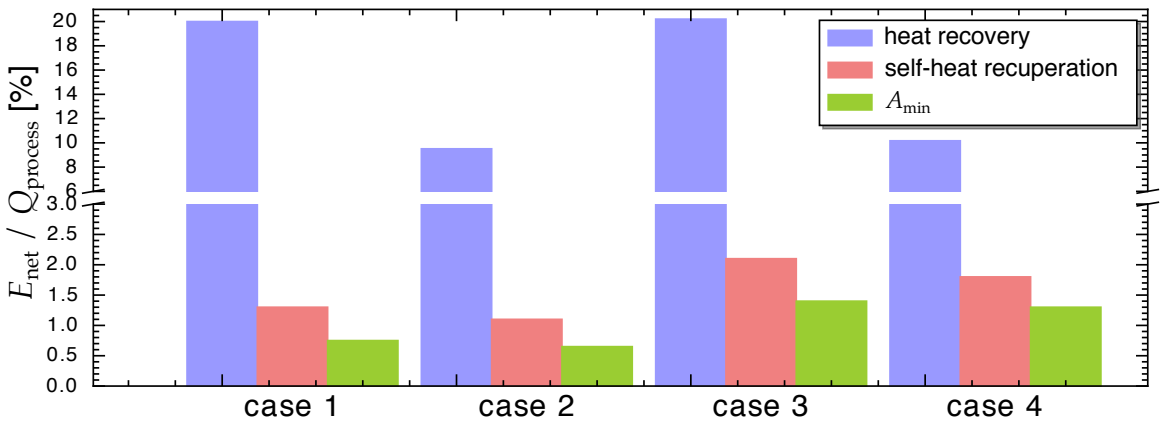

Figure 3.14: Comparison of energy consumption between benchmark process, self-heat recuperative process and minimum exergy destruction

change, ΔT_{min}, is proportional to the net work needed for heat circulation. E_{net}. Smaller temperature difference during heat exchange will result in slower heat transfer, but will result in smaller exergy destruction due to heat exchange and thus smaller energy consumption. Also temperature difference is preferred small in the perspective of magnetic field, because it is difficult to create strong magnetic field using permanent magnets and extra energy will be consumed due to joule heating if electromagnets are used.

The effect of irreversibility during magnetization and demagnetization process has been discussed in subsection 3.3.2. Due to the temperature gradient of the magnetocaloric working material, the local magnetic permeability of the material may vary largely. Thus, factor that should be taken into account is the demagnetization effect. It is also known that the demagnetization effect tends to take place at a lower field below 2 T [86]. Since the demagnetization effect is dependent on geometry and non-uniform properties of the magnetic material, thus needs to be taken into account when designing the actual device.

When the process material is magnetocaloric, though there are some research performed using magnetocaloric particles in suspension (i.e. ferrofluid and MR fluid) [87], the process material is likely to be solid. If this is the case, it will be difficult to flow the process material and exchange heat in counterflow. For the process material heat to be circulated, a working fluid will be needed as shown in Fig. 3.15. Minimum temperature difference needed for heat exchange, ΔT_{min}, is needed for counterflow heat transfer in the two HEXs. Thus, doubling the exergy destruction due to heat exchange and also doubling the total net work input, E_{net}.

Different cycle patterns

Two patterns for processes with set temperature, T_{set}, above the environmental temperature, T_0, can be presumed depending on the temperature at which the magnetization and demagnetization takes place and similarly, two patterns for processes with set temperature, T_{set}, below the environmental temperature, T_0, can be presumed (Fig. 3.16). Patterns 1 and 2 are processes with set temperature, T_{set}, above environmental temper-

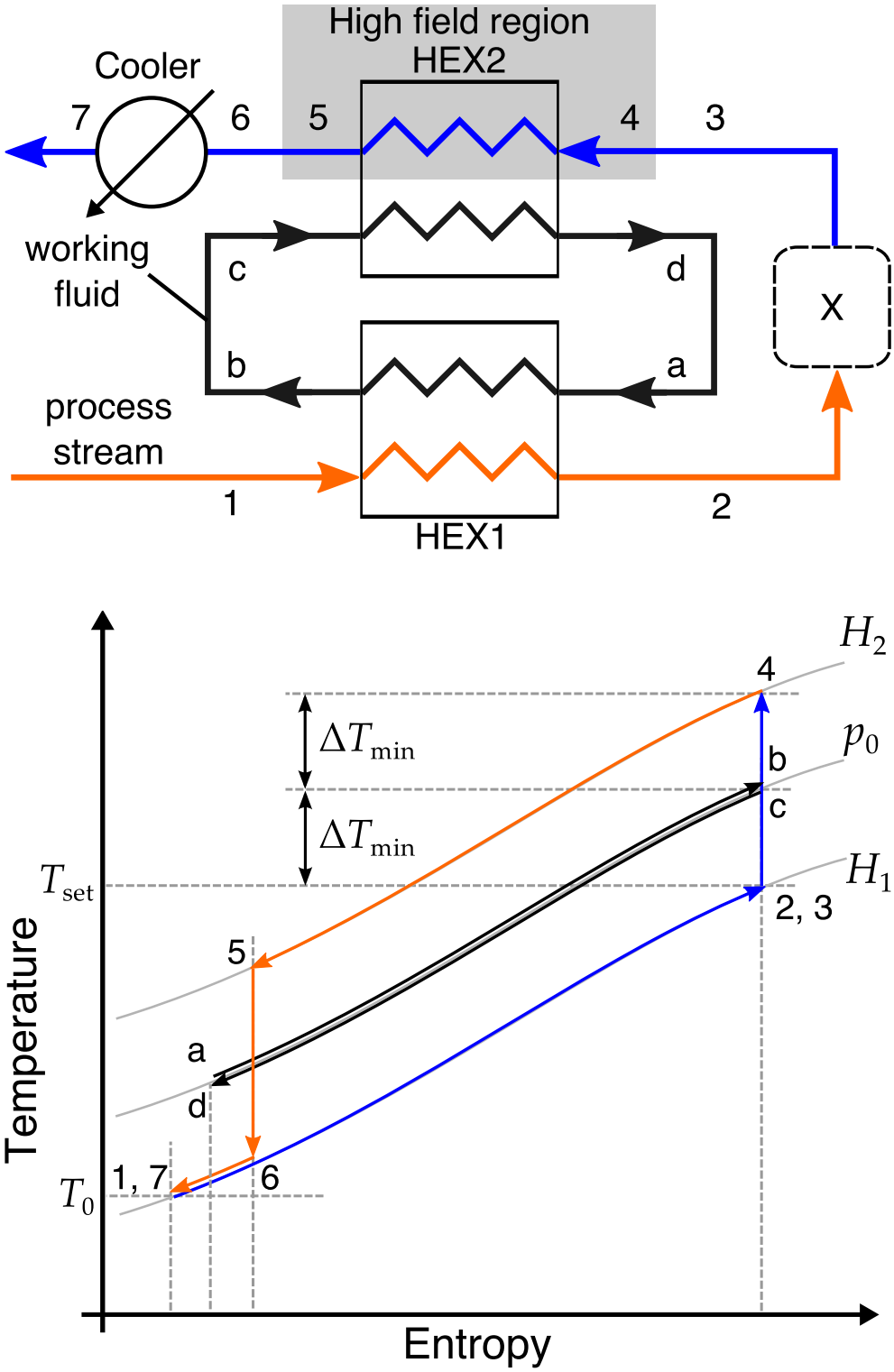

Figure 3.15: Process flow diagram (top) and temperature − entropy diagram (bottom) of a magnetocaloric heat circulator when process material is a magnetocaloric solid and working fluid is used to transfer heat

ature, T_0. In pattern 1, the temperature difference is larger between state points 4 and 2 than that between state points 5 and 1 ($\Delta T_{42} > \Delta T_{51}$). In this case, the minimal temperature difference is ΔT_{51}. On the contrary, in pattern 2, the temperature difference is larger between state points 5 and 1 than that between state points 4 and 2 ($\Delta T_{51} > \Delta T_{42}$). Hence, the minimal temperature difference is ΔT_{42}. A similar discussion can be made processes with set temperature, T_{set}, below environmental temperature, T_0, where the minimal temperature difference is the temperature difference between state points 3 and 5, ΔT_{35}, for pattern 3 and the temperature difference between state points 2 and 6, ΔT_{26}, for pattern 4. The magnetic flux density is determined such that the smallest temperature difference is larger than the minimum temperature difference required for heat exchange, ΔT_{min}. In all cases, the net work input, E_{net}, is equal to the energy discarded at the cooling water, Q_{discard}. All conditions calculated are categorized as pattern 2 because the adiabatic temperature difference, ΔT_{ad}, decreases with distance from the Curie temperature, θ_{C}, which is at 293.15 K for Gd. In actuality, magnetocaloric material with optimal Curie temperature in between the magnetizing and demagnetizing temperature will need to be chosen in order to satisfy the minimum temperature difference required for heat exchange with limited magnetic flux density.

Comparison with an ideal process

In section 2.2.4, the theoretical minimum exergy destruction during heat exchange was calculated for Nitrogen at 1 [atm]. Similarly, the theoretical minimum exergy destruction during heat exchange for magnetocaloric material can be calculated. The condition that is required to obtain the theoretical minimum exergy destruction during heat exchange is as follows.

$$C'_{H,p}\left(T, p, H\right) = C_{H,p}\left(T + \Delta T_{\mathrm{min}}, p, H\right) \tag{3.31}$$

From Eq. 2.20 and Eq. 2.21, the theoretical minimum entropy generation, ΔS_{gen}, and the theoretical minimum exergy destruction, A_{min}, can be calculated.

Fig. 3.17 shows the temperature-entropy diagram of theoretical minimum exergy de-

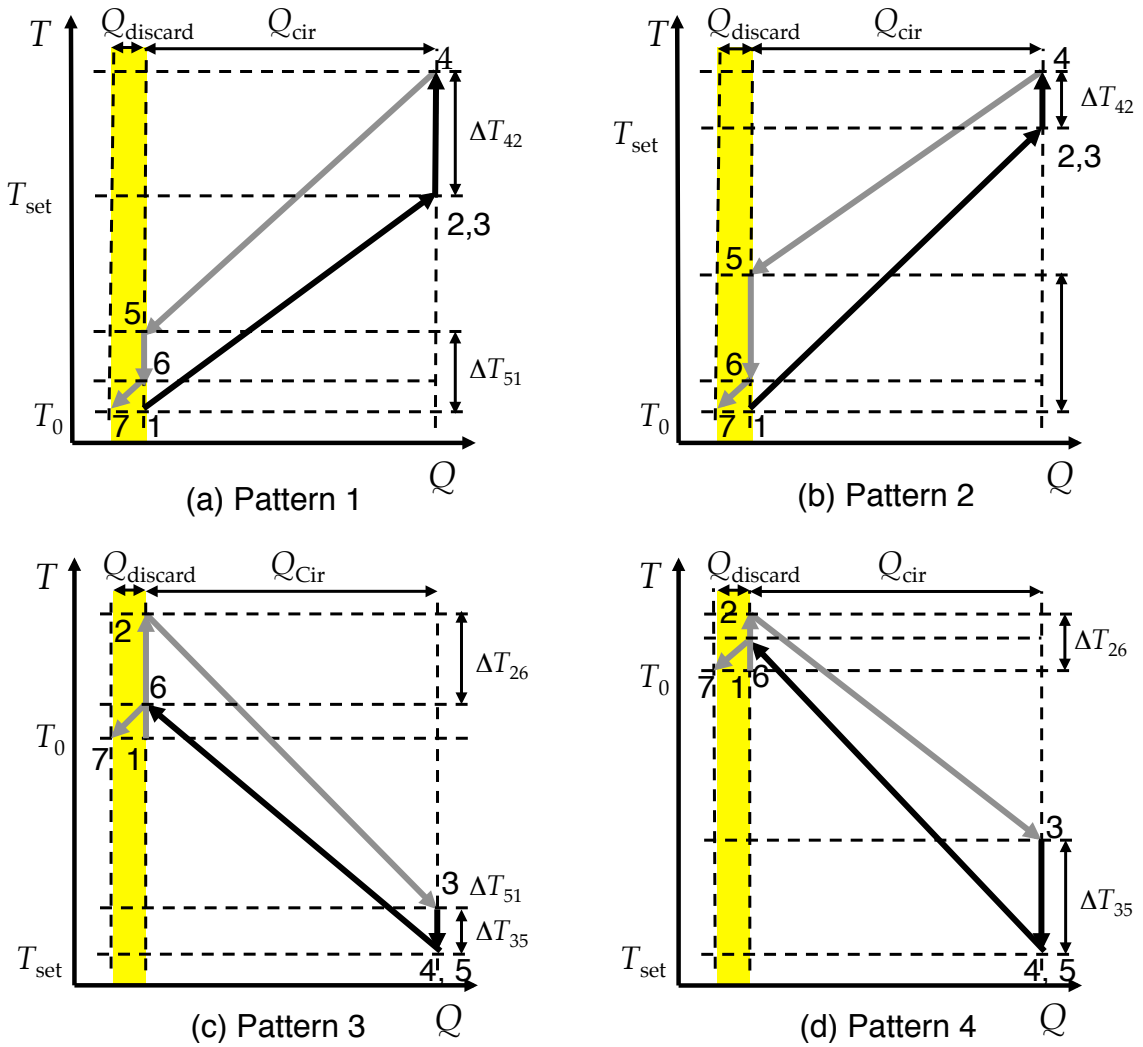

Figure 3.16: Temperature-heat diagrams of different magnetocaloric heat circulator patterns. Pattern 1 and 2 are processes with set temperature, T_{set}, above the environmental temperature, T_0, and pattern 3 and 4 are processes with set temperature, T_{set}, below the environmental temperature, T_0

struction for Gd at 1 T during heat exchange when the minimum temperature difference during heat exchange, ΔT_{min}, is set to 2 K and temperature-entropy diagram of magnetocaloric heat circulator for magnetocaloric process material when heat is circulated between 298.15 K and 318.15 K (case 2). It can be seen that compared to the case when the temperature difference during heat exchange is fixed to 2 K throughout the heat exchange, heat is exchanged at a larger temperature difference for the magnetocaloric heat circulator, resulting in extra exergy destruction.

When the same amount of heat is being circulated for the ideal case (i.e. $Q_{\mathrm{cir}} = 3366$ J kg^{-1}), the theoretical minimum exergy destruction, A_{min}, when the temperature difference during heat exchange, ΔT_{min}, is set to 2 K is 21.8 J kg^{-1} and the cold process stream temperature is changed from 298.15 to 318.15. Compared to the minimum exergy destruction during heat exchange case, about 1.6 times amount of net input work, E_{net}, is needed for heat circulation in magnetocaloric heat circulator ($E_{\mathrm{net}} = 35.9$ J kg^{-1}). Larger difference between the minimum exergy destruction and the ideal case seen compared to the self-heat recuperative process for Nitrogen using compression (subsection 2.2.4) because Gd is subjected to differing magnetic field in the vicinity of Curie temperature, θ_{C}, where the specific change in heat capacity variation is observed. Thus, the isomagnetic lines furthers from parallel compared to vapor compression of Nitrogen.

In order to further reduce the exergy destruction during heat exchange in a magnetocaloric heat circulator, magnetic field gradient can be set so that Eq. 3.31 can be obtained.

It is possible to circulate the heat of incompressible process fluids using compression if the gaseous material was used as the working material as it was the case for using magnetocaloric materials. Fig 3.18 shows the comparison between heat circulators which use compression and magnetocaloric effect. The initial temperature, T_0, was set to 298.15 [K], set temperature, T_{set}, 318.15 [K] and the minimum temperature difference needed for heat exchange, ΔT_{min}, as 2.0 [K]. The process fluid was water for both cases while the working material for the magnetocaloric effect case was Gd and carbon dioxide for the

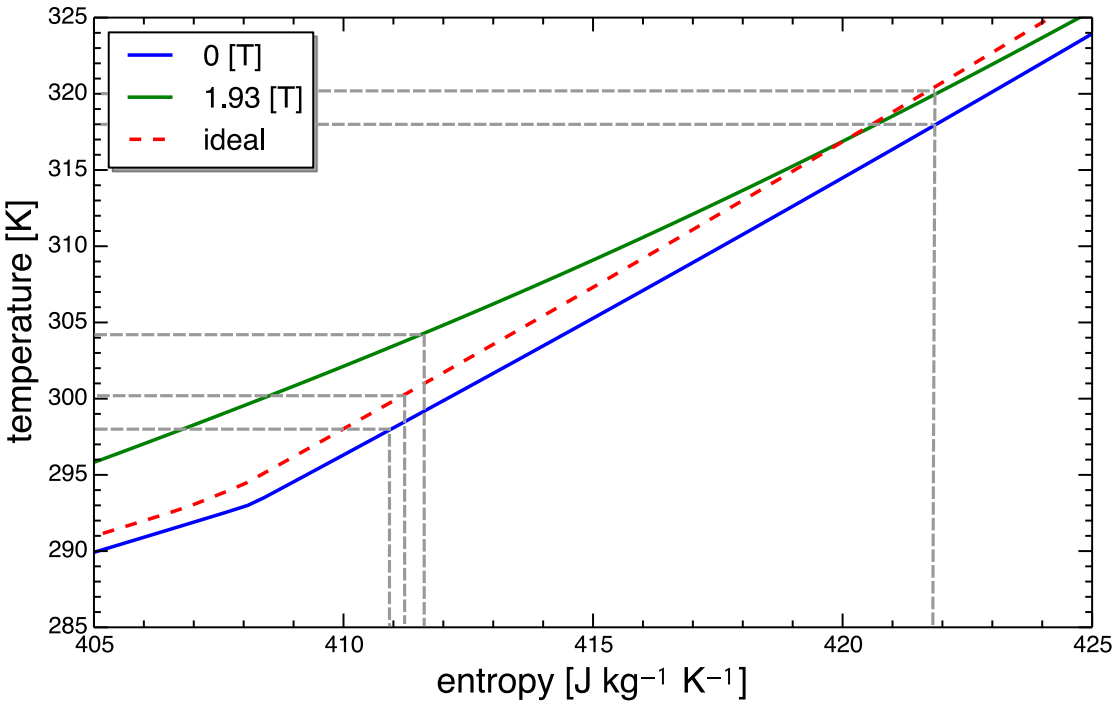

Figure 3.17: Temperature-entropy digram of theoretical minimum exergy destruction during heat exchange and magnetocaloric heat circulator

compressive case.

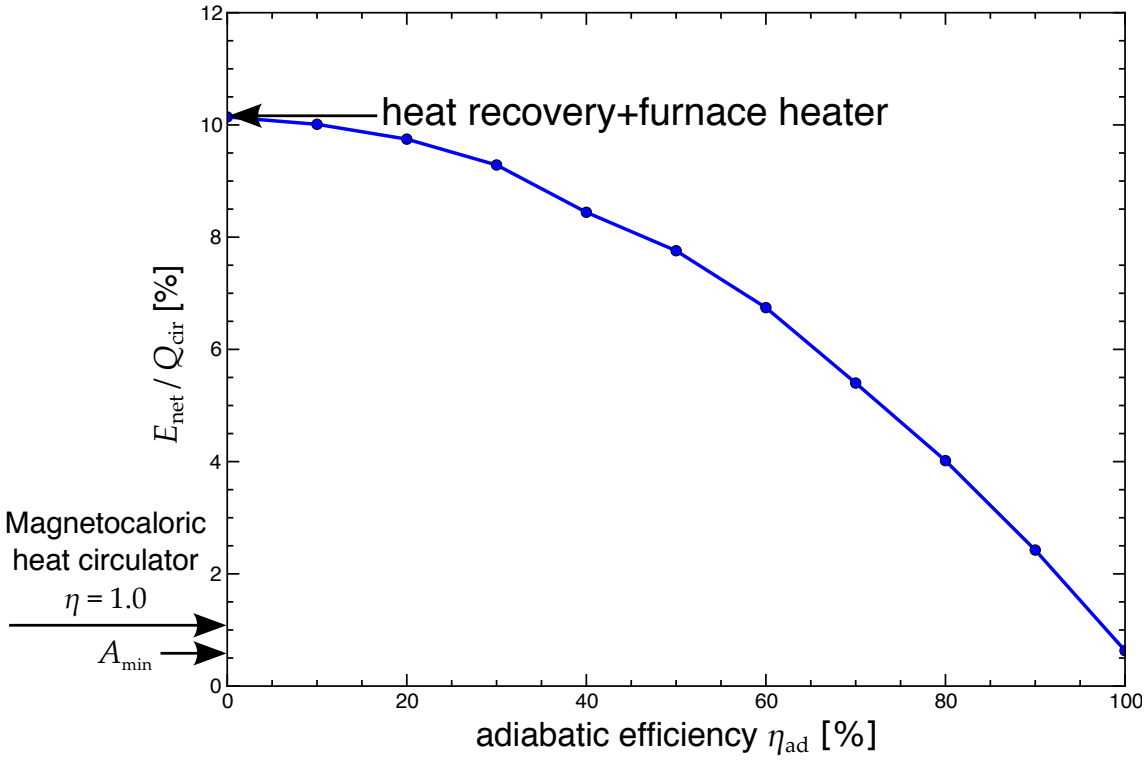

Figure 3.18: Comparison of heat circulators of using magnetocaloric effect and compressors at different adiabatic efficiency

From Fig. 3.18, it can be seen that although in the case for compressors, if the adiabatic efficiency is at 100%, the energy consumption is very close to the minimum exergy destruction due to heat exchange, A_{min}, already at around adiabatic efficiency of 95%, because the pressure applied to gain a temperature difference of 2 [K] is very small to affect the heat capacity of carbon dioxide, the energy consumption exceeds the energy consumption of a magnetocaloric heat circulator.

Magnetocaloric heat circulator and magnetic heat pump

Vast amount of research has been performed on the cycle analysis of magnetic heat pumps [88]. Kitanovski *et al.* has proposed new thermodynamic cycles so that further

efficiency can be gained from magnetic heat pumping [51]. Although heat pumps are well known to reduce the exergy destruction and energy consumption in thermal processes, often the heat capacity of the feed and effluent process stream do not match.

Fig. 3.19 shows the temperature-entropy diagram of a magnetic heat pump system when the heat is pumped from a heat source at T_c to heat sink at T_h. The magnetic heat pump system consist of a magnetocaloric material (1-2-3-4) and a working fluid (a-b-c-d). The temperature of the working fluid is raised (a $\rightarrow$ b) by receiving the heat from the magnetocaloric material (3 $\rightarrow$ 4). Then, the pumped heat, Q_h , is transferred to the heat sink (b $\rightarrow$ c). The remaining heat is transferred to the magnetocaloric material for regeneration (c $\rightarrow$ d, 1 $\rightarrow$ 2). After, heat, Q_c, is transferred from the heat source to the magnetocaloric material and comes back to its original state (d $\rightarrow$ a). In a magnetic heat pump, the heating capacity, Q_h, or the cooling capacity, Q_c, will be used to heat or cool the process material. In a magnetocaloric heat circulator, the process material heat is circulated.

In a magnetic heat circulator, the adiabatic temperature change, ΔT_{ad}, is equal to the larger out of the sum of ΔT_{3b}, ΔT_{bc} and ΔT_{c2} and ΔT_{4a}, ΔT_{ad} and ΔT_{d1}. While in a magnetocaloric heat circulator, the adiabatic temperature change, ΔT_{ad}, will be equal to the larger out of the sum of ΔT_{3b} and ΔT_{c2} and ΔT_{4a} and ΔT_{d1} because there are no heat load to be provided or to provide. This may be advantageous for cases when large magnetic field is difficult to produce.

3.5 Applications

A heat circulator is a system where the process stream heat can be circulated within. Unlike a heat pump where the heat is pumped in or pumped out of a process, the heat circulator can only be applied to processes where the heat can be circulated within. One example of an application is separation processes. Since separation itself does not involve reaction heat, the effect of applying self-heat recuperation is quite drastic. Fig. 3.20 shows

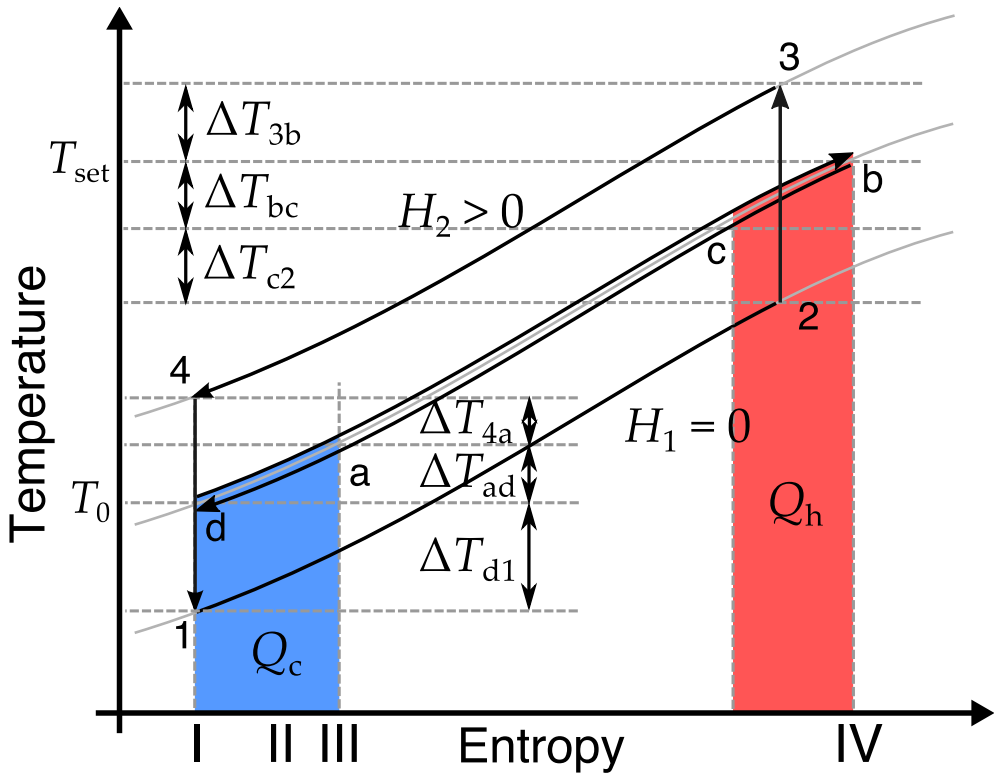

Figure 3.19: Temperature-entropy diagram of magnetic heat pump system

a schematic of a separation process. The feed process stream is cooled so that it is below the boiling point of one of its composing gas. If the separated gas at low temperature is needed for product, all of the energy has to be inserted, but it is often the case that after separation, the temperature of the process stream comes back up to the initial inlet temperature (i.e. for cryogenic air separation process for oxy-combustion, the oxygen is created at cryogenic temperature but is fed to the furnace at a higher temperature). If that is the case, the heat can be circulated by applying a heat circulator.

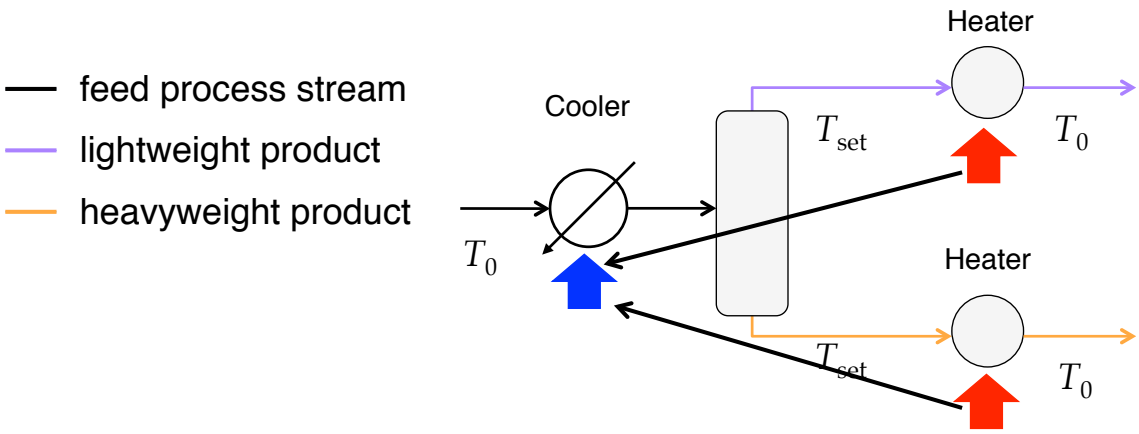

Figure 3.20: Schematic of a separation process

Fig. 3.21 shows the schematic image of a separation process where AMR heat circulator has been applied. The feed process steam can be split so that its heat capacity will match the effluent lightweight product and heavyweight product. Two beds will be needed for heat circulation of the two split streams.

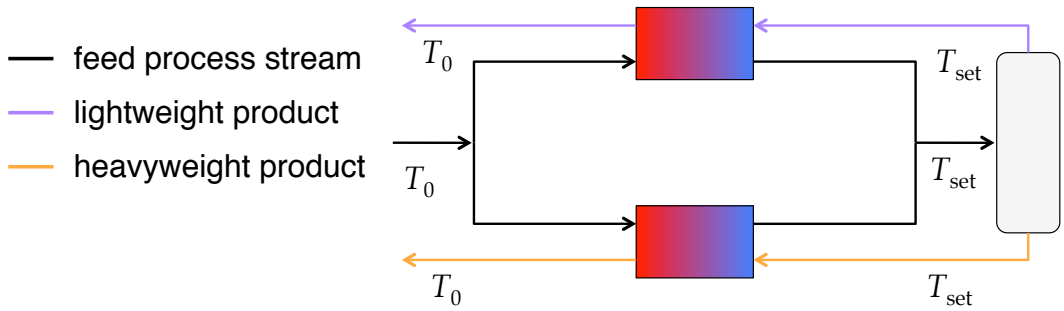

Figure 3.21: Schematic of a separation process where AMR heat circulator is applied

3.6 Conclusion

In this chapter a self-heat recuperative process that utilizes MCE for heat exergy recuperation is proposed. A system in which MCE is applied to self-heat recuperation is called magnetocaloric heat circulator. In a magnetocaloric heat circulator, magnetization and demagnetization is applied instead of compression and expansion. When magnetocaloric material is subjected to field variation, a reversible temperature change can be obtained, thus recuperating the heat carried by the magnetocaloric material. All process stream heat is recirculated inside the system without heat addition. It is shown that means to recuperate the process stream heat for heat circulation is not limited to compression and can be realized by enforcing a change of state by providing work.

The energy consumption and the ability of heat circulation of magnetocaloric heat circulator for magnetocaloric process material and non-magnetocaloric process material is analyzed in terms of temperature-entropy diagram. The results obtained were compared with a benchmark process with heat recovery, It was made clear that the total energy consumption can be reduced to 4.8-18.2% by applying the magnetocaloric heat circulator. Also, the energy consumption of a magnetocaloric heat circulator has been compared with the theoretical minimum exergy destruction during heat exchange when the minimum temperature difference during heat exchange, ΔT_{min}, is fixed. It was seen that exergy destruction in a magnetocaloric heat circulator is quite close to the theoretical minimum exergy destruction, A_{min}. The difference was due to the fact that magnetic field variation is subjected in the vicinity of the Curie temperature, θ_{C}, of the magnetocaloric material where specific large entropy change of magnetic spins can be observed.

Theoretical energy consumption for circulating heat of process stream using magnetocaloric materials as working materials where compared with case when gaseous material where used as working material. It was seen that the effect of adiabatic efficiency has large impact on the energy consumption when the temperature range in which the heat is circulated is small. This indicated that the magnetocaloric heat circulators maybe

applied to small size applications with small temperature range for heat circulation, due to its high adiabatic efficiency.

Although heat circulation is temperature is limited by the Curie temperature of the ferromagnetic material, the magnetocaloric heat circulator can be counted as one of the future options for energy saving in certain thermal processes.

Chapter 4

Conceptual design, mathematical model of AMR heat circulator

4.1 Introduction

The concept of applying MCE to a self-heat recuperative process has been proposed and its theoretical energy saving potential has been analyzed in Chapter 3. A process for magnetocaloric working material and non-magnetocaloric working material is proposed, but usually the process materials that we want to heat or cool is non-magnetocaloric. In this chapter, an active magnetic regenerative (AMR) heat circulator, which enables exergy recuperation for non-magnetocaloric process material is proposed. An AMR cycle is used to enable a quasi-counterflow heat exchange between the magnetocaloric working material and the process stream. A mathematical one-dimensional model is constructed to understand its thermal characteristics and its energy saving performance.

Initially, the concept of AMR has been presented by Brown as explained in subsection 1.4.3. In a magnetic heat pump that uses active magnetic regeneration, the regenerator made of magnetocaloric material works as a regenerator and for heat exergy recuperation. Many designs of magnetic heat pumps are proposed with difference magnetic field source, AMR configuration, and different magnetocaloric materials [44, 89].

In order to understand the thermal behavior and to implement the AMRR to applications, much effort has been put into transient modeling the device. Allab *et al.* built a simple one-dimensional model of a reciprocating AMR where the magnetocaloric material is a thin plate [90], in a model by Shir *et al.*, the dominating equation was divided for the magnetocaloric material and the fluid in the regenerator [91]. Siddikov *et al.* fitted the heat capacity and the entropy change of the magnetocaloric material to an equation so that it can be calculated from the temperature and the applied magnetic field [92]. Peterson *et al.* constructed a two-dimensional model [93], made a comparison with a one-dimensional model [94] and concluded that a one-dimensional model is insufficient to obtain the temperature profile and the energy consumption of an AMRR. Then, a three-dimensional model was made by Bouchard *et al.* for detailed understanding of the dynamics inside the regenerator bed. Instead of a three-dimensional model, Nielsen *et al.* included the parasitic thermal losses in a two-dimensional model [96]. Aprea and Maiorino [97] and Sarlah *et al.* [98], built a dimensionless model so that it is flexible and possible to compare different geometries and magnetocaloric materials. Kim and Jeong considered the impurity of the magnetocaloric material and implemented them into the model [99]. Park *et al.* included a third equation where the heat temperature evolution of the wall is included [100]. In the work by Rowe, a simple model where the overall energy balance of the AMRR can be obtained easily was presented [101, 102].

In all of the previous applications of the active magnetic regenerator, the use was for heat pumping, especially for refrigeration. The mathematical models were also made for heat pumping applications. In the AMR heat circulator proposed in this chapter, the AMRR is modified so that it can be used for heat circulating applications. Fig. 4.1 shows a schematic diagram of an active magnetic regenerator for heat pumping applications. In a magnetic heat pump, the device is closed and the heat pumping load is obtained from the heat exchanger at both ends. The heat that the working fluid receives from a heat source, Q_c is pumped utilizing the MCE of a magnetocaloric material. If an AMR heat pump was used to heat the process fluid at environmental temperature T_0, the pumped heat is given

to the process fluid at the hot heat exchanger as, Q_h, to reach its set temperature, T_{set}, for a particular application at X.

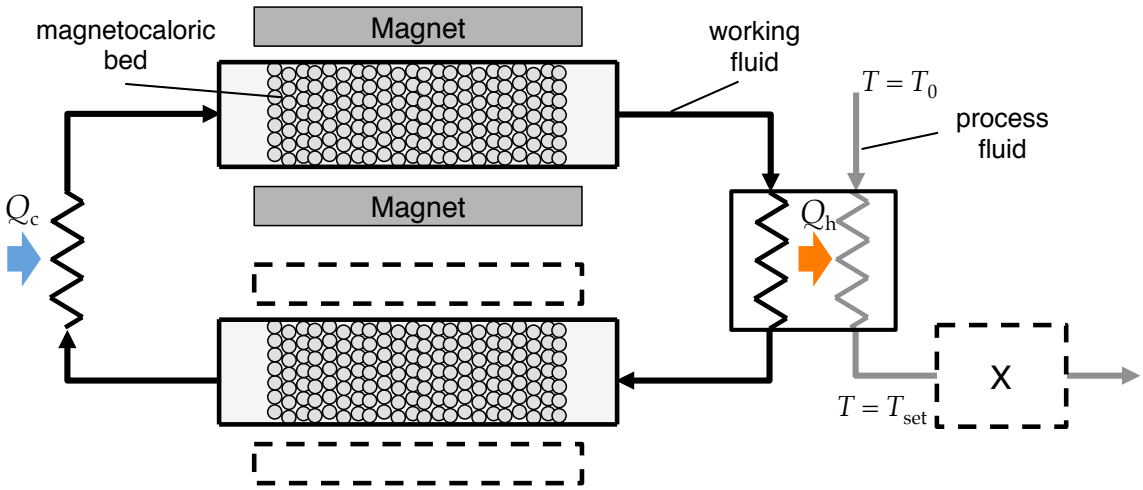

Figure 4.1: Schematic diagram of an active magnetic regenerative heat pump system

4.2 Active magnetic regenerative heat circulator

In an AMR heat circulator, the device is open so that the heat is transferred directly to the process stream as opposed to AMR heat pumps where the device was closed. The process stream itself runs through the magnetocaloric AMR bed. A heat pump pumps heat from a certain heat source to a certain heat sink, but the heat load and heat capacity of the process stream are often different from those of the pumped heat. Where in a heat circulator, the heat sink and the heat source is the process stream itself. Thus, the heat load and capacity of the process stream will always be close to equal, resulting in to smaller temperature difference throughout the heat exchange and reduction in exergy destruction.

Fig. 4.2 shows the schematic diagram of an AMR heat circulator for self-heat recuperation using MCE for non-magnetocaloric process materials. A magnetized bed of magnetocaloric material and a demagnetized bed of magnetocaloric material is set with temperature gradient so that both bed is hot on the right side of the figure and cold on the left side of the figure. The process stream enters the magnetized bed at environmental temperature, T_0, and receives heat from the magnetocaloric material so that it exits the bed at set temperature, T_{set}, for the next process X. Via the next process, the process stream at set temperature, T_{set}, enters the demagnetized bed where it gives its heat to the magnetocaloric material and is cooled close to environmental temperature, T_0. The same amount of heat received from the magnetized magnetocaloric material is given to the demagnetized magnetocaloric material. The process stream is cooled at the cooler to environmental temperature, T_0. Gradually, the temperature of the magnetized bed will decrease and the temperature of the magnetized bed will increase. After a certain period of time, the magnetized bed is demagnetized while the demagnetized bed is magnetized. The process fluid is always provided to the magnetized bed. From cyclically switching magnetization and demagnetization, quasi-counterflow heat exchange between the magnetocaloric working material and the process stream can be obtained and the process

stream heat can continuously be circulated.

Work is needed to demagnetize the magnetocaloric bed, w_{demag}, and part of the work can be recovered during magnetization, w_{mag}. The net energy input, E_{net}, will be the sum of the two works as it was for the magnetocaloric heat circulators discussed in Chapter 2. The two beds can be configured as shown in Fig 4.3. Okamura *et al.* [65] constructed an AMRR based on a configuration with revolving magnetocaloric material beds for heat pumping. Here, the device is open so that it can be used for heat circulation. The two beds revolve so that one bed is magnetized while the other is magnetized. The torque needed for revolving the bed will be the difference between the torque needed to demagnetize the bed and torque that is applied by the magnetic field when magnetizing the bed. Also, as the bed revolves, the process fluid always automatically enters the magnetized bed.

In an AMR heat circulator, no make-up heat is added to raise the temperature of the process fluid to its set temperature, T_{set}. After the heat of the process fluid is transferred to the ferromagnetic material, it is recuperated through magnetization. The recuperated heat is given back to the process fluid so that it is recirculated. The temperature difference during heat exchange between the process fluid and ferromagnetic material is kept minimal, leading to a drastic reduction in energy consumption.

Many AMR heat pump configuration has been proposed by past researchers. Scarpa *et al.* classified these researches [81]. In most of the AMR heat pumps classified by Scarpa *et al.*, the configuration can be modified so that it can be used as heat circulators instead of heat pumps.

The magnetocaloric material inside the bed can be configured as plate, particles, bulk ...etc. Although the adiabatic temperature change, ΔT_{ad}, is merely a few Kelvins per Tesla, and the strength of the magnetic field is limited to about 2 T at most when using permanent magnets, the heat exchange between the process fluid and the magnetocaloric material is direct, meaning that heat can be exchanged with very small temperature difference, ΔT_{min}, if configured well. Here, the bed consists of magnetocaloric material particles so that large surface area and heat transfer coefficient can be obtained.

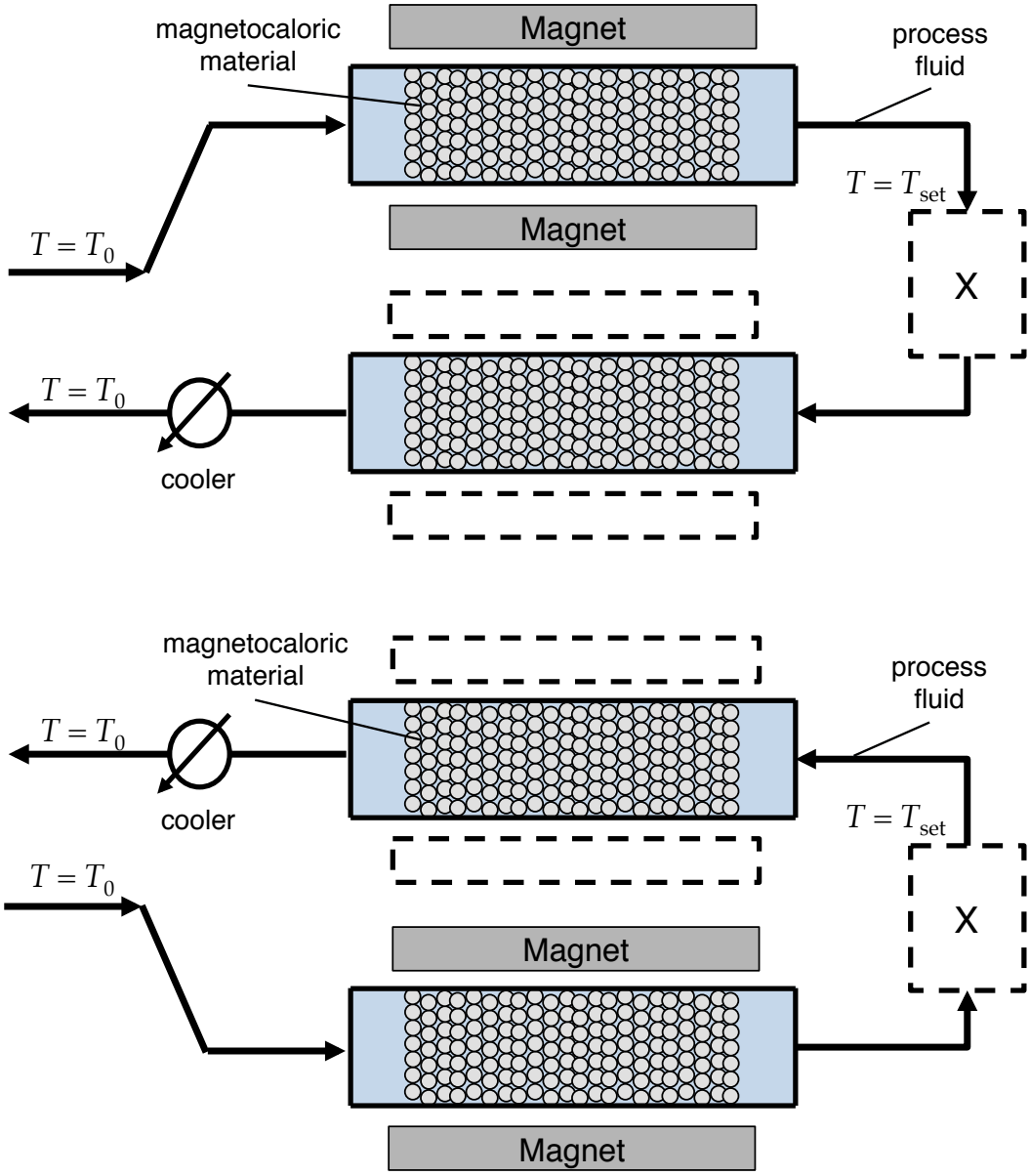

Figure 4.2: Schematic diagram of an AMR heat circulator for self-heat recuperation. After a certain period of time, the magnetized bed is demagnetized while the demagnetized bed is magnetized (top to bottom). The process fluid is always provided to the magnetized bed.

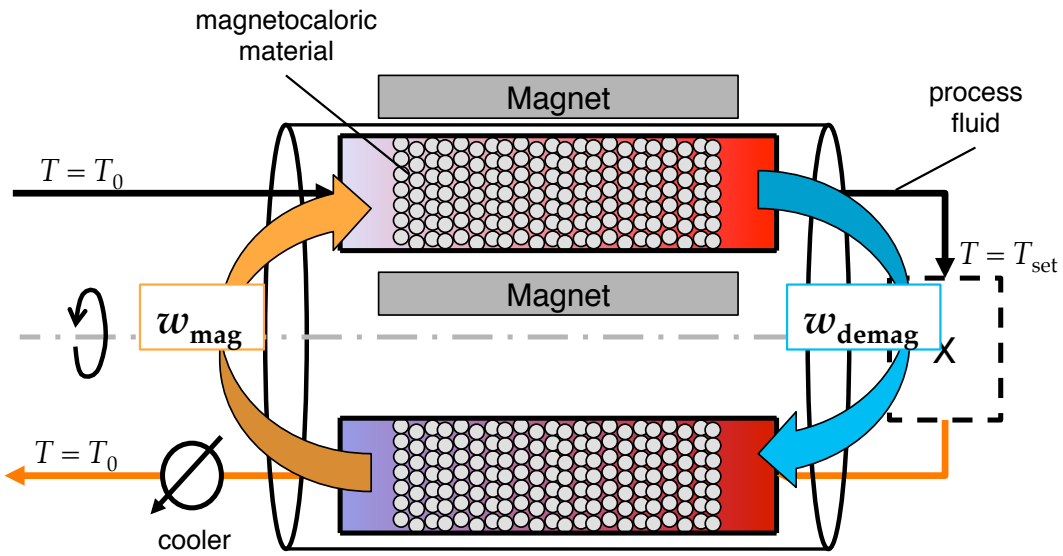

Figure 4.3: AMR heat circulator with revolving magnetocaloric beds

Figure 4.4 shows heat pump and heat circulator using active magnetic regeneration. Since the objective of a heat pump is to pump the heat of a cold reservoir to a hot reservoir, it requires two heat exchangers at the two ends. The working fluid flows back and forth to carry the heat. On the other hand, in the case of heat circulators, it does not supply or take away heat from an outside system, besides the small amount of heat discarded at the end of the cycle. Thus, the two heat exchangers are taken away, and the system is open, so that the process stream is able to flow in and out. For a process where a raise in the temperature of the process fluid is needed, all of the heat at the hot end will be returned to the bed.

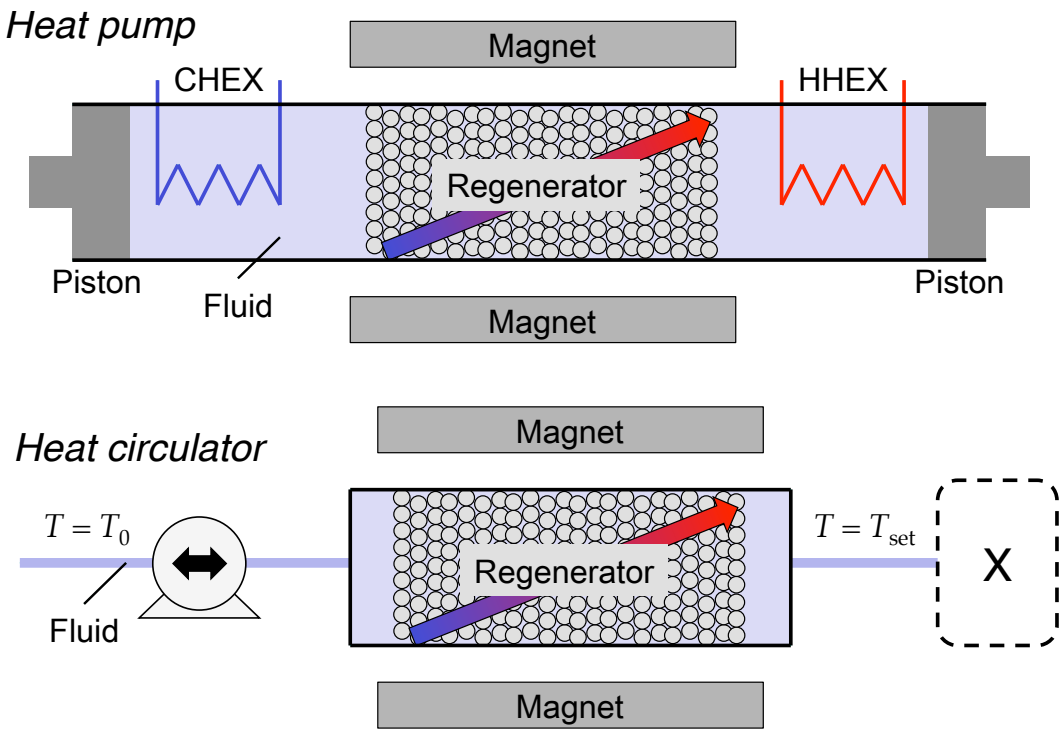

Figure 4.4: Heat pump and heat circulator using active magnetic regeneration

4.3 Construction of a mathematical model

4.3.1 Active magnetic regenerative heat circulator cycle

In order to verify the energy saving potential and understand the heat circulating capability of a magnetocaloric heat circulator, a simple one-dimensional mathematical model is constructed. The AMR heat circulator design shown in Fig 4.2 and 4.3 are made of two packed bed of magnetocaloric materials. Focusing on one of the two magnetocaloric beds, the cycle of AMR heat circulator consists of four cyclic steps 4.5.

1. **Magnetization:** Magnetic field is applied to the magnetocaloric bed, leading to an increase in the temperature of the magnetocaloric material. The temperature of the process fluid follows the temperature of the magnetocaloric material. During magnetization, the flow of the process stream is stopped.

2. **Cold blow:** Process fluid at environmental temperature, T_0, flows into the magnetocaloric bed. The process fluid receives heat from the magnetocaloric material and leaves the bed at temperature near the set temperature, T_{set}. The magnetic field is still applied, thus it is an isomagnetic cooling process from the point of view of magnetocaloric material.

3. **Demagnetization:** Magnetic field is removed from the magnetocaloric bed, leading to a decrease in the temperature of the magnetocaloric material. The temperature process fluid follows the temperature of the magnetocaloric material. The flow of the process stream is stopped.

4. **Hot blow:** Process stream at set temperature flows into the magnetocaloric bed. The process fluid gives its heat to the magnetocaloric material and leaves the bed at a temperature above environmental temperature, T_0. The process fluid is then cooled the cooler so that its temperature is T_0. The magnetic field is not varied, thus it is an isomagnetic heating process from the point of view of magnetocaloric material.

The four cycles are repeated continuously so that the heat is stably circulated. In a magnetocaloric heat circulator in Chapter 2, the process consisted of a isomagnetic heating, adiabatic magnetization, isomagnetic cooling and adiabatic demagnetization. Here, during magnetic field variation, heat exchange between the magnetocaloric material and the process fluid, thus the cycle of AMR consists of isomagnetic heating, polytrope magnetization, isomagnetic cooling and polytrope heating. If the magnetization and demagnetization is done quickly, they can be assumed as adiabatic. Since the two beds undergo the same cycle but only with a phase difference of half a cycle, in the mathematical simulation focusing on one bed is enough.

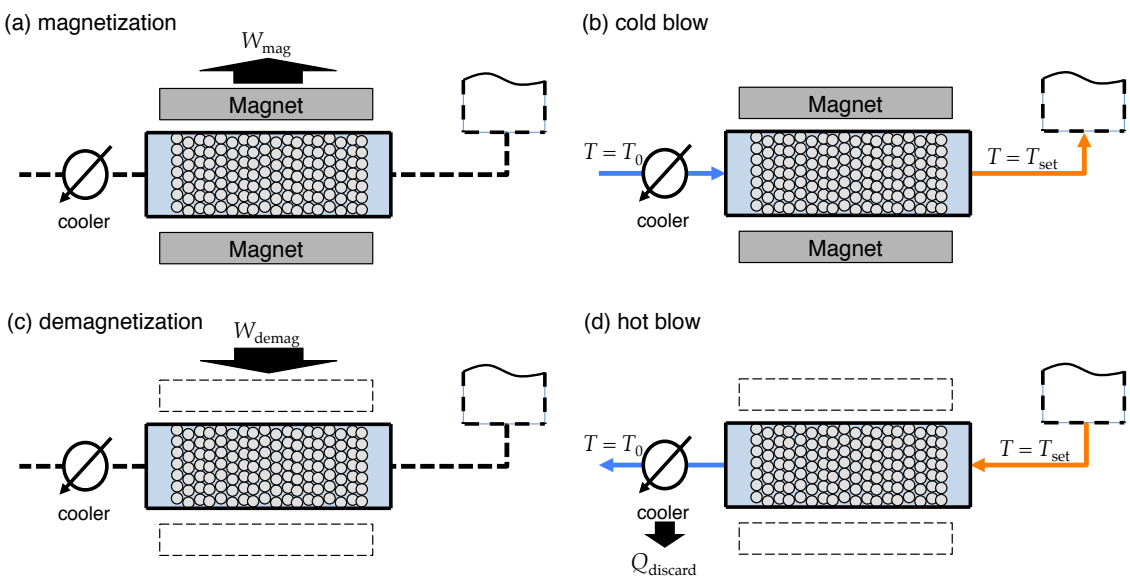

Figure 4.5: The four steps for self-heat recuperation in the open active magnetic regenerator: (a) magnetization step, (b) cold blow step, (c) demagnetization step and (d) hot blow step

Fig. 4.6 shows the time variation and magnetic field strength $\mu H(t)$ and mass flow rate of the process fluid $\dot{m}_f(t)$. The strength of the applied magnetic field is between μH_1 and μH_2. It is noted that the flow of process fluid is stopped during the magnetization

and demagnetization steps.

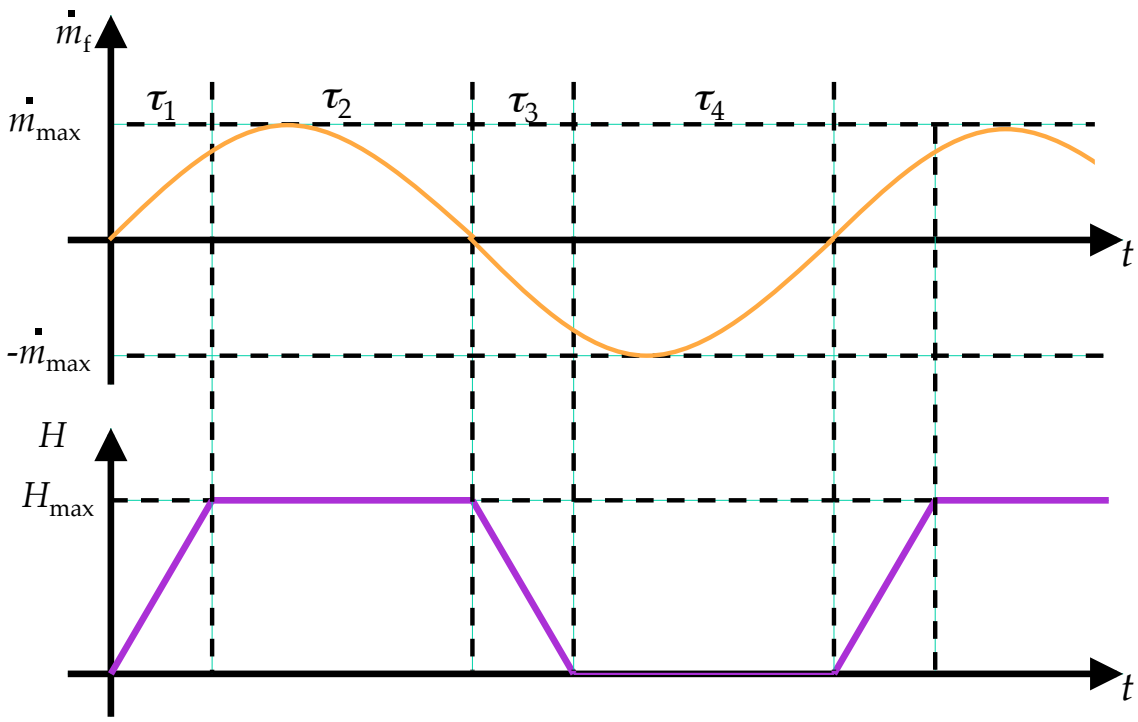

Figure 4.6: Characteristic of time in an open active magnetic regenerator cycle. The magnetic field is applied and removed during the magnetization step and the demagnetization step respectively. The flow rate is at maximum during the cold blow step and at minimum during the hot blow step

4.3.2 One-dimensional mathematical model

Some assumptions were made in constructing the mathematical model as shown below:

1. The inlet temperature profile during the hot blow is equal to the outlet temperature profile of the cold blow thus no heat is discarded at the hot end.

2. The fluid flow is parallel and uniform in any cross section so that the problem can be assumed one-dimensional.

3. The solid in the bed is uniformly distributed.

4. The adiabatic efficiency during magnetization and demagnetization is 100/

5. There are no demagnetization effect.

Considering the assumptions made above, a mathematical model of an AMR heat circulator was constructed. The energy balance of the working magnetocaloric material and process fluid is as shown in Fig. 4.7. The energy input to the working material is the sum of heat input by conduction, work input by magnetocaloric effect and heat input due to convective heat transfer with the process fluid. The energy input to the process fluid is the sum of heat input by conduction and mass transfer and convective heat transfer with the working magnetocaloric material. The difference of input and output energy is stored as the internal energy. From the energy balance, the following equations can be realized

$$\rho_{\mathrm{f}} c_{\mathrm{f}} A_{\mathrm{cs}} \epsilon \frac{\partial T_{\mathrm{f}}}{\partial t} + \dot{m}_{\mathrm{f}} c_{\mathrm{f}} \frac{\partial T_{\mathrm{f}}}{\partial x} = A_{\mathrm{cs}} \epsilon k_{\mathrm{f}} \frac{\partial^2 T_{\mathrm{f}}}{\partial x^2} - h a_{\mathrm{s}} (T_{\mathrm{f}} - T_{\mathrm{s}}) \tag{4.1}$$

$$\rho_{\mathrm{s}} c_{\mathrm{s}} A_{\mathrm{cs}} (1-\epsilon) \frac{\partial T_{\mathrm{s}}}{\partial t} = A_{\mathrm{cs}} (1-\epsilon) k_{\mathrm{s}} \frac{\partial^2 T_{\mathrm{s}}}{\partial x^2} + h a_{\mathrm{s}} (T_{\mathrm{f}} - T_{\mathrm{s}}) + (\mathrm{MCE})_{\mathrm{s}} \tag{4.2}$$

ρ, c, k, and T denote density, heat capacity, heat conductivity and temperature respectively, and the subscripts f and s denote fluid (process fluid) and solid (working material) respectively. A_{cs}, ϵ, $\dot{m}_{\mathrm{f}}$ and a_{s} denote the cross sectional area, porosity, flow rate and heat transfer surface. h is the solid-fluid heat transfer coefficient for a packed bed of spherical solids and is calculated using the equation by Whitaker [103]:

$$\frac{h d_{\mathrm{p}}}{k_{\mathrm{f}}} \frac{\epsilon}{1-\epsilon} = \left(0.5 Re_{\mathrm{p}}^{0.5} + 0.2 Re_{\mathrm{p}}^{\frac{2}{3}} \right) Pr^{\frac{1}{3}} \tag{4.3}$$

where d_{p}, Pr and Re_{p} are the diameter of the spheres, Prandtl number and Reynolds number of the process fluid, respectively.

The final term in Eq. 4.2 represents the energy input by the MCE due to the differing of the magnetic field at constant temperature. The amount of work input by differing the

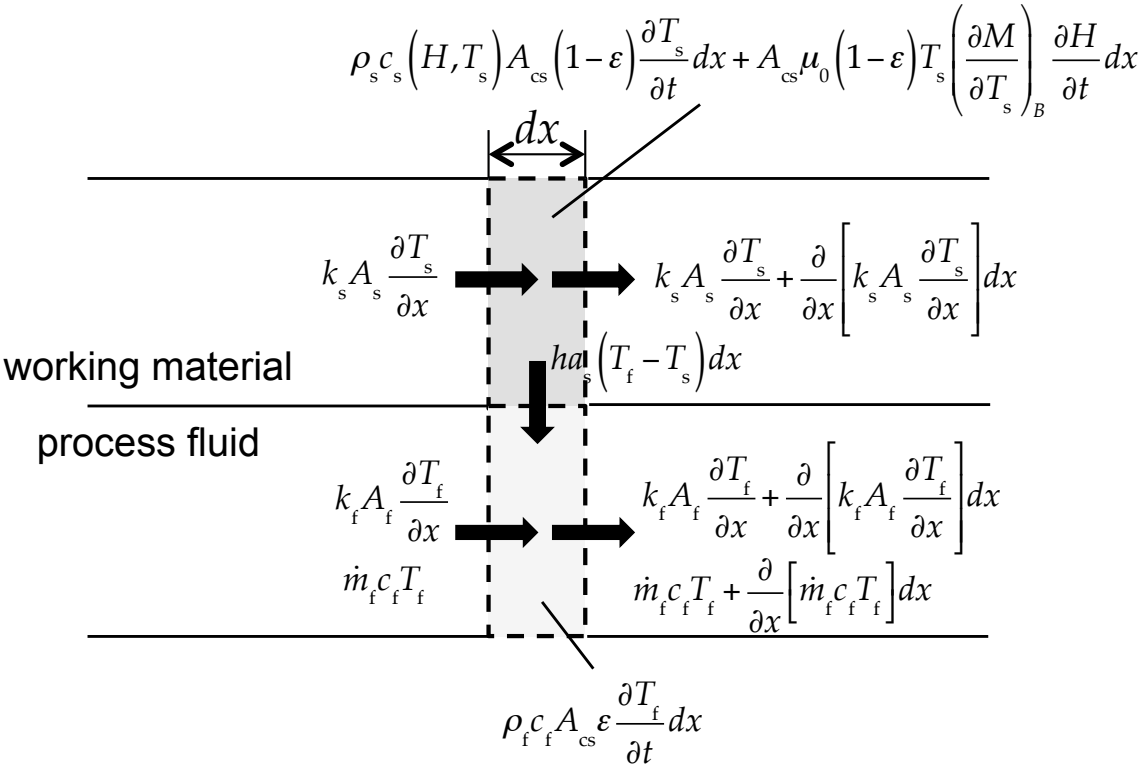

Figure 4.7: Energy balance for the process fluid and the working material during the open active magnetic regenerator cycles

magnetic field at constant temperature is defined as:

$$(\mathrm{MCE})_\mathrm{s} = A_\mathrm{cs}\mu_0(1-\epsilon)T_\mathrm{s}\frac{\partial M}{\partial T_\mathrm{s}}\frac{\partial H}{\partial t} \tag{4.4}$$

where M is the strength of magnetization.

The strength of magnetization, M, is calculated by using the molecular field model explained in 3.4.1. Fig. 4.8 shows the comparison of adiabatic temperature change, ΔT_ad, of gadolinium between calculation by molecular field model and values measured by Benford and Brown [50].

The heat capacity of the process material; water was assumed constant and unaffected by the temperature, strength of magnetic field and pressure. The heat capacity of the magnetocaloric working material differs largely when temperature or strength of applied field is varied. Thus, the transition of heat capacity can be calculated integrating Eq. 3.30.

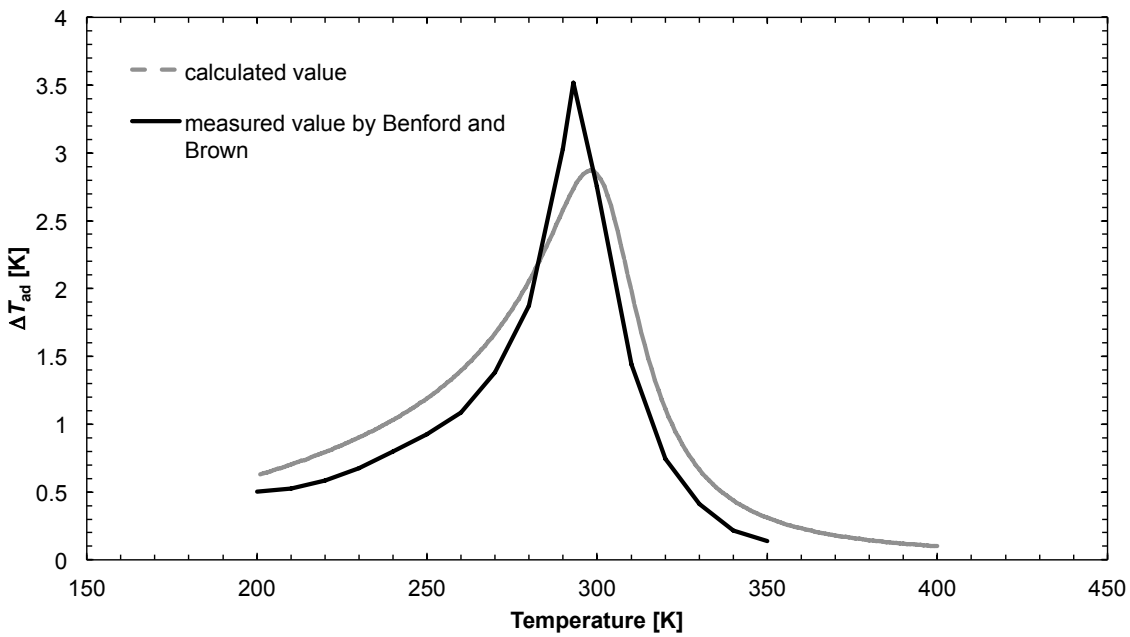

Figure 4.8: Comparison of adiabatic temperature change, ΔT_ad, of gadolinium when strength of magnetic field was varied from 0 to 1 [T] between calculation by molecular field model and values measured by Benford and Brown [50]

The initial condition for the process fluid and the magnetocaloric working material was set to the environmental temperature, $T_0 = 293.15[\mathrm{K}]$:

$$T_{\mathrm{f}}(0, x) = T_{\mathrm{s}}(0, x) = T_0 \tag{4.5}$$

The boundary condition during the magnetization and demagnetization step is

$$\frac{\partial T_{\mathrm{f}}}{\partial x} = \frac{\partial T_{\mathrm{s}}}{\partial x} = 0 \tag{4.6}$$

at both ends so that the bed is maintained adiabatic. The boundary condition during the cold blow step is

$$T_{\mathrm{f}}(T, 0) = T_0 \tag{4.7}$$

while the boundary condition during the hot blow step is

$$T_{\mathrm{f}}(t, l_{\mathrm{b}}) = T_{\mathrm{f}}\left(t - \frac{1}{2f}, l_{\mathrm{b}}\right) \tag{4.8}$$

where f denotes the frequency of the cycle and l_{b} denotes the length of the bed. No heat is discarded by the process fluid during the cold blow step and all of the heat that exits the bed during the cold blow step returns and enters the bed during the hot blow step.

It is assumed that a temperature gradient between the hot and the cold end of the bed will gradually increase. Eventually, the temperature of the hot end should saturate at a temperature where the heat will be circulated. The cycle is run a number of times until the temperature of the process fluid saturates and fulfills the following condition

$$T_{\mathrm{f}}(t, x) = T_{\mathrm{f}}\left(t - \frac{1}{f}, x\right) + \delta \tag{4.9}$$

where δ is the set tolerance. Until Eq. 4.9 is satisfied, the AMR heat circulator is still at its starting sequence. When Eq. 4.9 is satisfied, the cycle is assumed to have saturated and the heat circulation has begun.The set temperature, T_{set}, is determined as the average temperature of the process fluid at the hot end of the bed during the cold blow.

In order to determine the net work input, E_{net}, the heat discarded, Q_{discard}, can be calculated with the below equation,

$$Q_{\mathrm{discard}} = \int_{t_{\mathrm{m}}+t_{\mathrm{cb}}+t_{\mathrm{d}}}^{t_{\mathrm{m}}+t_{\mathrm{cb}}+t_{\mathrm{d}}+t_{\mathrm{hb}}} \dot{m}_{\mathrm{f}}(t) c_{\mathrm{f}} \left(T_{\mathrm{f}}(t, l_{\mathrm{b}}) - T_0\right) dt \tag{4.10}$$

From the energy balance, it is known that the heat discarded, Q_{discard}, is equal to the net work input, E_{net}, for self-heat recuperative processes.

Also, the heat that is circulated after the temperature gradient has saturated, is determined by

$$Q_{\text{cir}} = \int_{t_{\text{m}}}^{t_{\text{m}}+t_{\text{cb}}} \dot{m}_{\text{f}}(t) c_{\text{f}} \left(T_{\text{f}}(t, l_{\text{b}}) - T_0 \right) dt \tag{4.11}$$

The geometry of the AMR bed and the parameters of the mathematical simulation area summarized in table 4.1.

Table 4.1: Modeling parameters for the active magnetic regenerative heat circulator simulation

parameters		units	value
environmental temperature	T_0	[K]	290.15
pitch	$1/f$	[s]	4.0
bed length	l_{b}	[mm]	50.0
bed diameter	d_{b}	[mm]	7.8
cross sectional area	A_{cs}	[m^2]	3.14×10^{-4}
void ratio	ϵ	[-]	0.66
maximum mass flow rate	$\dot{m}_{\text{f}}$	[kg s^{-1}]	1.6×10^3
sphere diameter	d_{p}	[mm]	0.85
high magnetic field	μH_2	[T]	1.00
low magnetic field	μH_1	[T]	0.0
set tolerance	δ	[K]	0.02

Comparison with mathematical model of AMRR

Figure 4.9 shows the difference in mathematical model of AMR heat pumps and AMR

heat circulators. In both cases, the energy balance of the bed is the same, thus the governing equation is the same. However, the boundary condition of the two are different. In an AMR heat pump, there are two heat exchangers at the two ends of the bed. Thus, the temperature of the two ends of the bed is the temperature of the cold and the hot reservoir. Heat leaves from the hot end of the bed and enters at cold end of the bed but the working fluid stays in the bed. On the other hand, in the boundary condition for AMR heat circulators, the temperature of the cold end is fixed to the environmental temperature, T_0. The system is open, so the process fluid flows in and out of the system, but all of the heat that flows out from the hot end is returned.

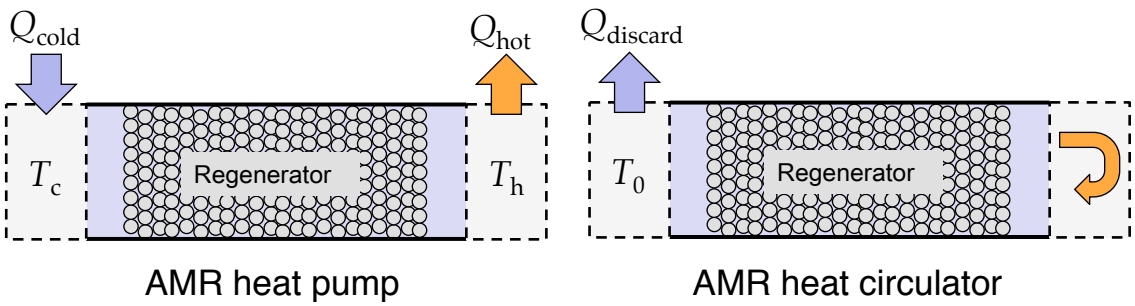

Figure 4.9: Comparison of boundary conditions for AMR heat pump and AMR heat circulators

4.4 Simulation results

4.4.1 Heat circulating potential

Fig. 4.10 shows the temperature profile of the hot, middle and cold end of the magnetocaloric bed at start up. It can be seen that the temperature difference between the hot and the cold end gradually increases, thus the temperature gradient of the magnetocaloric bed is increasing. The temperature of the cold end is kept at around 290.15 [K] because the process fluid is always provided at environmental temperature, T_0, 290.15 [K]. The rate in which the temperature gradient increases gradually decreases as it undergoes the AMR cycles. This is because as the temperature gradient grows larger, the amount of heat discarded with the process fluid and heat conduction of the bed increases, while the heat provided by the MCE of the magnetocaloric working material decreases as the temperature moves further from the Curie temperature, θ_C. Eventually the amount of heat discarded and provided matches leading to the saturation of temperature gradient.

After about 2000 [s] (500 cycles), the temperature gradient of the magnetocaloric bed saturates, so that the heat of the process stream is circulated in between 293 [K] and 308 [K]. In a self-heat recuperative process, the heat which is the subject of circulation is required to be provided initially. Thus, in a self-heat recuperative process with compressors, an additional fired heater was needed for the providing of heat at the start up sequence. In the AMR heat circulator, the initial heat which is the subject of circulation can be provided without an additional heat source.

Fig. 4.11 shows the temperature profile of the process fluid at the hot end of the bed after saturation. The temperature of the process fluid increases during the magnetization step, decreases during the cold blow step, decreases further during the demagnetization step and increases to the initial temperature of the cycle during the hot blow step. Process stream heat is transferred to the magnetocaloric working material during the demagnetization and hot blow steps, recuperated, and transferred back to the process fluid during the magnetization and cold blow steps. The following process X (Fig.4.2) is maintained

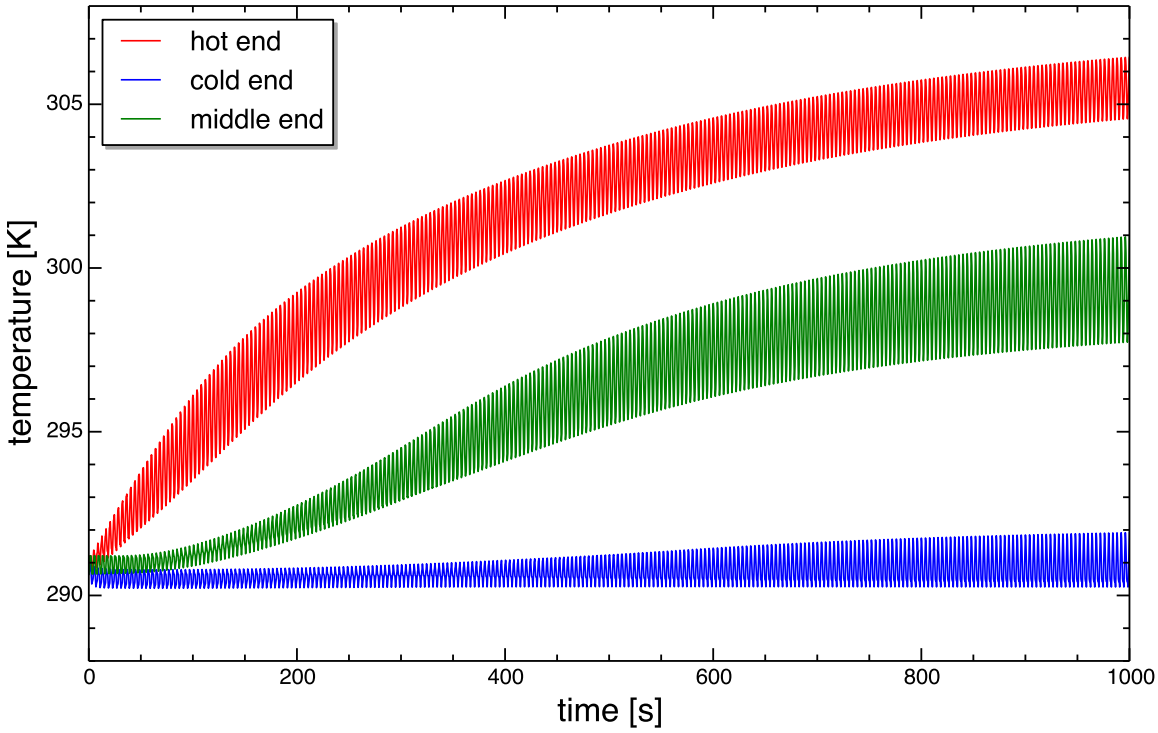

Figure 4.10: Temperature profile of the hot, middle and cold end of the magnetocaloric bed at start up

in the temperature range between 305.5 and 307.5 [K].

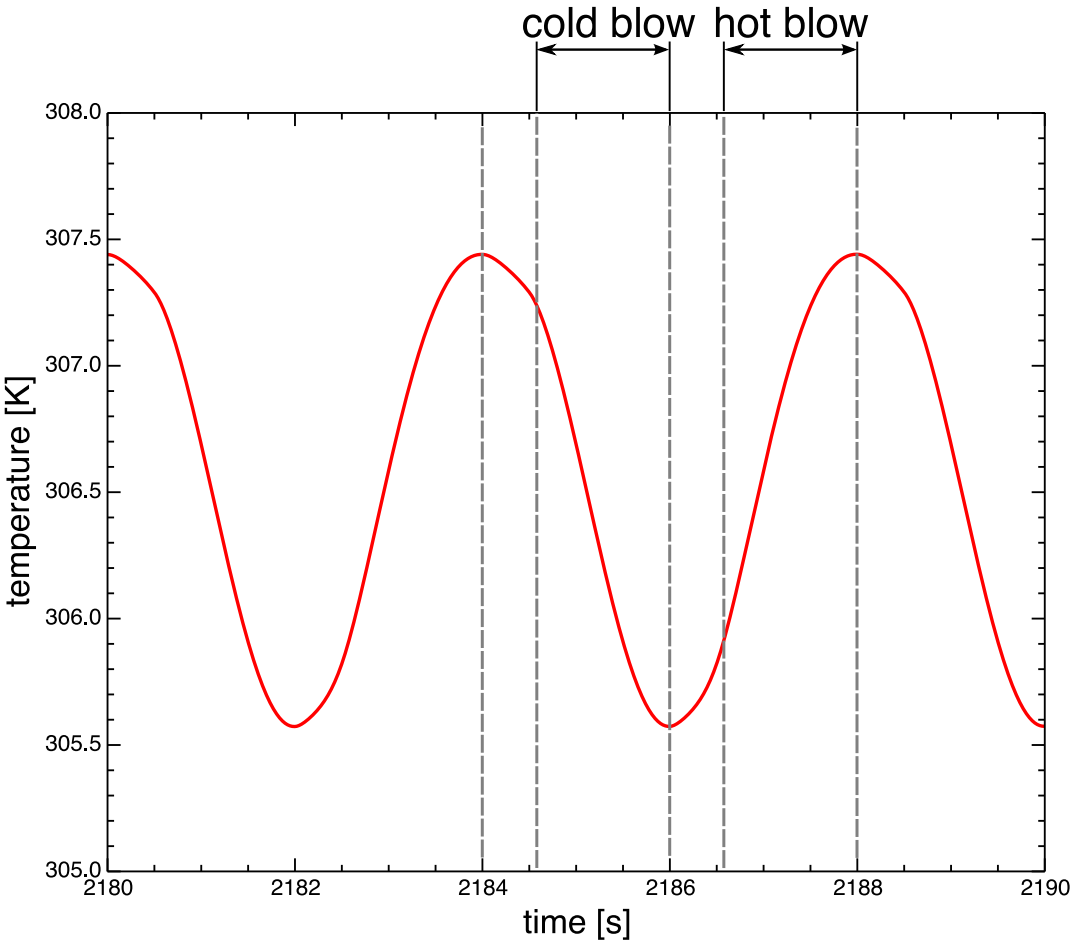

Figure 4.11: Temperature profile of process fluid at the hot end of the regenerator bed

Fig. 4.12 shows the temperature profile of the process fluid and the magnetocaloric working material at the middle of the bed. It can be seen that the temperature of the magnetocaloric working material increases when the bed is magnetized and decreases when the bed is demagnetized. The temperature of the process fluid follows the temperature of the magnetocaloric working material. The magnetization and the demagnetization is performed in 0.5 [s], the temperature of the magnetocaloric material changes rapidly in those regions.

Fig. 4.13 shows the temperature of the bed before and after each AMR cycle steps;

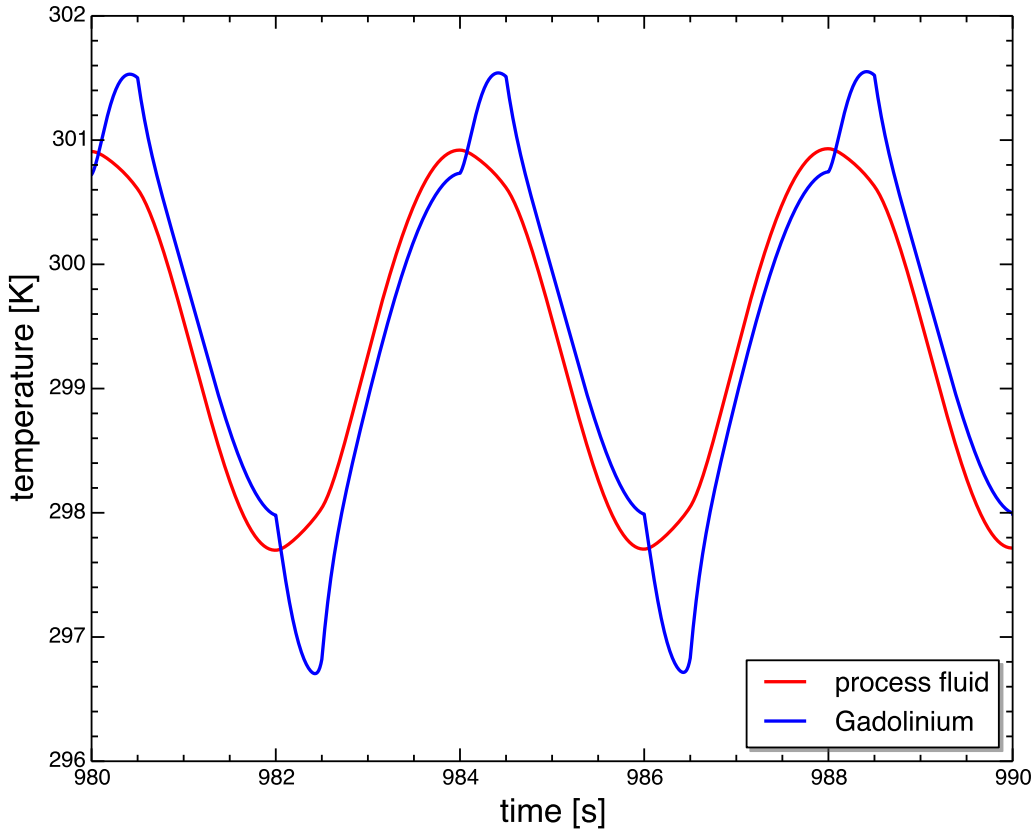

Figure 4.12: Temperature profile of the process fluid and working material at the middle of the bed

magnetization step, cold blow step, demagnetization step and hot blow step after saturation. It can be seen there is a temperature gradient in the AMR bed from cold to hot end. The temperature profile changes as the bed undergoes the cycle. It can be seen the temperature at the middle of the bed changes largely compared to the two ends. Since the AMR heat circulator applies a quasi-counterflow heat exchange, it will consume larger energy compared to self-heat recuperative process that implies a counterflow heat exchange. Since each micro-sections in the bed draws its own cycle, large temperature change will result in larger energy consumption. Detailed discussion is made in Section 4.4.2.

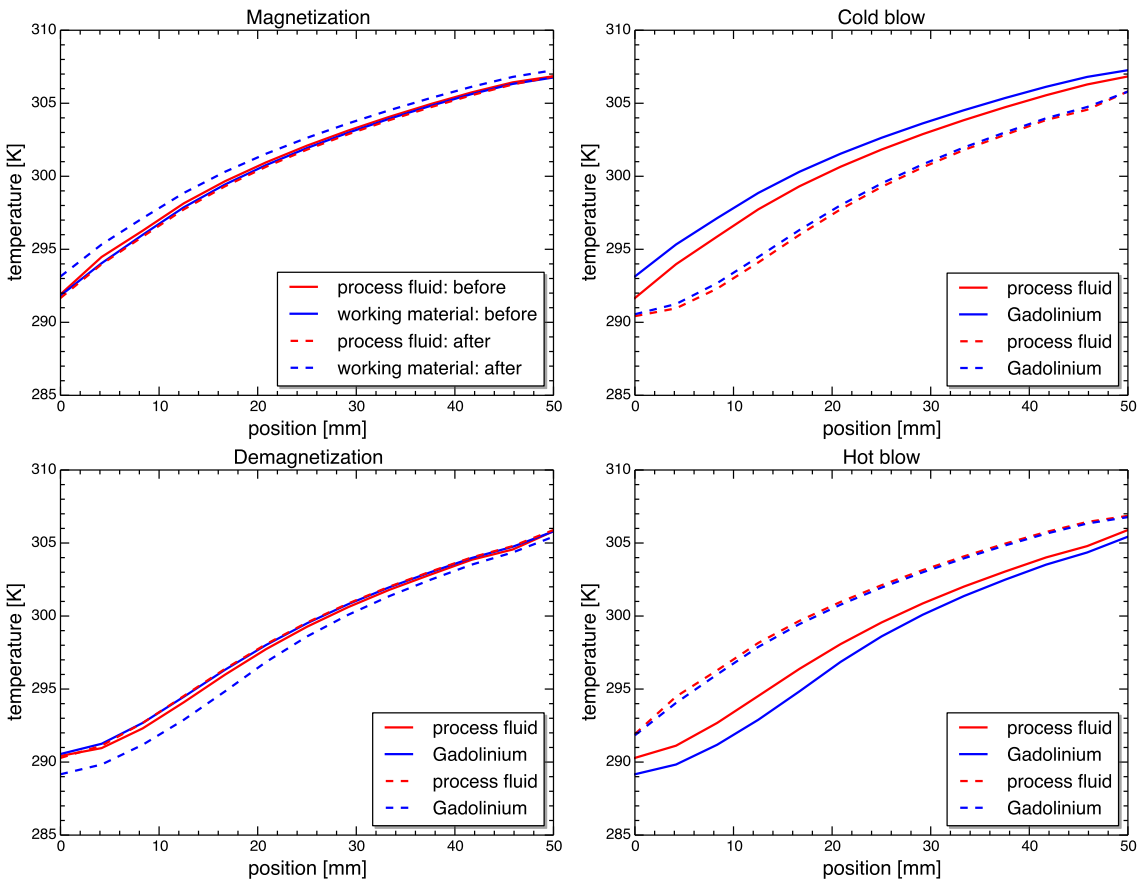

Figure 4.13: Temperature of AMR bed before and after each AMR cycle steps

4.4.2 Energy consumption

The total energy consumption determined from the heat discarded at the cooler, Q_{discard}, is 0.338 [J cycle^{-1}] in the temperature range between 293 [K] and 308 [K]. The circulated heat is the heat carried by the process fluid during cold blow step, and can be calculated as 14.4 [J cycle^{-1}]. If the heat that was circulated by the heat circulator was provided with a heat pump, the energy consumption is equivalent to a heat pump with coefficient of performance (COP) of 42.6. The heat of the process stream can be circulated with mere 2.35 % of the amount of heat circulated.

The reverse Carnot efficiency when the heat was circulated in between 293 [K] and 308 [K] can be calculated as 18.9 [-], which is much smaller than the COP equivalence value of an AMR heat circulator. This is because, in the case of a heat pump, waste heat or environmental heat needs to be pumped to heat the process stream and the heat capacity and the temperature in which the heat can be provided to the heat pump does not match the heat capacity and the temperature of the process fluid. Where in the case of a heat circulator, the heat capacity and the temperature of the heat source, which is the process stream itself, matches the heat capacity and the temperature of the heat sink, hence the exergy destruction due to heat exchange, A_{HEX}, can be reduced.

The Net work input, E_{net}, needed for heat circulation can also be derived from a temperature-entropy diagram of the working magnetocaloric material. Fig. 4.14 shows the temperature-entropy diagram of the magnetocaloric working material for one AMR cycle after the temperature gradient in the AMR bed has reached saturation. In Fig. 4.14, the temperature-entropy diagram is divided into 12 micro-sections. Each micro-section in the AMR bed draws its own cycle and the net work input, E_{net}, is equal to the sum of the areas of the cycles drawn for the micro-sections.

From Fig. 4.14, it can be seen that the cycle of the micro-sections are extended, indicating the wide temperature range in which the micro-sections go through. Fig. 4.15 shows the temperature-entropy diagram of the working magnetocaloric material plotted

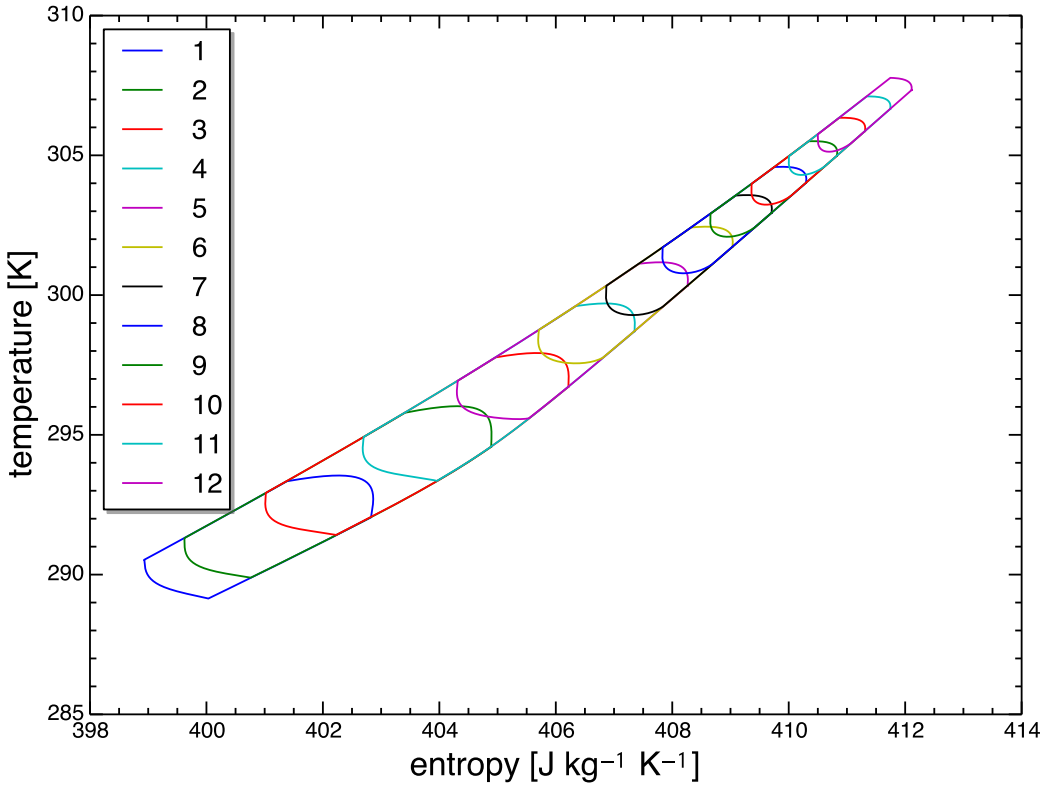

Figure 4.14: Temperature-entropy diagram of the working magnetocaloric material divided into micro-sections

versus position. The volume of the figure multiplied by the weight per cross sectional area in which the magnetocaloric working material occupies in the AMR bed is the net work input, E_{net}.

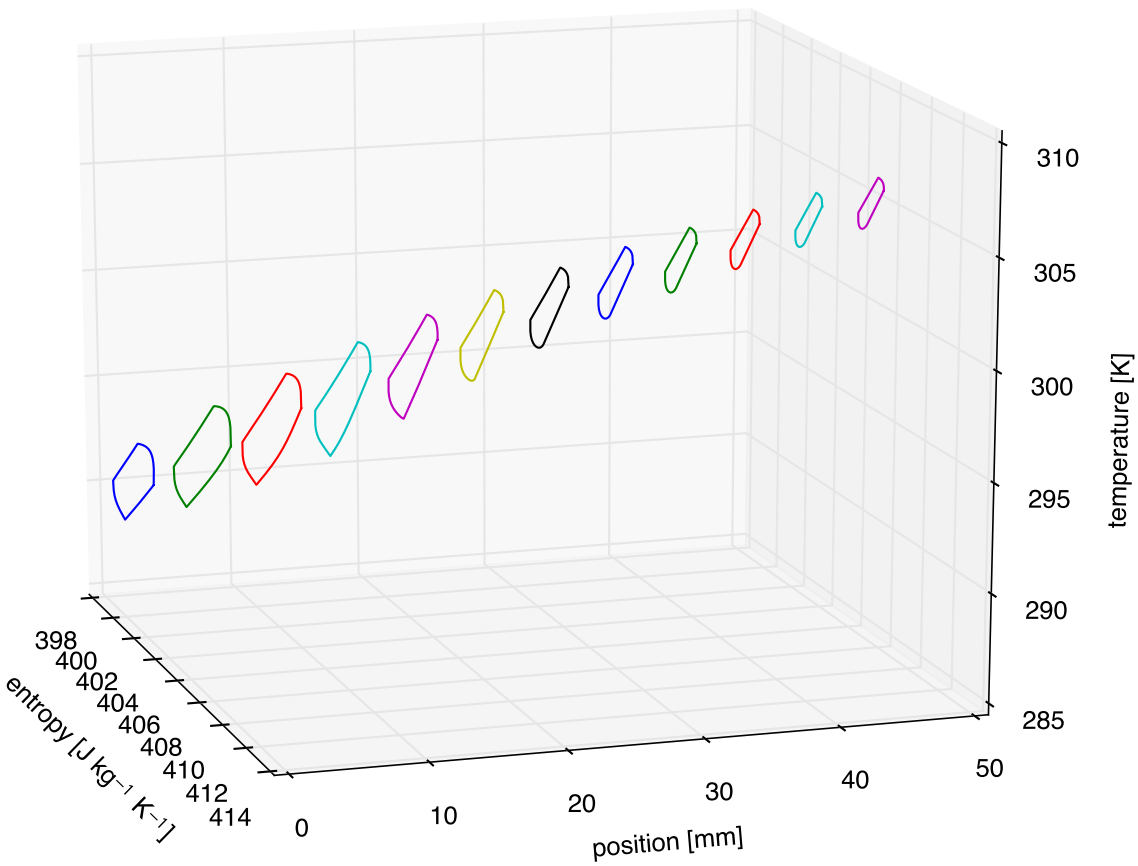

Figure 4.15: Temperature-entropy diagram of the working magnetocaloric material plotted versus position

From the isomagnetic lines in the temperature-entropy diagram, in a magnetocaloric heat circulator where the heat was circulated in between 293 [K] and 308 [K], with a counter-flow heat exchanger, the amount of net work, E_{net}, needed for heat exchange is 0.175 [J cycle^{-1}] which is 1.22 % of the amount of heat circulated (equivalent to heat pump of 81.9). The minimum temperature difference needed for heat exchange, ΔT_{min}, is 0.7 [K]. The minimum exergy destruction when the temperature difference was fixed

to 0.7 [K] is 0.128 [J cycle^{-1}] which is 0.89 % of the amount of heat circulated (equivalent to heat pump with COP of 112.3). It can be seen that the net work input, E_{net}, needed for heat circulation in the AMR heat circulator shows a value reasonably close to these values. These values will be the limits in which the amount of net work input, E_{net}, can be reduced to by further optimization of parameters and changing the ways in which the heat of the process stream is recuperated. The results are summarized in Table 4.2.

Table 4.2: Comparison of minimum (case 1), derived from temperature-entropy diagram (case 2), and derived from simulation (case 3) net work input, E_{net}, and the heat circulated, Q_{cir}

case	Q_{process}	E_{net}	$E_{\mathrm{net}}/Q_{\mathrm{process}}$
1		0.128 [J cycle^{-1}]	0.89 %
2	14.4 [kJ cycle^{-1}]	0.175 [J cycle^{-1}]	1.22 %
3		0.338 [J cycle^{-1}]	2.35 %

The reason why AMR heat circulator consumes more energy than the case where heat exchange is counter flow is because some heat circulated by the working material does not exit the bed. Fig. 4.16 shows a schematic temperature-entropy diagram of an AMR cycle. The bed is divided into three micro-sections. The heat that the working material circulated is the sum of the area colored yellow, blue and red. However, the heat that actually exits the bed is the area surrounded in green. Some of the heat that the working material circulated are used for raising the temperature of the bed and never leaves the bed. In order to gain the maximum efficiency, the parameters of the bed has to be optimized so that small amount of heat as possible is used to raise the temperature of the bed, i.e. the temperature fluctuation of the bed is minimized.

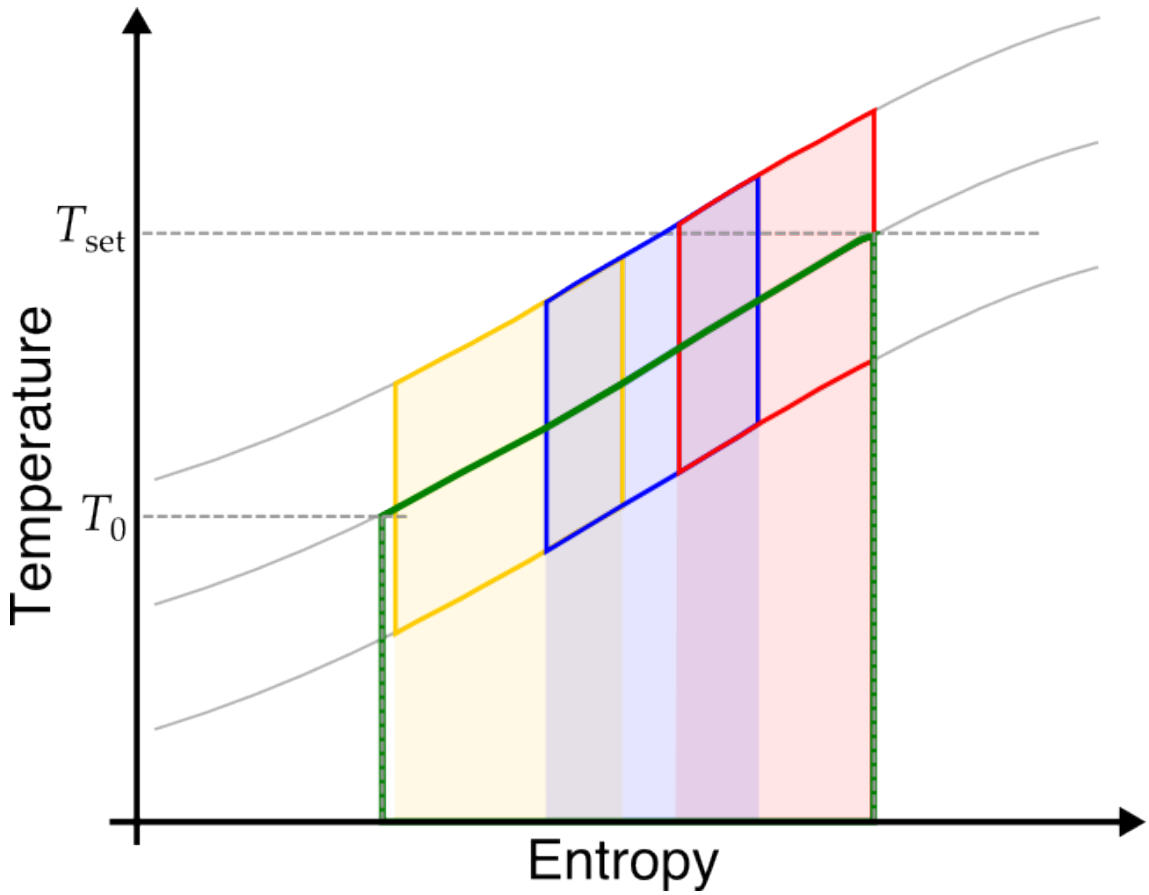

Figure 4.16: Schematic temperature-entropy diagram of an AMR cycle

4.4.3 Effect of parameters

In order to gain the maximum efficiency for the needed temperature difference, the effect of aspect ratio of the bed, cycle length, particle diameter, flow ratio and time needed for field variation was investigated. The energy balance of the magnetocaloric bed is made of three aspects, the magnetic work input, E_{net}, heat that is discarded through conduction of the process fluid, Q_{cond}, and heat that is carried out with the mass of the process fluid, Q_{mass}. When the temperature of the bed has saturated, the value of the three balance, which can be written as $E_{\mathrm{net}} = Q_{\mathrm{mass}} + Q_{\mathrm{cond}}$, in another words,

$$\int^{\tau}\int^{l_{\mathrm{B}}} \dot{m}_{\mathrm{f}} c_{\mathrm{f}} \frac{\partial T_{\mathrm{f}}}{\partial x} dxdt + \int^{\tau}\int^{l_{\mathrm{B}}} A_{\mathrm{cs}} \epsilon k_{\mathrm{f}} \frac{\partial^2 T_{\mathrm{f}}}{\partial x^2} dxdt = \int^{\tau}\int^{l_{\mathrm{B}}} h a_{\mathrm{s}} (T_{\mathrm{s}} - T_{\mathrm{f}}) dxdt \tag{4.12}$$

If $E_{\mathrm{net}} > Q_{\mathrm{mass}} + Q_{\mathrm{cond}}$, more energy is being supplied compared to the heat discarded, thus will be stored as internal energy and the temperature of the bed will rise. When $E_{\mathrm{net}} < Q_{\mathrm{mass}} + Q_{\mathrm{cond}}$, more energy is being discarded compared to the energy being supplied, thus the temperature of the bed will decrease.

Since the temperature in which the AMR heat circulate changes, it is difficult to compare efficiency. Here we have decided to use the ratio of net work input, E_{net}, and minimum exergy destruction, A_{min}. The ratio can be written as,

$$\frac{E_{\mathrm{net}}}{A_{\mathrm{min}}} = \frac{E_{\mathrm{net}}}{Q_{\mathrm{actual}}} \frac{Q_{\mathrm{actual}}}{Q_{\mathrm{cir}}} \frac{Q_{\mathrm{cir}}}{A_{\mathrm{min}}} \tag{4.13}$$

$$= \frac{Q_{\mathrm{actual}}}{Q_{\mathrm{cir}}} \frac{E_{\mathrm{net}}}{Q_{\mathrm{actual}}} \frac{Q_{\mathrm{cir}}}{A_{\mathrm{min}}} \tag{4.14}$$

when using Gd as the working material, the magnetic field is varied between 0 and 1 [T], and the temperature in which the heat is circulated is limited to few 10 Kelvins near the Curie temperature, $\frac{E_{\mathrm{net}}}{Q_{\mathrm{actual}}} \frac{Q_{\mathrm{cir}}}{A_{\mathrm{min}}}$ is around 1.7. This value is the closest you can get to A_{min} as long as you are under those conditions. Thus, it can be assumed that the ratio between E_{net} and A_{min} will approach asymptotically to 1.7 through optimization of the parameters.

Fig. 4.17 shows the relation between energy efficiency and set temperature and aspect ratio of the AMR bed. The aspect ratio was varied so that the volume (i.e. the amount

of Gd) does not change. It can be seen that with higher aspect ratio, due to the effect of heat conduction, the saturating temperature, T_{set}, will increase. The effect will saturate as the aspect ratio increases. The ratio between net work input, E_{net}, and minimum exergy destruction, A_{min}, increases slightly. It can be assumed that this is the result of amount of circulated heat increasing. In the simulation, heat loss has been neglected, so in actual case, higher aspect ratio will result in higher heat loss and thus lower efficiency and lower saturating temperature, T_{set}, depending on how much effort is made to insulate the system. Also, large area of magnetic field will be needed to uniformly magnetize a bed with high aspect ratio. Despite those factors, it can be said that higher aspect ratio is desired, for higher saturating temperature, T_{set}, can be obtained and the effect to energy efficiency is slight.

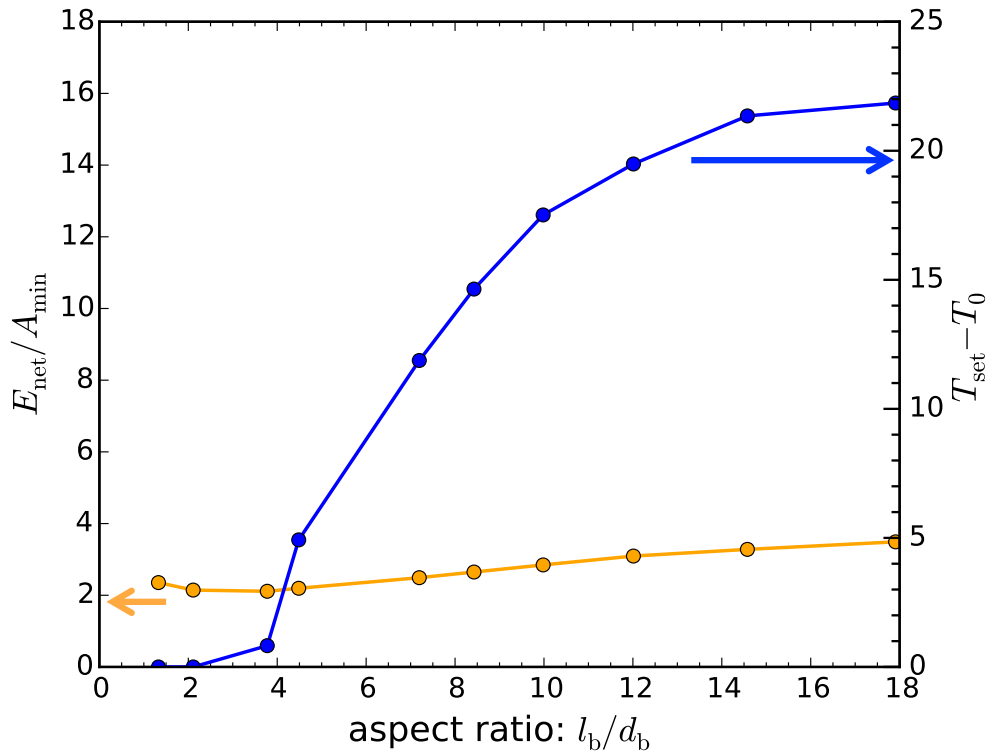

Figure 4.17: Saturating temperature and energy consumption versus aspect ratio of the AMR bed

Fig. 4.18 shows the effect of fluid flow rate to E_{net}/A_{min} and $T_{set} - T_0$. It can be seen that $T_{set} - T_0$ has an optimal point where maximum value can be obtained. The heat that is carried out from the bed is either result of conduction or carried out by the fluid flow. With low flow rate, the effect of conduction is large and with high flow rate, the effect of heat carried out by the fluid becomes large. When the fluid flow rate is low, E_{net}/A_{min} is low because, a large portion of the circulated heat does not exit the bed. As the flow rate increases, much heat is carried out of the bed so the E_{net}/A_{min} value decreases. Although the effect of pressure loss is very small, E_{net}/A_{min} increases slightly at high flow rates. Thus it can be said that there is an optimal fluid flow rate where the maximum $T_{set} - T_0$ and the minimum E_{net}/A_{min} can be gained.

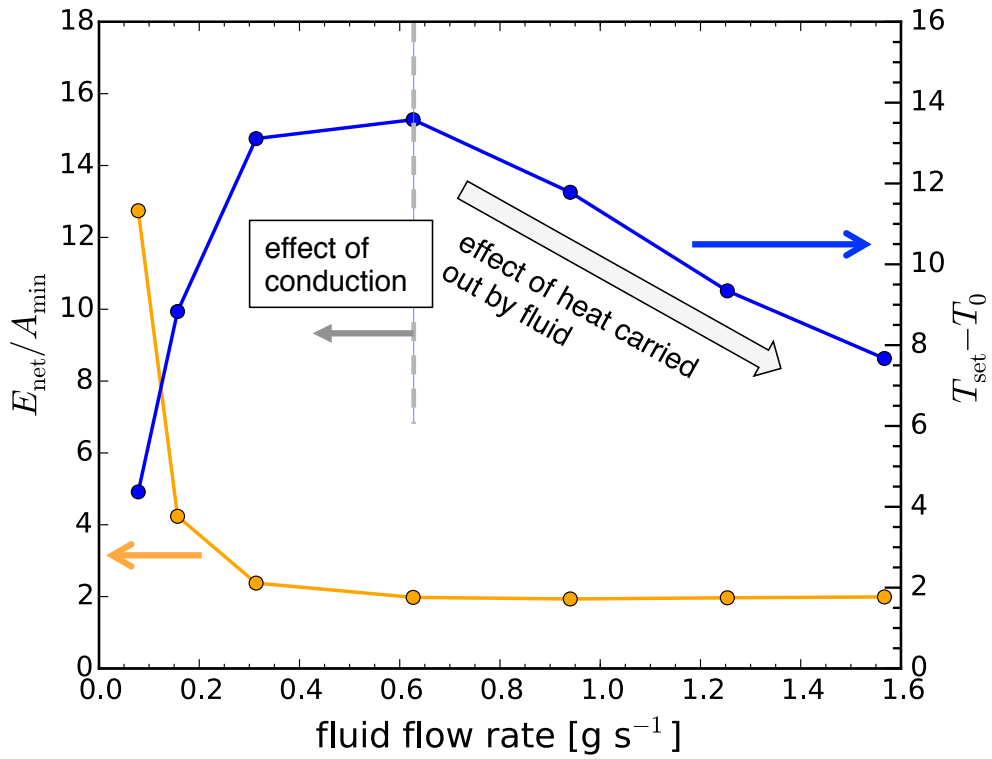

Figure 4.18: Saturating temperature and energy consumption versus fluid flow rate

Fig. 4.19 shows the effect of cycle length or frequency and particle size to $T_{set} - T_0$

and E_{net}/A_{min}. It can be seen from the shape of the figure that the effect of cycle length is similar to the effect of fluid flow rate. An optimal point for $T_{set} - T_0$ where the effect of conduction and heat carried out by the process fluid is minimum exists. For E_{net}/A_{min}, the value decreases as the cycle length increases and increases slightly after 8 [s] due to pressure loss. With smaller particle size, a higher heat transfer coefficient can be obtained. Due to higher heat transfer coefficient, smaller particle size results in generally higher $T_{set} - T_0$ value and higher E_{net}/A_{min} value.The Biot number for the three particle sizes are all well below 1 (around 0.3-0.4), thus, the effect of heat conduction in the particles are neglected. The optimal cycle length where the maximum $T_{set} - T_0$ can be gained decreases with higher heat transfer coefficient. It can be said that although higher saturation temperature can be obtained with higher heat transfer coefficient, the efficiency will become low.

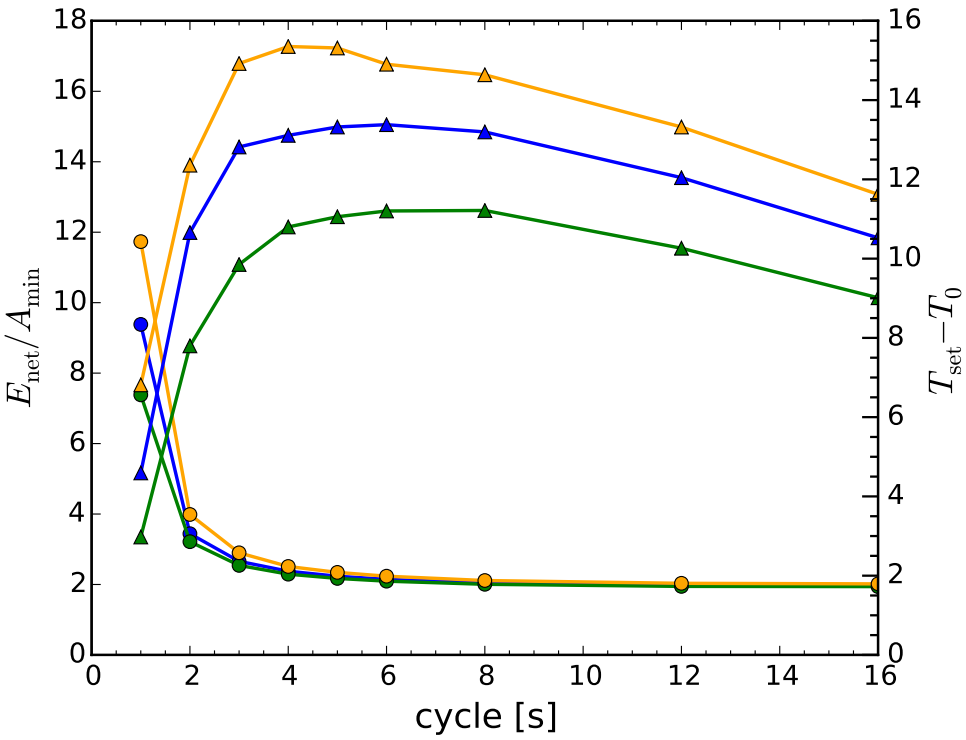

Figure 4.19: Saturating temperature and energy consumption versus cycle length with different particle diameter

Fig. 4.20 shows the effect of field variation time to $T_{\mathrm{set}} - T_0$ and $E_{\mathrm{net}}/A_{\mathrm{min}}$. Faster magnetization and demagnetization time will result in larger heat transfer temperature during heat exchange, ΔT_{HEX}, thus larger $T_{\mathrm{set}} - T_0$ can be gained. As for $E_{\mathrm{net}}/A_{\mathrm{min}}$, slightly higher value can be obtained with faster field variation time, because the cycle draws close to adiabatic magnetization. Faster field variation tie is advantageous for both energy efficiency and saturation temperature perspective.

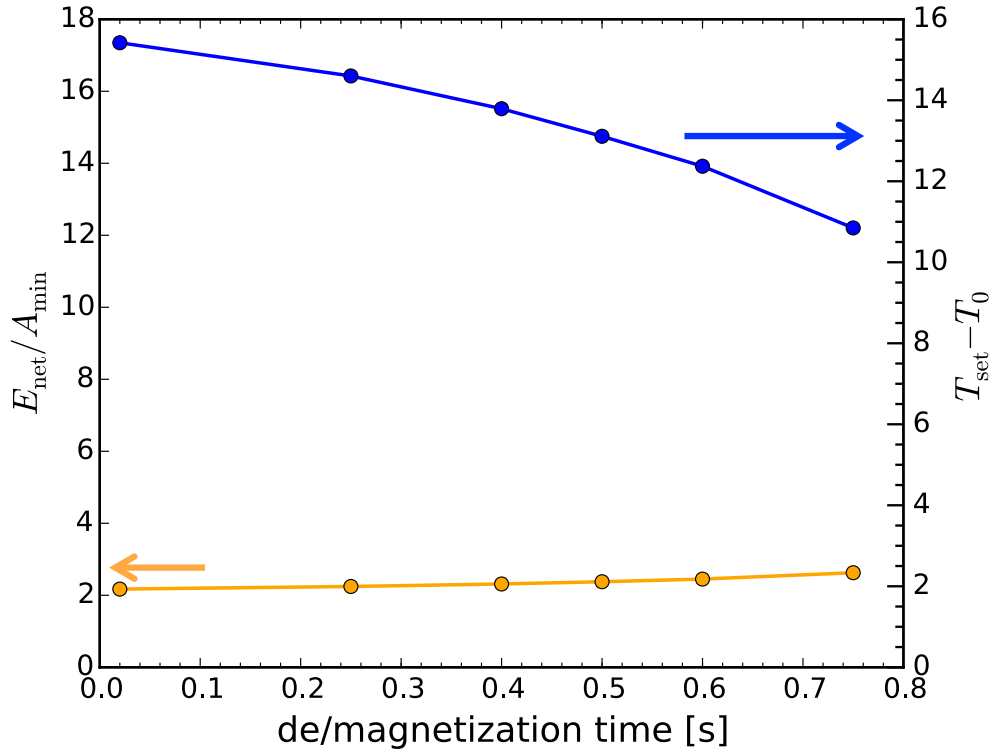

Figure 4.20: Saturating temperature and energy consumption versus time needed for magnetization and demagnetization

In actually installing AMR heat circulator to an application, the required set temperature, T_{set} will be set. Also, it is likely that the amount of usable magnetocaloric material, magnetic field and required amount of heat circulated is set. Thus, it will be needed to optimize the parameters so as to satisfy these requirements with the highest efficiency. It was seen that the larger aspect ratio, $l_{\mathrm{b}}/d_{\mathrm{b}}$, and smaller particle diameter is desirable to

obtain larger saturation temperature. There is an optimal point where the effect heat convection and heat carried out by the fluid is minimized for fluid flow rate and cycle time. The effect of these parameters are not so large from the energy efficiency point of view and the ratio between the net energy consumption and the minimum exergy destruction, $E_{\mathrm{net}}/A_{\mathrm{min}}$, converge to a value around 2.0.

4.5 Conclusion

In this chapter, an AMR heat circulator for realizing self-heat recuperation using MCE to save energy in thermal processes was proposed. Taking the magnetocaloric heat circulator proposed in Chapter 2, one step further, a method to actually circulate process stream heat has been proposed. In the AMR heat circulator, instead of employing compression, the process stream heat is recuperated by the MCE of magnetocaloric materials. Rather than using the active magnetic regenerator for heat pumping, it was applied for heat circulation. The process fluid heat is recirculated by magnetocaloric working material that undergoes an AMR heat circulation cycle of magnetization and demagnetization. No additional heat is added to increase the process stream temperature from environmental temperature, T_0, to its set temperature T_{set}, but demagnetization work was provided.

A mathematical one dimensional model was constructed in order to evaluate the heat circulating and energy saving potential of the AMR heat circulator. It was seen that the AMR heat circulator was capable of circulating the heat within the system at very low work input. The required work needed for heat circulation was reasonably close to the minimum exergy destruction during heat exchange, A_{loss}, derived from the temperature-entropy diagram. The difference was due to the temperature change of the magnetocaloric working material during the hot and cold blow step. The temperature-entropy diagram indicated that the AMR heat circulator has the potential to drastically reduce the total energy consumption in a thermal process. Furthermore, the effect of parameters such as the aspect ratio, fluid flow rate, particle diameter, cycle frequency and field variation time has been investigated and the overall trend has been elucidated. There is an optimal fluid flow rate and cycle time which maximized the effect of conduction and minimizes the effect of heat carried out by the fluid, to obtain the largest saturation temperature. Smaller particle size and larger aspect ratio is advantageous in order to gain large saturation temperature. The effect of these parameters where small for energy efficiency.

Chapter 5

Experimental study of AMR heat circulator

5.1 Introduction

In Chapter 4, active magnetic regenerative (AMR) heat circulator which enables self-heat recuperative processing using magnetocaloric effect has been proposed and a simple one-dimensional mathematical model is constructed. The basic behavior and its energy saving potential has theoretically been confirmed. However AMR heat circulator includes a complex heat transfer between the process stream and the working material. Thus, the model is in need of verification.

This chapter examines the measurement of the temperature evolution of the magnetocaloric bed and the work needed to circulate the heat using gadolinium and water as magnetocaloric working material and process fluid, respectively using a newly constructed AMR heat circulator. The experimental result has been compared with the mathematical simulation using the model constructed in Chapter 4.

5.2 Experimental method

The basic concept of AMR heat circulator has been explained in section 4.2. Similarly to the mathematical model, in the experiment, a single packed bed of magnetocaloric material is considered. An experimental setup of the AMR heat circulator has been newly constructed to examine its heat circulation potential and its energy saving consumption. The schematic of experimental setup configuration is shown in Fig. 5.1.

In this research, Gd was used as the magnetocaloric working material for its well studied magneto-thermal properties [48]. Water as the process fluid. The temperatures of the two ends and middle of the magnetocaloric bed were measured by using T type thermocouples. The temperature were measured for a certain period of time so that the change of the temperature gradient in the bed of magnetocaloric material can be monitored. A pressure sensor was placed just outside the two ends of the magnetocaloric bed so that the time evolution of process fluid velocity and the effect of pressure loss to the total energy consumption can be calculated. Permanent magnet is placed to creates the magnetic field. In order to control the magnetization and demagnetization of the bed, an actuator pushes and pulls the bed in and out of the permanent magnet. Synchronized with the control of magnetization and demagnetization by the actuator, a tubing pump was used to control the flow rate and the flow direction of the process fluid. The process fluid exchanged heat with the cooling water before entering the cold end of the bed to ensure that the initial temperature, T_0, was kept constant. Thermocouples were used to measure the temperature of the cooling water. A piezoelectric sensor was inserted between the actuator and the bed of magnetocaloric material so that the magnetizing and demagnetizing work can be calculated from the output force and the distance that the bed was moved.

The permanent magnet was manufactured by TOWA Industrial Co, Ltd., and is capable of providing a maximum magnetic field of 1.07 [T] and over 0.7 [T] within 30 [mm] radius from the point at which the field was at a maximum. The distribution of the

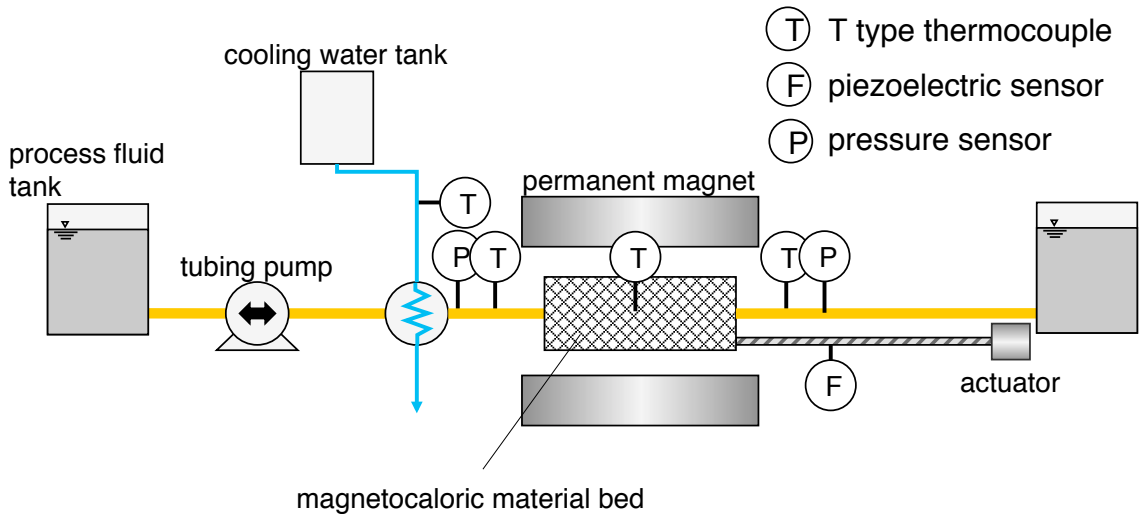

Figure 5.1: Schematic of the experimental arrangement for the active magnetic regenerative heat circulator

strength of the magnetic field at the middle of the space between the magnet is shown in Fig. 5.2. The experimental apparatus is depicted in Fig 5.3.

The sampling frequency of the thermocouple, pressure sensor and force sensor was set to 100 Hz. For the thermocouples, in order to ensure time and temperature resolution, a circuit using an instrumentation amplifier (LT1167) was set. The controlling of the system and the logging of the measured values were done by using LabVIEW 2013 by National Instruments.

Crushed Gd, passed through an 850 [mm] sieve, was packed inside an acrylic tube with an inner diameter of 8.0 [mm]. The bed length, l_b, was 50 [mm] and the void ratio, ϵ, was 0.65. The fluid flow rate, $\dot{m}_f$, was varied between 0.4 and 6.9 [g s^{-1}]. The frequency of the AMR cycle, f, was set to 0.25 [Hz]. The process fluid goes through an aluminum tube (diameter: 1.0 [mm]) with cooling water set to 290.15 [K]. Fig. 5.4 shows a schematic diagram of the magnetocaloric material bed used for experimental investigation of AMR heat circulator. A photo of the magnetocaloric bed is shown in Fig. 5.5.

Photos of the experimental apparatus are shown in Fig 5.6. The photo on the top is the permanent magnet as the field source and the magnetocaloric bed controlled by the

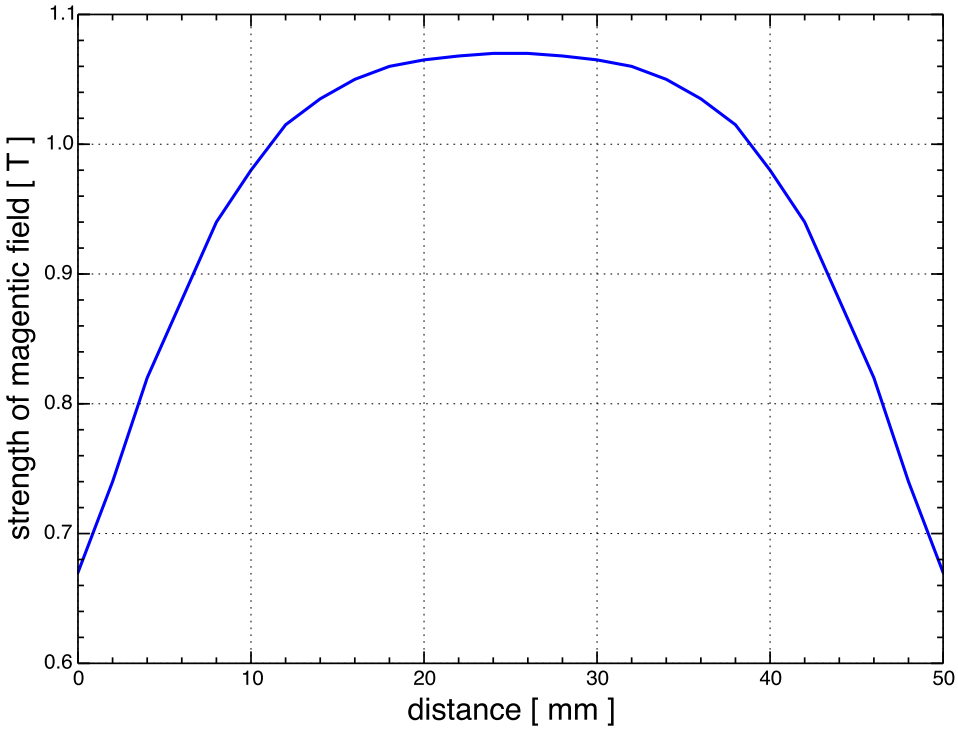

Figure 5.2: Distribution of magnetic field strength by TOWA Industrial Co, Ltd.

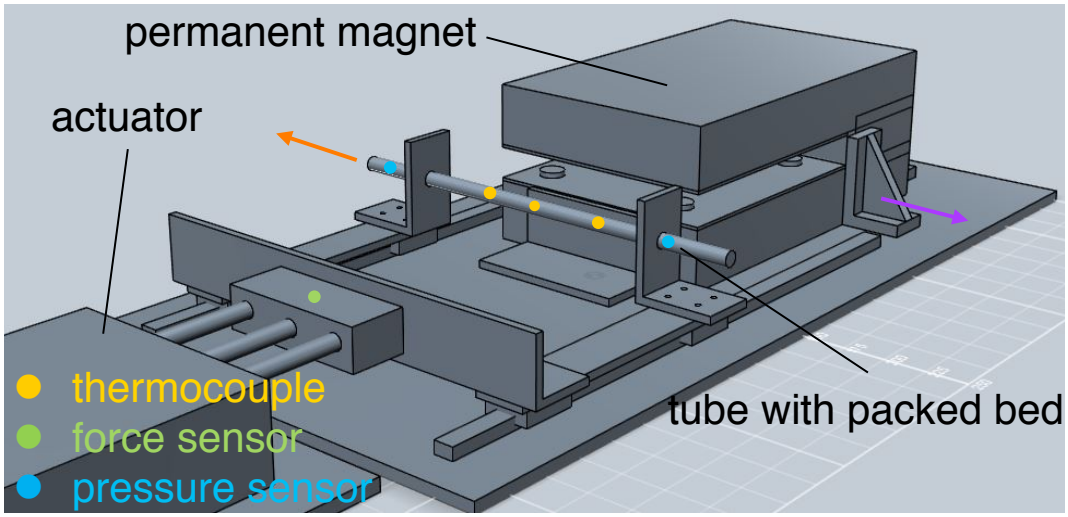

Figure 5.3: Configuration of the experimental arrangement for the active magnetic regenerative heat circulator

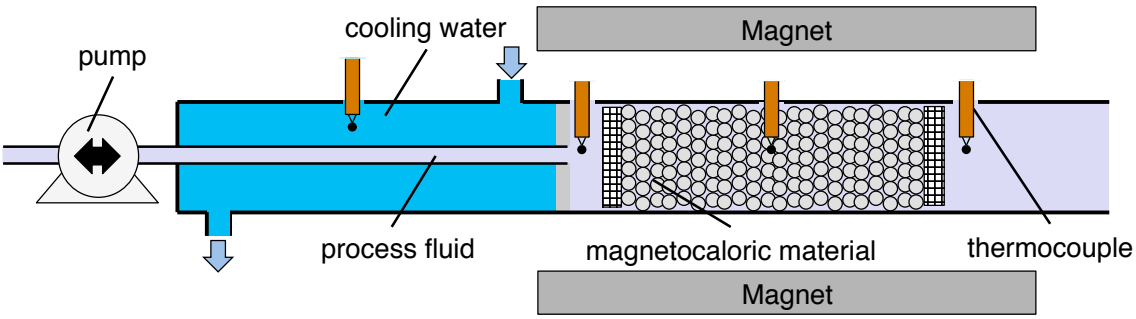

Figure 5.4: Schematic of AMR heat circulator magnetocaloric material bed

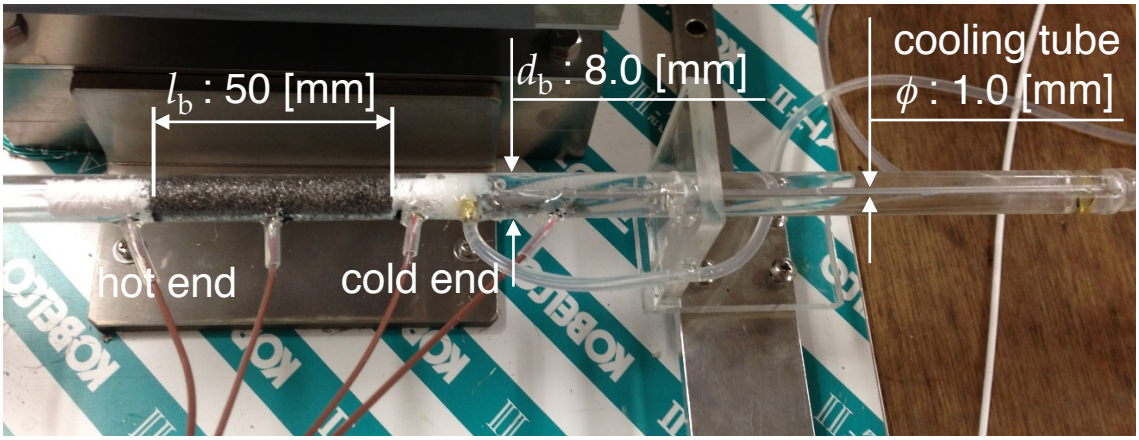

Figure 5.5: Photo of AMR heat circulator magnetocaloric material bed

actuator. The bed is pushed into the permanent magnet for magnetization. The photo on the bottom is the experimental apparatus drawn back. The tubing pump controls the direction and the flow rate of the process fluid, the flexible tube leads to the cooler above the photo.

Table 5.1 shows the parameters for the AMR heat circulator experiments summarized.

Table 5.1: Parameters for the active magnetic regenerative heat circulator experiments

parameters		units	value
environmental temperature	T_0	[K]	296.15
AMR cycle frequency	f	[Hz]	0.25
bed length	l_b	[mm]	50.0
bed diameter	d_b	[mm]	8.0
void ratio	ϵ	[-]	0.65
set mass flow rate	$\dot{m}_\mathrm{f}$	[g s^{-1}]	$0.04 - 0.69$
Gd particles diameter	d_p	[mm]	< 0.85
maximum magnetic field	μH_2	[T]	1.07

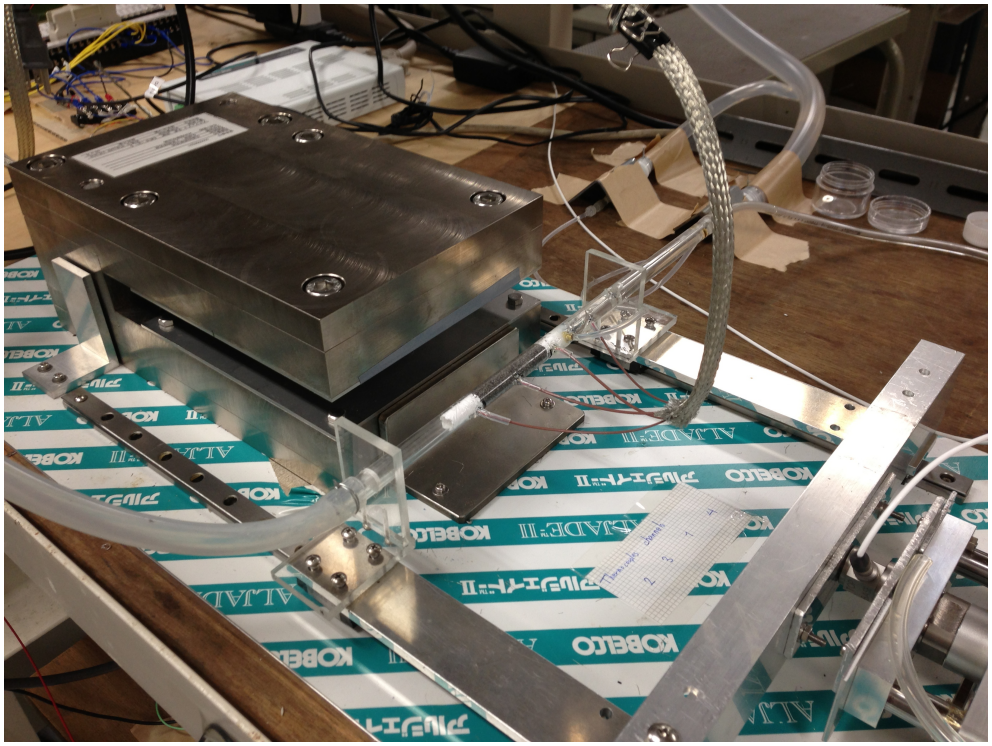

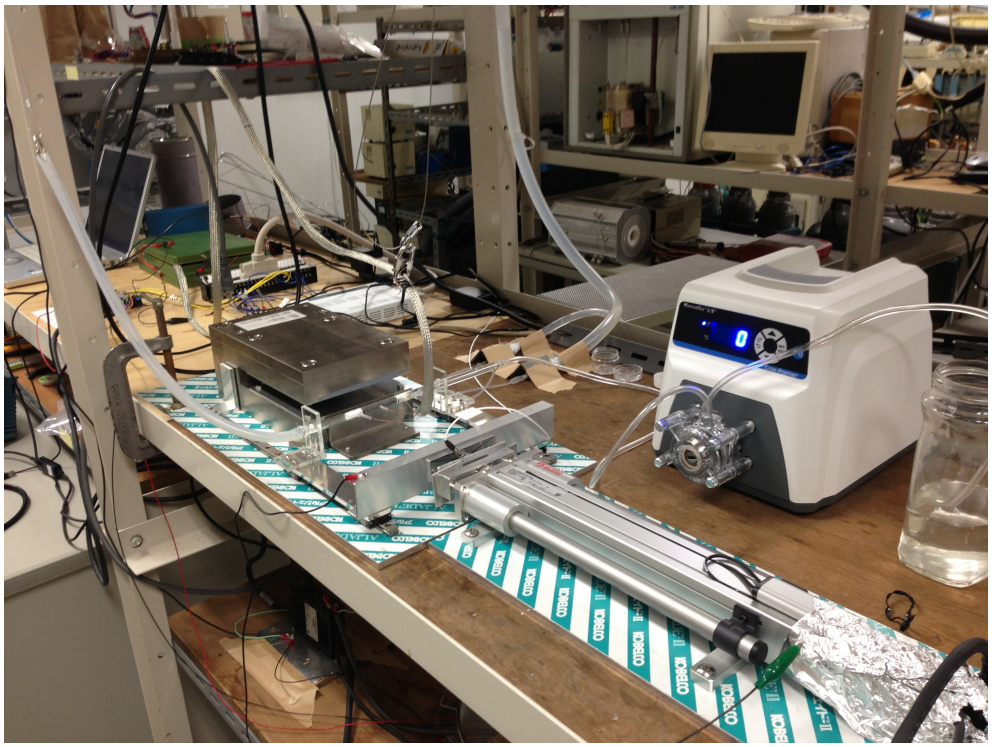

Figure 5.6: Photo of AMR heat circulator experimental apparatus. Magnet and magnetocaloric bed (top) and actuator and tubing pump (bottom)

5.3 Experimental results

5.3.1 Time evolution of bed temperature

Fig. 5.7 (top) shows the temperature evolution of the magnetocaloric packed bed when magnetic field was varied from 0 to 1.07 T, while the bed was filled with water as process fluid. The sharp peaks are due to electromagnetic induction when the thermocouples were inserted to the magnetic field and are of no relevance, thus it was removed from the results as shown in Fig. 5.7 (bottom). Due to the MCE of Gd, it can be seen the temperature of the bed had been changed. A temperature difference of about 0.6 K was seen for magnetization and demagnetization. Considering the void ratio, ϵ, as 0.65 and the heat capacity of water ($c_{\mathrm{f}} = 4.18 \times 10^6$ [J m^{-3} K^{-1}]) and Gd ($c_{\mathrm{s}} \approx 1.19 \times 10^6$ [J m^{-3} K^{-1}]) the adiabatic temperature difference, δT_{ad}, of magnetocaloric material can be calculated to be about 3.3 [K], which is correct value that the MCE of Gd should be showing.

Fig. 5.8 shows the time profile of the bed temperature when the fluid flow, $\dot{m}_{\mathrm{f}}$, was set to 0.16 [g s^{-1}]. Initially, the bed temperature was uniformly at 292 [K]. The temperature difference between the two ends of the bed gradually increases as it undergoes the AMR cycles. After 120 cycles, the temperature difference between the hot and the cold end, ΔT, was around 6.5 [K]. This point is where the heat provided by MCE balanced with the heat discarded from the process fluid. Which will be the startup sequence, because in a self-heat recuperative process, the heat that will be circulated will need to be provided initially. From 120 cycles onwards, the temperature difference between the hot and the cold end of the magnetocaloric packed bed has saturated and will not change, meaning the heat of the process fluid is circulated in between 290.5 [K] and 297.0 [K]. The reason that the temperature difference between the two ends of the magnetocaloric packed bed saturates is because the largest entropy change for the magnetocaloric material can be gained in the vicinity of the Curie temperature; $\theta_{\mathrm{C}} = 293.0$ [K] in the case of Gd. As the temperature moves further from the Curie temperature, θ_{C}, the entropy change gained by the MCE will decrease so that smaller adiabatic temperature difference, ΔT_{ad}, i.e. less

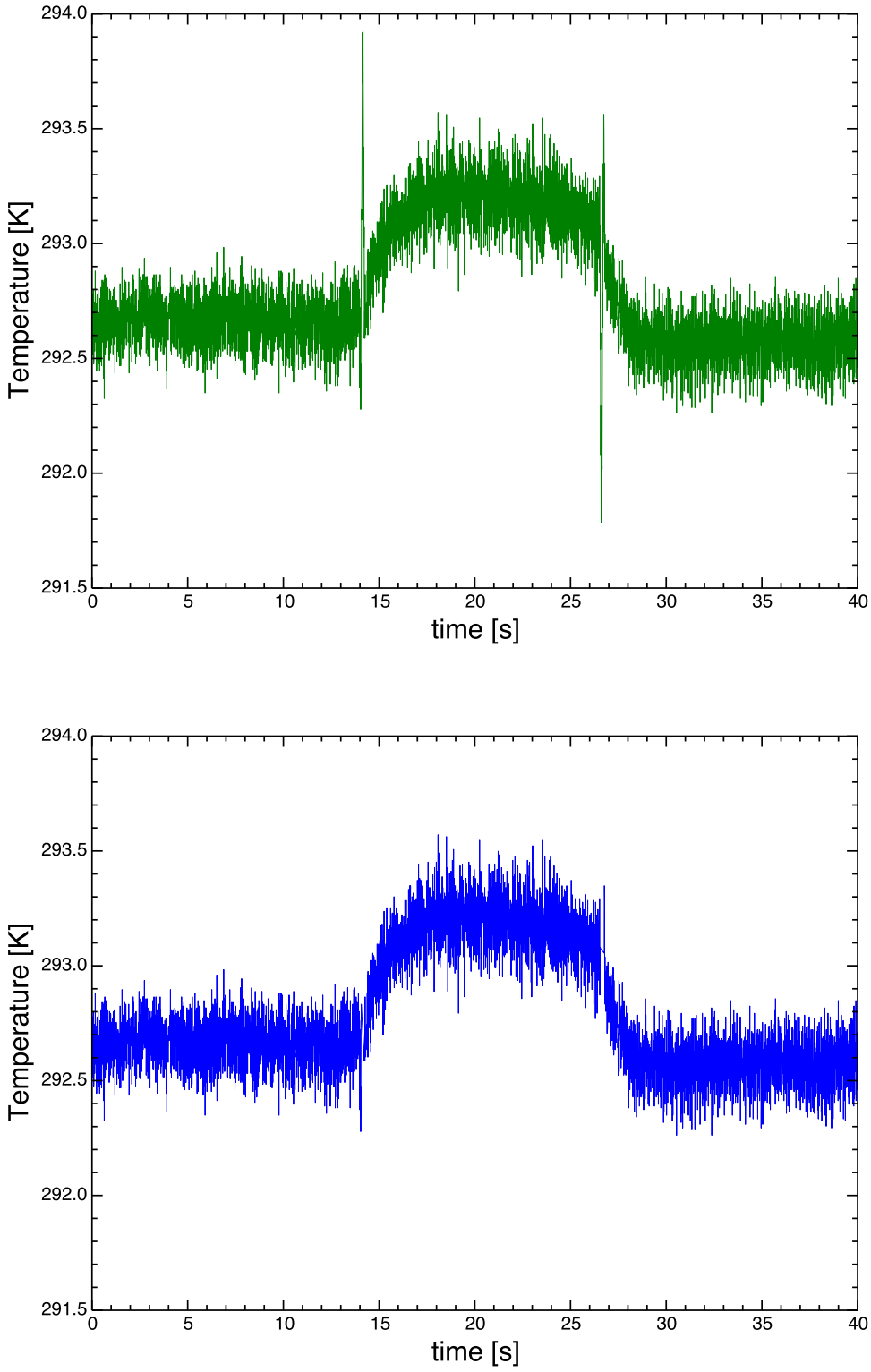

Figure 5.7: Temperature of the magnetocaloric packed bed subjected to a varying field from 0 to 1.07 T, raw data (top) and effect of electromagnetic induction removed (bottom)

heat is gained from the magnetocaloric material after its magnetization. With the set condition, it will take 120 cycles (480 [s]) for start up and is capable of circulating the heat between 6.5 K.

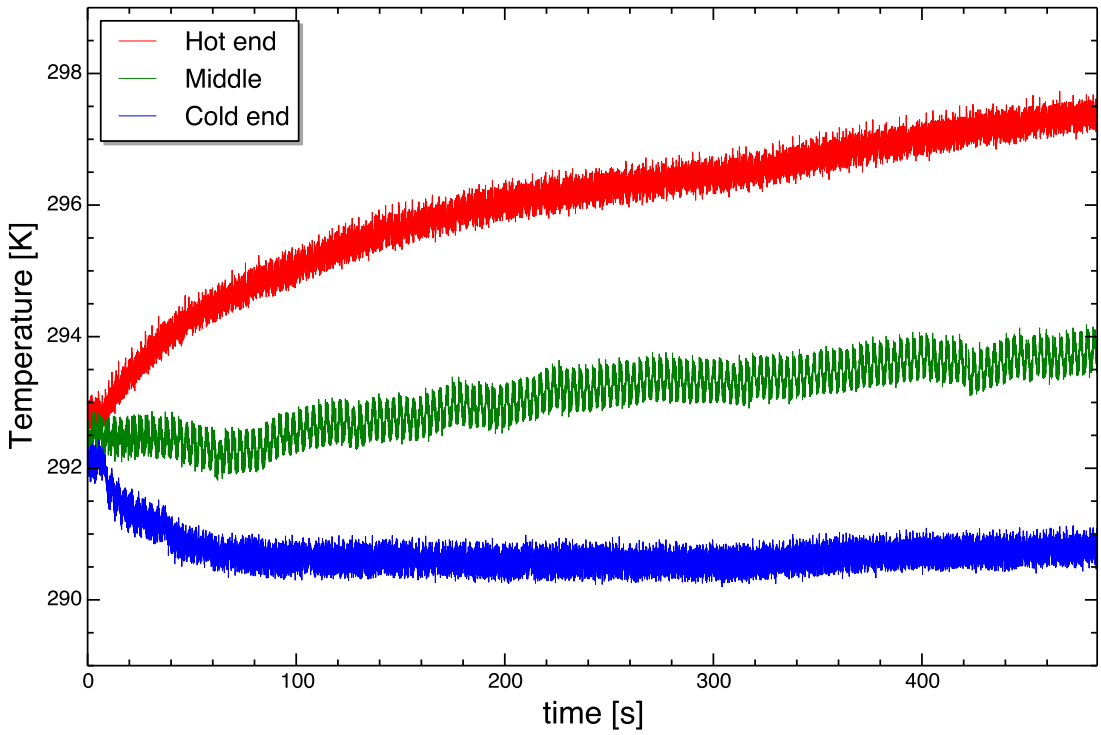

Figure 5.8: Time profile of the magnetocaloric packed bed temperature in the active magnetic regenerative heat circulator

Fig. 5.9 shows the effect of flow rate on the temperature difference between the hot end and the cold end, ΔT, when it has reached saturation (i.e. where the heat started to circulate). It can be seen that above about 0.16 [ml s^{-1}], the larger the flow rate the smaller the temperature difference. This is because a larger quantity of heat is discarded with the process fluid as the flow rate increases. The heat provided by the MCE balanced the heat discarded from the process fluid. A decrease in the temperature difference in the region with a flow rate below 0.16 [g s^{-1}], can be predicted because the effect of thermal conduction becomes significant compared to the heat being carried with the process fluid.

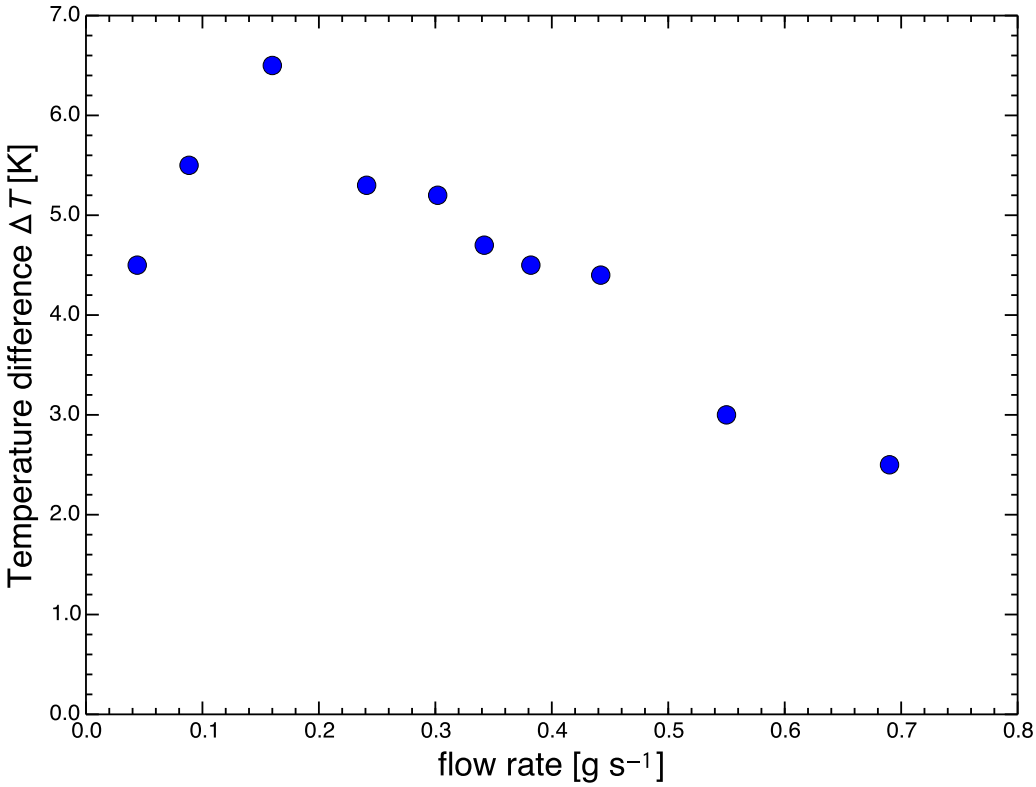

Figure 5.9: Temperature difference between the two ends of the magnetocaloric packed bed at saturation versus the flow rate of the process fluid

It was seen from the experimental results that it is possible to circulate the process stream heat near the Curie temperature, θ_C, of the working magnetocaloric material by applying MCE to self-heat recuperation technology. Although the temperature range in which the process stream heat can be circulated is limited by the Curie temperature of the process material, it is possible to widen the temperature range by using a so called layered bed technique, where magnetocaloric materials with different Curie temperatures are lined in the bed [104].

5.3.2 Energy consumption

The net work, E_{net}, input for the AMR heat circulator can be obtained from the force prevailing, f, during the magnetocaloric packed bed as it is inserted and removed from the magnet and the distance, x, travelled by the bed.

$$W_{\text{mag,demag}} = \int f dx \tag{5.1}$$

Fig. 5.11 shows the output from the piezoelectric sensor for a flow rate of 0.16 [ml s^{-1}]. The force after temperature saturation (120 cycles) has been measured and subtracted from the force measured without the magnet, to cancel the effects of friction and acceleration. The smaller peaks reflect the magnetic force owing to magnetization and the larger peaks as a result of demagnetization.

The area of the peaks when the time axis has been converted to distance represent the work needed for magnetization and demagnetization. The total distance that the actuator moved in one run was 67.6 [mm], maximum speed of 300.0 [mm s^{-1}], and the acceleration and the deceleration was both set to 2.0 [mm s^{-2}]. An average of 5 cycles (120-125 cycles) has been taken to obtain the magnetization work, w_{mag}, of 0.32 [J cycle^{-1}] (minimum 0.27 [J cycle^{-1}], maximum 0.37 [J cycle^{-1}]) and demagnetization work, w_{demag}, of 0.48 [J cycle^{-1}] (minimum 0.38 [J cycle^{-1}], maximum 0.52 [J cycle^{-1}]). The difference between the two work values is the net work input, E_{net}, 0.16 [J cycle^{-1}], provided that the work during magnetization is recovered. Assuming that the process fluid temperature moves

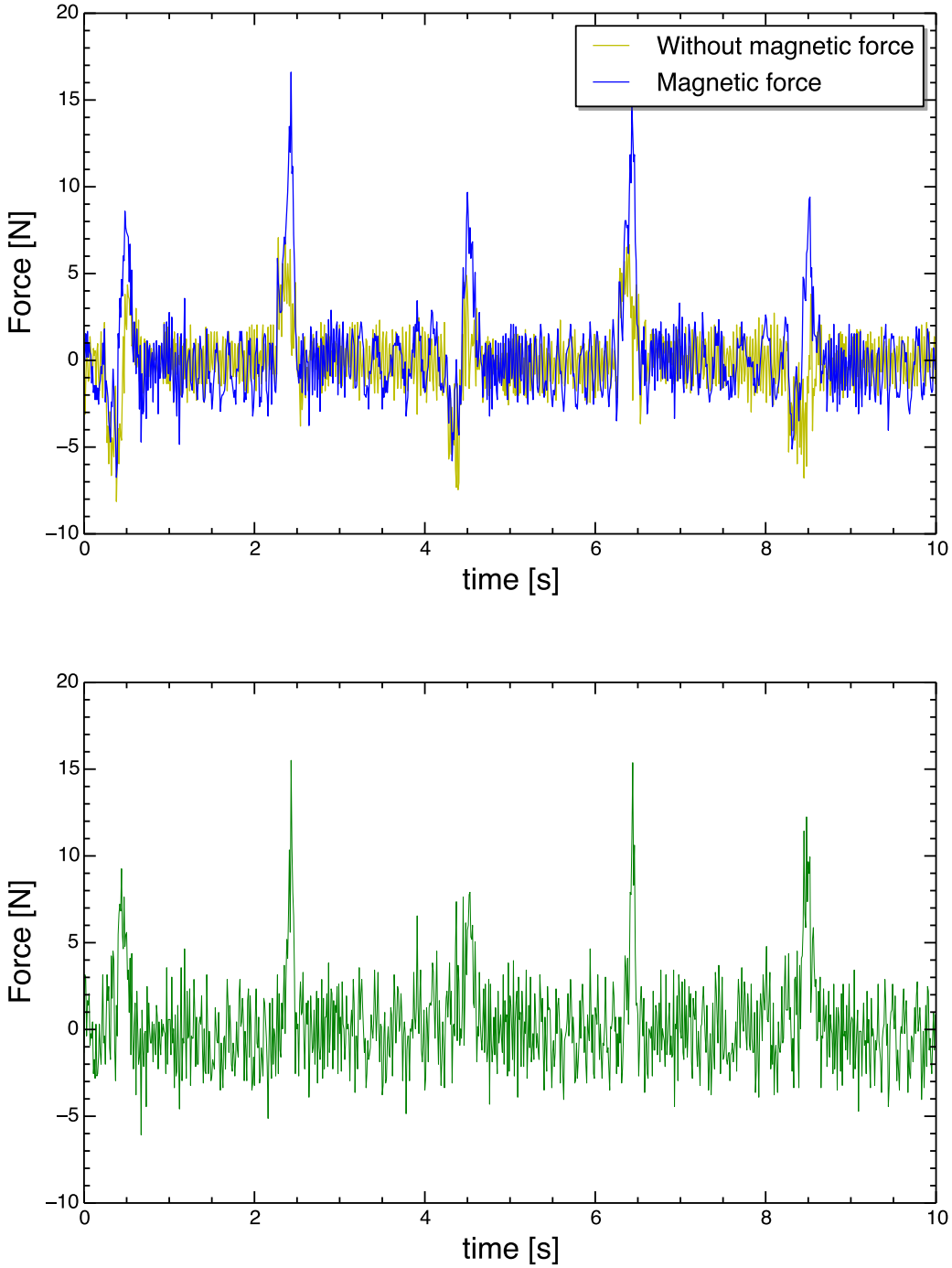

Figure 5.10: Measured force of the magnetocaloric packed bed with and without the magnet (top) and the arithmetic difference between the two forces (bottom)

between 289.5 and 297.0 [K] at 0.16 [g s^{-1}], the circulated heat during one cycle can be calculated as, 8.70 [J $cycle^{-1}$]. This indicates that the system has the potential of reducing the energy consumption to mere 1.8% in contrast to the case where heat is provided external to the system.

When the minimum temperature difference during heat exchange, ΔT_{min}, is decided, the minimum work input needed for heat circulation can be calculated as shown in subsection 2.2.4. The exergy destruction during heat exchange when the heat exchange between the hot and cold fluid was ΔT_{min}, throughout the heat exchange is the minimum work input needed, thus, when the heat capacity of the hot and cold fluid matches. The minimum temperature needed for heat exchange, ΔT_{min}, was derived from the temperature-entropy diagram when the magnetocaloric material; Gd was subjected to a magnetic field of, H_1 (= 0 [T]) and H_2 (= 1.07 [T]). In between 289.5 and 297.0 [K], the smallest adiabatic temperature change ,ΔT_{ad}, is obtained at 297.0 [K]. From the mean field approximation introduced in subsection 3.4.1, the adiabatic temperature change can be calculated as,

$$\Delta T_{\mathrm{ad}}\left(297.0[\mathrm{K}], 0[\mathrm{T}], 1.07[\mathrm{T}]\right) = 3.2[\mathrm{K}] \tag{5.2}$$

The smallest temperature difference during heat exchange should be approximately the half of the adiabatic temperature change, ΔT_{ad} where it is minimum. Thus, the minimum temperature difference during heat exchange, ΔT_{min}, is assumed as 1.6 [K]. The minimum work input derived from the exergy difference during heat exchange is 18.2 [J kg-Gd^{-1}] when 1.66 [kJ kg-Gd^{-1}] of process stream heat is circulated. Which means that theoretically all of the process stream heat can be circulated with mere 1.1 % of the total heat circulated.

The difference between the theoretical minimum exergy destruction when the minimum temperature difference during heat exchange when, ΔT_{min}, is set and the experimentally obtained value can be assumed to be caused by (1) heat loss, (2) dependency of heat capacity to the magnetic field near the Curie temperature, θ_{C}, of the magnetocaloric material, (3) pressure loss, (4) distribution of magnetic field and (5) loss due to overlap-

ping of the cycles AMR cycles when the bed was divided into micro-sections.

From Fig. 5.2 it can be seen that the effect of distribution of magnetic field is not so large since the strength of magnetic field is quite uniform near the region where the strength of magnetic field is maximum.

Fig. 5.11 shows the magnetocaloric heat circulator cycle drawn on a temperature-entropy diagram when heat was circulated in between 290.5 and 297.0 [K]. The strength of the magnetic field, H_1 and H_2, are 0 [T] and 1.07 [T] respectively so that it matches the experimental conditions. In this case, the input work needed for heat circulation is 20.9 [J kg-Gd^{-1}] when process stream heat of 1.66 [kJ kg-Gd^{-1}] is circulated which means that the process stream heat can be circulated with 1.3 % of the total heat circulated if the process stream heat was circulated using MCE of Gd at 0 [T] and 1.07 [T]. The comparison of net work input needed for heat circulation are summarized in Table 5.2. It can be seen that experimental value are showing a reasonably close value to the theoretical minimum work input and that the dependency of Gd's heat capacity to the strength of applied magnetic field accounts for about 30 % of the extra work needed for heat circulation.

Table 5.2: Comparison of minimum (case 1), numerically derived (case 2), and experimentally derived (case 3) net work input,$w$net, and the heat circulated, Q_{cir}

case	Q_{cir}	E_{net}	$E_{\mathrm{net}}/Q_{\mathrm{cir}}$
1	1.66 [kJ kg-Gd^{-1}]	18.2 [J kg-Gd^{-1}]	1.1 %
2	1.66 [kJ kg-Gd^{-1}]	20.9 [J kg-Gd^{-1}]	1.3 %
3	8.70 [J cycle^{-1}]	0.16 [J cycle^{-1}]	1.8 %

Fig. 5.12 shows the comparison between the theoretical minimum exergy destruction, A_{min}, energy consumption derived from temperature-entropy diagram of Gd and energy consumption derived experimentally. The amount of heat circulated, Q_{cir}, is set to 8.70

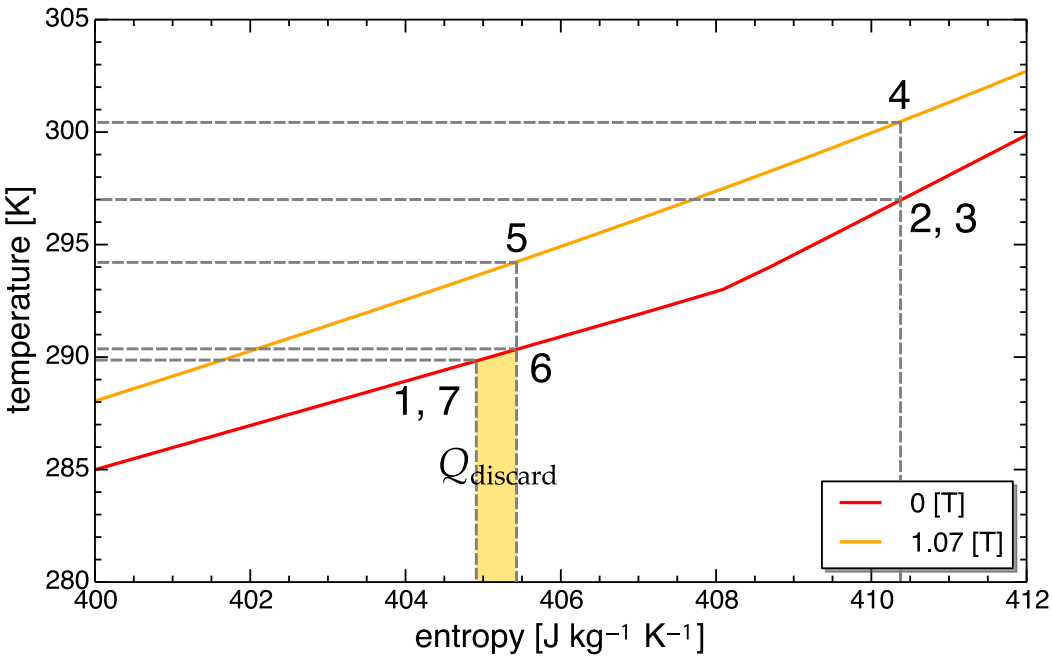

Figure 5.11: Magnetocaloric heat circulator cycle drawn on a temperature-entropy diagram when heat was circulated in between 290.5 and 297.0 [K]

[J cycle^{-1}]. Error bar representing the uncertainty of force measurement has been set on the experimental bar graph.

When there is pressure loss, all of the pump work is transformed into heat at process stream temperature, meaning that if the temperature of the process stream is low, large amount of exergy will be destructed. Fig. 5.13 shows the evolution of the pressure difference, Δp, at the two ends of the magnetocaloric bed in the case when the maximum flow rate, $\dot{m}_{\mathrm{f}}$, was set to 0.16 [g s^{-1}]. The maximum pressure loss is around -10.0 [kPa]. If we assume that the evolution of the mass flow rate changes as shown in Fig. 5.13, the pressure loss after one cycle can be calculated as, 2.5 [mJ cycle^{-1}]. Which only accounts for mere 1.6 % of the total work input for the experimental value (case 3). Thus, it can be said that although pressure loss also leads to irreversibility during heat transfer, the effect is usually very small.

The AMR heat circulator applies a quasi-counter flow heat exchange between the

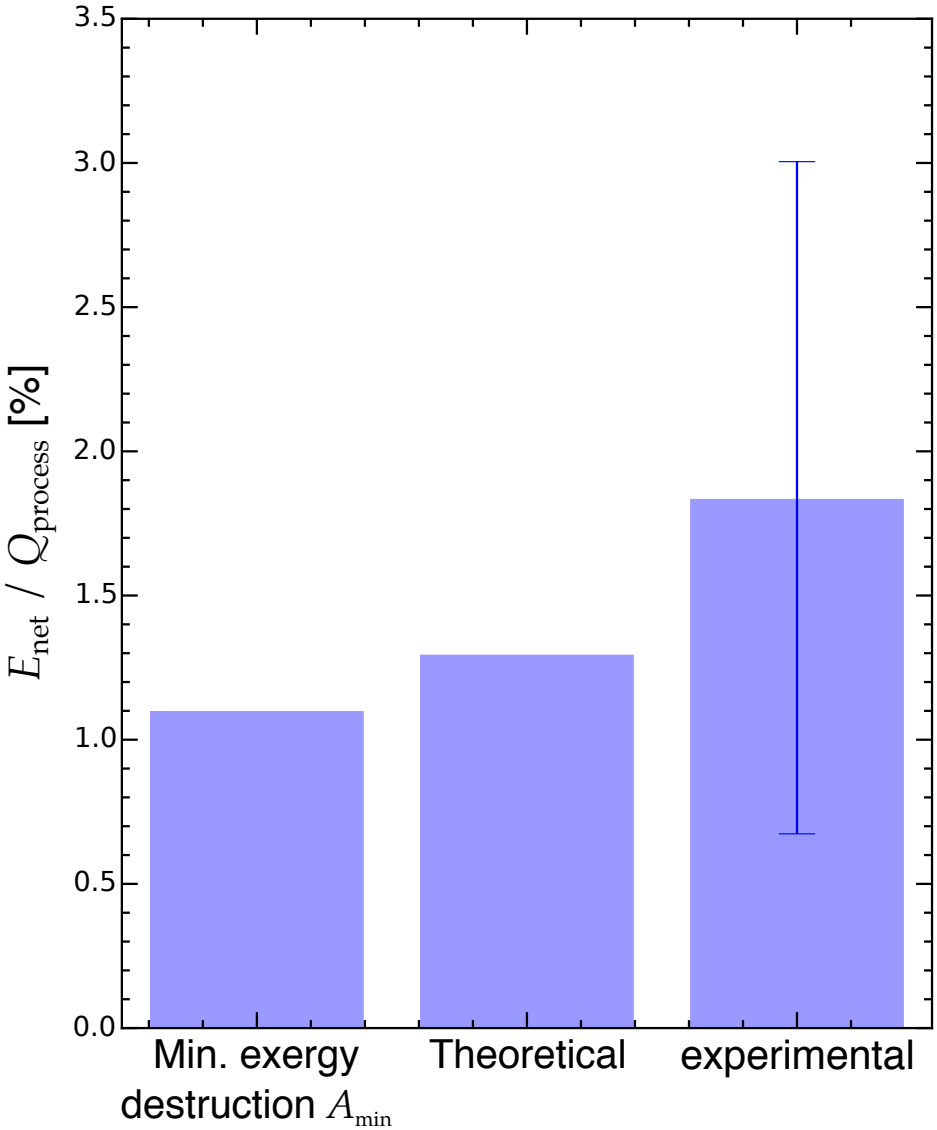

Figure 5.12: Comparison of energy consumption between the theoretical minimum exergy destruction, derived from temperature-entropy diagram, derived from experiment

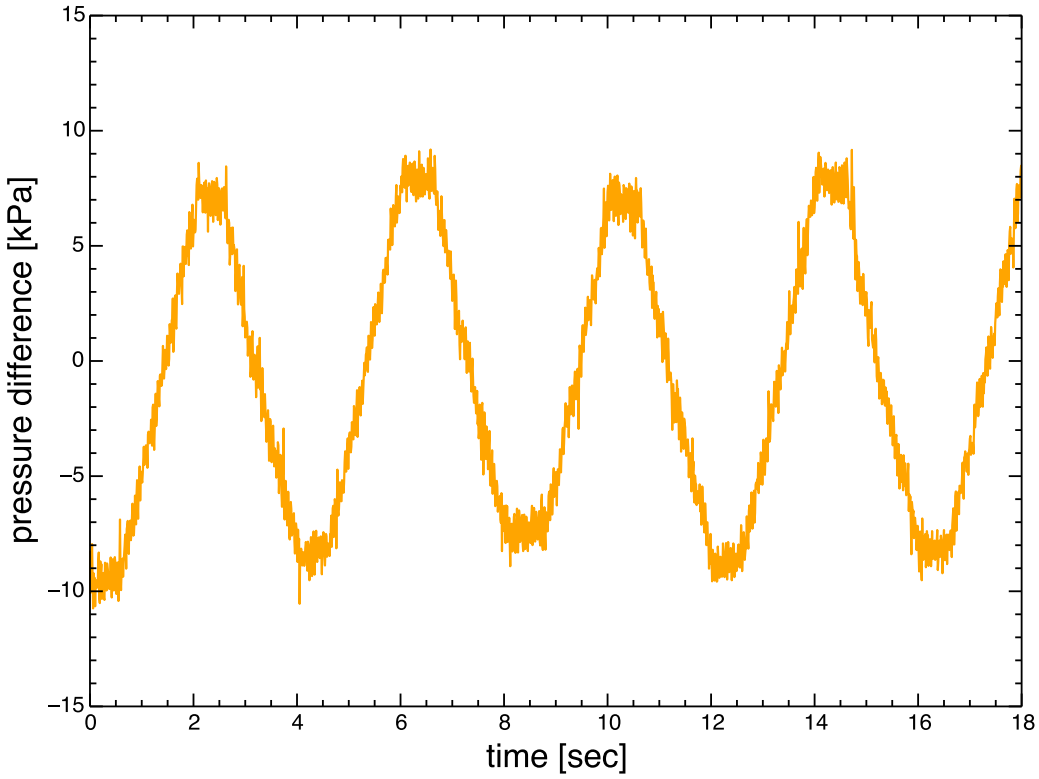

Figure 5.13: Evolution of pressure difference, Δp, at the two ends of the magnetocaloric bed

process stream and the magnetocaloric working material. In the case of calculation of net work input for magnetocaloric heat circulator, the heat exchange between the magnetocaloric working material and the process stream is assumed to be performed in counter flow. During the hot and cold blow step, as the magnetocaloric working material exchange heat with the flowing process stream, the overall temperature will be changed, and the temperature difference between the process stream and the magnetocaloric working material will decrease. If the AMR bed was divided into small sections, each section will draw a heat pump cycle as shown in Fig. 5.14. The net work input for the AMR heat circulator is the sum of the areas surrounded by the heat pump cycle drawn for each divided sections. This means that the net work input for the AMR heat circulator will become larger than the net work input for the case where a counter-flow heat exchange is applied. By increasing the frequency of the AMR cycle, f, it will become possible to realize the net work input being reduced to a value closer to the theoretical net work input. Detailed discussion of the effect of quasi-counter flow heat exchange has been made in section 4.4.2.

Through experimental investigation the heat circulating potential of the AMR heat circulator has been confirmed. Although the temperature difference in which the heat was circulated was merely 6.5 [K] in the experimental investigation, with different magnetocaloric materials, it will become possible to enlarge the temperature difference. Also the amount of input work needed to circulate the heat was very small due to small temperature difference, ΔT_{HEX}, during heat exchange and application of self-heat recuperation technology.

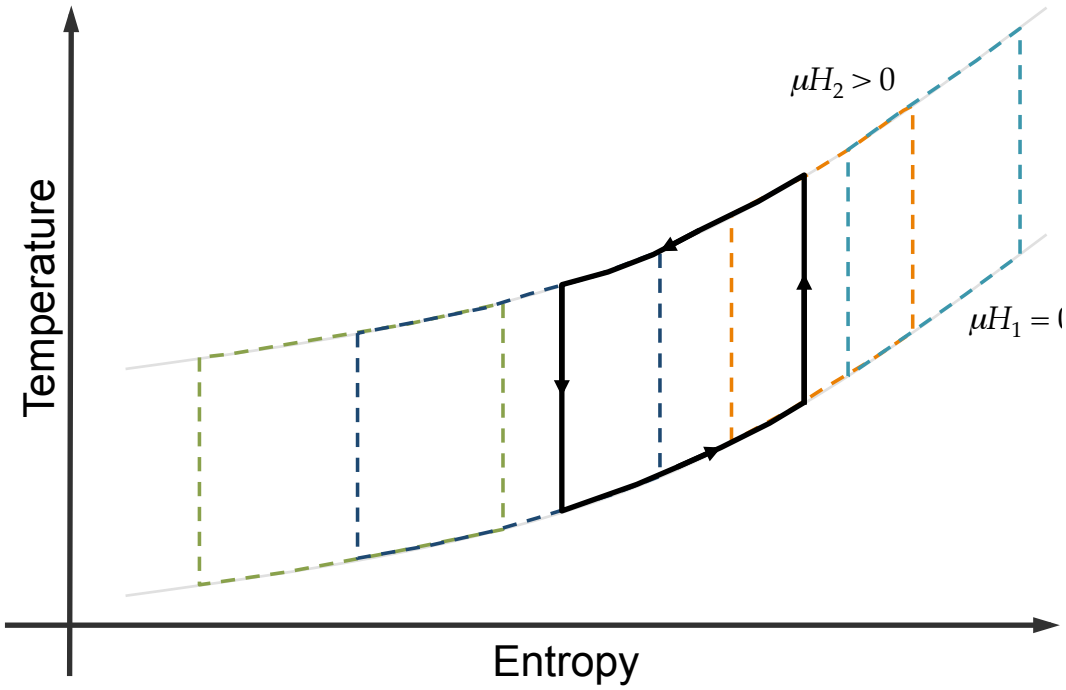

Figure 5.14: Temperature-entropy diagram of an active magnetic regenerative heat circulator divided into micro-sections

5.4 Mathematical model verification

5.4.1 Implement of parameter

In Chapter 4, a mathematical model of an AMR heat circulator has been constructed. Fig. 5.15 shows the time profile of the magnetocaloric packed bed temperature when the parameters for the experiment was implemented to the one dimensional mathematical model. It can be seen that compared to the experimental value, in the mathematical model, much larger temperature gradient is created. The difference can assumed to be caused by heat loss, the molecular field model of MCE, and non-uniformity of the Gadolinium particles resulting in lower heat transfer coefficient, h.

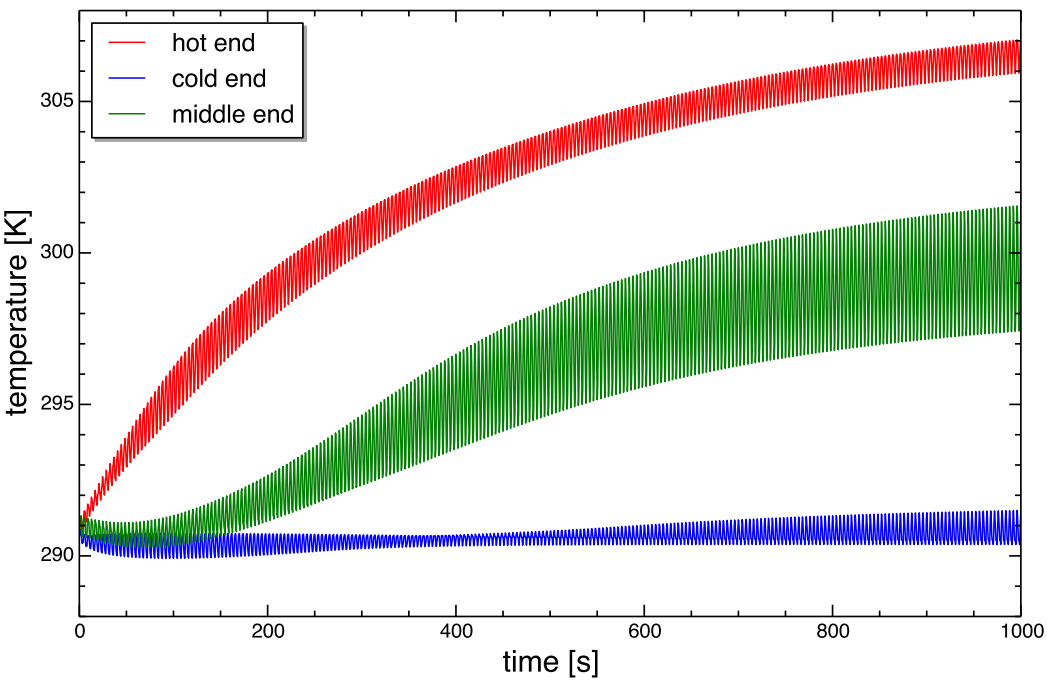

Figure 5.15: Time profile of the magnetocaloric packed bed temperature when the parameters for experiment were implemented to the mathematical model

Fig. 5.16 shows the temperature-entropy diagram of the AMR bed divided into micro-sections calculated by the mathematical model after saturation. The temperature-entropy

diagram does not follow the isobaric line of 0 [T] and 1.07 [T] because the magnetic field created by the permanent magnet was not uniform (Fig. 5.2). Thus, less heat is provided through the MCE at the two ends where the magnetic field is weak.

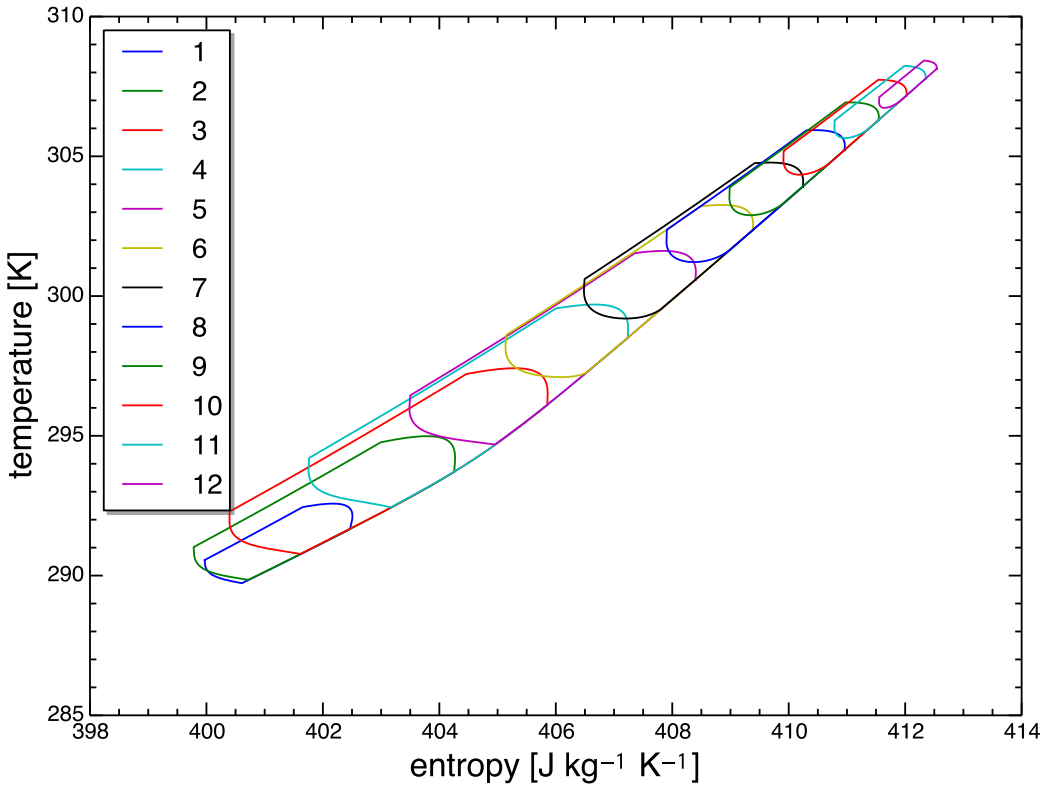

Figure 5.16: Temperature-entropy diagram of the magnetocaloric packed bed divided into micro-sections when the parameters for the experiment were implemented

5.4.2 Model enhancement

In the simulation, the temperature range in which the process stream heat was circulated was much larger than the temperature range obtained in the experiment. Since in the constructed model, the bed was assumed adiabatic towards the environment, heat conduction through the acrylic wall, heat convection between the wall and the process fluid and heat convection between the wall and the environment was considered [99]. The

governing equation derived from the energy conservation of the wall is,

$$\rho_{\mathrm{w}} c_{\mathrm{w}} \frac{\partial T_{\mathrm{w}}}{\partial t} = k_{\mathrm{w}} \frac{\partial^2 T_{\mathrm{w}}}{\partial x^2} + h_{\mathrm{i}} a_{\mathrm{wi}} (T_{\mathrm{f}} - T_{\mathrm{w}}) + h_{\mathrm{amb}} a_{\mathrm{wo}} (T_{\mathrm{amb}} - T_{\mathrm{w}}) \tag{5.3}$$

T_{w}, T_{amb}, ρ_{w}, c_{w}, k_{w}, h_{i}, h_{amb}, a_{wi} and a_{wo} denotes the temperature of the wall, temperature of the ambient ($= T_0$), density of the wall ($= 1180$ [kg m^{-3}]), specific heat capacity of the wall ($= 1.47 \times 10^3$ [J kg^{-1} K^{-1}]), heat conduction rate of the wall ($= 0.19$ [W m^{-1} K^{-1}]) heat convection rate between the wall and the process fluid, heat convection rate between the wall and the ambient, specific heat transfer area between the wall and the process fluid and specific heat transfer area between the wall and the ambient.

The heat convection rate between the wall and the process fluid, h_{i} was assumed the same as the heat transfer rate between the process fluid and the magnetocaloric working material, h by Whitaker [103]. The heat convection between the wall and the ambient was derived from the following equation,

$$\frac{h_{\mathrm{amb}} d_{\mathrm{bo}}}{k_{\mathrm{a}}} = 1.03 \times C_{\mathrm{T}} Ra^{0.25} \tag{5.4}$$

d_{bo} and k_{a} are the outer diameter of the AMR bed ($= 10$ [mm]) and heat conduction rate of air ($= 2.57 \times 10^{-2}$ [W m^{-1} K^{-1}]). C_{T} is

$$C_{\mathrm{T}} = \left(\frac{0.75 Pr_{\mathrm{a}}}{2.4 + 4.9 Pr_{\mathrm{a}}^{0.5} + 5 Pr_{\mathrm{a}}} \right)^{0.25} \tag{5.5}$$

Pr_{a} is the Prandtl number of air. The Rayleigh number, Ra, is

$$Ra = g\beta \frac{(T_{\mathrm{w}} - T_{\mathrm{amb}}) d_{\mathrm{bo}}^3 Pr_{\mathrm{a}}^2}{\nu_{\mathrm{a}}^2} \tag{5.6}$$

g, β are the gravitational acceleration ($= 9.80665$ [m s^{-2}]) and coefficient of thermal expansion of an ideal gas.

A term for the heat transfer between the wall and the process fluid has been added to the energy balance governing equation of the process fluid

$$\rho_{\mathrm{f}} c_{\mathrm{f}} A_{\mathrm{cs}} \epsilon \frac{\partial T_{\mathrm{f}}}{\partial t} + \dot{m}_{\mathrm{f}} c_{\mathrm{f}} \frac{\partial T_{\mathrm{f}}}{\partial x} = A_{\mathrm{cs}} \epsilon k_{\mathrm{f}} \frac{\partial^2 T_{\mathrm{f}}}{\partial x^2} - h a_{\mathrm{s}} (T_{\mathrm{f}} - T_{\mathrm{s}}) + h_{\mathrm{i}} a_{\mathrm{wi}} (T_{\mathrm{w}} - T_{\mathrm{amb}}) \tag{5.7}$$

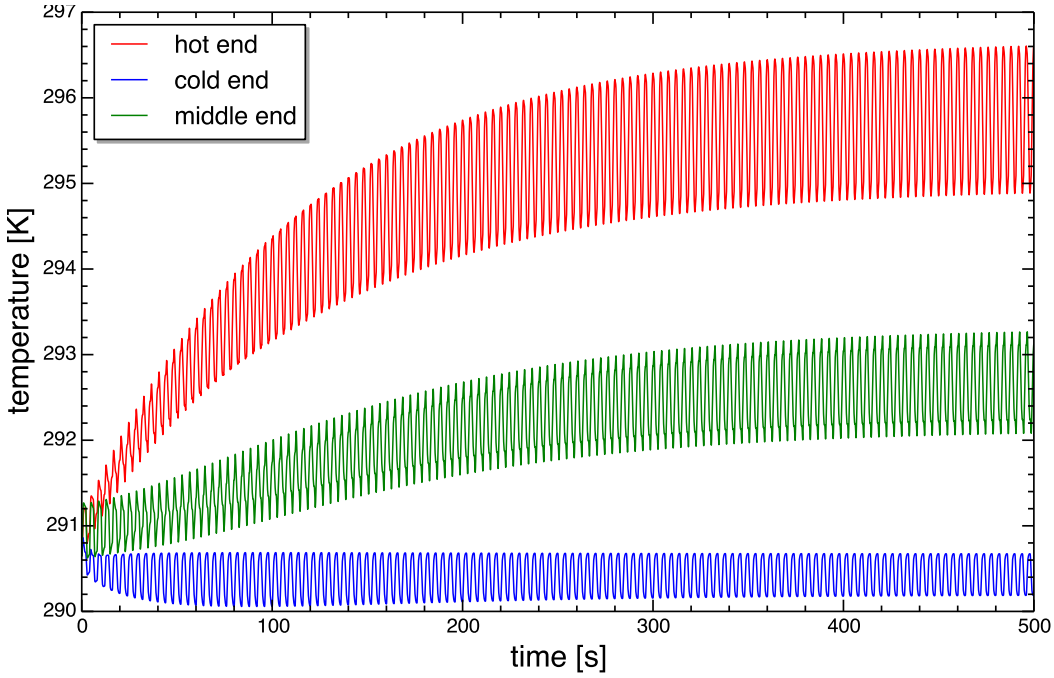

Figure 5.17: Temperature profile of the AMR heat circulator calculated using the enhanced mathematical model

The temperature profile of the AMR heat circulator calculated enhanced mathematical model is shown in Fig. 5.17. It can be seen that after saturation, the heat is circulated in between 290.5 and 295.7 [K], which is in better agreement with the experimental results.

Other factors that has influence on the difference between the experimentally obtained results and the mathematical model are, the amount of heat calculated by MCE and non-uniformity of the Gd particles resulting in lower heat transfer coefficient.

5.5 Conclusion

In this chapter, an AMR heat circulator was newly constructed for experimental investigations. The objective of the experimental investigation was to evaluate the heat circulation and AMR heat circulator and energy saving potentials. In the newly constructed AMR heat circulator, MCE is applied to recuperate the heat exergy of the process fluid so that it can be reused to heat the feed process fluid and realize self-heat recuperation.

In the newly constructed AMR heat circulator, Gd particles under 850 [$^{-}$m] were used as the working magnetocaloric material. Water was used as the process fluid. The AMR bed underwent the AMR cycle in between 0 [T] and 1.07 [T] and was able to circulate heat of 8.70 [J cycle^{-1}] in between 289.5 and 297.0 [K] with mere 0.16 [J cycle^{-1}], which is only 1.8 % of the amount of heat circulated.

The work obtained experimentally was compared with the theoretical minimum exergy due to heat exchange. The obtained result was reasonably in good agreement, indicating that the high energy saving potential of AMR heat circulator.

Additionally, the obtained results were compared with the mathematical model constructed in Chapter 4. The mathematical model was enhanced so that heat loss was considered in the model. The saturation temperature of the AMR bed temperature was in better agreement with the experimental value. However, although the saturation temperature was in a better agreement, the temperature fluctuation and the time needed for saturation still does not match the experimental results and thus, the model is still in need of intensification.

In this chapter, the energy saving potential of the AMR heat circulator based on the concept of magnetocaloric heat circulation has been verified.

Chapter 6

Conclusions and future works

6.1 Conclusion

The first paper published on self-heat recuperation technology was in 2009. Since then, it has proven to have great potentials in energy reduction for vast amount of processes. In a self-heat recuperative process, the feed process stream is adiabatically compressed to gain enough temperature difference needed for heat exchange. Then, all of the process stream heat is circulated within the process with no make-up heat added. If the application of self-heat recuperation technology can be extended, it will have a large impact in the amount of fuel consumption and CO_2 emission.

In the conventional self-heat recuperative processes, compressors were used to recuperate the heat exergy of the process stream. However, compressors can only be applied to gaseous process streams and the adiabatic efficiency can become quite low when implemented to small size applications. In this research, a self-heat recuperative process which utilizes magnetocaloric effect instead of compression has been proposed. First, in order to properly evaluate thermal processes and a reference factor which accounts for the minimum exergy destruction, A_{min}, for heat exchange has been set. Then, the magnetocaloric heat circulator has theoretically been evaluated. Active magnetic regenerative heat circulator has been presented to actualize self-heat recuperation using magne-

tocaloric effect. The AMR heat circulator has been analyzed by a one-dimensional model and experimentally to verify its heat circulating and energy saving potentials.

In Chapter 2, thermal processes were analyzed in terms of irreversibility and exergy. The exergy destructions due to heat transfer and combustion were graphically presented in the temperature-entropy diagram. Also, a method to obtain the minimum exergy destruction for a thermal process when the minimum temperature difference during heat exchange, ΔT_{min}, has been presented. It was seen that exergy destruction for thermal process is minimum when the temperature difference during heat exchange, ΔT_{HEX}, is at ΔT_{min} throughout the heat exchange. The value can be used as a reference factor when evaluating different thermal processes. The exergy destruction of a simple thermal process, thermal process with feed-effluent heat exchanger, and self-heat recuperative thermal process were compared with the minimum exergy destruction during heat exchange. The results showed that the self-heat recuperative process has the least exergy destruction because, 1) exergy is not destroyed in the process of creating heat for provision, and 2) since the heat source and the heat sink is the process stream itself, the amount of heat and the heat capacity matches, leading to small exergy destruction during heat exchange.

In Chapter 3, amongst the several methods to recuperate the heat exergy of the process stream, magnetocaloric effect was chosen and applied to self-heat recuperation. The presented magnetocaloric heat circulator can be applied to process stream that is liquid. The theoretical limit of energy reduction by applying a magnetocaloric heat circulator has been evaluated in terms of temperature-entropy diagram. From the evaluation, it was seen that the magnetocaloric heat circulator has potential of drastic energy reduction by circulating the process stream heat in the vicinity of the Curie temperature, θ_{C}, of the magnetocaloric working material. The energy consumption of heat circulator using magnetocaloric effect and compressors were compared. It was seen that the effect of adiabatic efficiency is large when the temperature range in which the heat is circulated is small. Indicating the potential of magnetocaloric heat circulators for small size applications.

In Chapter 4, an active magnetic regenerative heat circulator to realize self-heat recu-

peration using magnetocaloric effect has been proposed. The AMR heat circulator adopts a quasi-counterflow heat exchange between the process stream and the magnetocaloric working material. In an AMR heat circulator, the heat exchange between the process stream and the magnetocaloric working material can be made small due to heat exchange in packed bed form. A one dimensional mathematical model of an AMR heat circulator has been constructed. From the simulation using the mathematical model, it was seen that the AMR heat circulator has great potential to reduce energy consumption in thermal processes in the vicinity of Curie temperatures, θ_C, of the magnetocaloric working material. Furthermore it was found that in order to obtain high saturation temperature, there is an optimal point for fluid flow rate and cycle time where the effect of convection is maximized and the effect of heat carried out by the process fluid is minimized. Smaller particle size and larger aspect ratio, l_b/d_b, is advantageous if one is in need of large saturation temperature. The effect of these parameters to the energy efficiency; here defined as the ratio of net energy input and minimum exergy destruction, E_{net}/A_{min}.

In Chapter 5, an AMR heat circulator has newly been constructed to verify its potentials seen from the simulation performed in Chapter 4. Gadolinium was used as the magnetocaloric working material and water as process fluid. The time evolution of the temperature gradient inside the magnetocaloric bed was measured along with the magnetic work needed for heat circulation. The ability to circulate the heat of a liquid process stream in the vicinity of the Curie temperature of the magnetocaloric working material with small work input has been verified. The obtained results were compared with the value obtained by the simulation. The model was intensified with by including the heat capacity of the wall surrounding the bed. Although the saturation temperature was in better agreement with the experimental value, the saturation time and the temperature fluctuation during the AMR cycle does not match as well as the saturation temperature.

The two reference factor set for evaluating self-heat recuperative processes, $E_{net}/Q_{process}$ and $A_{min}/Q_{process}$ can be used to understand the energy saving potential of self-heat recuperative process and also understand how far the process is from the theoretical mini-

mum. The proposed heat circulator that uses magnetocaloric effect showed great potential of energy saving compared to conventional energy saving technologies based on heat recovery, but requires more energy than the heat circulator which utilizes compression. The difference is caused by the dependency of heat capacity to magnetic field and the fact that active magnetic regeneration implies a quasi-counterflow heat exchange thus a part of input energy is used to raise the temperature of the AMR bed. The simulation model built was able to capture the trend of the temperature profile during the AMR cycle and the effect of parameters, but is still in need of intensification to predict the saturation temperature.

6.2 Future works

6.2.1 Minimum exergy destruction

In Chapter 2 a method to obtain the minimum exergy destruction, $A_{\min}$, in thermal processes when the minimum temperature difference during heat exchange, $\Delta T_{\min}$, is decided. In the method, exergy destruction due to combustion and exergy destruction due to heat exchange has been taken into account. Here, in a heat exchanger, it is assumed that the exergy destruction due to heat transfer is much larger than the exergy destruction due to pressure loss. However, since the exergy destruction due to heat exchange is proportional to the minimum temperature difference during heat exchange, if the heat exchanger is enhanced to decrease the minimum temperature during heat exchange, there will be trade off between the exergy destruction due to heat exchange and exergy destruction due to pressure loss (i.e. the heat transfer coefficient, h, can be increased drastically by applying a fluidized bed, but the pressure loss will increase severely as well). Thus, it can be said that there will be some optimal point where the sum of exergy destruction due to heat transfer and exergy destruction due to pressure loss will be minimized. We will be needing to develop methodology to obtain the minimum exergy destruction for thermal processes including pressure loss.

6.2.2 Enhancement of magnetocaloric heat circulator

In Chapter 3, a method to obtain the theoretical energy consumption for a magnetocaloric heat circulator using a temperature-entropy diagram is presented. Chapter 4 and 5 describes the Active Magnetic Regenerative heat circulator which can actualize the concept of magnetocaloric heat circulation. It was described that the applying of a quasi-counterflow heat exchange between the process fluid and the magnetocaloric working material, results in extra energy consumption. The AMR heat circulator consists of numbers of parameters including geometries of the regenerative bed, characteristics and the flow rate of the process material, characteristics of the magnetocaloric working material,

cycle frequency. . . etc. A method in which to optimize these parameters to obtain the maximum temperature difference for heat circulation, or the maximum efficiency is needed. The characteristics of the magnetocaloric working material also relies on the material which is used. Since in order to obtain the maximum entropy change due to field variation, the magnetocaloric working material is used in the vicinity of the turning point, making their physical parameters difficult to characterize. It is needed to enhance the mathematical model of the AMR heat circulator so that it can be implemented to various magnetocaloric working material and configure an optimization method. Furthermore, it is possible to have different magnetocaloric materials with different Curie temperatures, θ_C, a so called 'layered bed technique' to enlarge the temperature difference in which the AMR heat circulator circulates. If this method is to be implemented, additional parameters such as the number of layers, length of each layer must be optimized as well.

For the enhancement of the device itself, a method to obtain the "ideal" adiabatic temperature change, ΔT_{ad}, during heat exchange is needed. It was described in Chapter 2 the method to obtain the minimum exergy destruction, A_{min}, for thermal processes is when the temperature difference during heat exchange is ΔT_{min} from start to end. If the gradient of the magnetic field can be controlled so that the adiabatic temperature change, ΔT_{ad}, is equal to the minimum temperature difference needed for heat exchange, ΔT_{min}, it will become possible to minimize the exergy destruction for magnetocaloric heat circulators. Another method to obtain the ideal distribution of adiabatic temperature change, ΔT_{ad}, is by layering different magnetocaloric materials with a distribution of Curie temperatures, θ_C. A precise model of a magnetocaloric heat circulator is needed for optimizing the magnetic field, or the distribution of the magnetocaloric materials.

Appendix A

Calculation of heat exergy

Often, the exergy rate of heat is expressed by Eq. 2.8. This can be applied if the heat source which holds the heat can has a heat capacity of infinite. The case can be realized with latent heat. Fig. A.1 shows the temperature-entropy diagram for heat source with heat capacity of infinite. Since the integration of temperature by entropy resembles heat, the area surrounded in purple is the amount of total energy that the heat holds. The maximum work that can be obtained from this heat can be calculated by the well known, Carnot efficiency as

$$w_{\max} = Q\frac{T - T_0}{T} \tag{A.1}$$

Thus, the area colored in yellow is the amount of maximum work, or the exergy which the heat holds.

When we evaluate the exergy of heat at a certain temperature, it is important to consider the carrier of the heat. If the carrier of the heat is sensible heat, the amount of exergy that the heat holds can be calculated by Eq. 2.11. Fig. A.2 shows the temperature-entropy diagram of heat source for sensible heat. The area surrounded by the purple line is the total amount of heat which is held by the sensible heat. It is noted that the area shape is not rectangular as it was the case for latent heat. The maximum work can be calculated as

$$w_{\max} = Q - T_0(S - S_0) \tag{A.2}$$

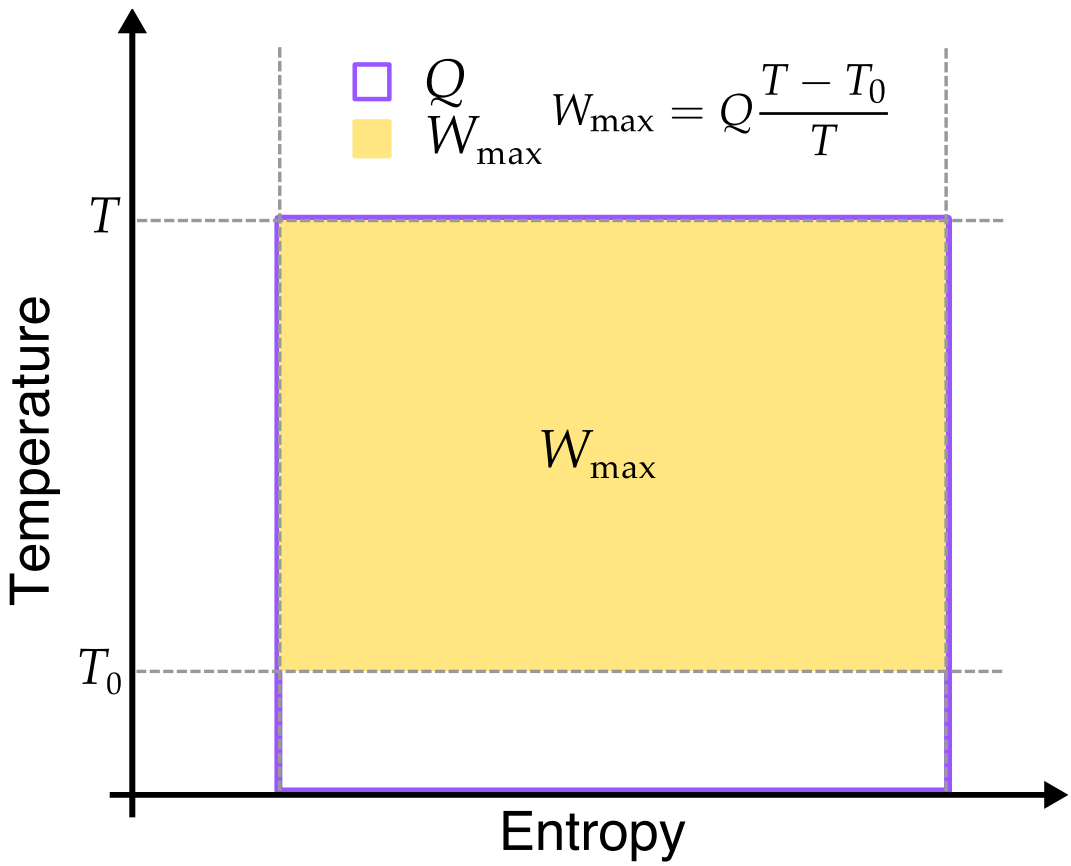

Figure A.1: Temperature-entropy diagram showing exergy of heat for latent heat

The yellow area represents the maximum work, $W_{\max}$, or the amount of exergy that the sensible heat holds.

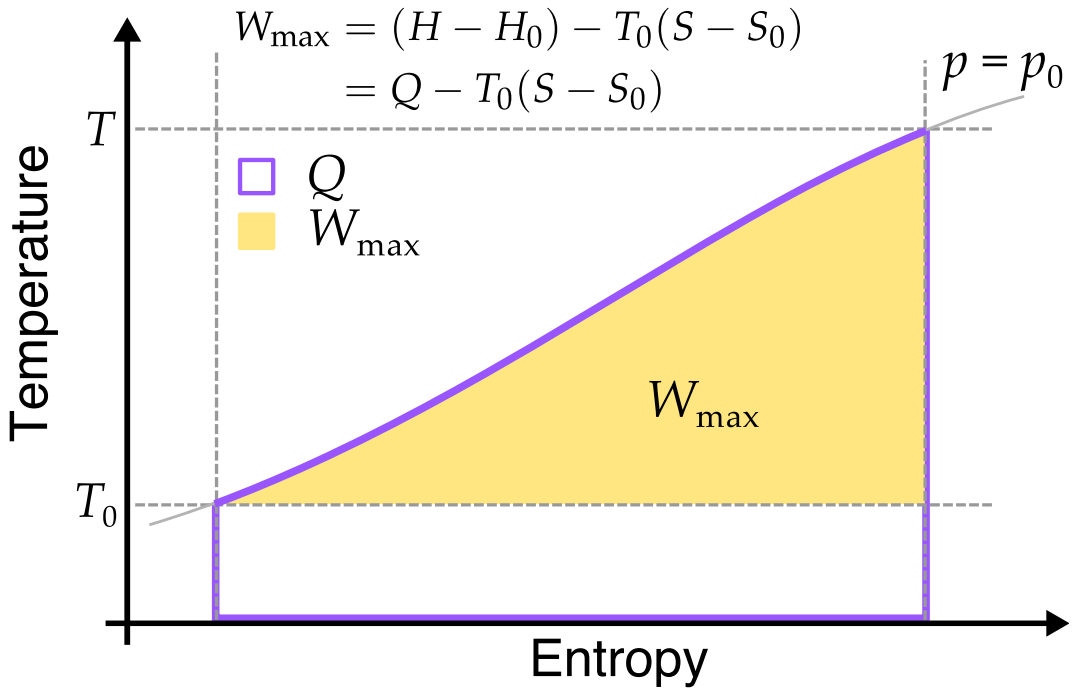

Figure A.2: Temperature-entropy diagram showing exergy of heat for sensible heat

Fig. A.3 shows the comparison of heat exergy rate carried by different carriers. Carnot resembles the latent heat case, and the rest are for the sensible heat. It can be seen that there are slight differences between the carriers due to the difference of heat capacity.

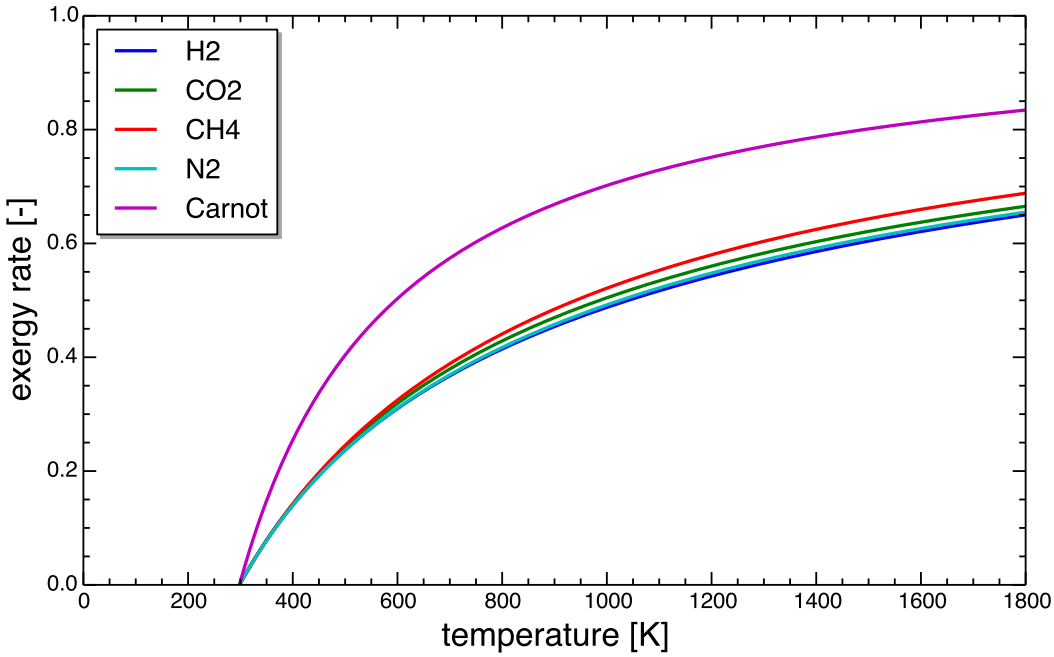

Figure A.3: Comparison of exergy rate at different temperatures, depending on the carrier of the heat

Literatures cited

[1] Boden, T A, G Marland, and R J Andres. 2010. "Global, Regional, and National Fossil-Fuel CO2 Emissions." Carbon Dioxide Information Analysis Center, Oak Ridge National Laboratory, U.S. Department of Energy, Oak Ridge, Tenn., U.S.A.

[2] Shafiee, S, and E Topal. 2009. "When Will Fossil Fuel Reserves Be Diminished?" *Energy Policy* **37** (1): 181 – 89.

[3] National Greenhouse Gas Inventory Report of JAPAN. (2014) Ministry of Environment, Japan. Greenhouse Gas Inventory Office of Japan (GIO), CGER, NIES

[4] Maruoka, N, K Sato, J Yagi, and T Akiyama. 2002. "Development of PCM for Recovering High Temperature Waste Heat and Utilization for Producing Hydrogen by Reforming Reaction of Methane." *ISIJ International* **42** (2): 215 – 219.

[5] Linnhoff, B, and E Hindmarsh. 1983. "The Pinch Design Method for Heat Exchanger Networks." *Chemical Engineering Science* **38** (5): 745 – 763.

[6] Linnhoff, B, and A R Eastwood. 1987. "Overall Site Optimization by Pinch Technology." *Chemical Engineering Research and Design* **65**: 138 – 144.

[7] Matsuda, K, Y Hirochi, H Tatsumi, and T Shire. 2009. "Applying Heat Integration Total Site Based Pinch Technology to a Large Industrial Area in Japan to Further Improve Performance of Highly Efficient Process Plants." *Energy* **34** (10): 1687 – 1692.

[8] Zhao, Z, G Liu, and X Feng. 2006. "New Graphical Method for the Integration of Hydrogen Distribution Systems." *Industrial & Engineering Chemistry Research* **45** (19): 6512 – 6517.

[9] Zhelev, T.K., and N Bhaw. 2000. "Combined Water – oxygen Pinch Analysis for Better Wastewater Treatment Management." *Waste Management* **20** (8): 665 – 670.

[10] Alwi, W, S Rafidah, N E M Rozali, Z Abdul-Manan, and J J Kleme š . 2012. "A Process Integration Targeting Method for Hybrid Power Systems." *Energy* **44** (1): 6 – 10.

[11] Kansha, Y, N Tsuru, K Sato, C Fushimi, and A Tsutsumi. 2009. "Self-Heat Recuperation Technology for Energy Saving in Chemical Processes." *Industrial & Engineering Chemistry Research* **48** (16): 7682 – 7686.

[12] Aspelund, A, D O Berstad, and T Gundersen. 2007. "An Extended Pinch Analysis and Design Procedure Utilizing Pressure Based Exergy for Subambient Cooling." *Applied Thermal Engineering* **27** (16): 2633 – 2649.

[13] Tsutsumi, A. 2004. "Advanced IGCC/IGFC using exergy recuperation technology." *CCT Journal* **11**: 17 – 22.

[14] Kuchonthara, P, S Bhattacharya, and A Tsutsumi. 2005. "Combination of Thermochemical Recuperative Coal Gasification Cycle and Fuel Cell for Power Generation." *Fuel* **84** (7-8): 1019 – 1021.

[15] Tsutsumi, A. 2012. "Innovative Energy Saving Technology by Exergy Recuperation." *Journal of the Japan Institute of Energy* **91** (7): 592-598.

[16] Kuchonthara, P, and A Tsutsumi. 2006. "Energy-Recuperative Coal-Integrated Gasification / Gas Turbine Power." *Journal of Chemical Engineering of Japan* **39** (5): 545 – 552.

[17] Dincer, I, and M A Rosen. 2007. ”Exergy: Energy, Environment and Sustainable Development.” Elsevier Science

[18] 吉田邦夫編、(1999). エクセルギー工学—理論と実際. 共立出版

[19] Cox, J.D.; Wagman, D.D.; Medvedev, V.A., CODATA Key Values for Thermodynamics, Hemisphere Publishing Corp., New York, 1984, 1.

[20] Chase, M.W., Jr., NIST-JANAF Thermochemical Tables, Fourth Edition, J. Phys. Chem. Ref. Data, Monograph 9, 1998, 1-1951.

[21] 信澤寅男、(1980). エネルギー工学のためのエクセルギー入門. オーム社

[22] Yaws, C. (1998). ”Chemical Properties Handbook: Physical, Thermodynamics, Environmental Transport, Safety & Health Related Properties for Organic & (Mcgraw-Hill Handbooks).”

[23] Kansha, Y, N Tsuru, C Fushimi, K Shimogawara, and A Tsutsumi. 2010. “An Innovative Modularity of Heat Circulation for Fractional Distillation.” *Chemical Engineering Science* **65** (1). 330 − 334.

[24] Kansha, Y, N Tsuru, C Fushimi, and A Tsutsumi. 2010. “Integrated Process Module for Distillation Processes Based on Self-Heat Recuperation Technology.” *Journal of Chemical Engineering of Japan* **43** (6): 502 − 507.

[25] Kansha, Y, N Tsuru, C Fushimi, and A Tsutsumi. 2010. “New Design Methodology Based on Self-Heat Recuperation for Production by Azeotropic Distillation.” *Energy & Fuels* **24** (11): 6099 − 6102.

[26] Matsuda, K, K Kawazuishi, Y Kansha, C Fushimi, M Nagao, H Kunikiyo, F Masuda, and A Tsutsumi. 2011. “Advanced Energy Saving in Distillation Process with Self-Heat Recuperation Technology.” *Energy* **36** (8) 4640-4645.

[27] Kansha, Y, A Kishimoto, T Nakagawa, and A Tsutsumi. 2011. "A Novel Cryogenic Air Separation Process Based on Self-Heat Recuperation." *Separation and Purification Technology* **77** (3). 389 – 396.

[28] Kishimoto, A, Y Kansha, C Fushimi, and A Tsutsumi. 2011. "Exergy Recuperative CO2 Gas Separation in Post-Combustion Capture." *Industrial & Engineering Chemistry Research* **50**: 10128 – 10135.

[29] Kishimoto, A, Y Kansha, C Fushimi, and A Tsutsumi. 2012. "Exergy Recuperative CO2 Gas Separation in Pre-Combustion Capture." *Clean Technologies and Environmental Policy* **14** (3): 465 – 474.

[30] Fushimi, C, Y Kansha, M Aziz, K Mochidzuki, S Kaneko, A Tsutsumi, K Matsumoto, et al. 2010. "Novel Drying Process Based on Self-Heat Recuperation Technology." *Drying Technology* **29** (1): 105 – 110.

[31] Aziz, M, Y Kansha, A Kishimoto, Y Kotani, Y Liu, and A Tsutsumi. 2012. "Advanced Energy Saving in Low Rank Coal Drying Based on Self-Heat Recuperation Technology." *Fuel Processing Technology* **104** 16 – 22.

[32] Aziz, M, C Fushimi, Y Kansha, K Mochidzuki, S Kaneko, A Tsutsumi, K Matsumoto, et al. 2011. "Innovative Energy-Efficient Biomass Drying Based on Self-Heat Recuperation Technology." *Chemical Engineering & Technology* **34** (7): 1095 – 1103.

[33] Liu, Y, M Aziz, C Fushimi, Y Kansha, K Mochidzuki, S Kaneko, A Tsutsumi, et al. 2012. "Exergy Analysis of Biomass Drying Based on Self-Heat Recuperation Technology and Its Application to Industry: A Simulation and Experimental Study." *Industrial & Engineering Chemistry Research* **51** (30): 9997 – 10007.

[34] Liu, Y, M Aziz, Y Kansha, S Bhattacharya, and A Tsutsumi. 2014. "Application of the Self-Heat Recuperation Technology for Energy Saving in Biomass Drying System." *Fuel Processing Technology* **117** 66 – 74.

[35] Mizuno, H, Y Kansha, A Kishimoto, and A Tsutsumi. 2012. “Thermal Seawater Desalination Based on Self-Heat Recuperation.” *Clean Technologies and Environmental Policy* **15** (5): 765 – 769.

[36] Mizuno, H, Y Kansha, A Kishimoto, and A Tsutsumi. 2012. “Thermal Desalination Process Based on Self-Heat Recuperation.” *Chemical Engineering Transactions* **29**: 379 – 384.

[37] 新日鉄住金エンジニアリングニュースリリース. 2012. バイオエタノール製造コストを大幅削減！～自己熱再生理論を用いた省エネ蒸留プロセス実証試験～ http://www.eng.nssmc.com/news/detail/131

[38] Tishin, A M, Y I Spichkin. 2003. ”Magnetocaloric effect and its Applications” CRC Press

[39] Pecharsky, V K, and K A Gschneidner. 1999. “Magnetocaloric Effect and Magnetic Refrigeration.” *Journal of Magnetism and Magnetic Material*s **200**: 44 – 56.

[40] Warburg, E. 1881. ”Magnetische untersuchungen.” *Annalen der Physik* **249**: 141-164.

[41] Debye, P. 1926. ”Einige bemerkungen zur magnetisierung bei tiefer temperatur.” *Annalen der Physik* **386**: 1154-1160.

[42] Giauque, W. F. 1927. ”A thermodynamic treatment of certain magnetic effects. A proposed method of producing temperatures considerably below 1 absolute.” *Journal of the American Chemical Society* **49**: 1864-1870.

[43] Gschneidner, K A, and V K Pecharsky. 2000. “Magnetocaloric Materials.” *Annual Review of Material Science* **30**(1): 387 – 429.

[44] Yu, B, M Liu, P W Egolf, and A Kitanovski. 2010. “A Review of Magnetic Refrigerator and Heat Pump Prototypes Built before the Year 2010.” *International Journal of Refrigeration* **33** (6): 1029 – 1260.

[45] Pecharsky, V K, K A Gschneidner, A Pecharsky, and A M Tishin. 2001. "Thermodynamics of the Magnetocaloric Effect." *Physical Review B* **64** (14): 144406.

[46] Kihara, T, Y Kohama, Y Hashimoto, S Katsumoto, and M Tokunaga. 2013. "Adiabatic Measurements of Magneto-Caloric Effects in Pulsed High Magnetic Fields up to 55 T." *The Review of Scientific Instruments* **84** (7): 074901.

[47] Kitanovski, A, and P W Egolf. 2006. "Thermodynamics of Magnetic Refrigeration." *International Journal of Refrigeration* **29** (1): 3 – 21.

[48] Dan' kov, S Y, A M Tishin, V K Pecharsky, and K A Gschneidner. 1998. "Magnetic Phase Transitions and the Magnetothermal Properties of Gadolinium." *Physical Review B* **57**(6): 3478 – 3490.

[49] Bednarz, G, D J W Geldart, and M A White. 1993. "Heat Capacity of Gadolinium near the Curie Temperature." *Physical Review B* **47**(21): 247 – 259.

[50] Benford, M, and G V Brown. 1981. "T-S Diagram for Gadolinium near the Curie Temperature." *Journal of Applied Physics* **52**(3): 2110 – 2012.

[51] Kitanovski, A, U Plaznik, J Tušek, and A Poredoš. 2014. "New Thermodynamic Cycles for Magnetic Refrigeration." *International Journal of Refrigeration* **37**: 28 – 35.

[52] Iwasaki, W. 2003. "Magnetic Refrigeration Technology for an International Clean Energy Network Using Hydrogen Energy (WE-NET)." *International Journal of Hydrogen Energy* **28**(5): 559 – 567.

[53] Numazawa, T, K Kamiya, T Utaki, and K Matsumoto. 2014. "Magnetic Refrigerator for Hydrogen Liquefaction." *Cryogenics* (in press)

[54] Yayama, H, Y Hatta, and A Tomokiyo. 2000. "Hybrid Cryogenic Refrigerator Combining Magnetic- and Gas-Cooling System." *Physica B: Condensed Matter* **284-288**: 2016 – 2017.

[55] Tishin, A M, and Y I Spichkin. 2014. "Recent Progress in Magnetocaloric Effect: Mechanisms and Potential Applications." *International Journal of Refrigeration* **37**: 223 – 229.

[56] Collins, S and F J Zimmerman. 1953. "Cyclic Adiabatic Demagnetization." *Physical Review* **90**(5): 991-992.

[57] Heer, C V, C B Barnes, and J G Daunt. 1954. "The Design and Operation of a Magnetic Refrigerator for Maintaining Temperatures below 1° K." *Review of Scientific Instruments* **25**(11): 1088.

[58] Brown, G V. 1976. "Magnetic Heat Pumping near Room Temperature." *Journal of Applied Physics* **47**(8): 3673 – 3780.

[59] Steyert, W A. 1978. "Stirling cycle Rotating Magnetic Refrigerators and Heat Engines for Use near Room Temperature." *Journal of Applied Physics* **49**(3): 1216 – 1226.

[60] Barclay, J A and W A Steyert. "Active Magnetic Regenerator." U.S. Patent No.4332135, June 1, 1982.

[61] Zimm, C, A Jastrab, A Sternberg, V Pecharsky, K Gschneidner Jr., M Osborne and I Anderson. 1998. "Description and Performance of a Near-Room Temperature Magnetic Refrigerator." *Advances in Cryogenic Engineering: Proceedings of the Cryogenic Engineering Conference* **43**: 1759-1766.

[62] Hirano, N, S Nagaya, M Takahashi, T Kuriyama, K Ito, and S Nomura. 2002. "Development of Magnetic Refrigerator for Room Temperature Application." *Advances in Cryogenic Engineering: Proceedings of the Cryogenic Engineering Conference* **47**: 1027 – 1035.

[63] Blumenfeld, P E, F C Prenger, and A Sternberg. 2002. "High Temperature Superconducting Magnetic Refrigeration." *Advances in Cryogenic Engineering: Proceedings of the Cryogenic Engineering Conference* **47**: 1019 – 1927.

[64] Bohigas, X, E Molins, A Roig, J Tejada, and X X Zhang. 2000. "Room-Temperature Magnetic Refrigerator Using Permanent Magnets." *IEEE Transactions on Magnetics* **36**(3): 538 – 544.

[65] Okamura, T, K Yamada, N Hirano, and S Nagaya. 2006. "Performance of a Room-Temperature Rotary Magnetic Refrigerator." *International Journal of Refrigeration* **29**(8): 1327 – 1331.

[66] Zimm, C, A Boeder, J Chell, A Sternberg, A Fujita, S Fujieda, and K Fukamichi. 2006. "Design and Performance of a Permanent-Magnet Rotary Refrigerator." *International Journal of Refrigeration* **29**(8): 1302 – 1306.

[67] Engelbrecht, K, D Eriksen, C R H Bahl, R Bj ø rk, J Geyti, J a Lozano, K K Nielsen, F Saxild, A Smith, and N Pryds. 2012. "Experimental Results for a Novel Rotary Active Magnetic Regenerator." *International Journal of Refrigeration* **35**(6): 1498 – 1505.

[68] Nielsen, K K, J Tu š ek, K Engelbrecht, S Schopfer, A Kitanovski, C R H Bahl, A Smith, N Pryds, and A Poredo š . 2011. "Review on Numerical Modeling of Active Magnetic Regenerators for Room Temperature Applications." *International Journal of Refrigeration* **34**(3): 603-616.

[69] Tura, A, K K Nielsen, and A Rowe. 2012. "Experimental and Modeling Results of a Parallel Plate-Based Active Magnetic Regenerator." *International Journal of Refrigeration* **35** (6): 1518 – 1527.

[70] Tishin, A M. 1990. "Magnetocaloric Effect in Strong Magnetic Fields." *Cryogenics* **30**: 127 – 36.

[71] Allen, G, U Bianchi, and C Price. 1963. "Thermodynamics of Elasticity of Natural Rubber." *Transactions of the Faraday Society* **59**: 2493-2502.

[72] Cui, J, Y Wu, J Muehlbauer, Y Hwang, R Radermacher, S Fackler, M Wuttig, and I Takeuchi. 2012. "Demonstration of High Efficiency Elastocaloric Cooling with Large ΔT Using NiTi Wires." *Applied Physics Letters* **101** (7): 073904.

[73] Scott, J F. 2011. "Electrocaloric Materials." *Annual Review of Materials Research* **41** (1): 229 – 240.

[74] Neese, B, B Chu, S G Lu, Yong Wang, E Furman, and Q M Zhang. 2008. "Large Electrocaloric Effect in Ferroelectric Polymers near Room Temperature." *Science* **321** (5890): 821 – 823.

[75] Mischenko, A S, Q Zhang, J F Scott, R W Whatmore, and N D Mathur. 2006. "Giant Electrocaloric Effect in Thin-Film $PbZr_{0.95}Ti_{0.05}O_3$." *Science* **311** (5765): 1270 – 1271.

[76] Sari, O, and M Balli. 2014. "From Conventional to Magnetic Refrigerator Technology." *International Journal of Refrigeration* **37**: 8 – 15.

[77] Oliveira, N A, and P J Ranke. 2010. "Theoretical Aspects of the Magnetocaloric Effect." *Physics Reports* **489** (4-5). 89 – 159.

[78] Ožbolt, M., A. Kitanovski, J. Tušek, and A. Poredoš. 2014. "Electrocaloric vs. Magnetocaloric Energy Conversion." *International Journal of Refrigeration* **37**: 16 – 27.

[79] Balli, M, and C Mahmed. 2011. "On the Magnetic Forces in Magnetic Cooling Machines: Numerical Calculations and Experimental Investigations." *IEEE Transactions on Magnetics* **47**(10): 3383 – 3886.

[80] Coelho, A A, S Gamma, A Magnus and G Carvalho. 2009. "Prototype of a Gd-based rotating magnetic refrigerator for work around room temperature." *Proceedings of the Third International Conference on Magnetic Refrigeration at Room Temperature*, Des

Moines, Iowa, USA, 11 – 15, May. International Institute of Refrigeration, Paris, 381 – 386.

[81] Scarpa, F, G Tagliafico, and L A Tagliafico. 2012. "Classification Proposal for Room Temperature Magnetic Refrigerators." *International Journal of Refrigeration* **35**(2): 453 – 458.

[82] Basso, V, C P Sasso, G Bertotti, and M LoBue. 2006. "Effect of Material Hysteresis in Magnetic Refrigeration Cycles." *International Journal of Refrigeration* **29**(8): 1358 – 1365.

[83] Arnold, D S, A Tura, A Ruebsaat-Trott, and A Rowe. 2014. "Design Improvements of a Permanent Magnet Active Magnetic Refrigerator." *International Journal of Refrigeration* **37**: 99 – 105.

[84] Pecharsky, V K, K A Gschneidner, Y Mudryk, and D Paudyal. 2009. "Making the Most of the Magnetic and Lattice Entropy Changes." *Journal of Magnetism and Magnetic Materials* **321**(21): 3541 – 3547.

[85] Kitanovski, A, and P W Egolf. 2009. "Application of Magnetic Refrigeration and Its Assessment." *Journal of Magnetism and Magnetic Materials* **321**(7): 777 – 781.

[86] Peksoy, O, and A Rowe. 2005. "Demagnetizing Effects in Active Magnetic Regenerators." *Journal of Magnetism and Magnetic Materials* **288**: 424 – 432.

[87] Rosensweig, R E. 2006. "Refrigeration Aspects of Magnetic Particle Suspensions." *International Journal of Refrigeration* **29**(8): 1250 – 1258.

[88] Romero Gó mez, J, R Ferreiro Garcia, A De Miguel Catoira, and M Romero Gomez. 2013. "Magnetocaloric Effect: A Review of the Thermodynamic Cycles in Magnetic Refrigeration." *Renewable and Sustainable Energy Reviews* **17**: 74 – 82.

[89] Gschneidner, K A, and V K Pecharsky. 2008. "Thirty Years of near Room Temperature Magnetic Cooling: Where We Are Today and Future Prospects." *International Journal of Refrigeration* **31**(6): 945 – 961.

[90] Allab, F, A Kedous-Lebouc, J M Fournier, and J P Yonnet. 2005. "Numerical Modeling for Active Magnetic Regenerative Refrigeration." *IEEE Transactions on Magnetics* **41**(10): 3757 – 3759.

[91] Allab, F, A Kedous-Lebouc, J M Fournier, and J P Yonnet. 2005. "Numerical Modeling for Active Magnetic Regenerative Refrigeration." *IEEE Transactions on Magnetics* **41**(10): 3757 – 3759.

[92] Siddikov, B M, B A Wade, and D H Schultz. 2005. "Numerical Simulation of the Active Magnetic Regenerator." *Computers & Mathematics with Applications* **49**: 1525 – 1538.

[93] Petersen, T F, N Pryds, A Smith, J Hattel, H Schmidt, and H J Hogaard Knudsen. 2008. "Two-Dimensional Mathematical Model of a Reciprocating Room-Temperature Active Magnetic Regenerator." *International Journal of Refrigeration* **31**(3): 432 – 443.

[94] Petersen, T F, K Engelbrecht, C R H Bahl, B Elmegaard, N Pryds, and A Smith. 2008. "Comparison between a 1D and a 2D Numerical Model of an Active Magnetic Regenerative Refrigerator." *Journal of Physics D: Applied Physics* **41**(10): 105002.

[95] Bouchard, J, H Nesreddine, and N Galanis. 2009. "Model of a Porous Regenerator Used for Magnetic Refrigeration at Room Temperature." *International Journal of Heat and Mass Transfer* **52**(5): 1223 – 1329.

[96] Nielsen, K K, C R H Bahl, A Smith, R Bj ø rk, N Pryds, and J Hattel. 2009. "Detailed Numerical Modeling of a Linear Parallel-Plate Active Magnetic Regenerator." *International Journal of Refrigeration* **32**(6): 1478 – 1486.

[97] Aprea, C, and A Maiorino. 2010. "A Flexible Numerical Model to Study an Active Magnetic Refrigerator for near Room Temperature Applications." *Applied Energy* **87** (8): 2690 – 2098.

[98] Sarlah, A, and A Poredoš. 2010. "Dimensionless Numerical Model for Simulation of Active Magnetic Regenerator Refrigerator." *International Journal of Refrigeration* **33**(6): 1061 – 1067.

[99] Kim, Y, and S Jeong. 2011. "Numerical Simulation and Its Verification for an Active Magnetic Regenerator." *International Journal of Refrigeration* **34**(1)R: 204 – 215.

[100] Park, I, Y Kim, and S Jeong. 2013. "Development of the Tandem Reciprocating Magnetic Regenerative Refrigerator and Numerical Simulation for the Dead Volume Effect." *International Journal of Refrigeration* **36**(6): 1741 – 1749.

[101] Rowe, A. 2012. "Thermodynamics of Active Magnetic Regenerators: Part I." *Cryogenics* **52**(2): 111 – 118.

[102] Rowe, A. 2012. "Thermodynamics of Active Magnetic Regenerators: Part II." *Cryogenics* **52** (2): 119 – 128.

[103] Whitaker, S. 1972. "Forced Convection Heat Transfer Correlations for Flow in Pipes, Past Flat Plates, Single Cylinders, Single Spheres, and for Flow in Packed Beds and Tube Bundles." *AIChE Journal* **18**(2): 361 – 371.

[104] Engelbrecht, K, C R H Bahl, and K K Nielsen. 2011. "Experimental Results for a Magnetic Refrigerator Using Three Different Types of Magnetocaloric Material Regenerators." *International Journal of Refrigeration* **34**(4) 1132 – 1140.

Publications

Journals

[1] **Yui Kotani**, Yasuki Kansha, Atsushi Tsutsumi, "Self-heat recuperation using magnetocaloric effect", *Chemical Engineering Transaction* (2012) **29** 373-378.

[2] Muhammad Aziz, Yasuki Kansha, Akira Kishimoto, **Yui Kotani**, Yuping Liu, Atsushi Tsutsumi, "Advanced energy saving in low rank coal drying based on self-heat recuperation technology", *Fuel Processing Technology* (2012) **104** 16-22.

[3] **Yui Kotani**, Muhammad Aziz, Yasuki Kansha, Chihiro Fushimi, Atsushi Tsutsumi, "Magnetocaloric Heat Circulator based on Self-Heat Recuperation Technology", *Chemical Engineering Science* (2013) **101** 5-12.

[4] **Yui Kotani**, Yasuki Kansha, Atsushi Tsutsumi, "Conceptual design of an active magnetic regenerative heat circulator based on self-heat recuperation technology", *Energy* (2013) **55** 127-133.

[5] **Yui Kotani**, Yasuki Kansha, Atsushi Tsutsumi, "Active Magnetic Regenerative Heat Circulator for Energy Saving in Thermal Process", *Chemical Engineering Transaction* (2013) **35** 229-234.

[6] Yasuki Kansha, **Yui Kotani**, Muhammad Aziz, Akira Kishimoto, Atsushi Tsutsumi, "Design and Evaluation of a Self-Heat Recuperative Thermal Process Based on Thermodynamic Irreversibility and Exergy", *Journal of Chemical Engineering of Japan*

(2013) **46** 87-91.

[7] **Yui Kotani**, Yasuki Kansha, Ishizuka Masanori, Atsushi Tsutsumi, "Experimental investigation of an active magnetic regenerative heat circulator applied to self-heat recuperation technology", *Applied Thermal Engineering* (2014) **70** 1202-1207.

[8] **Yui Kotani**, Yasuki Kansha, Ishizuka Masanori, Atsushi Tsutsumi, "Theoretical and experimental investigation on the energy consumption of self-heat recuperation using magnetocaloric effect", *Chemical Engineering Transactions* (2014) **39** 175-180.

Books

[1] **小谷 唯**,『熱エネルギーの高効率活用技術と省エネルギー（仮）』, フロンティア出版, 2014 （提出済）

International Conference

◯ for oral presentation, □ for poster presentation

[1] ◯ **Yui Kotani**, Muhammad Aziz, Yasuki Kansha, Chihiro Fushimi, Atsushi Tsutsumi, "Magnetic Heat Circulator Based On Self-Heat Recuperation", 2011 American Institute of Chemical Engineers Annual Meeting (2011 AIChE), 763e, Minneapolis, US (2011.10)

[2] □ **Yui Kotani**, Muhammad Aziz, Yasuki Kansha, Chihiro Fushimi, Atsushi Tsutsumi, "Magnetic Heat Circulator Based On Self-Heat Recuperation" , International Symposium on Exploring the Frontiers of Academic Collaboration between UAE and Japan − Petroleum and Energy-related Technologies, Tokyo, JPN (2011.12)

[3] □ **Yui Kotani**, Yasuki Kansha, Atsushi Tsutsumi, "Self-heat recuperation using magnetocaloric effect" 15th Conference Process Integration, Modeling and Optimization for Energy Saving and Pollution Reduction (PRES2012), P7.73, Prague, CSK (2012.8)

[4] ◯ **Yui Kotani**, Yasuki Kansha, Atsushi Tsutsumi, "Simulation of Self-Heat Recuperation Using Magnetocaloric Effect", 2012 American Institute of Chemical Engineers Annual Meeting (2012 AIChE), 350c, Pittsburg, US (2012.10)

[5] ◯ Yasuki Kansha, Yuping Liu, **Yui Kotani**, Hiroyuki Mizuno, Atsushi Tsutsumi, "Self-Heat Recuperation and Its Applications in Chemical Industries", 2012 American Institute of Chemical Engineers Annual Meeting (2012 AIChE), 350b, Pittsburg,

US (2012.10)

[6] ◯ **Yui Kotani**, Yasuki Kansha, Atsushi Tsutsumi, "Self-Heat Recuperation using Magnetocaloric Effect", GMSI-COSM-UT2 Workshop 2012 (Univ. of Tokyo and Univ. of Toronto Graduate Student Workshop), Tokyo, JPN (2012.6)

[7] ◯ Yasuki Kansha, Masanori Ishizuka, **Yui Kotani**, Atsushi Tsutsumi, "Evaluation of Exergy loss in heat exchangers", 9th World Congress of Chemical Engineering 15th Asian Pacific Confederation of Chemcial Engineering Congress (WCCE 9 & APCChE 15 APCChe 2013) Seoul, KOR (2013.8)

[8] ◯ **Yui Kotani**, Yasuki Kansha, Atsushi Tsutsumi, "Active magnetic regenerative heat circulator for energy saving in thermal process", 16th Conference Process Integration, Modeling and Optimization for Energy Saving and Pollution Reduction (PRES2013), 2.1.3, Rodos, GRC (2013.9)

[9] ◯ **Yui Kotani**, Yasuki Kansha, Atsushi Tsutsumi, "Proposition of active magnetic regenerative heat circulator for self-heat recuperation in thermal processes", Postgraduate Colloquium for Environmental Research 2013 (POCER2013), 015, Genting Highland, MYS (2013.6)

[10] ◯ Yasuki Kansha, Masanori Ishizuka, **Yui Kotani**, Atsushi Tsutsumi, "Exergy Loss Minimization for Chemical Processes", International Conference on Green Energy and Technology (ICGET), Kitakyushu, JPN (2013.8)

[11] ◯ **Yui Kotani**, Yasuki Kansha, Masanori Ishizuka, Atsushi Tsutsumi, "Experimental Investigation of Self-Heat Recuperation Using Magnetocaloric Effect for Energy Saving in Thermal Processes", 2013 American Institute of Chemical Engineers Annual Meeting (2013 AIChE), 616e, San Francisco, US (2013.11)

[12] □ **Yui Kotani**, Yasuki Kansha, Masanori Ishizuka, Atsushi Tsutsumi, "Simulation and Experimental Evaluation of Self-heat Recuperation Using Magnetocaloric Ef-

fect", International Symposium on EcoTopia Science 2013 (ISETS '13), Nagoya, JPN (2013.12)

[13] ◯ Renaldo Rasfuldi, **Yui Kotani**, Yasuki Kansha, Atsushi Tsutsumi, "Self-Heat Recuperative Heat Circulation Processing with Thermoelectric Device", International Conference on Applied Energy (ICAE2014), Taipei, TAIWAN (2014.6)

[14] ◯ **Yui Kotani**, Yasuki Kansha, Masanori Ishizuka, Atsushi Tsutsumi, "Theoretical and experimental investigation on the energy consumption of self-heat recuperation using magnetocaloric effect", 17th Conference Process Integration, Modeling and Optimization for Energy Saving and Pollution Reduction (PRES2014), Prague, CZK (2014.8)（発表予定）

[15] ◯ **Yui Kotani**, Yasuki Kansha, Masanori Ishizuka, Atsushi Tsutsumi, "Magnetocaloric self-heat recuperation cycle for energy saving in thermal processes", 6th IIR/IIF International Conference on Magnetic Refrigeration (THERMAG VI), Victoria, CAN (2014.9)（発表予定）

[16] ◯ Masanori Ishizuka, Hiroyuki Mizuno, **Yui Kotani**, Yasuki Kansha, Atsushi Tsutsumi, "Modeling of Triple bed Circulation Fluidized Bed Flow behavior using Equivalent Electrical Circuit", The 4th Asian Conference on Innovative Energy & Environmental Chemical Engineering (4th ASCON-IEEChE), Yeosu, KOR (2014.11)（発表予定）

[17] ◯ Yasuki Kansha, Hiroyuki Mizuno, **Yui Kotani**, Masanori Ishizuka, Chunfeng Song, Qian Fu, Atsushi Tsutsumi, "Methanol Production Process Based on Self-Heat Recuperation" The 4th Asian Conference on Innovative Energy & Environmental Chemical Engineering (4th ASCON-IEEChE), Yeosu, KOR (2014.11)（発表予定）

[18] ◯ Toshihiro Kaseda, Yasuki Kansha, Ishizuka Masanori, Yui Kotani, Renaldo Rasfuldi, Atsushi Tsutsumi, "Self-heat recuperation by electrocaloric effect" The 4th

Asian Conference on Innovative Energy & Environmental Chemical Engineering (4th ASCON-IEEChE), Yeosu, KOR (2014.11)（発表予定）

[19] ◯ Toshihiro Kaseda, Yasuki Kansha, Masanori Ishizuka, **Yui Kotani**, Renaldo Rasfuldi, Atsushi Tsutsumi, "Self-heat recuperation system by Electrocaloric effect", 2014 American Institute of Chemical Engineers Annual Meeting (2014 AIChE), Atlanta, US（発表予定)

Domestic Conferences

◯ for oral presentation, □ for poster presentation

[1] ◯ **小谷 唯** Aziz Muhammad, 甘蔗 寂樹, 伏見 千尋, 堤 敦司,『自己熱再生に基づく磁気熱循環システム』 日本エネルギー学会第 20 回年次大会講演要旨集, 294-295 （2011.8）

[2] ◯ **小谷 唯** 『自己熱再生に基づく磁気熱循環システム』, 第 11 回コプロワークショップ「エネルギー・物質の併産（コプロダクション）およびエクセルギー再生による革新的省エネルギーと次世代産業基盤の構築」 講演要旨集, 49-58 （2012.2）

[3] ◯ **小谷 唯**, 甘蔗 寂樹, 堤 敦司『自己熱再生に基づく磁気ヒートサーキュレーター』 化学工学会第 77 年会, G222 （2012.3）

[4] ◯ **小谷 唯**, 甘蔗 寂樹, 堤 敦司『自己熱再生に基づいた AMR ヒートサーキュレーターの概念設計』 化学工学会第 78 年会 B306 （2013.3）

[5] ◯ **小谷 唯**, 甘蔗 寂樹, 石束 真典, 堤 敦司『磁気熱量効果を適用した自己熱再生システムの実験研究』 化学工学会第 45 回秋季大会, K123 （2013.9）

[6] ◯ **小谷 唯**,『熱プロセス省エネルギー化のための磁気熱循環システム』IIS PhD Student Live、1-13 （2013.7）

[7] □ Rasfuldi Renaldo, **小谷 唯**, 甘蔗 寂樹, 堤 敦司 『Self-Heat Recuperative Heat Circulation Processing with Thermoelectric Device』 化学工学会第 79 年会, SC2P53 （2014.3）

[8] ◯ **小谷 唯**, 甘蔗 寂樹, 石東 真典, 堤 敦司『磁気熱量効果を用いた熱循環システムの実験研究』 日本エネルギー学会第 23 回年次大会講演要旨集, 233 （2014.7）

[9] ◯ 甘蔗 寂樹、**小谷 唯**、Aziz Muhammad、岸本 啓、堤 敦司、『不可逆性とエクセルギーの観点からの自己熱再生熱プロセスの評価』、N121（2014.9）（発表予定）

[10] ◯ 加世田 敏宏、甘蔗 寂樹、石東 真典、**小谷 唯**、Renaldo Rasfuldi、堤 敦司、『誘電熱量効果を用いた自己熱再生システムの構築』、化学工学会第 46 回秋季大会、N120（2014.9）（発表予定）

[11] ◯ 石東真典、水野寛之、**小谷 唯**、甘蔗 寂樹、堤 敦司『大型三塔式循環流動層の粒子循環量制御のためのモデル化』 第 20 回流動化・粒子プロセッシングシンポジウム

Honors

[1] 平成 23 年度日本エネルギー学会「奨励賞」『自己熱再生に基づく磁気熱循環システム』受賞（35 歳以下若手研究者対象）

[2] 2012GMSI Summer Camp organized by the University of Tokyo Global Center of Excellence for Mechanical System Innovation "Award for Most Innovative Idea" Michael Barako, Bin Feng, **Yui Kotani**, Atsushi Kubo, Kenneth Mcnaney, Dhruba Panthi, Yonghua Zhao

[3] 1st Prize in the Competition for the Best Poster ZDENEK BURIANEC MEMORIAL AWARD Self-heat recuperation using magnetocaloric effect. **Y. Kotani**, Y. Kansha, A. Tsutsumi. 15th Conference on Process Integration, Modeling and Optimization for Energy Saving and Pollution Reduction PRES2012

[4] GMSI Project Based Learning award for Most Outstanding Project Execution. **Yui Kotani**, Xiao Chen, Mashiro Fujii and Yonghua Zhao

[5] Journal of Chemical Engineering Japan Outstanding Paper Award of 2013. Evaluation of a Self-Heat Recuperative Thermal Process Based on Thermodynamic Irreversibility and Exergy. Yasuki Kansha, **Yui Kotani**, Muhammad Aziz, Akira Kishimoto, Atsushi Tsutsumi

Acknowledgement

This work was conducted under direction of Prof. Atsushi Tsutsumi at Institute of Industrial Science, the University of Tokyo. I will like to express my deepest gratitude for always creating time for discussions and giving me insightful advices from different perspectives.

Great appreciation goes to my thesis committee, Prof. Naoki Shikazono, Prof.Ryo Shirakashi, Prof. Junichiro Shiomi and Prof. Masashi Tokunaga for their valuable comments.

Prof. Yasuki Kansha and Mr. Masanori Ishizuka at the Institute of Industrial Science, the University of Tokyo has always been my best advisers throughout the work. Their advices has been illuminating. I would like to express them my heartfelt appreciation.

My appreciation goes to Prof. Chihiro Fushimi at Tokyo Agriculture Engineering Technology, Prof. Muhammad Aziz at Tokyo Institute of Technology, Dr. Akira Kishimoto at Kobe Steel, LTD. and Dr. Hidetoshi Yamamoto for their close support and helpful suggestions.

Prof. Tetsuji Okamura at Tokyo Institute of Technology has kindly welcomed me to his laboratory for discussion. I am very much grateful.

I would like to thank the members of Tsutsumi laboratory for their support. I am in dept of Dr. Qian Fu, Dr. Chunfeng Song Dr. Bokkyu Choi, Dr. Dhruba Panthi and Dr. Yuping Liu. The discussions made with them has been highly suggestive. My appreciation goes to Ms. Seiko Honma and Ms. Sakura Haratani for their ensuring support that enabled the research go smoothly. My colleagues, Mr. Hiroyuki Mizuno, Mr. Mike

Musil, Mr. Junghee Jo, Mr. Toshihiro Kaseda, Mr. Renaldo Rasfuldi, Mr. Yusuke Sakakibara, Mr. Yusuke Shimizu, Mr. Yuan Tang and Mr. Lu Chen made my life as at the laboratory exciting and fruitful.

My acknowledgement goes to Japan Society of Promotion of Science (JSPS) who has financially supported this research.

Finally, I would like to express my warmest gratitude goes to my family and friends, especially my partner Eri who has been encouraged me greatly.